Absolute Cross Sections for Molecular Photoabsorption, Partial Photoionization, and Ionic Photofragmentation Processes

Cite as: Journal of Physical and Chemical Reference Data **17**, 9 (1988); https://doi.org/10.1063/1.555821
Submitted: 04 April 1987 . Published Online: 15 October 2009

J. W. Gallagher, C. E. Brion, J. A. R. Samson, and P. W. Langhoff

Absolute Cross Sections for Molecular Photoabsorption, Partial Photoionization, and Ionic Photofragmentation Processes

J. W. Gallagher, C. E. Brion,[a] J. A. R. Samson,[b] and P. W. Langhoff[c]

Joint Institute for Laboratory Astrophysics, University of Colorado and National Bureau of Standards, Boulder, Colorado 80309-0440

Received 4 April 1987; revised manuscript received 26 August 1987

A compilation is provided of absolute total photoabsorption and partial-channel photoionization cross sections for the valence shells of selected molecules, including diatomics (H_2, N_2, O_2, CO, NO) and triatomics (CO_2, N_2O), simple hydrides (H_2O, NH_3, CH_4), hydrogen halides (HF, HCl, HBr, HI), sulfur compounds (H_2S, CS_2, OCS, SO_2, SF_6), and chlorine compounds (Cl_2, CCl_4). The partial-channel cross sections presented refer to production of the individual electronic states of molecular ions and also to production of parent and specific fragment ions, as functions of incident photon energy, typically from ~20 to 100 eV. Total photoabsorption cross sections above the first ionization threshold are reported from conventional optical measurements obtained using line and continuum sources and from "equivalent-photon" dipole (e,e) electron scattering experiments. Partial photoionization cross sections for production of electronic states of molecular ions are obtained from photoelectron spectroscopy and from dipole $(e,2e)$ coincidence measurements. Photoionization mass spectrometry and dipole $(e, e+\text{ion})$ coincidence studies provide measurements of partial cross sections for ionic photofragmentation (i.e., dissociative photoionization). Photoelectron anisotropy factors, which together with electronic partial cross sections provide cross sections differential in photon energy and in ejection angle, are also reported. There is generally good agreement between cross sections measured by the physically distinct optical and dipole electron-impact methods. The cross sections and anisotropy factors also compare favorably with selected *ab initio* and model potential (X-alpha) calculations which provide a basis for interpretation of the measurements.

Key words: asymmetry parameter; beta; cross section; dissociative ionization; partial channel; photoabsorption; photofragmentation; photoionization.

Contents

1. Introduction 13
2. Definitions and Nomenclature 15
3. Experimental Methods 17
   3.1. Photon Measurements 17
      3.1.a. Total Photoabsorption and Photoionization Cross Sections 17
      3.1.b. Partial Photoionization Cross Sections 20
   3.2. Dipole Electron-Impact Measurements 21
      3.2.a. Total Photoabsorption Cross Sections 21
      3.2.b. Partial Photoionization Cross Sections 23
4. Theoretical Studies 25
   4.1. Cross-Sectional Expressions 25
   4.2. Dynamical Approximations 26
   4.3. Computational Approximations 26
5. Data Acquisition and Presentation 27
6. Conclusions and Evaluation 28
7. Acknowledgments 149
8. References 149

List of Tables

1. Photon and electron impact experiments 17
2. Data for H_2 30
3. Data for N_2 34
4. Data for O_2 40
5. Data for CO 47

[a] Department of Chemistry, University of British Columbia, Vancouver, B.C., Canada V6T 1Y6.
[b] Department of Physics, University of Nebraska, Lincoln, NE 68588-0111.
[c] Department of Chemistry and Supercomputer Computations Research Institute, Florida State University, Tallahassee, FL 32306. Present address: Department of Chemistry, Indiana University, Bloomington, IN 47405.

6. Data for NO 54
7. Data for CO_2 62
8. Data for N_2O 69
9. Data for H_2O 76
10. Data for NH_3 83
11. Data for CH_4 89
12. Data for hydrogen halides 94
13. Data for H_2S 106
14. Data for CS_2 112
15. Data for OCS 120
16. Data for SO_2 127
17. Data for SF_6 130
18. Data for Cl_2 140
19. Data for CCl_4 145

List of Figures

1. Photoelectron kinetic energy spectron for the water molecule 14
2. Parent- and fragment-ion spectrum obtained from dipole (e, e + ion) electron-ion coincidence study of the water molecule 14
3. Simple photoabsorption cell 18
4. Split-beam absorption cell 18
5. Double-ion chamber 19
6. Electron kinetic energy analyzers 20
7. Dipole (e, e) energy loss spectrometer 22
8. Dipole (e, $2e$) spectrometer 23
9. Dipole (e, e + ion) spectrometer 24
10. Total photoabsorption cross section for H_2: (a) low-energy range, (b) high-energy range 31
11. (a) Partial photoionization cross section for H_2; final ionic state = $X\,^1\Sigma_g^+$. (b) Photoelectron asymmetry parameter for H_2; final ionic state = $X\,^1\Sigma_g^+$ 32
12. Partial ionic photofragmentation cross sections for H_2; (a) product ion = H_2^+, (b) product ion = H^+ 33
13. Total photoabsorption cross section for N_2: (a) low-energy range, (b) high-energy range 35
14. Partial photoionization cross sections for N_2; (a) final ionic state = $X\,^2\Sigma_g^+$, (b) final ionic state = $A\,^2\Pi_u^+$, (c) final ionic state = $B\,^2\Sigma_u^+$ .. 36
15. Photoelectron asymmetry parameters for N_2; (a) final ionic state = $X\,^2\Sigma_g^+$, (b) final ionic state = $A\,^2\Pi_u^+$, (c) final ionic state = $B\,^2\Sigma_u^+$ .. 37
16. Partial photoionization cross sections for N_2; (a) final ionic state = $C\,^2\Sigma_u^+$, (b) final ionic state = $F\,^2\Sigma_g^+$, (c) final ionic state = $G\,^2\Sigma_g^+$. 38
17. (a) Partial photoionization cross section for N_2; final ionic state = $^2\Sigma_g$. (b) Partial ionic photofragmentation cross section for N_2, product ion = N_2^+. (c) Partial ionic photofragmentation cross section, product ion = N^+ 39
18. Total photoabsorption cross section for O_2: (a) low-energy range, (b) high-energy range 41
19. Partial photoionization cross sections for O_2; (a) final ionic state = $X\,^2\Pi_g^+$, (b) final ionic state = $a\,^4\Pi_u + A\,^2\Pi_u$, (c) final ionic state = $b\,^4\Sigma_g^-$ 42
20. Photoelectron asymmetry parameters for O_2; (a) final ionic state = $X\,^2\Pi_g^+$, (b) final ionic state = $a\,^4\Pi_u + A\,^2\Pi_u$, (c) final ionic state = $b\,^4\Sigma_g^-$ 43
21. Partial photoionization cross sections for O_2; (a) final ionic state = $B\,^2\Sigma^-$, (b) final ionic state = $^2\Pi_u + c\,^4\Sigma_u^-$, (c) final ionic state = $^2\Sigma_u^-$ 44
22. Partial photoionization cross sections for O_2; (a) PES peak at 33 eV, (b) final ionic state = $^{2,4}\Sigma_g^-$ 45
23. Partial ionic photofragmentation cross sections of O_2; (a) product ion = O_2^+; (b) product ion = O^+ 46
24. Total photoabsorption cross section for CO: (a) low-energy range, (b) high-energy range.. 48
25. Partial photoionization cross sections for CO; (a) final ionic state = $X\,^2\Sigma^+$, (b) final ionic state = $A\,^2\Pi$, (c) final ionic state = $B\,^2\Sigma^+$ 49
26. Photoelectron asymmetry parameters for CO; (a) final ionic state = $X\,^2\Sigma^+$, (b) final ionic state = $A\,^2\Pi$, (c) final ionic state = $B\,^2\Sigma^+$ 50
27. Partial photoionization cross sections for CO; (a) final ionic state = $C\,^2\Sigma^+$, (b) final ionic state = W (PES peak at 32 eV), (c) final ionic state = $^2\Sigma$ (PES peak at 35–45 eV) 51
28. (a) Partial photoionization cross section for CO, final ionic state = $W + {}^2\Sigma$ (PES peak at 30–44 eV); (b) Partial ionic photofragmentation cross section for CO, product ion = CO^+. (c) Partial ionic photofragmentation cross section for CO, product ion = C^+ 52
29. Partial ionic photofragmentation cross sections for CO; (a) product ion = O^+, (b) product ion = CO^{2+}, (c) product ion = C^{2+} 53
30. Total photoabsorption cross section for NO: (a) low-energy range, (b) high-energy range.. 55
31. Partial photoionization cross sections for NO; (a) final ionic state = $X\,^1\Sigma^+$, (b) final ionic state = $b\,^3\Pi$, (c) final ionic state = $c^3\Pi$ 56
32. Photoelectron asymmetry parameters for NO; (a) final ionic state = $X\,^1\Sigma^+$, (b) final ionic state = $b\,^3\Pi$, (c) final ionic state = $c^3\Pi$ 57
33. Partial photoionization cross sections for NO; (a) final ionic state = $A\,^1\Pi$, (b) final ionic state = $B\,^1\Pi$ 58
34. Partial photoionization cross sections for NO; (a) final ionic state = PES peak at 14–20 eV, (b) final ionic state = $c + B + B'$, (c) final ionic state = PES peak at 26–36 eV 59
35. (a) Partial photoionization cross section for NO, final ionic state = $^1\Pi + {}^3\Pi$; (b) Partial ionic photofragmentation cross section for NO, product ion = NO^+ 60
36. Partial ionic photofragmentation cross sections for NO; (a) product ion = N^+, (b) product ion = O^+, (c) product ion = NO^{2+} 61
37. Total photoabsorption cross section for CO_2: (a) low-energy range, (b) high-energy range.. 63

38. Partial photoionization cross sections for CO_2; (a) final ionic state = $X^2\Pi_g$, (b) final ionic state = $A^2\Pi_u + B^2\Sigma_u$, (c) final ionic state = PES peak at 22–40 eV 64
39. Photoelectron asymmetry parameters for CO_2; (a) final ionic state = $X^2\Pi_g$, (b) final ionic state = $A^2\Pi_u$, (c) final ionic state = $B^2\Sigma_u$ 65
40. (a) Partial photoionization cross sections for CO_2, final ionic state = $C^2\Sigma_g$, (b) photoelectron asymmetry parameter for CO_2, final ionic state = $C^2\Sigma_g$ 66
41. Partial ionic photofragmentation cross sections for CO_2; (a) product ion = CO_2^+, (b) product ion = CO^+, (c) product ion = O^+ 67
42. Partial ionic photofragmentation cross sections for CO_2; (a) product ion = C^+, (b) product ion = CO_2^{2+}, (c) product ion = C^{2+} 68
43. Total photoabsorption cross section for N_2O: (a) low-energy range, (b) high-energy range.. 70
44. Partial photoionization cross sections for N_2O; (a) final ionic state = $X^2\Pi$, (b) final ionic state = $A^2\Sigma$, (c) final ionic state = $B^2\Pi$ 71
45. Photoelectron asymmetry parameters for N_2O; (a) final ionic state = $X^2\Pi$, (b) final ionic state = $A^2\Sigma$, (c) final ionic state = $B^2\Pi$ 72
46. (a) Partial photoionization cross section for N_2O, final ionic state = $C^2\Sigma^+$, (b) photoelectron asymmetry parameter for N_2O, final ionic state = $C^2\Sigma^+$, (c) partial photoionization cross section for N_2O, final ionic state = PES peak at 24 eV 73
47. (a) Partial photoionization cross section for N_2O, final ionic state = PES peak at 22–42 eV. (b) Partial ionic photofragmentation cross sections for N_2O, product ion = N_2O^+. (c) Partial ionic photofragmentation cross sections for N_2O, product ion = NO^+ 74
48. Partial ionic photofragmentation cross sections for N_2O; (a) product ion = N_2^+, (b) product ion = O^+, (c) product ion = N^+ 75
49. Total photoabsorption cross section for H_2O: (a) low-energy range, (b) high-energy range.. 77
50. Partial photoionization cross sections for H_2O; (a) final ionic state = X^2B_1, (b) final ionic state = A^2A_1, (c) final ionic state = B^2B_2 78
51. Photoelectron asymmetry parameters for H_2O; (a) final ionic state = X^2B_1, (b) final ionic state = A^2A_1, (c) final ionic state = B^2B_2 79
52. (a) Partial photoionization cross section for H_2O, final ionic state = C^2A_1, (b) photoelectron asymmetry parameter for H_2O, final ionic state = C^2A_1 80
53. (a) Partial photoionization cross section for H_2O, final ionic state = C^2A_1, extended energy range. (b) Partial ionic photofragmentation cross section for H_2O, product ion = H_2O^+ ... 81
54. Partial ionic photofragmentation cross sections for H_2O; (a) product ion = OH^+, (b) product ion = H^+, (c) product ion = O^+ 82
55. Total photoabsorption cross section for NH_3: (a) low-energy range, (b) high-energy range.. 84
56. Partial photoionization cross sections for NH_3; (a) final ionic state = X^2A_1, (b) final ionic state = A^2E, (c) final ionic state = B^2A_1 85
57. Photoelectron asymmetry parameters for NH_3; (a) final ionic state = X^2A_1, (b) final ionic state = A^2E, (c) final ionic state = B^2A_1 86
58. Partial ionic photofragmentation cross sections for NH_3; (a) product ion = NH_3^+, (b) product ion = NH_2^+, (c) product ion = NH^+ 87
59. Partial ionic photofragmentation cross sections for NH_3; (a) product ion = N^+, (b) product ion = H^+ 88
60. Total photoabsorption cross section for CH_4; (a) low-energy range, (b) high-energy range.. 90
61. Partial photoionization cross sections for CH_4; (a) final ionic state = X^2T, (b) final ionic state = A^2A_1, (c) final ionic states = many-body states arising from inner valence ionization 91
62. Partial ionic photofragmentation cross sections for CH_4; (a) product ion = CH_4^+, (b) product ion = CH_3^+, (c) product ion = CH_2^+ 92
63. Partial ionic photofragmentation cross sections for CH_4; (a) product ion = CH^+, (b) product ion = H^+, (c) product ions = C^+ and H_2^+ 93
64. Total photoabsorption cross section for HF 95
65. Partial photoionization cross sections for HF; (a) final ionic state = $X^2\Pi$, (b) final ionic state = $A^2\Sigma^+$, (c) final ionic state = $B^2\Sigma^+$ ... 96
66. Partial ionic photofragmentation cross sections for HF; (a) product ion = HF^+, (b) product ion = F^+, (c) product ion = H^+ 97
67. (a) Total photoabsorption cross section for HCl. (b) Partial photoionization cross section for HCl, final ionic state = $X^2\Pi$. (c) Partial photoionization cross section for HCl, final ionic state = $A^2\Sigma^+$ 98
68. (a) Partial photoionization cross section for HCl, final ionic states = many-body states arising from inner valence ionization. (b) Photoelectron asymmetry parameter for HCl, final ionic state = $X^2\Pi$. (c) Photoelectron asymmetry parameter for HCl, final ionic state = $A^2\Sigma^+$ 99
69. Partial ionic photofragmentation cross sections for HCl; (a) product ion = HCl^+, (b) product ion = Cl^+, (c) product ion = H^+ 100
70. (a) Total photoabsorption cross section for HBr. (b) Partial photoionization cross section for HBr, final state = $X^2\Pi$. (c) Partial photoionization cross section for HBr, final state = $A^2\Sigma^+$ 101
71. (a) Partial photoionization cross section for HBr, final ionic states = many-body states arising from inner valence ionization. (b) Photoelectron asymmetry parameter for HBr, final ionic state = $X^2\Pi$. (c) Photoelectron asymmetry parameter for HBr, final ionic

state = $A\,^2\Sigma^+$ 102
72. Partial ionic photofragmentation cross sections for HBr; (a) product ion = HBr^+, (b) product ion = Br^+, (c) product ion = H^+ 103
73. Partial photoionization cross sections for HI; (a) final ionic state = $X\,^2\Pi$, (b) final ionic state = $A\,^2\Sigma^+$ 104
74. Photoelectron asymmetry parameters for HI: (a) final ionic state = $X\,^2\Pi$. (b) final ionic state = $A\,^2\Sigma^+$ 105
75. Total photoabsorption cross section for H_2S ... 107
76. Partial photoionization cross sections for H_2S; (a) final ionic state = $X\,^2B_1$, (b) final ionic state = $A\,^2A_1$, (c) final ionic state = $B\,^2B_2$ 108
77. Photoelectron asymmetry parameters for H_2S; (a) final ionic state = $X\,^2B_1$, (b) final ionic state = $A\,^2A_1$, (c) final ionic state = $B\,^2B_2$ 109
78. (a) Partial photoionization cross section for H_2S, final ionic state = C, (b) photoelectron asymmetry parameter for H_2S, final ionic state = C. (c) Partial ionic photofragmentation cross section for H_2S, product ion = H_2S^+ 110
79. Partial ionic photofragmentation cross sections for H_2S; (a) product ion = HS^+, (b)product ion = S^+, (c) product ion = H^+ 111
80. Total photoabsorption cross section for CS_2.... 113
81. Partial photoionization cross sections for CS_2; (a) final ionic state = $X\,^2\Pi_g$, (b) final ionic state = $A\,^2\Pi_u$, (c) final ionic state = $B\,^2\Sigma_u$ 114
82. Photoelectron asymmetry parameters for CS_2; (a) final ionic state = $X\,^2\Pi_u$, (b) final ionic state = $A\,^2\Pi_u$, (c) final ionic state = $B\,^2\Sigma_u$ 115
83. (a) Partial photoionization cross sections for CS_2; (a) final ionic state = $C\,^2\Sigma_g$, (b) final ionic state = $C\,^2\Sigma_g + D\,^2\Pi_u$, (c) final ionic state = $D\,^2\Pi_u$ 116
84. Photoelectron asymmetry parameters for CS_2; (a) final ionic state = $C\,^2\Sigma_g$, (b) final ionic state = $D\,^2\Pi_u$, (c) Partial photoionization cross section for CS_2, final ionic states = many-body states arising from inner valence ionization 117
85. Partial ionic photofragmentation cross sections for CS_2; (a) product ion = CS_2^+, (b) product ion = S_2^+, (c) product ion = CS^+ 118
86. Partial ionic photofragmentation cross sections for CS_2; (a) product ion = CS_2^{2+}, (b) product ion = S^+, (c) product ion = C^+ 119
87. Total photoabsorption cross section for OCS .. 121
88. Partial photoionization cross sections for OCS; (a) final ionic state = $X\,^2\Pi$, (b) final ionic state = $A\,^2\Pi + B\,^2\Sigma^+$, (c) final ionic states = many-body states arising from inner valence ionization 122
89. Photoelectron asymmetry parameters for OCS; (a) final ionic state = $X\,^2\Pi$, (b) final ionic state = $A\,^2\Pi$, (c) final ionic state = $B\,^2\Sigma^+$ 123
90. (a) Partial photoionization cross section for OCS, final ionic state = $C\,^2\Sigma^+$.(b) Photoelectron asymmetry parameter for OCS, final ionic state = $C\,^2\Sigma^+$ 124
91. Partial ionic photofragmentation cross sections for OCS; (a) product ion = OCS^+, (b) product ion = CS^+, (c) product ion = S^+ 125
92. Partial ionic photofragmentation cross sections for OCS; (a) product ion = CO^+, (b) product ion = O^+, (c) product ion = C^+ 126
93. (a) Total photoabsorption cross section for SO_2. (b) Partial ionic photofragmentation cross sections for SO_2, product ion = SO_2^+ 128
94. Partial ionic photofragmentation cross sections for SO_2; (a) product ion = SO^+, (b) product ion = O^+, (c) product ions = S^+, O_2^+ 129
95. Total photoabsorption cross section for SF_6: (a) low-energy range, (b) high-energy range.. 131
96. Partial photoionization cross sections for SF_6; PES peak at (a) 15.7, (b) 17.0, and (c) 18.3 eV 132
97. Partial photoionization cross sections for SF_6; PES peak at (a) 19.7 and (b) 22.5 eV 133
98. Photoelectron asymmetry parameters for SF_6; PES peak at (a) 15.7, (b) 17.0, and (c) 18.3 eV 134
99. Photoelectron asymmetry parameters for SF_6; PES peak at (a) 19.7 and (b) 22.5 eV 135
100. Partial ionic photofragmentation cross sections for SF_6; (a) product ion = SF_5^+, (b) product ion = SF_4^+, (c) product ion = SF_3^+ 136
101. Partial ionic photofragmentation cross sections for SF_6; (a) product ion = SF_2^+, (b) product ion = SF^+, (c) product ion = S^+ 137
102. Partial ionic photofragmentation cross sections for SF_6; (a) product ion = F^+, (b) product ion = SF_2^{2+}, (c) product ion = SF_3^{2+} 138
103. Partial ionic photofragmentation cross sections for SF_6; (a) product ion = SF_4^{2+}, (b) product ion = SF^{2+}, (c) product ion = S^{2+} 139
104. Total photoabsorption cross section for Cl_2..... 141
105. Partial photoionization cross sections for Cl_2; (a) final ionic state = $X\,^2\Pi_g$, (b) final ionic state = $A\,^2\Pi_u$, (c) final ionic state = $B\,^2\Sigma_g$ 142
106. Photoelectron asymmetry parameters for Cl_2; (a) final ionic state = $X\,^2\Pi_g$, (b) final ionic state = $A\,^2\Pi_u$, (c) final ionic state = $B\,^2\Sigma_g$ 143
107. Partial ionic photofragmentation cross secions for Cl_2; (a) product ion = Cl_2^+, (b) product ion = Cl^+, (c) product ion = Cl_2^{2+} 144
108. Partial photoionization cross sections for CCl_4; (a) final ionic state = $X\,^2T_1$, (b) final ionic state = $A\,^2T_2$, (c) final ionic state = $B\,^2E$..... 146
109. Photoelectron asymmetry parameters for CCl_4; (a) final ionic state = $X\,^2T_1$, (b) final ionic state = $A\,^2T_2$, (c) final ionic state = $B\,^2E$..... 147
110. Partial photoionization cross sections for CCl_4; (a) final ionic state = $C\,^2T_2$, (b) final ionic state = $D\,^2A_1$ 148
111. Photoelectron asymmetry parameters for CCl_4; (a) final ionic state = $C\,^2T_2$, (b) final ionic state = $D\,^2A_1$ 149

Glossary

σ_{abs}^{T} = total photoabsorption cross section
σ_{ion}^{T} = total photoionization cross section
Γ = total photoionization efficiency or quantum yield
σ_{ion}^{j} = partial photoionization cross section for production of a singly (or multiply) charged molecular ion in the electronic state j
BR^{j} = photoelectron branching ratio for production of a singly (or multiply) charged molecular ion in the electronic state j
β^{j} = photoelectron asymmetry parameter or angular anisotropy factor for production of the singly charged molecular ion in the electronic state j
σ_{ion}^{frag} = partial ionic photofragmentation cross section for production of a singly (or multiply) charged parent or fragment ion, including those resulting from ion pairs
BR^{frag} = ionic photofragmentation branching ratio for production of a singly (or multiply) charged parent or fragment ion, including those resulting from ion pairs
$\frac{df}{dE}$ = differential optical oscillator strength
$h\nu$ = incident photon energy
E = electron energy loss

1. Introduction

Molecular photoionization processes are of fundamental importance[1–23] and find application in a large number of scientific contexts, including studies in aeronomy,[24] astrophysics,[25] planetary sciences,[26] and radiation chemistry, physics, and biology.[27] Workers in these disciplines require reliable absolute cross sections for total photoabsorption, photoionization, partial photoionization, and for fragmentation processes over wide spectral ranges, particularly for use in modeling studies.[27–30] In addition, experimental total and partial cross sections are required for critical evaluation of theoretical and computational approximations to molecular photoionization processes.

Although continuing progress has been made in experimental studies of molecular total photoabsorption and total photoionization cross sections in the vacuum ultraviolet (VUV) and soft x-ray regions since the early 1950s,[31–44] quantitatively reliable absolute partial photoionization and ionic photofragmentation cross sections have been obtained only comparatively recently.[45–58] Theoretical calculations of partial photoionization cross sections at reliable levels of approximation have also appeared comparatively recently, in accordance with the development of refined computational techniques and the increasing availability of large high-speed digital computers.[59–71] In view of growing interest in molecular photoionization processes, particularly in the partial channels contributing to the overall photoabsorption, a compilation of partial cross-sectional data obtained largely in the last decade, in comparison with selected *ab initio* and model potential (X-alpha) calculations, is both timely and desirable.

The processes of primary interest here are one-photon, single ionization and subsequent fragmentation events. One-photon, multiple ionization may also be important, and in such cases these processes should be taken into account in the analysis and interpretation of experimental data. A detailed discussion of the complications that arise in measurements of single ionization in the presence of multiple ionization is given in Sec. 2. The one-photon, single ionization and subsequent fragmentation events can be written for a prototype molecule AB in the forms

$$AB + h\nu \rightarrow [AB^{+}]^{j} + e^{-}, \quad (1.1)$$

$$[AB^{+}]^{j} \rightarrow AB^{+} \text{ and/or } A + B^{+}. \quad (1.2)$$

Here, $h\nu$ is the incident photon energy, AB is a target molecule in the ground vibronic state with an essentially degenerate ensemble of rotational states, $[AB^{+}]^{j}$ is a molecular ion in the electronic excited state j, and e^{-} is the ejected electron carrying off kinetic energy. Because τ_e, the time scale for the electron photoejection process of Eq. (1.1), is generally much shorter ($\tau_e \sim 10^{-17}$ s) than τ_m, the time scale of the molecular ionic relaxation process ($\tau_m \sim 10^{-13}$ s) of Eq. (1.2),[51,72] the ion $[AB^{+}]^{j}$ is characterized experimentally by measurements of the ejected electron kinetic energy (i.e., binding energy) using photoelectron spectroscopy (PES) or the equivalent technique of dipole (e,2e) spectroscopy.[45–50] These generally reveal, at sufficiently high resolution, a series of well-defined vibrational structures associated with stable molecular ions or metastable predissociating ions, as well as vibrational continua associated with direct ionic fragmentation processes, for each accessible electronic ionic state. Figure 1 depicts the binding energy spectrum for the water molecule at electronic resolution.[73] The four groups of electrons shown are associated with production of the four lowest electronic states of H_2O^{+}, which correspond essentially to removal of electrons from the four outer molecular orbitals in H_2O.[74] The subsequent relaxation and fragmentation of these ionic states $[H_2O^{+}]^{j}$ [i.e., Eq. (1.2)] is studied by photoionization mass spectrometry (PIMS) or the equivalent technique of dipole (e,e + ion) coincidence spectroscopy. In Fig. 2 is shown a photoionization mass spectrum indicating the ions produced in the case of the water molecule.[73] However, coincidence measurements can establish the contribution of each state to each ionic fragment.

It is helpful in clarifying the aims and objectives of the present compilation to distinguish among three regions of valence-shell molecular photoprocesses: (i) The discrete absorption region, extending from the lowest electronic excitation energy to the lowest or first ionization potential. (ii) The "structured" ionization region extending from the first ionization potential to ~20 eV. In this region the ionization efficiency varies and is less than unity. Few accurate efficiency measurements have been made in this region. (iii) The smooth cross-sectional region extending above ~20 eV to several hundred eV, where inner-shell processes start to

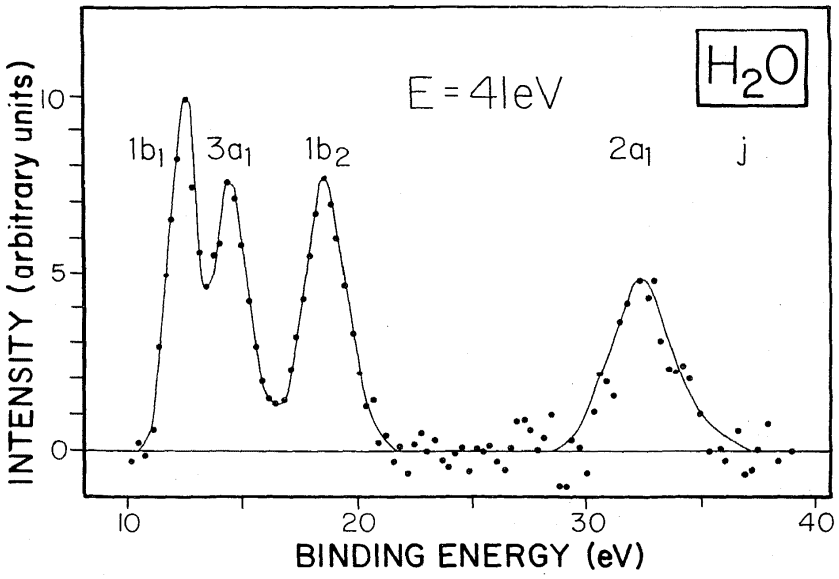

FIG. 1. Photoelectron kinetic energy spectrum for the water molecule at an incident photon energy of $h\nu = 41$ eV (Ref. 73). When suitably corrected for instrument function effects, the areas under the various peaks give branching ratios for production of the final ionic states to electronic resolution. Absolute partial cross sections are obtained by multiplication of the branching ratios with the total photoionization cross section.

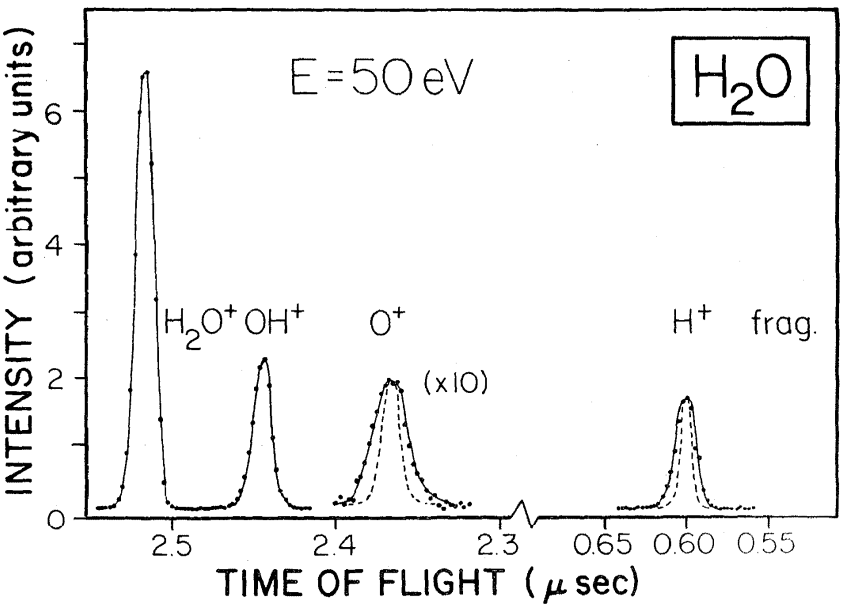

FIG. 2. Parent- and fragment-ion spectrum obtained from dipole $(e,e + \text{ion})$ electron-ion coincidence study of water molecules (Ref. 73). The areas under the peaks provide branching ratios for production of the indicated ions at 50-eV incident photon energy. Absolute parent- and fragment-ion partial photoionization cross sections are obtained by multiplication of the branching ratios with the total photoionization cross section. The dashed curves represent the width expected for fragment ions with thermal energy.

contribute.[75,76] The discrete absorption region (i) is not considered explicitly here. Reliable cross sections are still difficult to obtain in this spectral interval, due to the effects of finite instrumental resolution and the small intrinsic linewidths associated with rotational structure.[39] The structured region (ii) is of considerable interest in the present context, but it is premature to attempt a compilation of absolute cross-sectional data for this spectral region. The many important spectroscopic studies which have been made or are in progress in this interval include photoelectron spectroscopy to vibrational or even rotational resolution,[77] high-resolution fluorescence yield measurements,[78] high-resolution relative photoabsorption and photoionization with mass analysis measurements,[79] ion fluorescence depolarization studies,[80] threshold photoelectron spectroscopy,[81] and multiphoton ionization spectroscopy.[82] On the basis of these results, it is anticipated that a significant body of quantitatively reliable vibrationally resolved, partial cross sections will be available within a few years. In the smooth continuum region (iii), total photoabsorption and partial photoionization cross sections have been measured during the past several years using spectrometers with differing energy resolutions. The cross sections obtained from the different experiments compare favorably in almost all cases[45–58] and should therefore be largely independent of any future improvements in energy resolution. *It is this region to which the present compilation of total photoabsorption, partial-channel photoionization, and ionic photofragmentation cross sections for all valence-shell processes is directed.* Specifically excluded from the present article are inner-shell processes,[75,76] which constitute a topic suitable for a separate review.

The present report should be regarded as a logical continuation of earlier compilations and complementary to other more recent reviews. Early absolute photoabsorption and total photoionization cross sections in the visible and near-ultraviolet (UV) regions, and related aspects of photoelectron spectroscopy, have been reviewed previously from various perspectives,[1–23] and helpful bibliographies for these earlier data are available.[31–44] The comprehensive monograph of Berkowitz,[23] in particular, provides a detailed account of molecular photoionization and related studies up to 1978. Descriptions of experimental techniques for studying photoionization employing various optical sources[45–47,50,51,55,57,58] and the equivalent pseudophotons provided by electron-impact ionization and coincidence methods[48,49,52–54,56] are available. Photoabsorption and partial photoionization cross sections, as well as branching ratios, obtained from dipole (e,e), $(e,2e)$, and $(e,e+\text{ion})$ spectroscopy measurements up to approximately 1982 have been reported in cumulative tabulations.[53,54]

2. Definitions and Nomenclature

Definitions of the partial cross sections σ_{ion}^{j}, $\sigma_{\text{ion}}^{\text{frag}}$, and of the related branching ratios BR^{j}, BR^{frag}, both experimentally and theoretically, as well as of σ_{abs}^{T}, Γ, σ_{ion}^{T}, and of the anisotropy factors β^{j}, are given in this section. The effects of multiple ionization and pair production on measured values are discussed. All cross sections and related quantities are functions of the photon energy $h\nu$, although this dependence is generally not indicated explicitly in the following.

In providing the appropriate definitions, it is helpful to consider the three valence-shell photoprocesses that are relevant in the vacuum ultraviolet and soft x-ray intervals of interest here. These are the following.

(1) Excitation by photoabsorption into stable and/or dissociative neutral states (excluding ion-pair processes)

$$h\nu + \text{AB} \rightarrow \text{AB}^{*} \text{ and/or } \text{A} + \text{B}^{*}. \tag{2.1}$$

(2) Elastic and/or inelastic photon scattering:

$$h\nu + \text{AB} \rightarrow h\nu + \text{AB} \text{ and/or } h\nu' + \text{AB}^{*}. \tag{2.2}$$

Contributions from such processes are usually negligible and are not considered further in the present work.

(3) Photoionization as observed by either

(a) PES ($\tau_e \sim 10^{-17}$ s)

$$h\nu + \text{AB} \rightarrow [\text{AB}^{n+}]^{j} + ne^{-}, \tag{2.3}$$

where $[\text{AB}^{n+}]^{j}$ is a singly or multiply charged ion ($n \geqslant 1$) in state (j) which may be stable or unstable with respect to subsequent dissociation, or

(b) PIMS ($\tau_m \gtrsim 10^{-13}$ s)

$$h\nu + \text{AB} \rightarrow [\text{AB}^{n+}]^{j} + ne^{-} \begin{cases} \rightarrow \text{AB}^{n+} & (2.4) \\ \rightarrow \text{A}^{p+} + \text{B}^{q+} & (2.5) \\ \rightarrow \text{A}^{+} + \text{B}^{-}, & (2.6) \end{cases}$$

where Eq. (2.4) refers to production of singly or multiply charged stable parent ions of charge $n \geqslant 1$; Eq. (2.5) refers to production of fragment ions of charge p^{+} and q^{+}, where $p+q=n \geqslant 1$ and either p or q may be zero, and Eq. (2.6) refers to ion-pair production ($n=0$). All three processes [i.e., those defined by Eqs. (2.4)–(2.6)] are included in the general description "ionic photofragmentation" and are designated by the label "frag" in the symbols and equations used in the present work.

The total photoabsorption cross section (σ_{abs}^{T}) encompassing the above three groups of processes (1–3) may be written as

$$\sigma_{\text{abs}}^{T} = \sigma_{n} + \sigma_{\text{ion}}^{T}, \tag{2.7}$$

where σ_n is the cross section for neutral processes (1) and σ_{ion}^{T} is the total photoionization cross section (3). The latter quantity is defined by the relation[50]

$$\sigma_{\text{ion}}^{T} = \Gamma \sigma_{\text{abs}}^{T}, \tag{2.8}$$

where Γ is the total photoionization efficiency or quantum yield given by

$$\Gamma = \frac{\text{Number of ionizing events/s}}{\text{Number of photons absorbed/s}}. \tag{2.9}$$

The presence of distinct electronic and fragmentation time scales associated with Eqs. (2.3) and (2.4)–(2.6), respectively, and of the two classes of corresponding experiments (PES and PIMS) provides two distinct definitions of the term "ionizing events" appearing in the numerator of Eq. (2.9). Since PES measurements [Eq. (2.3)] cannot detect the ion-pair production events [Eq. (2.6)], the photoionization efficiency obtained is generally less than that obtained

from PIMS measurements which can be made to detect all the ionizing events required in Eq. (2.9); i.e., $\Gamma^{\rm PES} \leqslant \Gamma^{\rm PIMS} \equiv \Gamma$. For practical purposes this difference is usually of little importance, since the generally small pair-production cross section σ_{pp} is concentrated in a relatively narrow spectral band at low photon energy. Nevertheless, both ionization efficiencies are useful, as is clarified below.

A. Photoelectron spectroscopy

Following Eq. (2.9), the photoionization efficiency in this case may be written as

$$\Gamma^{\rm PES} = \frac{(N_1 + N_2/2 + N_3/3 + \cdots)}{\text{Number of photons absorbed/s}}, \qquad (2.10)$$

where $N_1, N_2, \ldots$ are the number of electrons produced/s by all single-, double-,... ionization events on the short time scale before any subsequent ionic photofragmentation. With this definition $\Gamma^{\rm PES} \leqslant 1$. The quantities $N_1, N_2, \ldots$ are generally not determined directly, but rather measurements are made of BR^j, the photoelectron branching ratio for production of a singly or multiply charged molecular ion $[\mathrm{AB}^{n+}]^j$ in the electronic state j, where

$$\mathrm{BR}^j = \frac{N^j/n}{(N_1 + N_2/2 + \cdots)}. \qquad (2.11)$$

Here, N^j is the number of photoelectrons produced/s from formation of these ions. With this definition $\sigma^j_{\rm ion}$, the partial photoionization cross section for production of a singly or multiply charged molecular ion in the electronic state j, is given by

$$\sigma^j_{\rm ion} = \mathrm{BR}^j \Gamma^{\rm PES} \sigma^T_{\rm abs}. \qquad (2.12)$$

Comparison of Eqs. (2.10) and (2.11) indicates $\Gamma^{\rm PES}$ is the correct photoionization efficiency to employ in determining $\sigma^j_{\rm ion}$.

In practice, it is experimentally difficult to disentangle the electron groups $N_1, N_2, \ldots$ associated with the separate photoionization processes of Eq. (2.3). Usually, double and higher ionization states ($[\mathrm{AB}^{n+}]^j, n > 1$) are not directly observed in conventional PES experiments because of the energy sharing by the two or more ejected electrons, resulting in a low intensity background upon which the largely discrete single-ionization spectrum is superimposed. Consequently, multiple ionization branching ratios are not measured, and the contribution of multiple ionization is not properly taken into account in obtaining one-electron BR^j values unless the weak continuous background kinetic energy spectrum of electrons associated with this process is explicitly subtracted from the measured signal.[47,50] Multiple ionization is usually small in the valence-shell spectral intervals of interest here,[19] and thus corrections are small in any event. In the absence of measured $\Gamma^{\rm PES}$ values, $\Gamma^{\rm PIMS}$ is usually employed in Eq. (2.12).

Closely related to each electronic partial photoionization cross section $\sigma^j_{\rm ion}$ is the corresponding photoelectron asymmetry parameter or angular anisotropy factor β^j. In the case of the single-ionization processes of central interest here, the two quantities together provide the one-electron electronic partial photoionization cross-section differential in ejection angle for unoriented molecular targets in the form[50]

$$d\sigma^j_{\rm ion}(\theta) = (\sigma^j_{\rm ion}/4\pi)[1 + \beta^j P_2(\cos\theta)]\, d\Omega, \qquad (2.13)$$

where $P_2(\cos\theta)$ is the second-degree Legendre polynomial and θ is the angle between the incident photon (linear) polarization direction and the mometum vector of the outgoing electron. Equation (2.13) rests on the familiar dipole approximation, which should hold well in the photon energy region of interest here.

B. Photoionization mass spectrometry

Following Eq. (2.9), the PIMS total photoionization efficiency may be written as

$$\Gamma^{\rm PIMS} = \frac{(\mathcal{N}_1 + \mathcal{N}_2 + \cdots \mathcal{N}_{pp})}{\text{Number of photons absorbed/s}}, \qquad (2.14)$$

where $\mathcal{N}_1$ and $\mathcal{N}_2, \ldots$ are the numbers of singly, doubly,... charged ions initially produced/s before any subsequent ionic photofragmentation occurs, and $\mathcal{N}_{pp}$ is the number of ion-pair events/s. With this definition $\Gamma^{\rm PIMS} (\equiv \Gamma) \leqslant 1$, and with the exception of the spectral interval where ion-pair production is non-negligible,

$$\Gamma^{\rm PES} \cong \Gamma^{\rm PIMS} = \Gamma. \qquad (2.15)$$

Although the definition of $\Gamma^{\rm PIMS}$ involves only the processes of Eqs. (2.3) and (2.6), any practical measurement also includes the processes of Eqs. (2.4) and (2.5). However, the correct values of $\Gamma^{\rm PIMS}$ are obtained directly from time-of-flight (TOF) mass spectrometer signals. This is because fragments produced upon dissociation of multiply charged molecular ions [Eq. (2.5)], which might be thought to give rise to multiple ionization events for a single absorbed photon, are counted collectively as a single event (that is, only the fastest fragment is detected), provided the detector efficiency is 100% for ions of all degrees of ionization.

The frequently employed ionic photofragmentation branching ratio $\mathrm{BR}^{\rm frag}$ for production of a singly or multiply charged parent or fragment ion of a particular type, including those from ions pairs, can be written as

$$\mathrm{BR}^{\rm frag} = \frac{N^{\rm frag}}{(\mathcal{N}_1 + \mathcal{N}_2 + \cdots \mathcal{N}_{pp})}, \qquad (2.16)$$

where $N^{\rm frag}$ is the number of ions/s of type "frag" actually observed. As indicated above, for PIMS-type measurements utilizing conventional TOF mass spectrometers the denominator of Eq. (2.16), is actually measured directly. Consequently,

$$\mathrm{BR}^{\rm frag} = \frac{N^{\rm frag}}{\Sigma_{\rm frag} N^{\rm frag}}. \qquad (2.17)$$

With this definition, $\sigma^{\rm frag}_{\rm ion}$, the partial photoionization cross section for production of an ion of any type "frag," is given by

$$\sigma^{\rm frag}_{\rm ion} = \mathrm{BR}^{\rm frag} \Gamma^{\rm PIMS} \sigma^T_{\rm abs}. \qquad (2.18)$$

Time-of-flight mass spectrometers as currently employed do not provide for measurement of cross sections for all possible fragmentation processes referred to in Eq. (2.18). Specifically, since only the fastest singly charged ionic fragment from a dissociating doubly charged molecular ion is observed, such cross sections are not commonly measured. Although their contributions are generally small for the va-

lence-shell photoionization processes of interest here, cross sections for dissociating multiply charged ions can be detected in suitably modified PIMS measurements, as is discussed in Sec. 3 below.

To summarize the foregoing partial cross-section expressions for both PES and PIMS measurements, emphasizing the small (usually negligible) differences inherent in the two ionization efficiencies employed:

$$\sigma_{\text{ion}}^{j} = \text{BR}^{j}\Gamma^{\text{PES}}\sigma_{\text{abs}}^{T} \cong \text{BR}^{j}\Gamma\sigma_{\text{abs}}^{T} \cong \text{BR}^{j}\sigma_{\text{ion}}^{T}, \quad (2.19)$$

and

$$\sigma_{\text{ion}}^{\text{frag}} = \text{BR}^{\text{frag}}\Gamma^{\text{PIMS}}\sigma_{\text{abs}}^{T} = \text{BR}^{\text{frag}}\Gamma\sigma_{\text{abs}}^{T} = \text{BR}^{\text{frag}}\sigma_{\text{ion}}^{T}. \quad (2.20)$$

From Eqs. (2.19) and (2.20), two alternative partitionings of the total photoionization cross section can be written in the forms,

$$\sigma_{\text{ion}}^{T} = \Sigma_{\text{frag}}\sigma_{\text{ion}}^{\text{frag}} \cong \Sigma_{j}\sigma_{\text{ion}}^{j}. \quad (2.21)$$

Cross sections σ are generally expressed in units of cm^2 or in megabarns ($1\ \text{Mb} = 10^{-18}\ \text{cm}^2$), and are related to the differential optical oscillator strength df/dE, where $E = h\nu$, by the expression[83]

$$\sigma[\text{Mb}] = \left(\frac{\pi e^2 h}{mc}\right)\frac{df}{dE}[\text{eV}^{-1}] = 109.75\,\frac{df}{dE}[\text{eV}^{-1}], \quad (2.22)$$

where the symbols in the factor $(\pi e^2 h/mc)$ have their usual meanings.

3. Experimental Methods

In this section, accounts are given of photon and electron-impact dipole-simulation techniques for measurements of the total photoabsorption, electronic partial photoionization, and ionic photofragmentation cross sections of unoriented molecules. Although the present description is largely self-contained, only essential features of the apparatus employed and measurement procedures are presented. More detailed descriptions have been reported previously elsewhere.[45–52]

The early measurements of partial photoionization cross sections as functions of photon energy utilized capillary discharge lamps and line sources[84] and predate the more widespread use in the mid 1970s of monochromated synchrotron-radiation sources and appropriately calibrated electron energy analyzers for photoabsorption and photoionization experiments. A significant parallel development during the past 15 yr employing dipole electron-molecule inelastic scattering techniques has provided quantitative simulations of conventional photoabsorption and photoionization experiments at continuously tunable energies corresponding to the UV and soft x-ray regions. These simulation techniques, aptly called the "poor-man's synchrotron," have provided a large body of data for comparison with photon measurements of absolute cross sections.[48] The present compilation reports results from both photon and dipole electron-molecule scattering experiments. In cases where parallel experiments have been done, there is a high degree of agreement between the results obtained by the two different methods. Table 1 indicates the photon and equivalent electron-impact experiments employed in measuring total and partial photoionization cross sections.

3.1. Photon Measurements

Aspects of the photon experiments listed in Table 1 are discussed briefly in this subsection.

3.1.a. Total Photoabsorption and Photoionization Cross Sections

Determinations of accurate absolute cross sections for partial photoionization processes require first measurement, as a function of energy, of the total absorption cross section σ_{abs}^{T} appearing in the familiar Lambert–Beer law,[47,50]

Table 1. Photon and Electron-Impact Experiments

Photon Experiment	Quantity Measured	Equivalent Electron-Impact Experiment
Total Photoabsorption	σ_{abs}^{T}	Electron-energy-loss spectroscopy, dipole (e,e)
Total Photoionization	σ_{ion}^{T}	Dipole (e,2e) or (e,e+ion) (from sums of partials)
Photoelectron spectroscopy	σ_{ion}^{j}, β^{j}	Electron energy loss — ejected electron coincidence, dipole (e,2e)
Photoionization mass spectrometry	$\sigma_{\text{ion}}^{\text{frag}}$	Electron-ion coincidence, dipole (e,e+ion)

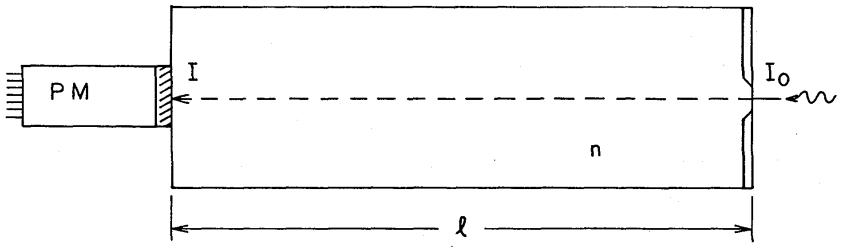

FIG. 3. Simple photoabsorption cell, where measurements must be made at different times of the incident light intensity with and without gas in the cell. Here, I_0 and I are, respectively, the incident and transmitted light intensity, n is the gas number density, l is the length of the cell, and PM is a photomultiplier (Refs. 47 and 50).

$$I = I_0 \exp(-\sigma^T_{\text{abs}} nl). \tag{3.1}$$

Here, n is the number density of the gas sample, and I_0 and I are, respectively, the intensities of the radiation of energy $h\nu$ incident on and transmitted a distant l through the absorbing gas. In addition, the total photoionization efficiency Γ or, equivalently, the total photoionization cross section σ^T_{ion} must be determined in order to make use of the partial-channel expressions of Eqs. (2.19) and (2.20). The total photoabsorption cross section is determined using Eq. (3.1) rewritten in the form

$$\sigma^T_{\text{abs}} = (1/nl)\ln(I_0/I), \tag{3.2}$$

which requires measurement of the ratio of light incident upon a sample to that transmitted by the sample, the path length l, and the number density n. Several techniques have been developed for this purpose.[47,50]

3.1.a.1. Simple Cell

An approach that has been used quite extensively in total photoabsorption measurements is depicted in Fig. 3.[50] It consists of a simple absorption cell of length l with an entrance window or narrow slit facing the incident radiation. The end of the cell is defined by an exit window coated with sodium salicylate followed by a photomultiplier (PM). The signal of intensity I_0 entering the empty cell is first recorded as a function of incident photon energy. The cell is then filled with a gas of number density n and the PM reading taken again to record the intensity I transmitted through the length l of the gas. The total cross section is then given by Eq. (3.2). The accuracy of this method depends upon, among other things, the light source intensity remaining constant during the course of the measurement. Unfortunately, few sources remain stable and reproducible to $\pm 1\%$ over suitable time periods. This is particularly true for synchrotron radiation from a storage ring, because the intensity of the radiation decreases naturally with time. Thus, techniques that measure I_0 and I simultaneously are generally preferred when a synchrotron source is employed.

3.1.a.2. Split Beam

In the split-beam method depicted in Fig. 4, a portion of the incident radiation strikes a mesh coated with sodium salicylate. The fluorescent radiation produced by the mesh is observed with a photomultiplier, the remainder of the incident beam being transmitted through the sample to another PM tube at the end of the absorption cell. Signals from the two PM tubes are balanced when there is no gas in the cell, so that the intensity of light transmitted through the cell in the

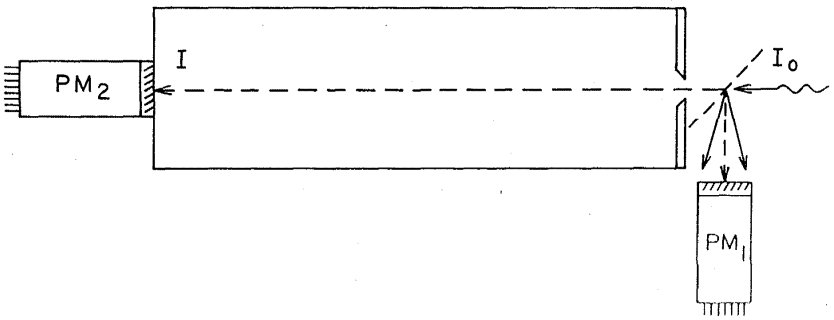

FIG. 4. Split-beam absorption cell utilizing a mesh coated with sodium salicylate or a mirror intercepting a fraction of the incident radiation at the entrance to the absorption cell to allow for the effects of incident intensity variation (Refs. 47 and 50). The arrangement is otherwise as in Fig. 3.

presence of absorption can be effectively corrected for variation in incident intensity.[50]

3.1.a.3. Double-Ion Chamber

A double-ionization chamber can provide simultaneous measurements of both the total absorption cross section σ^T_{abs} and the total positive-charge production efficiency, Γ', defined as[47]

$$\Gamma' = \frac{\text{Number of positive charges produced/s}}{\text{Number of photons absorbed/s}}. \quad (3.3)$$

Briefly, the apparatus depicted in Fig. 5 consists of a cylindrical absorption cell maintained at a positive potential with respect to two ion collector plates of equal lengths L. The symmetry of the design assures that the ions produced in two regions of the cell will be collected by the appropriate collector plate. Under these conditions the absolute cross section is given by[50]

$$\sigma^T_{abs} = (1/nL)\ln(i_1/i_2), \quad (3.4)$$

where i_1 and i_2 are the measured electrode currents. To determine Γ', we note that the numerator in Eq. (3.3) is given by the measured current $i_1 + i_2$ and the denominator by the difference between incident (I_0) and transmitted (I) light intensity. The latter is obtained from I_0 and the total absorption cross section using the Lambert–Beer law [Eq. (3.1)]. This provides an expression for Γ' in the form

$$\Gamma' = (i_1^2/e)/(i_1 - i_2)I_0, \quad (3.5)$$

where e is the magnitude of the electronic charge. Generally, a rare gas or other sample for which σ^T_{abs} and Γ' are well known is used to determine I_0.

Although Γ' as defined in Eq. (3.3) generally differs from Γ of Eq. (2.9), the two quantities can be related under appropriate conditions. Letting γ_1, γ_2,... denote the ionization efficiencies for one-, two-,... electron ionization, and γ_{pp} that for pair production, we have

$$\Gamma' = \gamma_1\left(1 + \frac{2\gamma_2}{\gamma_1} + \frac{3\gamma_3}{\gamma_1} + \cdots + \frac{\gamma_{pp}}{\gamma_1}\right), \quad (3.6)$$

and

$$\Gamma = \gamma_1\left(1 + \frac{\gamma_2}{\gamma_1} + \frac{\gamma_3}{\gamma_1} + \cdots + \frac{\gamma_{pp}}{\gamma_1}\right). \quad (3.7)$$

For photon energies below the double-ionization threshold $\Gamma' = \Gamma$, and the double-ion chamber technique allows Γ ($= \gamma_1$) to be determined absolutely in this energy range. For photon energies above the double-ionization threshold but below the triple-ionization threshold, the absolute value of γ_2 can be determined from mass spectrometer measurements of double-ionization events, although care must be taken to include any contribution from dissociative multiple ionization. Such complications are generally disregarded in molecular photoionization studies, the common practice being to set $\Gamma \cong \Gamma' \cong \gamma_1 \cong 1$ for sufficiently high photon energies. This approximation may not be warranted in all cases although corrections are generally small for valence-shell photoionization processes.

Errors in total absorption cross sections and ionization efficiencies arise primarily from measurement of the ratio I_0/I and of the number density of the gas. The errors in I_0/I, discussed previously in the literature,[50] should be limited to 1% or 2% in regions of continuous absorption. Larger errors can arise in highly structured spectral regions when the

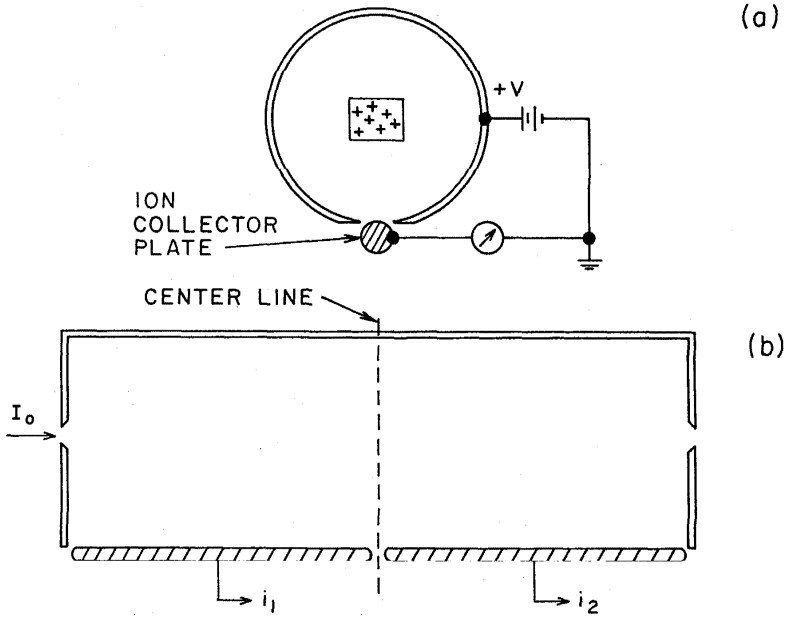

FIG. 5. Double-ion chamber; (a) cylindrical cross section and (b) side view. The ion currents i_1 and i_2 are collected, respectively, on two rods of equal lengths L located symmetrically about the center line of the ion chamber.

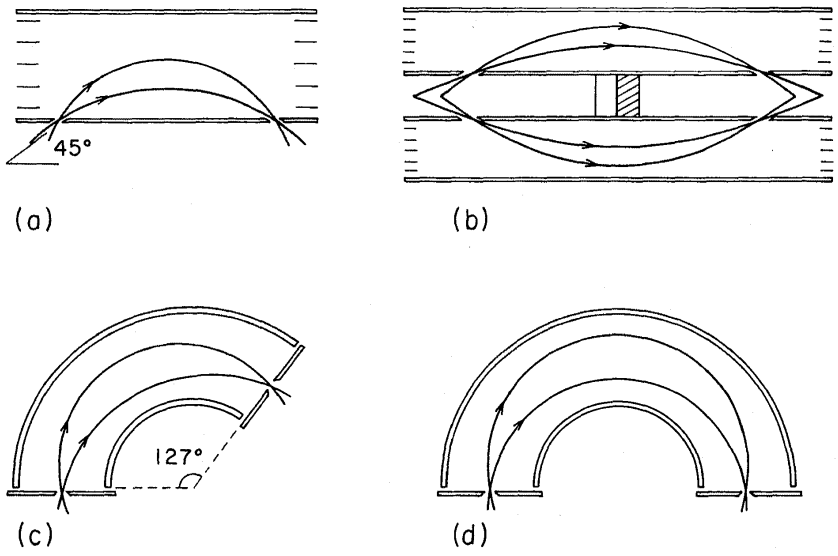

FIG. 6. Types of electron kinetic energy analyzers currently employed in photoelectron spectroscopy studies; (a) parallel plate, (b) cylindrical mirror, (c) 127° cylindrical, (d) 180° spherical.

bandwidth of the incident radiation is large relative to intrinsic widths. This particular difficulty has also been discussed extensively and is largely one of sensible data analysis.[39] Specifically, the defining cross-sectional expression [Eq. (3.1)] is generally inappropriate for analysis of data obtained in the presence of narrow spectral features. However, when the intrinsic spectral widths (corresponding to rotational structure, for example) are very narrow compared to the incident radiation bandwidths, and a very small stepping interval is used in the spectral scan, Eq. (3.1) is once again valid.[85] Great care must also be taken in measuring the pressure of the absorbing gas to obtain the number density. Many of the earlier absorption measurements used mercury McLeod gauges to measure pressures, giving rise to systematic errors caused by streaming effects of mercury atoms flowing towards a cold trap.[86] These difficulties have been overcome through use of capacitance-type manometers. However, errors of a few percent still can occur if temperature transpiration effects in the capacitance manometer are not considered.[87]

3.1.b. Partial Photoionization Cross Sections

PES and PIMS techniques are generally used to measure partial cross sections for production of ions in specific electronic states, and for production of parent or specific fragment ions, respectively. Other techniques, such as fluorescence excitation spectroscopy (FES), have also been used for these purposes, particularly in studies of structured spectral regions.[51] However, the fluorescence technique is not always useful in providing absolute partial cross sections, because of the possibility of cascading from higher excited states and the internal rearrangements that can take place. Consequently, this approach is not discussed further in the present compilation.

3.1.b.1. Electronic Partial Cross Sections

Absolute electronic partial photoionization cross sections are obtained from measurement of electronic branching ratios (BR^j) defined in Sec. 2. Various types of electron energy analyzers and modes of operation have been devised for performing these measurements, largely focusing on one-electron photoionization processes. The geometry of such PES experiments is shown in Fig. 6, which depicts four typical electron energy analyzers. In each case, electrons in a small solid angle $d\Omega$ are accepted by the analyzer at an angle θ relative to the incident light. For measurements of the branching ratio of Eq. (2.11) for $n = 1$, it is convenient to employ the magic angle ($\theta = 54.7°$) arrangement for which $P_2(\cos\theta) = 0$. In this case the number of electrons dN^j detected is proportional to σ^j_{ion} but independent of β^j [Eq. (2.13)], so the total numbers N^j in Eq. (2.11) that refer to integration over all solid angles can be replaced by those accepted in the solid angle $d\Omega$. Once the partial cross section σ^j_{ion} is determined from Eq. (2.12), the anisotropy factor β^j is obtained from measurement of the angular distribution of ejected electrons [Eq. (2.13)]. This is generally accomplished by either rotating the analyzer in a plane containing the incident light beam or in a plane at right angles to it. Alternatively, the analyzer can be fixed and the polarization of the light can be rotated if a polarizer is employed.

Photoelectron measurements must employ a suitably calibrated analyzer since the collecting efficiency of the apparatus is generally dependent on electron kinetic energy. Furthermore, as indicated above, photoelectron measurements are complicated by multiple ionization events, which produce a weak continuous background kinetic energy spectrum of electrons that must be subtracted from the measured signal in order to obtain the correct one-electron cross sections. Additionally, complications also arise when the inci-

dent radiation is not 100% polarized. These aspects of the measurement procedures have been discussed in considerable detail elsewhere and are not repeated here.[47,50]

Constant-ionic-state (CIS) techniques, in which incident photon energy and ejected electron kinetic energy are simultaneously scanned, are increasingly employed in measurements of electronic partial cross sections without prior explicit determination of branching ratios from individual photoelectron spectra obtained at a series of photon energies.[45–50,88,89] Such CIS measurements can be normalized to the total photoabsorption using a single set of branching ratios obtained at an optimum (low) photon energy where multiple ionization cannot occur but where the ionization efficiency is unity.[88,89] Partial cross sections obtained in this manner will be correct even at the higher photon energies where other complicating effects occur. Although accurate CIS measurements are generally more difficult to carry out, the more specific data obtained generally merit the effort.

3.1.b.2. Parent- and Fragment-Ion Cross Sections

Photoionization mass spectrometry techniques are generally employed to measure cross sections for production of parent and specific fragment ions. The appropriate branching ratios and the corresponding partial cross sections are given by Eqs. (2.16)–(2.18). Ion-pair production and dissociation of multiply charged ions into singly ionized fragments complicates determination of the number N^{frag} of one-electron ions of a given type. Additionally, most mass spectrometers will discriminate against energetic fragments due to the different response of the detector to ions of different mass and energy, and to the propensity for fast ions to be disproportionately sampled, because they move rapidly out of the ion extraction region. Techniques for overcoming these difficulties have been described previously elsewhere.[47,50] It should be noted that accurate values of the total cross section for fragmentation are obtained directly from the difference between total photoionization cross section and that for parent ion production. The latter is, of course, not sensitive to the extraction difficulties associated with fragment ions.

3.2. Dipole Electron-Impact Measurements

In the past decade methods have been developed for the quantitative study of molecular photoabsorption and partial-channel photoionization cross sections utilizing the virtual photon field of forward-scattered fast electrons.[48,49,52–54,56,76,87,90] These techniques have provided quantitative simulations of conventional photoabsorption, PES, and PIMS measurements in the equivalent photon energy range of ~5–1000 eV and the cross sections so obtained are effectively equivalent to those determined by photon techniques. Table 1 gives the electron-impact equivalents to the primary photon measurements. The electron-impact methods use electron energy-loss spectroscopy to simulate the initial photoabsorption, and coincidence counting of electrons and/or ions to obtain partial and fragment photoionization cross sections. In these methods the electron energy loss E is continuously variable and is the analog of a variable-energy photon source ($E = h\nu$). To understand this analogy, it is helpful to compare the processes of impact excitation of a molecule AB by an incident electron with energy E_0 and the resonant absorption of a photon

$$e^-(E_0) + AB \rightarrow AB^* + e^-(E_0 - E), \tag{3.8}$$

$$h\nu + AB \rightarrow AB^*. \tag{3.9}$$

In both excitation cases the energy $E = h\nu$ is deposited in the target molecule AB. Similarly, for ionization either by electron impact or photon absorption

$$e^-(E_0) + AB \rightarrow [AB^+ + e_{ej}^-(E - IP)] + e_{\text{scatt}}^-(E_0 - E), \tag{3.10}$$

$$h\nu + AB \rightarrow [AB^+ + e_{ej}^-(h\nu - IP)], \tag{3.11}$$

where IP is the molecular ionization potential. In each case, the energy E is deposited in the target species M and the (photo)ejected electron e_{ej}^- will carry away the excess energy, $E - IP$. In the electron-impact induced reaction (3.10), the dipole $(e,2e)$ or dipole $(e,e+\text{ion})$ coincidence methods are needed to kinematically characterize the "photoelectron" or "photoionization" processes, respectively. The electron-impact equivalents of the three primary experiments, photoabsorption,[48,49,56,91–95] PES,[96–98] and PIMS,[99–101] are discussed and described briefly in the following subsections.

3.2.a. Total Absorption Cross Sections

It has long been known that dipole excitation or ionization of atoms and molecules can be effected by electron collisions at vanishingly small momentum transfer.[91] Under the appropriate inelastic scattering conditions (high impact energy and zero-degree mean scattering angle), transitions obeying dipole (optical) selection rules are selectively induced in the target species, but with relative intensities that differ (by a known target-independent factor) from those observed by direct interaction with photons. The quantitative relation that exists between differential electron scattering ($d\sigma/dE$) and photoabsorption cross sections is given through the Bethe–Born relationship[48,49,56,91–95]

$$\frac{d\sigma(K)}{dE} = \frac{2}{E}\frac{k_f}{k_i}\frac{1}{K^2}\frac{df(K)}{dE}, \tag{3.12}$$

where k_i, k_f, and K are the incident, scattered, and transferred momenta, respectively, E is the energy loss, and $df(K)/dE$ is the so-called generalized (momentum-transfer dependent) oscillator strength density. The latter can be expanded in a series of terms in which the first is the optical or dipole oscillator strength df/dE of Eq. (2.22), with higher terms involving even powers of the momentum transfer K;

$$\frac{df(K)}{dE} = \left(\frac{df}{dE}\right) + AK^2 + BK^4 + \cdots. \tag{3.13}$$

Consequently, in the limit of zero momentum transfer, the generalized oscillator strength approaches the optical oscillator strength, and this provides the basis for determinations of cross sections for photoabsorption and photoionization from inelastic electron scattering measurements. Under these conditions (i.e., $K \rightarrow 0$)

$$\left(\frac{df}{dE}\right) = \frac{mc}{\pi e^2 h}\sigma_{\text{abs}}^T = \frac{E}{2}\frac{k_i}{k_f}K^2\frac{d\sigma(K)}{dE}. \tag{3.14}$$

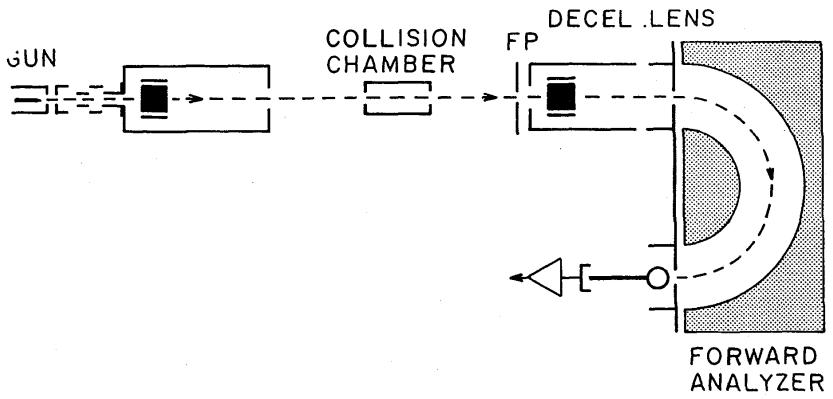

FIG. 7. Schematic of dipole (e,e) energy loss spectrometer used for studies of absolute photoabsorption (Ref. 97). FP is the focal plane.

This important relationship shows that not only are dipole transitions induced in the excitation and ionization of atomic and molecular targets by fast electrons, but that their absolute intensity can be obtained by kinematic conversion of the electron scattering cross section using the factor $E/2(k_i/k_f)K^2$.[48] (In practice this factor must be integrated over the experimental geometry.) The explicit extrapolation $K \to 0$ of Eq. (3.14) can be avoided by making direct measurement sufficiently close to the $(K = 0)$ optical limit. For valence-shell excitation or ionization this condition requires impact energies of at least 3 keV at a zero-degree scattering angle.

A schematic of a dipole (e,e) electron spectrometer suitable for total cross-section measurements is shown in Fig. 7. Its operation is described in detail elsewhere.[48,49,56] There are some unique features and also some limitations of the electron-impact simulation method of total photoabsorption measurement, however, which warrant additional discussion here.

It can be seen from Eq. (3.14) that the photoabsorption oscillator strength is related to the differential electron scattering cross section by the multiplicative factor $(E/2)(k_i/k_f)K^2$, which can be shown to be essentially proportional to E^3 (Refs. 48 and 56). That is, the optical photoabsorption cross section is derived from the forward electron scattering spectrum by multiplying with a kinematic factor of the order of E^3. (In practice, the exponent of E is approximately 2 due to the need for integration over the finite acceptance angle in the forward direction.[102]) Consequently, the electron scattering signal will fall off more rapidly with energy loss by a factor of $\sim E^3$ than does the photoabsorption cross section. Therefore, great care must be taken to exclude background due to stray electrons, particularly at higher values of E. This problem is analogous to that of stray light in optical spectrometers. Partial photoionization cross sections are similarly obtained by correcting the dipole $(e,2e)$ or $(e,e+\text{ion})$ coincident intensities by the same energy loss dependent factor. In the case of the coincidence photoionization experiments, the statistics result in an effective upper limit of the energy loss range ($\sim$1000 eV with present instrumentation). This limitation is much less severe in the case of the noncoincident dipole (e,e) experiment, where the signals are correspondingly much larger. All electron scattering work is done at sufficiently low pressures to avoid double scattering processes.

An advantage inherent in the electron-impact simulation method is that anomalous intensity effects due to finite linewidth cannot occur due to the nonresonant character of electron-impact excitation [Eq. (3.10)]. As a result, the entire oscillator strength is contained beneath the measured photoabsorption curve regardless of linewidth or energy resolution. By contrast, optical intensities, where excitation is of course resonant, can be very severely perturbed in those cases where natural linewidths are narrower in energy than the monochromator bandwidth. In the continuum, lower energy resolution is of little practical consequence except in areas of very sharp structure, but even in this case the electron-impact methods still give the correct contribution to the total cross section beneath the measured curve. In smooth continuum regions both high- and lower-resolution electron or photon experiments will give the same result for the cross section.

A further significant benefit in the dipole electron-impact experiment results from the flat virtual photon field induced in the target molecule by the passing fast electron.[48,56] The intensity of the pseudophotons produced is constant with energy loss E, and thus provides a flat virtual photon source which results in the correct relative spectral photoabsorption shape without measurement of exciting flux or target density (pressure). The absolute photoabsorption cross section can be determined directly without absolute measurements by making use of the Thomas–Reiche–Kuhn (TRK) sum rule relating the total photoabsorption oscillator strength integrated over all discrete and continuum states to the number of electrons in the target molecule.[48,56] To this end, the valence-shell electron energy loss spectrum is measured out to several hundred eV, with the small remaining intensity to higher energy being quite accu-

rately estimated (usually $\leqslant 5\%$) by extrapolation with the form $a\epsilon^{-b}$, where b typically has an effective value in the range 2–2.5.[48,56] Assuming shell separation, the total area is then normalized to the number of valence electrons plus a very small correction for Pauli excluded states (this usually involves a contribution of ~ 0.2 oscillator strength units).[56,103] By this means an absolute scale can be obtained with an accuracy of usually better than $\sim 5\%$. Alternatively, the Bethe–Born corrected energy loss spectrum may be normalized at a single energy loss or photon energy to a known optical absorption cross section.

3.2.b. Partial Photoionization Cross Sections

The absolute total photoabsorption cross section obtained as described above may be used in the derivation of absolute partial photoionization cross sections for electronic states of ions [dipole $(e,2e)$ method] or for molecular and dissociative photoionization [dipole $(e,e+\text{ion})$ method] from the respective coincidence measurements, Bethe–Born corrected in accordance with Eq. (3.14). Presently available dipole $(e,2e)$ and $(e,e+\text{ion})$ techniques are restricted to energy resolutions of 0.5–1.5 eV full width at half maximum (FWHM), due mainly to the thermal energy spread of the primary electron beam, precluding the observation of vibrational phenomena and closely spaced ionic states. It does, however, have the advantage of integrating over most or all of the Franck–Condon envelope, even in the constant-ionic-state mode described further below. The energy resolution limitations are less important in dipole $(e,e+\text{ion})$ spectroscopy. The resolution of existing dipole spectrometers could be improved by utilizing electron monochromators to give resolutions as good as 0.020 eV, since the incident electron beam flux required ($\sim 10^{-8}$ A) is well within the capabilities of presently available electron monochromation techniques.[76,90] The relative photoionization efficiency can be measured in both the dipole $(e,2e)$ and $(e,e+\text{ion})$ methods, as discussed further below.

Constant-ionic-state spectra can be measured for electronic states of ions by suitable tandem scanning of the incident electron energy loss and the ejected electron energy.[89] The (relative intensity) CIS scans may be put on an absolute photoionization cross-section scale by Eq. (3.14) and subsequent normalization to the already determined absolute total photoabsorption using a branching ratio (from a binding energy spectrum) at a suitable single energy E in the region where the ionization efficiency is unity. A similar procedure can also be used in the dipole $(e,e+\text{ion})$ spectrometer to obtain molecular and fragment-ion partial cross sections directly. In general, the CIS method should give more accurate results than the branching ratio method, since the normalization can usually be done at an energy high enough to ensure that the ionization efficiency is unity, but low enough to avoid the complications arising from multiple ionization and other many-body effects in inner-valence regions. In most studies the CIS and branching-ratio (PES) modes can both be used, with the comparison providing a consistency check on the results.[89]

3.2.b.1. Electronic Partial Cross Sections

The general procedure employed in this case is similar to that of photon methods as described above. In Fig. 8 is shown a schematic of the dipole $(e,2e)$ spectrometer presently in use. Electrons in the forward scattering direction undergoing an energy loss E are detected in coincidence with the ejected electrons. The magic-angle (54.7°) ejected-electron analyzer must be calibrated for transmission efficiency as a function of kinetic energy, and also for any variation in flight time.[96–98] Both factors can be accounted for in a single transmission function, $T(\epsilon)$, which can vary by at least an order of magnitude over a 10-eV range of electron kinetic energy ϵ. The greatest uncertainties in $T(\epsilon)$ occur at kinetic energies below 5 eV (i.e., near photoionization thresholds), and errors in $T(\epsilon)$ function are likely to be the main reasons for discrepancies between $(e,2e)$ and optical PES partial cross sections in the near threshold region. Because of the coincident nature of the measurements in dipole $(e,2e)$ bind-

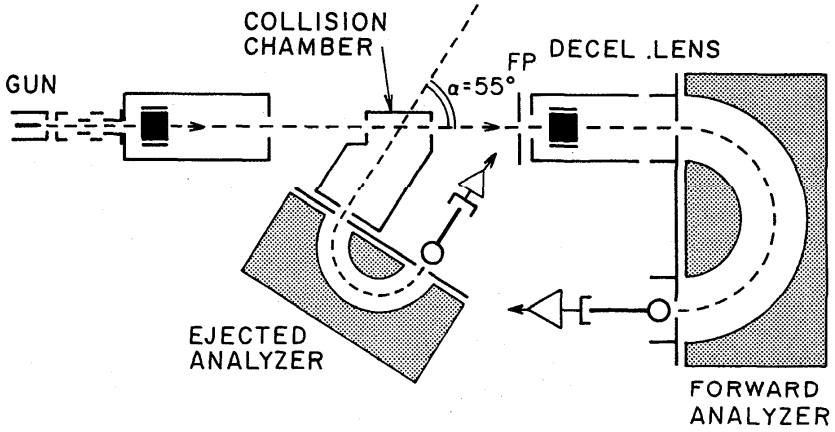

FIG. 8. Schematic of dipole $(e,2e)$ spectrometer used for measurement of absolute partial photoionization cross sections for production of ionic states (Ref. 97).

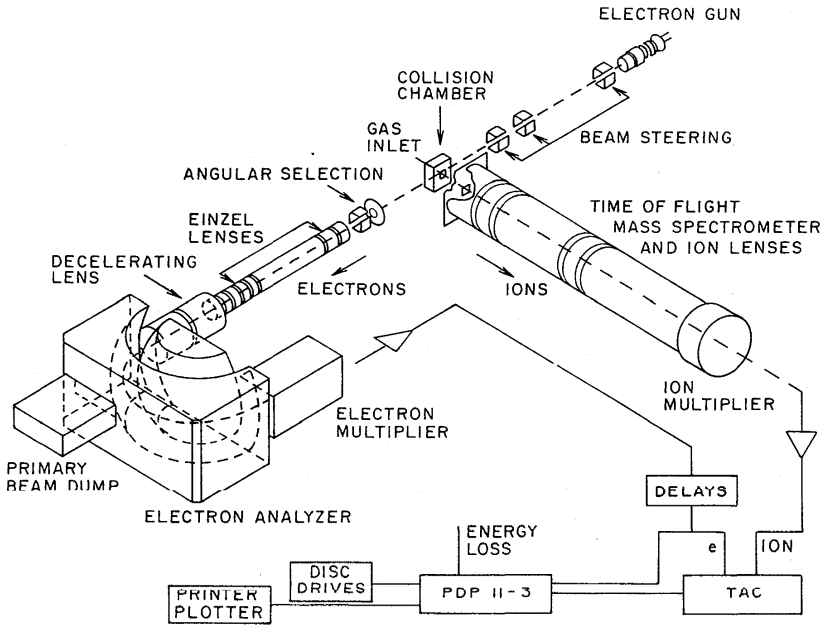

FIG. 9. Schematic of dipole (e,e + ion) spectrometer used for measurement of absolute photoionization cross section for molecular and dissociative ionization (Refs. 97–101).

ing-energy spectra, double or multiple ionization (molecular or dissociative) will result in detection of a single ejected electron which may appear at any kinetic energy due to energy sharing. In contrast, in optical PES, two or more electrons are detected as a continuum reflecting the energy sharing, and double ionization events are thus counted twice.

3.2.b.2. Parent- and Fragment-Ion Cross Sections

Parent- and fragment-ion cross-section measurements employing dipole electron-impact techniques follow generally the optical approach described above. In Fig. 9 is shown the (e,e + ion) spectrometer presently in use.[99,101] Time-of-flight mass-analyzed ions are detected in coincidence with forward-scattered, energy-loss-selected electrons. It is vital that all fragment ions be collected, regardless of the kinetic energy of fragmentation, if true absolute partial cross sections for dissociative ionization channels are to be measured employing any PIMS instrument. Most conventional mass spectrometers, which collect mainly thermal-energy ions, can therefore discriminate severely against fragment ions with kinetic energies greater than ~0.5 eV. Such instrumentation is therefore not normally suitable for obtaining correct fragment ion yields, since in such cases energetic fragment intensities can be in error by as much as an order of magnitude.[79] Because of the large kinetic energies involved, the dipole (e,e + ion) spectrometer is designed to collect all fragment ions with up to 20 eV excess kinetic energy with 100% efficiency.[99–101]

The (e,e + ion) spectrometer uses a time-to-amplitude converter (TAC) to measure the electron-ion coincidence. Use of the TAC method can lead to inaccuracies in the case of significant dissociative double photoionization (e.g., $AB^{2+} \rightarrow A^+ + B^+$). Although the number of ionizing events is correctly registered, only the fastest (lightest) fragment ion would normally be detected from each double dissociative ionization event. Such doubly dissociative processes are usually negligible, certainly below ~60 eV, but in some cases (e.g., SF_6) this is not the case, and spurious results may be obtained. In simple homonuclear diatomic molecules, the correct single fragment-ion partial cross section has been obtained by determining the difference between the total photoionization and the molecular (parent) ion cross sections.[104] This method cannot be extended beyond homonuclear diatomic species except as a check on the total dissociative photoionization cross section.

3.2.b.3. Photoionization Efficiency

The relative photoionization efficiency may be determined separately in both the dipole ($e,2e$) and the (e,e + ion) spectrometers by summing the electronic ionic state or total ion (molecular and dissociative) count rates and dividing by the forward scattering (noncoincident) signal. In all molecules studied to date the photoionization efficiencies above ~20 eV have been found to be constant, a value that can be sensibly normalized to unity in this region. The normalized photoionization efficiency so obtained may be used together with branching ratios to partition the total photoabsorption into partial photoionization cross sections at each value of E. This procedure assumes contributions from multiple ionization and ion-pair productions are negligible.

The total photoabsorption, photoionization efficiency, and branching ratios (or CIS scans), as well as the total and partial photoionization cross sections, may all be determined

over a wide energy range in a single instrument in the case of both dipole $(e,2e)$ and $(e,e+\text{ion})$ spectroscopies. This provides important consistency checks with a given method and also between the two spectroscopies. The sums of the partial cross sections for electronic states of ions and for molecular dissociative fragments must be equal to each other and each must be equal to the total photoabsorption multiplied by the photoionization efficiency over the entire photon energy range. This has also provided a useful means of determining the detailed, quantitative dipole breakdown pathways of molecules.[49,73,105]

4. Theoretical Studies

The theoretical basis for one-photon, one-electron molecular photoionization calculations was provided some years ago in the form of state-to-state cross-section expressions differential in energy and photoemission angle,[106–108] as adapted for applications to many-electron atoms and molecules.[109–116] These expressions entail calculations of appropriate initial and final states for use in the dipole matrix element, generally evaluated employing the length form.[108] Recent developments in this area involve the formulation of sensible dynamical approximations and the implementation of efficient computational procedures for carrying out the necessary calculations.[59–71] In this section, cross-section expressions are given, the dynamical approximations currently employed are described briefly, and aspects of the computational procedures introduced are indicated. The results of selected *ab initio* and model potential (X-alpha) calculations are reported with the corresponding measured data.

4.1. Cross-Sectional Expressions

A formal expression for the one-electron photoionization cross section is given by the nonrelativistic quantum mechanical formula[108]

$$d\sigma^{j}_{\text{ion}} = (2\pi e^2/hc)h\nu|\langle\phi_j(\mathbf{k})|\boldsymbol{\epsilon}\cdot\boldsymbol{\mu}|\phi\rangle|^2 d\Omega. \qquad (4.1)$$

Here, $d\sigma^{j}_{\text{ion}}$ is the differential photoionization cross section for electron ejection with momentum $\mathbf{k}$ into the solid angle $d\Omega$ upon production of the molecular ion in state j from the initial molecule AB by action of the incident photon. The unit vector $\boldsymbol{\epsilon}$ gives the direction of the incident light polarization, $h\nu$ is the photon energy, the symbols in the first parentheses on the right-hand side of Eq. (4.1) have their customary meanings, $\boldsymbol{\mu}$ is the molecular dipole-moment operator, and ϕ and $\phi_j(\mathbf{k})$ are initial and final molecular wavefunctions, respectively.[109–116] Since the function ϕ describes a neutral bound-state molecule AB, it is normalized to unity in the conventional manner and labeled with appropriate quantum numbers. These refer ultimately to nuclear spin states, total angular momentum and its projection, parity, and energy ordering, although introduction of the Born–Oppenheimer approximation and the appropriate Hund's coupling scheme for nuclear, electronic, and rotational angular momenta gives rise to the familiar electronic, vibrational, and rotational quantum numbers.[117] The final-state function $\phi_j(\mathbf{k})$ describes the photoejected electron as well as the state of the molecular ion produced, and can be written in the form $\phi_{\mathbf{k}}^{(-)}\otimes\phi_j$, where the symbol $\otimes$ implies a coupling that takes cognizance of total wavefunction antisymmetry and of other possible requirements, such as spin multiplicity, for appropriate Hund's cases.[110–116] The appropriate continuum state $\phi_{\mathbf{k}}^{(-)}$ is quantized in the direction of the outgoing electron and in kinetic energy, quantities both specified by the labeling vector $\mathbf{k}$.[108] Furthermore, $\phi_{\mathbf{k}}^{(-)}$ must satisfy so-called incoming-wave asymptotic boundary conditions if Eq. (4.1) is to be employed,[107] and is normalized in the so-called Dirac delta-function sense in kinetic energy $t=\frac{1}{2}k^2$ and emission angle Ω, so that[117]

$$\langle\phi_{\mathbf{k}'}^{(-)}|\phi_{\mathbf{k}}^{(-)}\rangle = \delta(t'-t)\delta(\Omega'-\Omega). \qquad (4.2)$$

The wavefunction ϕ_j describes the molecular ion in state j, involving quantum numbers similar to those employed for the initial state ϕ. However, in contrast to ϕ, ϕ_j describes either vibrationally stable parent-ion states, unstable predissociating states, or directly dissociative states. In the two latter cases, continuous labels specifying fragmentation kinetic energy and the direction of separation arise, and so the label j is, strictly speaking, inadequate. This complication is avoided in the present development by regarding ϕ_j as appropriate for the metastable ionic state $[AB^+]^j$ of Eqs. (1.1) and (2.3) formed prior to the possibly dissociative processes of Eqs. (1.2) and (2.4)–(2.6). Since available experimental data do not generally provide fragmentation kinetic energy or angular distributions, and there are few corresponding theoretical studies available, the restriction is not an essential one for present purposes.

Although the state-to-state expression of Eq. (4.1) is of considerable interest in connection with rotationally resolved cross sections, there are at present few data available pertaining to these quantities. In the present development, attention focuses on electronic partial photoionization cross sections and ionic photofragmentation cross sections, in which cases considerable data are now available. The differential cross section to electronic resolution can be obtained from Eq. (4.1) for rotationally resolved processes by introduction of the appropriate initial-state Boltzmann weighting factors and summation and/or integration over all rotational, vibrational, and additional subsidiary quantum labels associated with final states.[111,116] Alternatively, it is also possible to treat the molecular rotational degrees of freedom classically at the outset, to define vibronic cross sections for fixed molecular orientation, and to perfom an average of all equally weighted orientations appropriate for the gas-phase targets of interest here.[110,112] The formal cross-sectional expression employed in the latter case is identical with that of Eq. (4.1), where now ϕ and ϕ_j refer to vibronic wavefunctions, and there is an explicit dependence in the dipole matrix element on the Euler orientation angles of the molecular target which must be averaged over.[110] Finally, in the simplest approach the vibrational degrees of freedom are disregarded, providing vertical electronic cross sections that correspond to summation over the vibrationally resolved expressions in the Franck–Condon approximation.[110–116] In order to proceed further with the cross-sectional evaluation it is necessary to introduce specific dynamical approximations for the necessary electronic wavefunctions.

4.2. Dynamical Approximations

The large majority of molecular photoionization calculations performed to date employ the Born–Oppenheimer and Franck–Condon approximations, Hartree–Fock initial wavefunctions for the electronic part of ϕ, Koopmans ionic core functions for the electronic part of ϕ_j, and a variety of choices for the continuum function $\phi_{\mathbf{k}}^{(-)}$, as described in the following subsection. In this approximation the partial channels to electronic resolution are defined by the orbital that is removed in forming the appropriate Koopmans core state, and the continuum function $\phi_{\mathbf{k}}^{(-)}$ is determined by the corresponding hole-state potential or an approximation to it. Under these conditions, the state-to-state cross-sectional expressions to either rotational or vibrational resolution both provide, upon appropriate summation over rotational and/or vibrational states electronic cross sections in the form[109–119]

$$d\sigma^j_{\text{ion}} = (\sigma^j_{\text{ion}}/4\pi)[1 + \beta^j P_2(\cos\theta)]d\Omega, \tag{4.3}$$

where

$$P_2(\cos\theta) = \tfrac{1}{2}(3\cos^2\theta - 1), \tag{4.4}$$

is the second-degree Legendre polynomial, θ is the angle between $\mathbf{k}$ and $\boldsymbol{\epsilon}$, and σ^j_{ion} and β^j are the electronic partial photoionization cross section and angular anisotropy factor, respectively, for the final electronic ionic state $[AB^+]^j$ of Eq. (1.1). If the incident radiation is unpolarized, the appropriate cross section is

$$d\sigma^j_{\text{ion}} = (\sigma^j_{\text{ion}}/4\pi)[1 - \tfrac{1}{2}\beta^j P_2(\cos\theta)]d\Omega, \tag{4.5}$$

where θ is now the angle between $\mathbf{k}$ and the photon propagation direction, but σ^j_{ion} and β^j are unchanged.

The electronic partial cross section σ^j_{ion} corresponds to the classical angle average of the three body-frame cross sections for polarization along the three principle axes of electric polarizability, whereas the angular anisotropy factor β^j provides a description of the angular distribution of photoejected electrons. Although explicit expressions for σ^j_{ion} and β^j have been given in the literature in terms of partial-wave expansions and one-electron radial matrix elements, these are sufficiently complicated to make their presentation here unwarranted.[110–116] In an alternative development, wavefunctions of body-frame point-group symmetry are employed in cross-sectional calculations, avoiding the more conventional partial-wave expansion.[65] These functions are to be understood as the linear combinations of so-called eigenchannel states that provide the appropriate polarization cross sections.[68] Although the development also provides a basis for constructing angular anisotropy factors, calculations of β^j values employing these methods have only recently been reported in the literature.

4.3. Computational Approximations

Various approximations to the electronic wavefunctions required in the cross-sectional expression of Eqs. (4.1)–(4.5) have been employed to date. With the exception of a very few specific cases cited below, these have been in single-channel or single-configuration approximations, generally employing Hartree–Fock target functions, as indicated above. In this approximation, the electronic partial cross sections refer to removal of electrons from individual canonical Fock orbitals, in accordance with the Koopmans approximation.[59] Calculations of the final-state functions involve the construction of a photoejected electron wave $\phi_{\mathbf{k}}^{(-)}$ satisfying incoming-wave boundary conditions in the presence of a static potential which is noncentral and also nonlocal (exchange potential), and which becomes Coulombic for large separations. The approximations employed to date for the final state include the following types of wavefunctions and potentials.

A. Plane waves

In this case the potential is set to zero, constituting the simplest possible approximation to the ionization function. Numerous calculations have been reported in this approximation using initial-state Hartree–Fock orbitals.[16] The cross sections and anisotropy factors so obtained are qualitatively and quantitatively unsatisfactory, providing little if any help in interpreting measured values. In particular, the cross sections all vanish at threshold, in contrast to the predictions of the Wigner threshold law for Coulombic systems,[120] the high-energy limit obtained is unsatisfactory, ambiguities arise in connection with orthogonality between initial- and final-state wavefunctions, and the very interesting resonance features that arise from the short-range portions of molecular potentials are not included in the approximation. Such calculations are possibly useful, however, for negative-ion photodetachment cross sections, in which cases the correct potential is weak and asymptotically non-Coulombic.

B. Single-center Coulomb waves

The potential refers to that of a unit positive charge in this case, generally placed at the center of mass. Partial cross sections so obtained using Hartree–Fock initial orbitals can be satisfactory at higher photon energies, in which case the Coulomb limit is approached. At lower energies such cross sections generally provide only a background value, since they do not include the effects of the short-range molecular ionic field, which can give rise to appreciable differences from the Coulomb values even in so-called single-center (e.g., hydride) systems. In particular, shape resonance features are not predicted. Additionally, introduction of orthogonality constraints between the continuum state and the occupied orbitals can give rise to cross sections that include spurious irregular spectral features.[121]

C. Two center Coulomb waves

This approximation, appropriate for homonuclear diatomic molecules, employs a pair of fractional charges (usually $+\frac{1}{2}$) to represent the molecular ionic field.[122] As in the single-center Coulomb approximation, cross sections useful at high photon energy are obtained in this way. However, the important distorting effects of the short-range molecular potential are not included, giving generally unsatisfactory results below ~ 50 eV, and orthgonality constraints can produce spurious spectral features.

D. Local molecular potentials

Potentials of the Khare, Sternheimer, or X-alpha type, in which the nonlocal exchange part is replaced with a local approximation, have been employed extensively in molecular photoionization calculations.[60,63,69,70,123,124] In the widely adopted multiple scattering X-alpha approximation, use of an external sphere outside of which the potential is taken as Coulombic insures that the appropriate high photon energy limit is obtained. The short-range molecular potential is simulated with atomic spheres, in which there are largely effective Coulomb potentials,[123] and interstitial regions in which the potential is constant. These particle-in-Coulomb-boxes potentials can reproduce aspects of measured photoionization cross sections, although results obtained from various workers in specific cases can differ by factors of two or more due to ambiguities in choice of potential parameters. Although these approaches are not *ab initio* in nature, and consequently generally are not quantitative, they predict the existence of resonance features in calculated cross sections, aiding in the interpretation of measured values. However, the energies of these features are usually incorrect. Care must be exercised, however, in spuriously accounting for channel-coupling or other configuration-mixing processes in measured cross sections on basis of a single-channel model. Local potentials of the Sternheimer or inversion type are largely of unknown accuracy when applied to molecules. These are designed to provide theoretical insights into photoionization cross sections, rather than to provide quantitatively reliable values.[124]

E. *Ab initio* static-exchange potentials

This approximation employs a static noncentral, nonlocal (exchange) potential obtained from neutral target Hartree–Fock orbitals, minus that of the ionized electron.[59,62,64–68,71] All one-electron effects are included except for the polarization and relaxation the remaining core feels upon ionization. The latter effect is taken into account in an approximate way by employing ionic-state molecular orbitals.[67] Calculations indicate the approach provides a useful first approximation free from ambiguity to photoionization cross sections, and furnishes a basis for subsequent introduction of polarization, relaxation, and channel-coupling effects. Moreover, cross sections corresponding to so-called satellite or many-electron ionization channels are also obtained from static-exchange calculations in the intensity-borrowing sudden approximation.[62] Computational difficulties have hampered static-exchange calculations in the past, although good agreement is now obtained employing various numerical techniques. Single-center expansions of ionization functions, supplemental with basis-set representations of exchange potentials, now provide cross sections for linear molecules that are in good accord from different groups.[64,66,67,71] Completely square-integrable methods, when implemented properly, provide cross sections in these cases that are in accord with the single-center expansion methods, and are similarly applicable to polyatomic molecules,[65,68] and to these calculations of angular distributions.[125] In some cases, correlated ground-state wavefunctions have been used in conjunction with static-exchange final states.[71]

F. Coupled-channel calculations

General procedures for the study of channel-coupling effects are provided by the so-called multichannel quantum defect theory.[126] In this development, cross-sectional expressions are parameterized in terms of quantities that are generally slowly varying functions of photon energy and are consequently amenable to calculation. Computational studies of channel-coupling effects have been reported at the static-exchange level in time-dependent Hartree–Fock calculations.[127–129] The ionic cores employed in this approach refer to the Koopmans approximation, with ionization functions for each electronic channel determined in the presence of configuration mixing in the single-excitation or ionization approximation. Additionally, particle-hole terms are also incorporated into the development, which corrects to a certain extent for two-electron correlation terms in the ground-state functions. Calculations to date in this approach include the use of local approximations to the Koopmans core potentials,[128,129] and the neglect of particle-hole terms.[130]

Although the foregoing approximations all have been employed in varying degrees, only *ab initio* static-exchange and local potential (X-alpha) calculations are reported here to aid in interpretation of spectral variations in the experimentally observed cross sections, in accordance with the widespread use of these approximations.

5. Data Acquisition and Presentation

Experimental and theoretical data compiled here are obtained from published results in the open literature, as well as from private communications. Cross sections ($\sigma^T_{\rm abs}, \sigma^j_{\rm ion}, \sigma^{\rm frag}_{\rm ion}$) and anisotropy factors (β^j) are extracted from journal and manuscript figures using standard digitization techniques, or read from tables, and entered into a data base. Tables 2–19 list the data sources for each molecule chronologically by year of publication. Also indicated are the following. (1) Whether the work was experimental (E) or theoretical (T). (2) The method used to acquire the data, where P≡photon methods (i.e., photoabsorption, PES, PIMS), DIP≡electron-impact simulation techniques [i.e., dipole (e,e), $(e,2e)$, and $(e,e+\text{ion})$ methods], StEx≡static-exchange calculations, and CI≡configuration interaction calculations. (3) The method used for experimental normalization, where AB≡true absolute determination, i.e., by measurement of n and I_0 (see Sec. 3), TRK≡Thomas–Reiche–Kuhn sum rule method (assuming valence-shell separation), NM≡normalization to a "known" cross section at a single energy. (4) The specific electronic states of the parent ion for which partial photoionization cross sections $\sigma^j_{\rm ion}$ are given. (5) Specific molecular ions and dissociative fragments for which cross sections $\sigma^{\rm frag}_{\rm ion}$ are given. (6) The specific electronic states of the parent ion for which asymmetry parameters (β^j) are given. (7) The energy range for which data are given.

All measured and calculated photoabsorption cross sections $\sigma^T_{\rm abs}$ for a specific molecule are plotted together on

an individual figure as a function of the photon energy $h\nu$. Similarly, all cross sections σ^j_{ion} and asymmetry parameters β^j for production of a specific final state j of the parent ion, as well as cross sections $\sigma^{\text{frag}}_{\text{ion}}$ for production of a molecular ion or specific dissociative fragment, are plotted on individual figures as functions of the incident photon energy. Measured cross sections and asymmetry parameters are indicated by separate points, while calculated data are given as lines. The threshold energy for the relevant photoionization process, obtained from literature values,[4,7,131–136] is indicated by a vertical dotted line on each figure. All cross sections are given in both Mb (10^{-18} cm^2) on the left and as oscillator strengths (eV^{-1}) [see Eq. (2.22)] on the right of the figures. A tabular listing of all data presented in the figures is available in JILA Data Center Report No. 32.

6. Conclusions and Evaluation

The summary tables and figures show the experimental data and selected calculations accumulated to the end of 1986 for the absolute cross sections for photoabsorption, partial photoionization for production of electronic states of ions, and for ionic photofragmentation processes, all as functions of photon energy in the range above the first ionization threshold to ~100 eV. Data for photoelectron asymmetry or angular anisotropy parameters are also shown. The target molecules include commonly encountered homonuclear and heteronuclear diatomics, linear and bent triatomics, as well as a number of polyatomic molecules of general interest.

In most cases, the original publications provide little direct information of the author's assessment of accuracy of the measured data. However, where several different, independent measurements exist (e.g., N_2, CO, O_2, NO, CO_2, N_2O,...), the degree of agreement and extent of scatter of data points among the various measurements provides a critical indication of reliability. Good agreement between measured data sets is a particularly stringent criterion of reliability in the present work, because of the unique circumstances associated with the two types of methods used, i.e., conventional photoabsorption techniques and the corresponding dipole electron-molecule scattering techniques. These two techniques are based on processes and instrumentation that are completely different, physically distinct, and totally independent. Furthermore, in almost all cases, their normalization methods are completely different in both principle and practice. In the photon experiments, the absolute scale is established from true absolute determinations of light fluxes and particle densities. In contrast, the dipole electron-scattering methods utilize Bethe–Born conversion factors and Thomas–Reiche–Kuhn sum rule normalization (for subshell) of the oscillator strength scale, with no absolute measurements necessary. The degree of agreement between results obtained under these totally different experimental circumstances is an excellent indicator of accuracy. For most of the commonly encountered small molecules both experimental techniques have been used, and the figures show that excellent agreement generally exists between the respective data sets. In these cases, high confidence can be placed in these data.

With the above considerations in mind, it can be stated that in almost all cases the absolute photoabsorption cross sections (σ^T_{abs}) are considered to be accurate to better than $\pm$ 10% over the energy ranges shown, and in many cases (N_2, CO, O_2, NO, CO_2, N_2O, H_2O, NH_3, CH_4, H_2S, CS_2, COS), to better than $\pm$ 5%. Examination of the figures shows that a few data sets may be less accurate than $\pm$ 10% in certain energy ranges, particularly in the immediate threshold region. Difficulties commonly encountered in photoabsorption measurements which may contribute to inaccuracies in measured data include: (i) stray light, (ii) higher-order radiation, (iii) determination of light flux, and (iv) determination of target density. The largest errors in absolute photoabsorption measurements apparently occur as a result of uncertainties in the measurement of particle density. In the dipole (e,e) method important sources of uncertainty include: (i) stray electrons, (ii) validity of shell separation in TRK sum rule normalization, and (iii) extrapolation of the high-energy absorption tail to infinite photon energy.

The situation is more complex in the case of absolute partial cross sections for photoionization processes (σ^j_{ion} and $\sigma^{\text{frag}}_{\text{ion}}$). Here, the techniques are more difficult, and the signals smaller in both direct photoionization methods and their electron-impact counterparts.

In the case of PES [or $(e,2e)$], σ^j_{ion} are obtained from photoelectron branching-ratio measurements and the absolute total photoabsorption cross section and photoionization efficiency (or total photoionization cross section). Alternatively, CIS scans suitably normalized using a single set of branching ratios at a single photon energy are employed. In order to eliminate angular distribution effects, the signal is normally sampled in a small acceptance cone centered about the magic angle. Such magic angle PES [or $(e,2e)$] signals are necessarily small compared with the partial photoionization signals sampled in PIMS [or $(e,e+\text{ion})$], which usually involve collection over all angles. A further source of error in PES [or $(e,2e)$] is in the accuracy with which the electron transmission efficiency T is known, particularly at lower electron kinetic energies (i.e., near threshold). Such uncertainties are probably the reason for the near threshold discrepancies observed in a few cases; for example, in the σ^j_{ion} measurements reported by different groups for NO and H_2O. However, in most other cases, good agreement has been obtained from different experiments.

Assessment of the accuracy of measured σ^j_{ion} involves several considerations. First, the reproducibility of the photoelectron branching ratio or CIS measurements reported by different groups using the two independent experimental methods is a good indicator of the accuracy of the primary measurements. These cross sections are subject to inaccuracies arising from the contributions of multiple ionization processes and the continua associated with ionic states having steeply repulsive potential energy curves. Weak many-body ionization states which are either not observed or improperly detected also lead to inaccuracies above photon energies of ~30 eV.[89] Inaccuracies in the near threshold regions can arise from nonspectral backgrounds of low kinetic energy electrons. Consideration of these effects, togeth-

er with the reproducibility of the data shown, suggests that the measured σ^{j}_{ion} are accurate to within $\pm 15\%$ in most cases. However, in the case of ionic states of very low yield, the inaccuracies are expected to be somewhat larger.

The accuracy of $\sigma^{\text{frag}}_{\text{ion}}$ is generally higher than that of σ^{j}_{ion}, since the fragments are collected over all angles. Failure to collect all energetic fragments can be a major source of error in mass spectrometer experiments. The large ion drawout fields currently used in the source region ensure complete collection of energetic fragment ions, irrespective of the kinetic energy of fragmentation. Consequently, the branching ratios, and therefore the $\sigma^{\text{frag}}_{\text{ion}}$ are essentially free of such kinetic-energy discrimination effects. A further possible source of inaccuracy arises from failure to detect one of the fragment ions in double dissociative photoionization (i.e., $AB^{2+} \rightarrow A^{+} + B^{+}$). The time-to-amplitude converter detectors used in both PIMS and dipole $(e,e + \text{ion})$ experiments will normally only detect the faster of the two ions (A^{+},B^{+}) exiting the TOF tube. Errors due to these effects are only likely to be significant for valence-shell processes above photon energies of 40–50 eV. A consideration of these factors and of the data presented leads to the conclusion that the $\sigma^{\text{frag}}_{\text{ion}}$ are accurate to within $\pm 10\%$ for all except the lowest abundance ions.

It is evident from the figures that the calculated partial-channel photoionization cross sections reported provide values that are, in most cases, in sensible accord with the measured values. A useful comparison between static-exchange and X-alpha results is given in the case of H_2. Generally, when results of these two methods differ significantly (e.g., N_2O, CS_2, OCS), the static-exchange results are in better accord with measured values. Discrepancies between measured values and single-channel, static-exchange calculations can generally be expected in threshold regions, where polarization effects, possible non-Franck–Condon behavior, and contributions from autoionization, all neglected in the *ab initio* studies, are important. Additionally, channel-coupling effects, particularly in threshold regions and in the presence of two or more intravalence excitations, and the failure of the Koopmans approximations for molecules containing heavier atoms, can lead to discrepancies between measured values and static-exchange calculations. It should be noted that the single-channel, static-exchange approximation will provide reliable cross sections in the high-energy limit, even in the presence of the complicating factors indicated above, provided the intensity-borrowing effects of higher-lying many-electron ionic states are accounted for by using appropriate spectroscopic factors. Finally, the precision with which static-exchange cross sections can be calculated at present is indicated in those figures containing results from two or more groups for a given cross section. There are some significant differences between static-exchange calculations in open-shell molecules (NO, O_2) and/or in channels that include shape-resonance features (e.g., NO, O_2, CO_2), in which cases the cross sections are particularly sensitive to both initial- and final-state wavefunctions.

Table 2. Data for H_2.

Reference	Author	Year	E/T	Method	Experimental normalization	Cross Sections			Betas	Photon energy range (eV)
						Abs	State specific partials	Molecular ions and dissociative fragments	State	
166	Cook	1964	E	P	AB	✓				16- 22
172	Denne	1970	E	P	AB	✓				150-280
179	Fryar	1973	E	P	NM			H_2^+,H^+		21- 41
138	Backx	1976	E	DIP	TRK	✓				10- 70
138	Backx	1976	E	DIP	TRK			H_2^+,H^+		15- 70
207	Lee	1976	E	P	AB	✓				17- 70
167	Davenport	1977	T	Xα	---		X			15- 24
176	Dutta	1977	T	StEx	---				X	20- 40
223	ONeil	1978	T	CI-StEx	---		X			15- 37
223	ONeil	1978	T	CI-StEx	---			H_2^+,H^+		15- 40
213	Marr	1980	E	P	---				X	17- 30
123	Thiel	1981	T	Xα	---				X	18- 50
244	Southworth	1982	E	P	---				X	19- 26
201	Itikawa	1983	T	CI	---				X	17- 21
228	Raseev	1983	T	StEx	---		X			15- 23
165	Collins	1984	T	StEx	---				X	19- 31
237	Samson	1984	E	P	AB			H_2^+,H^+		18- 41
236	Samson	1985	E	P	AB	✓				15-124

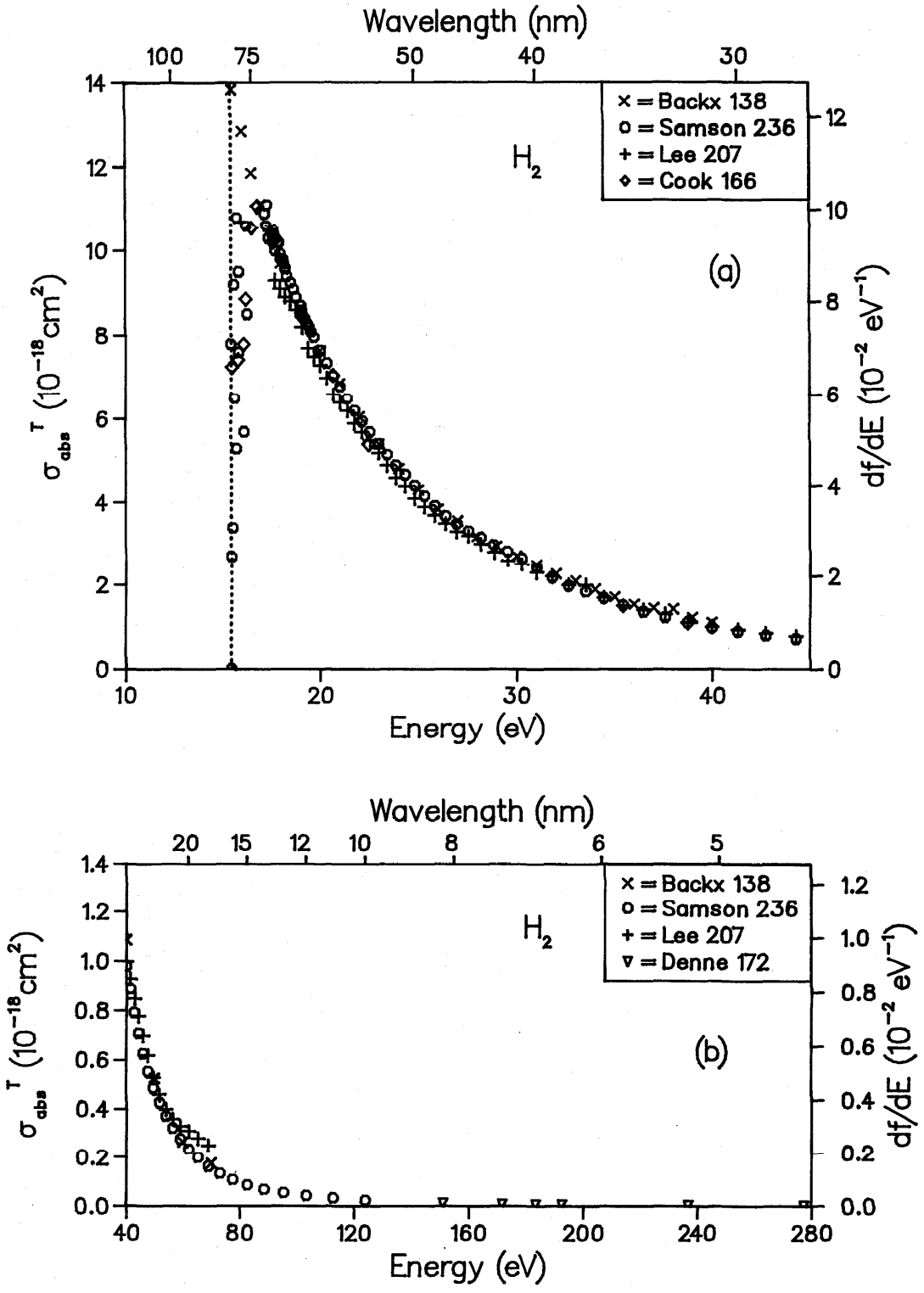

FIG. 10. Total photoabsorption cross section for H_2: (a) low-energy range, (b) high-energy range.

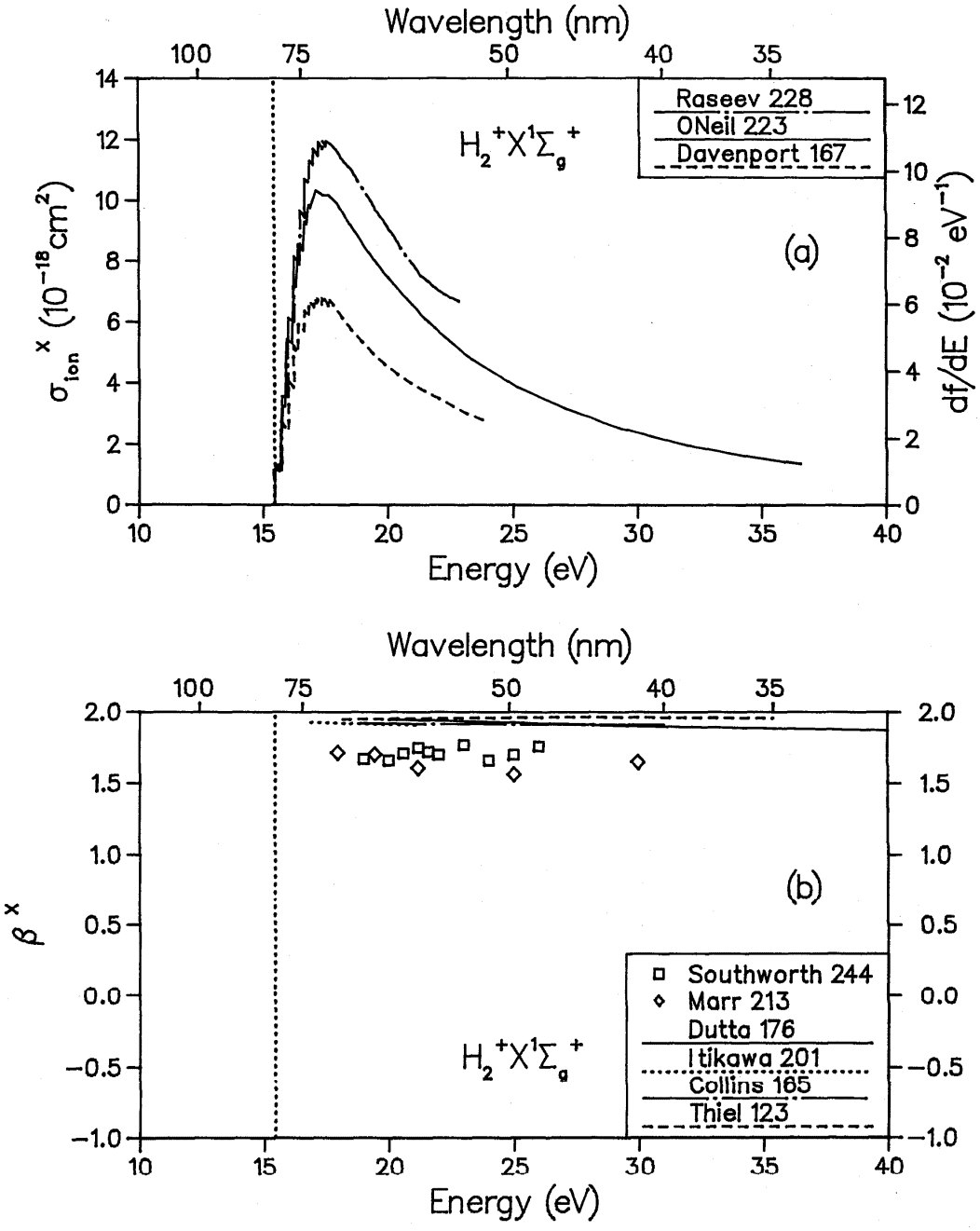

FIG. 11. (a) Partial photoionization cross section for H_2; final ionic state $= X^1\Sigma_g^+$. (b) Photoelectron asymmetry parameter for H_2; final ionic state $= X^1\Sigma_g^+$.

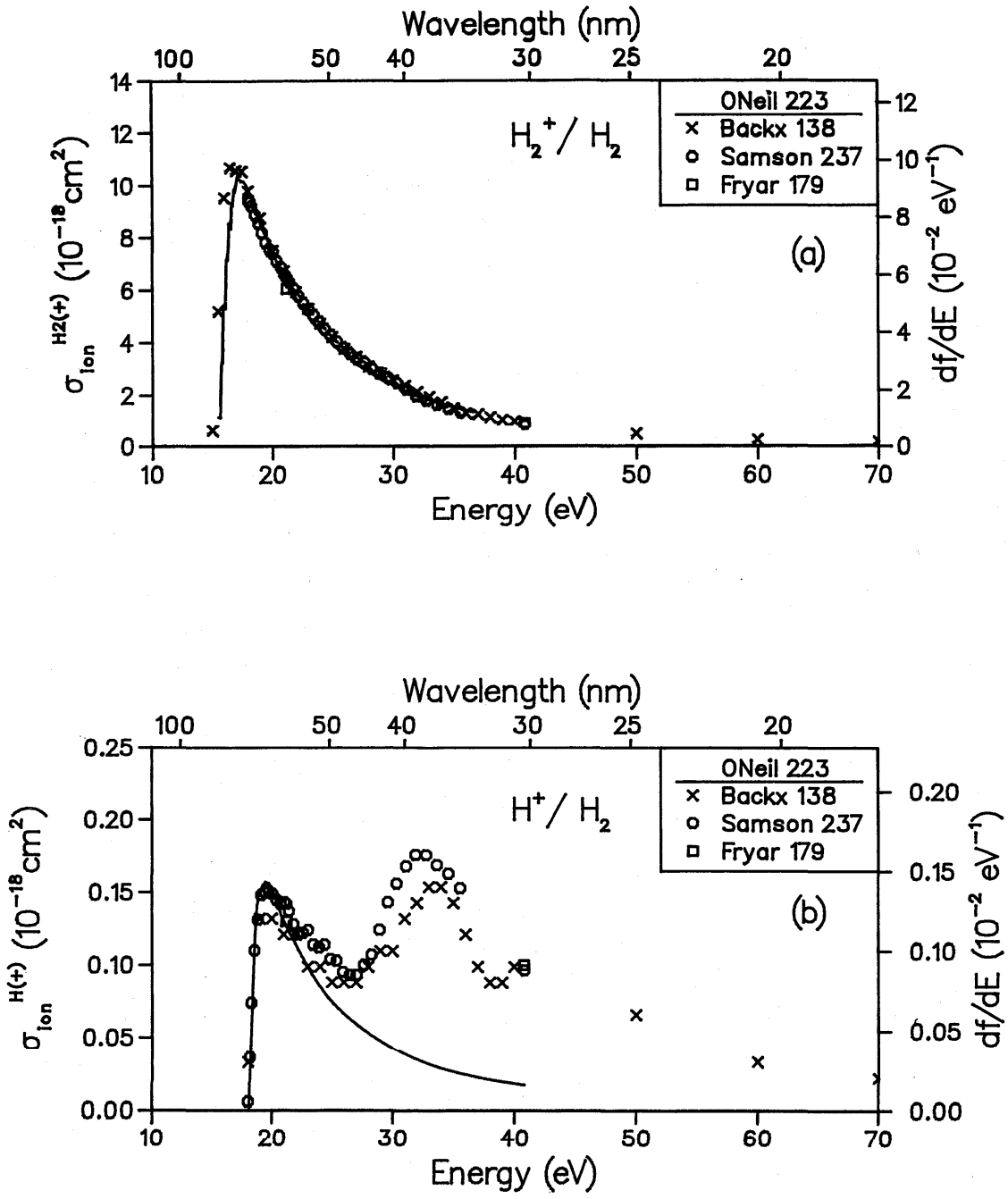

FIG. 12. Partial ionic photofragmentation cross sections for H_2; (a) product ion = H_2^+, (b) product ion = H^+.

Table 3. Data for N_2.

Reference	Author	Year	E/T	Method	Experimental normalization	Cross Sections: Abs	Cross Sections: State specific partials	Cross Sections: Molecular ions and dissociative fragments	Betas: State	Photon energy range (eV)
172	Denne	1970	E	P	AB	✓				150-525
179	Fryar	1973	E	P	NM			N^+, N_2^+		20- 41
208	Lee	1973	E	P	AB	✓				19- 70
254	Watson	1973	E	P	AB	✓				17- 33
168	Davenport	1976	T	Xα	---		X,A,B			16- 42
190	Hamnett	1976	E	DIP	TRK		X,A,B,F,$(2\sigma_g^{-1})$			18- 50
256	Wight	1976	E	DIP	TRK	✓				18- 70
256	Wight	1976	E	DIP	TRK			N^+, N_2^+		18- 60
170	de Reilhac	1977	E	P	AB	✓				24-125
88	Plummer	1977	E	P	NM		X,A,B			20- 40
235	Samson	1977	E	P	AB		X,A,B			16- 41
258	Woodruff	1977	E	P	AB		X,A,B			19- 37
164	Cole	1978	E	P	AB	✓				35-250
214	Marr	1979	E	P	---				X,A,B	21- 42
252	Wallace	1979	T	Xα	---				X,A,B	17-150
198	Holmes	1980	E	P	---				A	18- 20
203	Krummacher	1980	E	P	NM		C,F,G,$(2\sigma_g^{-1})$			43- 65
206	Langhoff	1981	T	CI	---		C,F,G,$(2\sigma_g^{-1})$			38- 67
212	Lucchese	1982	T	StEx/CI	---		X,A,B		X,A,B	15- 41
a	Adam	1983	E	P	---				B	28- 38
221	Morin	1983	E	P	NM		$(2\sigma_g^{-1})$			35- 58
165	Collins	1984	T	StEx	---		X		X	16- 40
184	Grimm	1984	E/T	P	---				X,A,B	40- 70
236	Samson	1984	E	P	AB			N^+,N_2^+		15-107
236	Samson	1986	E	P	AB	✓				15-107
243	Southworth	1986	E	P	---				X,B	16- 38

[a]M. Y. Adam, P. Morin, P.Lablangue and I. Nenner, taken from Ref. 243.

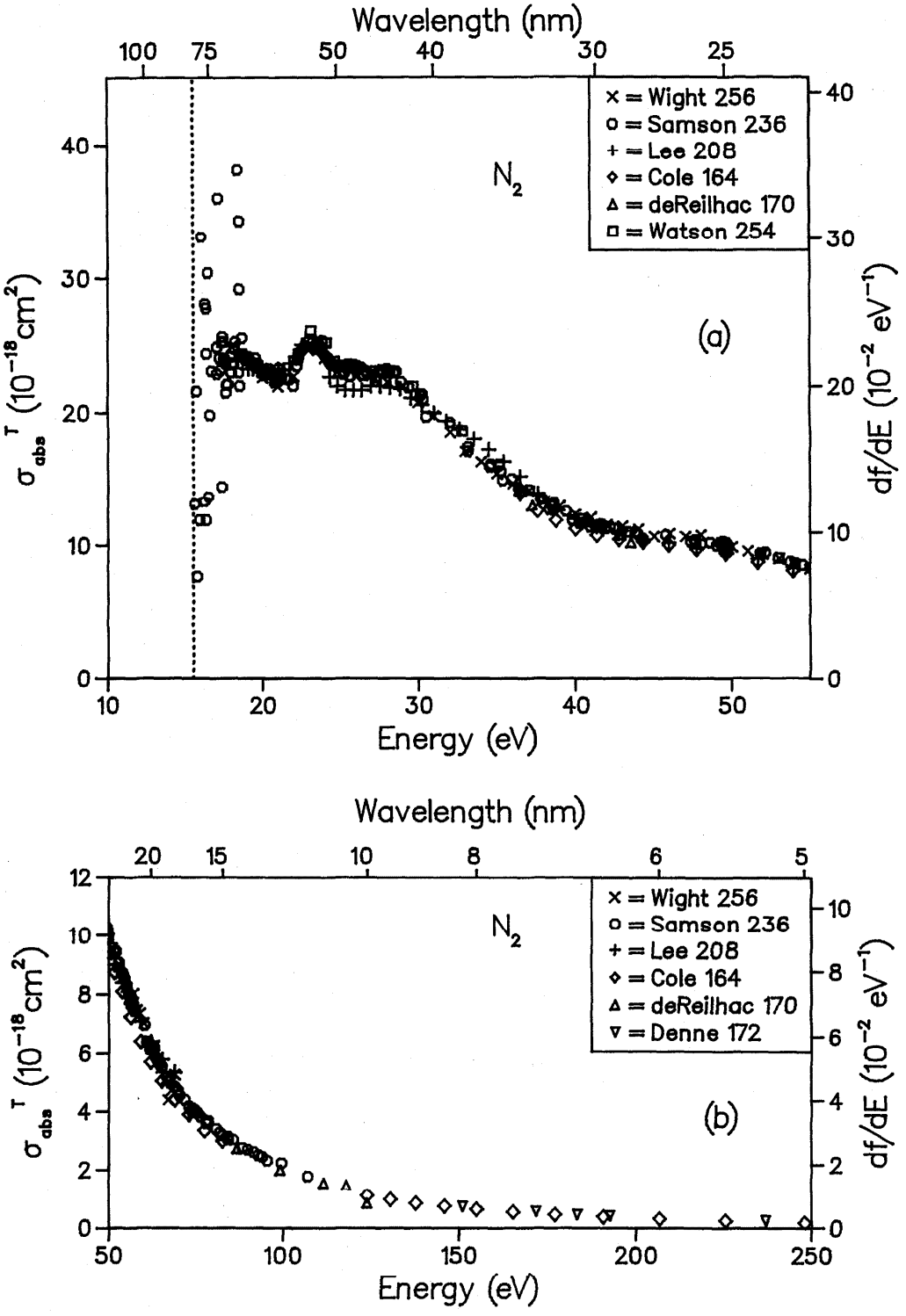

FIG. 13. Total photoabsorption cross section for N_2: (a) low-energy range, (b) high-energy range.

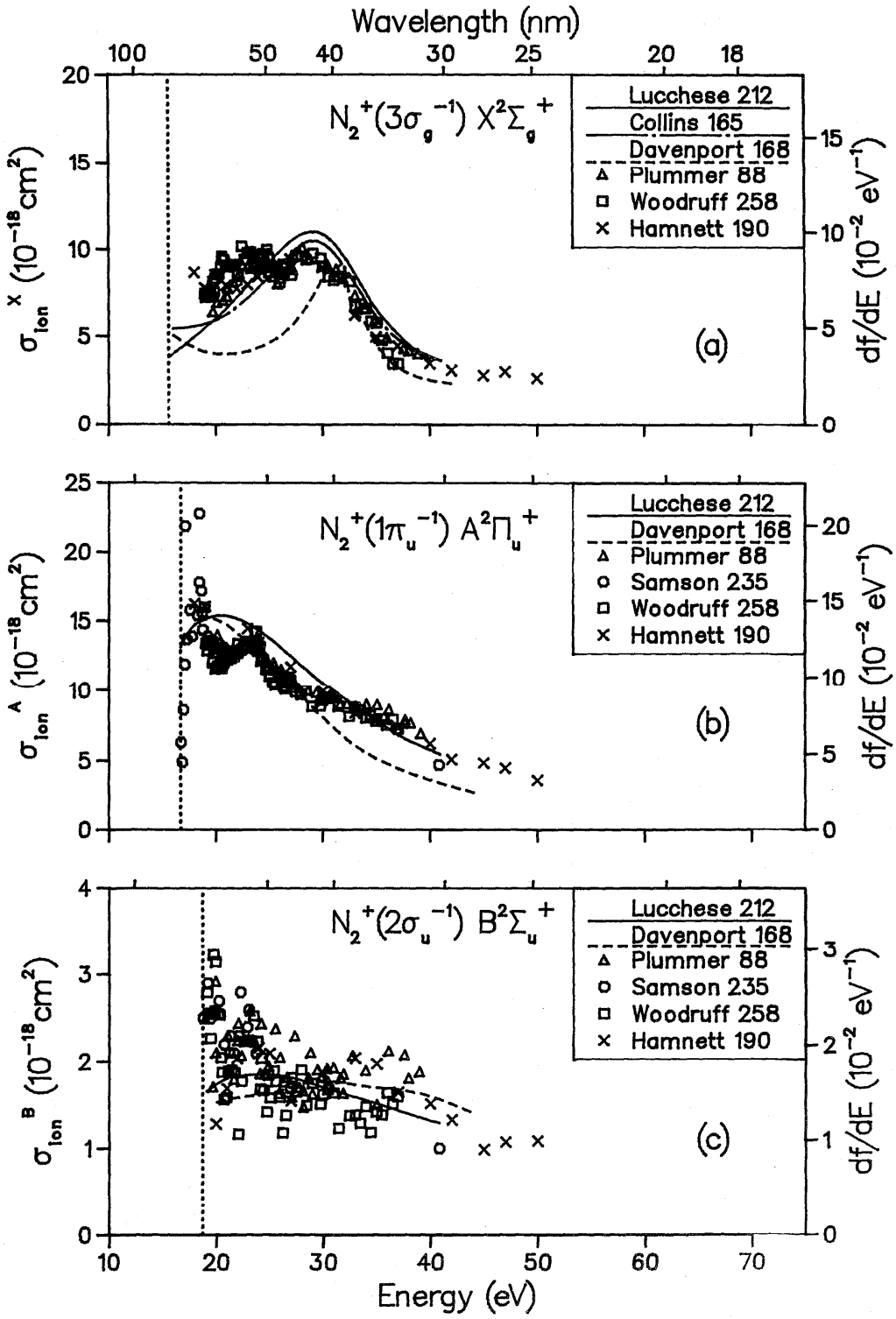

FIG. 14. Partial photoionization cross sections for N_2; (a) final ionic state = $X^2\Sigma_g^+$, (b) final ionic state = $A^2\Pi_u^+$, (c) final ionic state = $B^2\Sigma_u^+$.

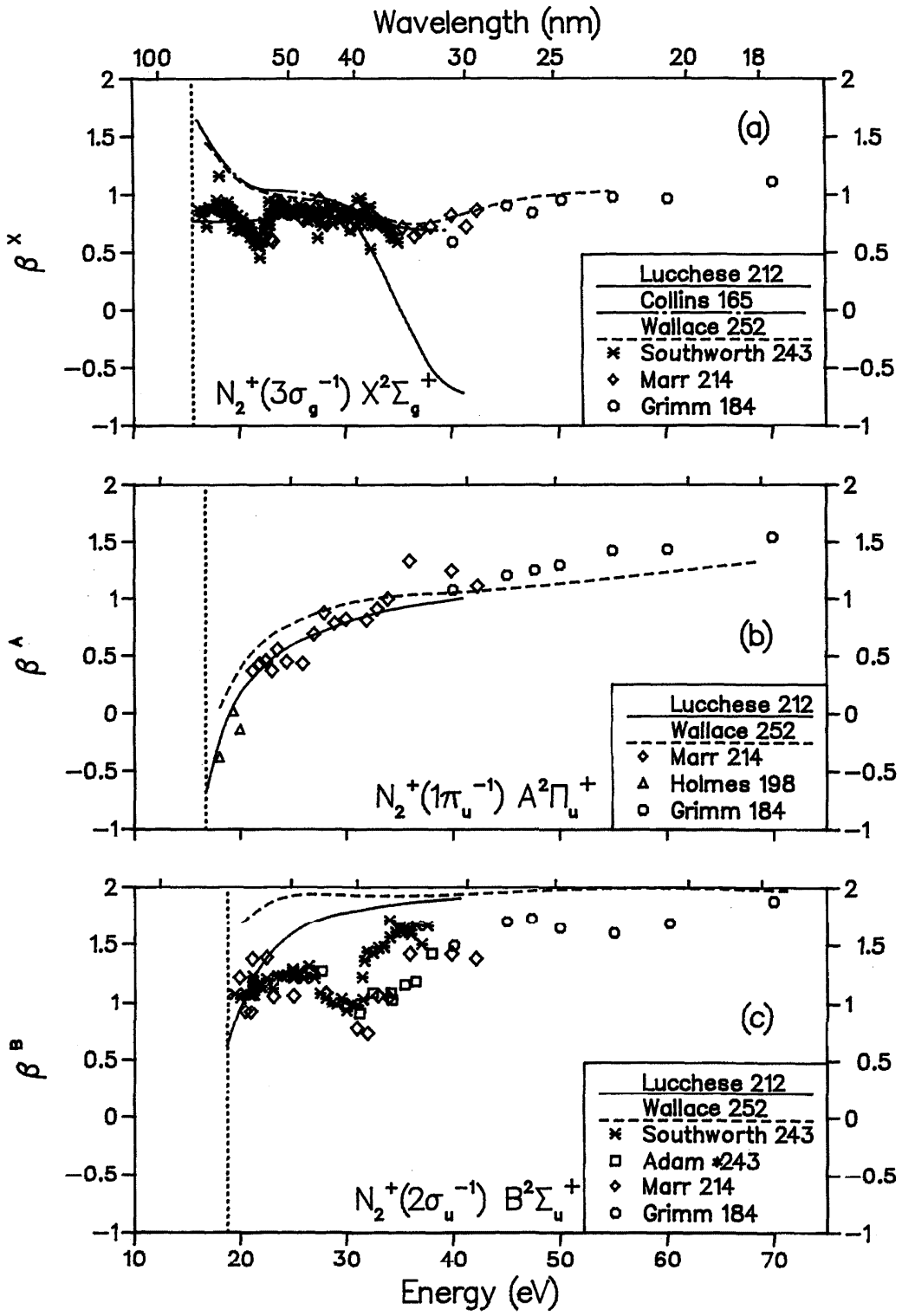

FIG. 15. Photoelectron asymmetry parameters for N_2: (a) final ionic state $= X^2\Sigma_g^+$, (b) final ionic state $A^2\Pi_u^+$, (c) final ionic state $= B^2\Sigma_u^+$.

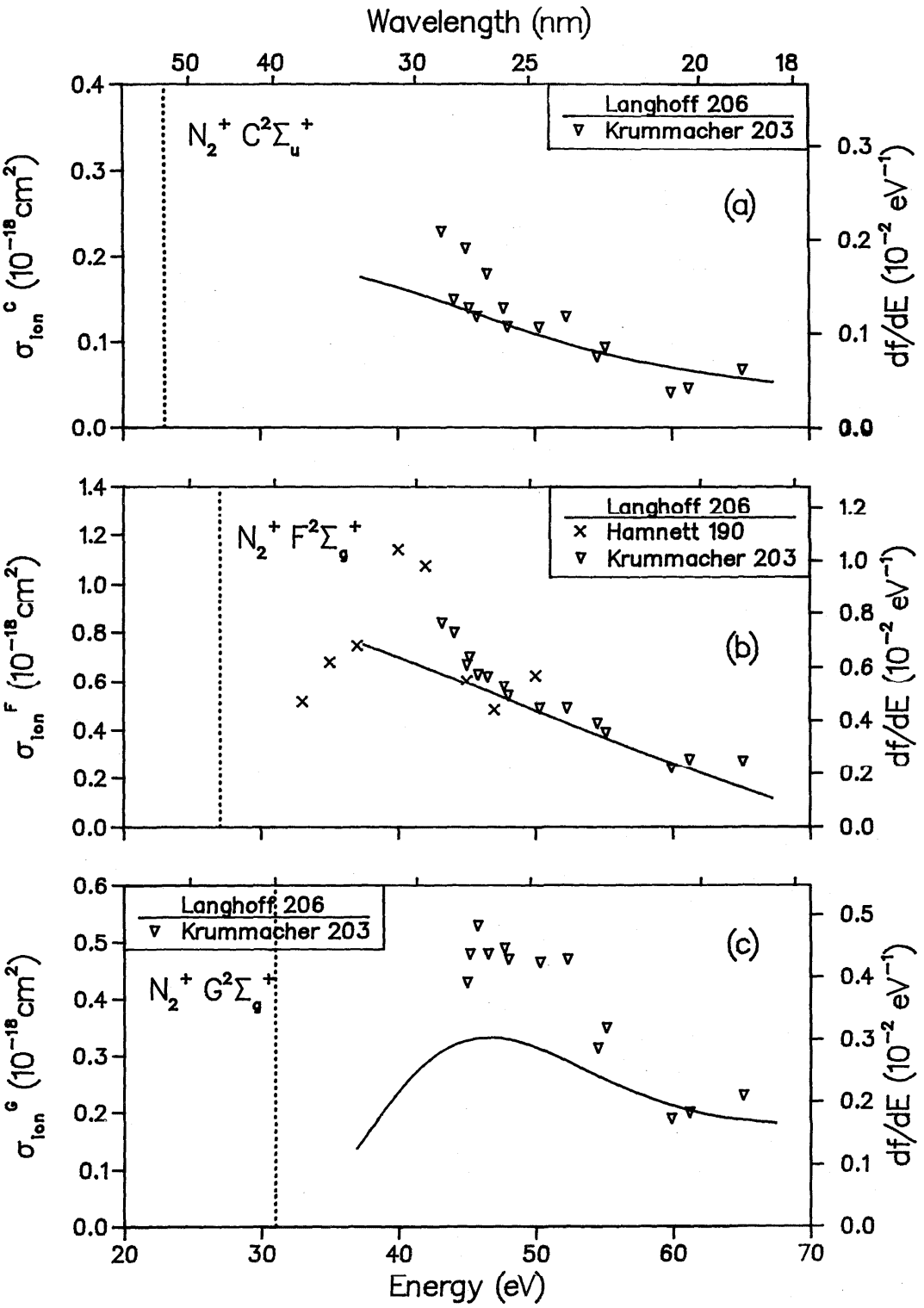

FIG. 16. Partial photoionization cross sections for N_2; (a) final ionic state $= C^2\Sigma_u^+$, (b) final ionic state $= F^2\Sigma_g^+$, (c) final ionic state $= G^2\Sigma_g^+$.

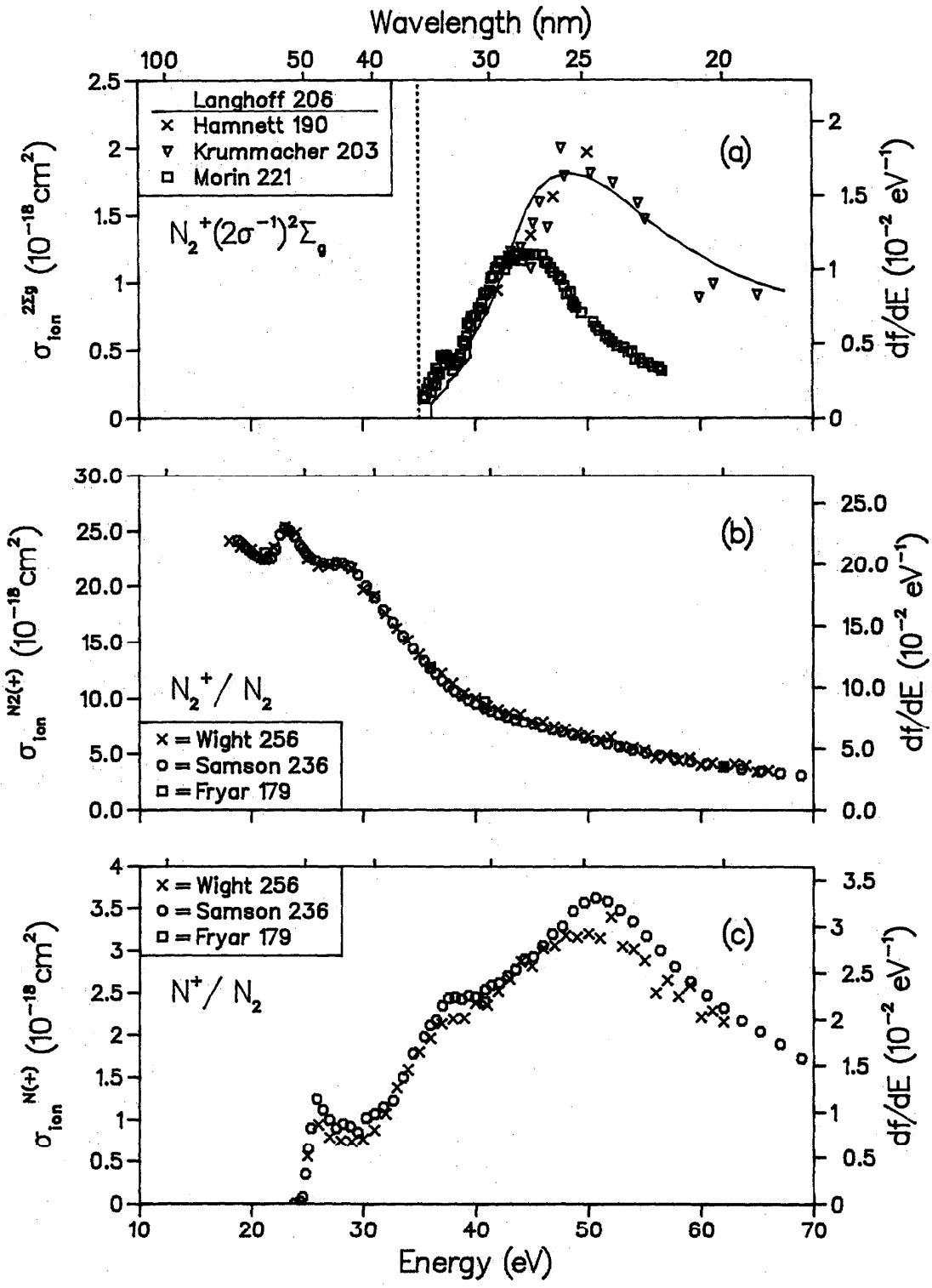

FIG. 17. (a) Partial photoionization cross section for N_2; final ionic state = $^2\Sigma_g$. (b) Partial ionic photofragmentation cross section for N_2, product ion = N_2^+. (c) Partial ionic photofragmentation cross section, product ion = N^+.

Table 4. Data for O_2.

Reference	Author	Year	E/T	Method	Experimental normalization	Cross Sections: Abs	Cross Sections: State specific partials	Cross Sections: Molecular ions and dissociative fragments	Betas: State	Photon energy range (eV)
172	Derne	1970	E	P	AB	✓				150-525
179	Fryar	1973	E	P	NM			O^+, O_2^+		20- 40
208	Lee	1973	E	P	AB	✓				17- 70
255	Watson	1973	E	P	AB	✓				20- 30
170	de Reilhac	1977	E	P	AB	✓				24-124
234	Samson	1977	E	P	AB		X,a+A,b,B			16- 41
164	Cole	1978	E	P	AB	✓				36-250
218	McCoy	1978	E	P	AB				X	19- 44
219	Mehlman	1978	E	P	AB	✓				36-207
149	Brion	1979	E	DIP	TRK	✓				5-275
149	Brion	1979	E	DIP	TRK		X,a+A+b,E,C, $^2\Sigma_u^-$,33 eV, $^{2,4}\Sigma_g^-$			17- 75
149	Brion	1979	E	DIP	TRK			O^+, O_2^+		11- 75
205	Langhoff	1979	T	StEx	---		X,b,B			12- 70
181	Gerwer	1980	T	StEx	---		X,a+A			17- 70
185	Gustaffson	1980	E	P	NM		X,a+A,b,B			20- 45
198	Holmes	1980	E	P	---				X,a+A,b	15- 20
229	Raseev	1981	T	StEx	---		b,B			18- 25
123	Thiel	1981	T	Xα	---		X		X	16- 50
175	Dittman	1982	T	Xα	---		a+A,b,B		a+A,b	16- 50
222	Morin	1982	E	P	NM		b,B			18- 24
104	Samson	1982	E	P	AB			O^+, O_2^+		18-103
236	Samson	1984	E	P	AB	✓				12-107

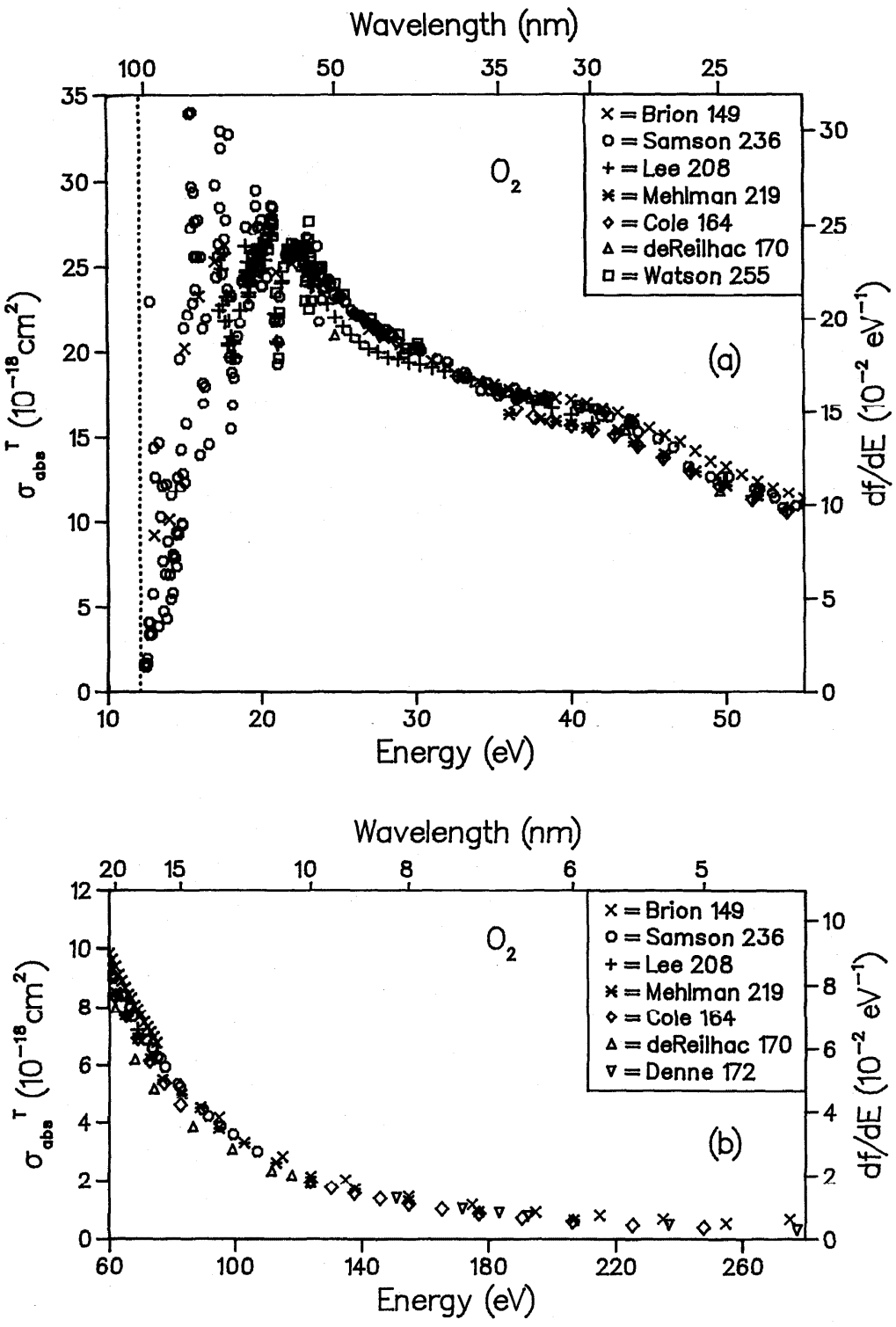

FIG. 18. Total photoabsorption cross section for O_2: (a) low-energy range, (b) high-energy range.

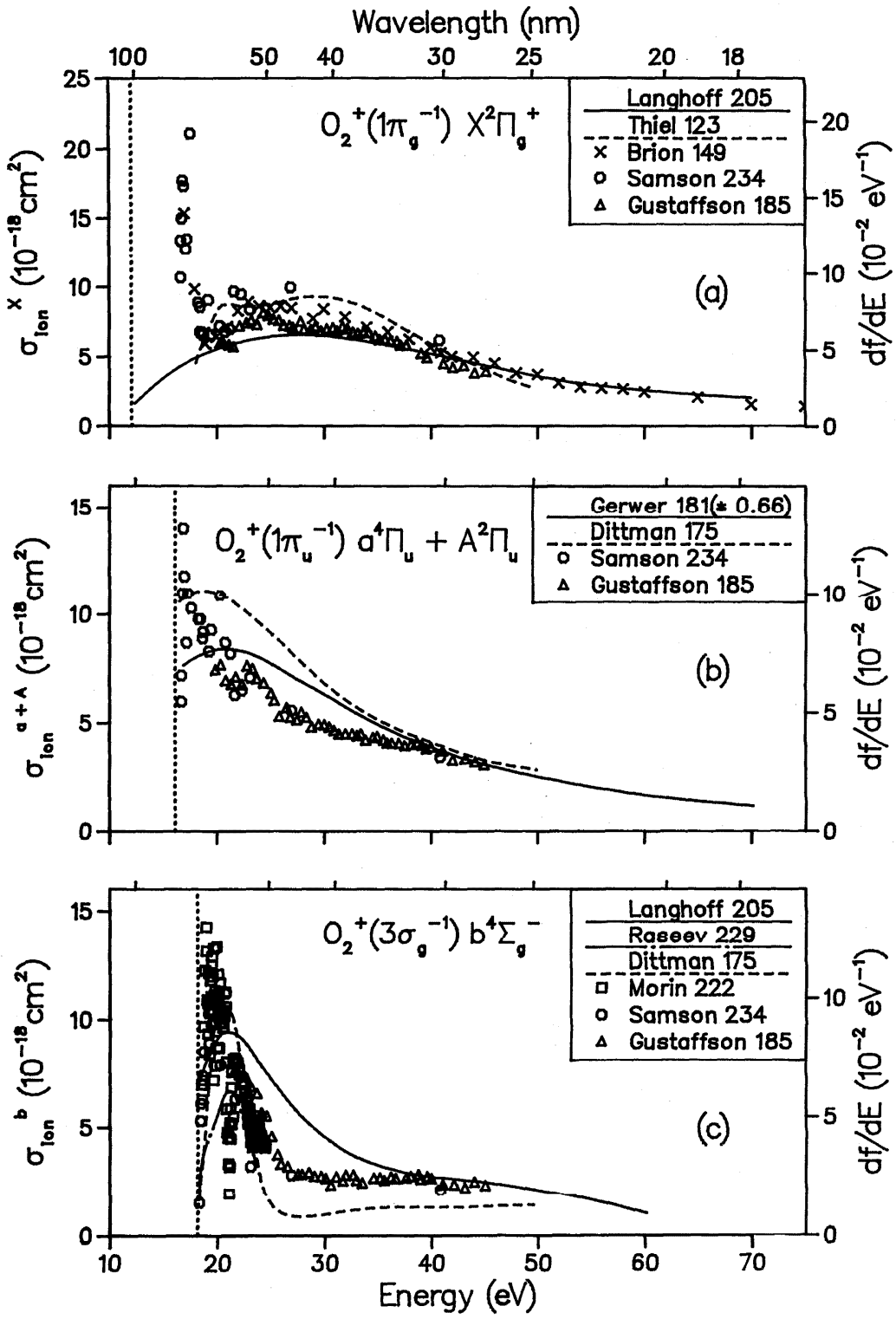

FIG. 19. Partial photoionization cross sections for O_2; (a) final ionic state = $X^2\Pi_g^+$, (b) final ionic state = $a^4\Pi_u + A^2\Pi_u$, (c) final ionic state = $b^4\Sigma_g^-$.

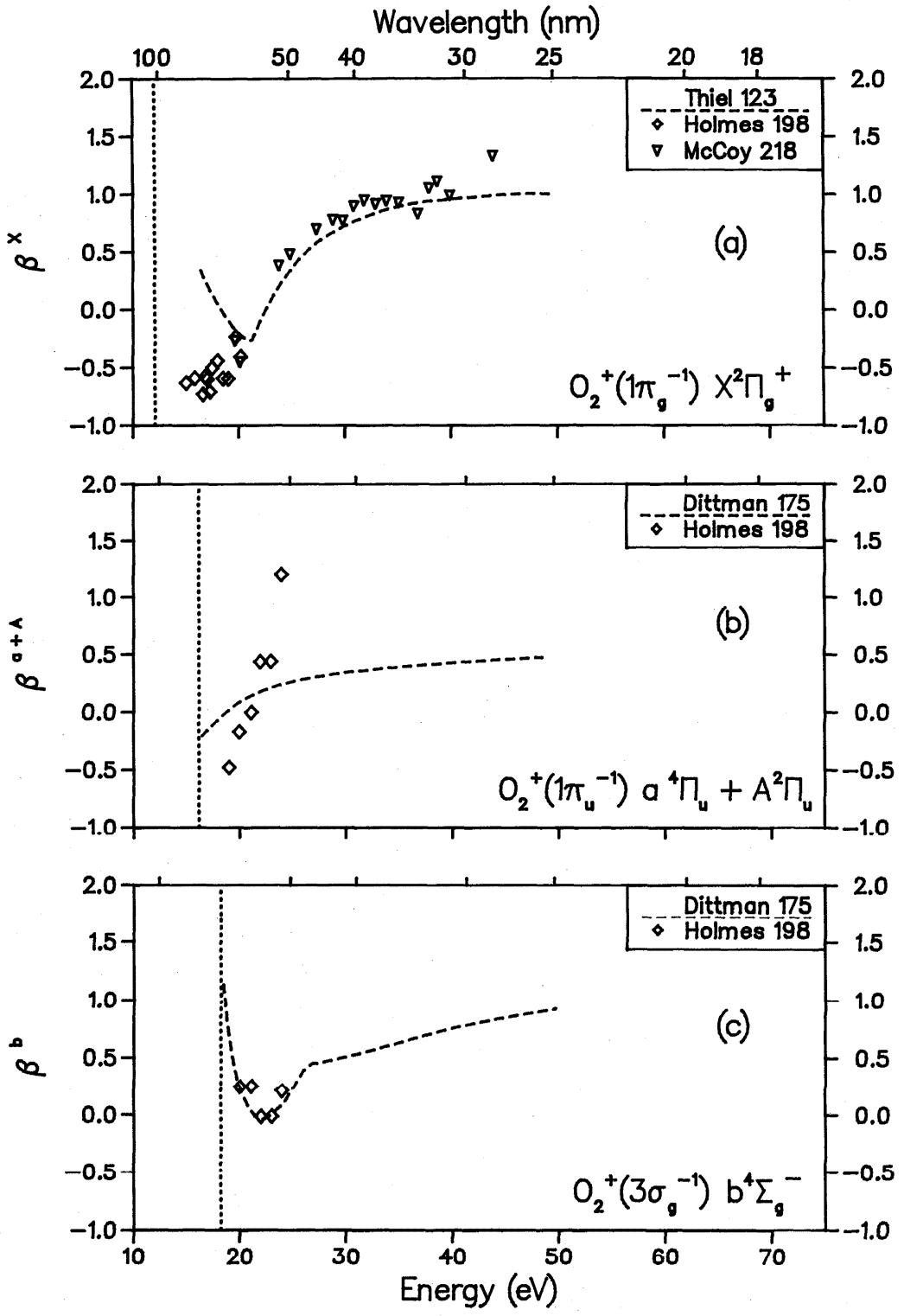

FIG. 20. Photoelectron asymmetry parameters for O_2; (a) final ionic state $= X^2\Pi_g^+$, (b) final ionic state $= a^4\Pi_u + A^2\Pi_u$, (c) final ionic state $= b^4\Sigma_g^-$.

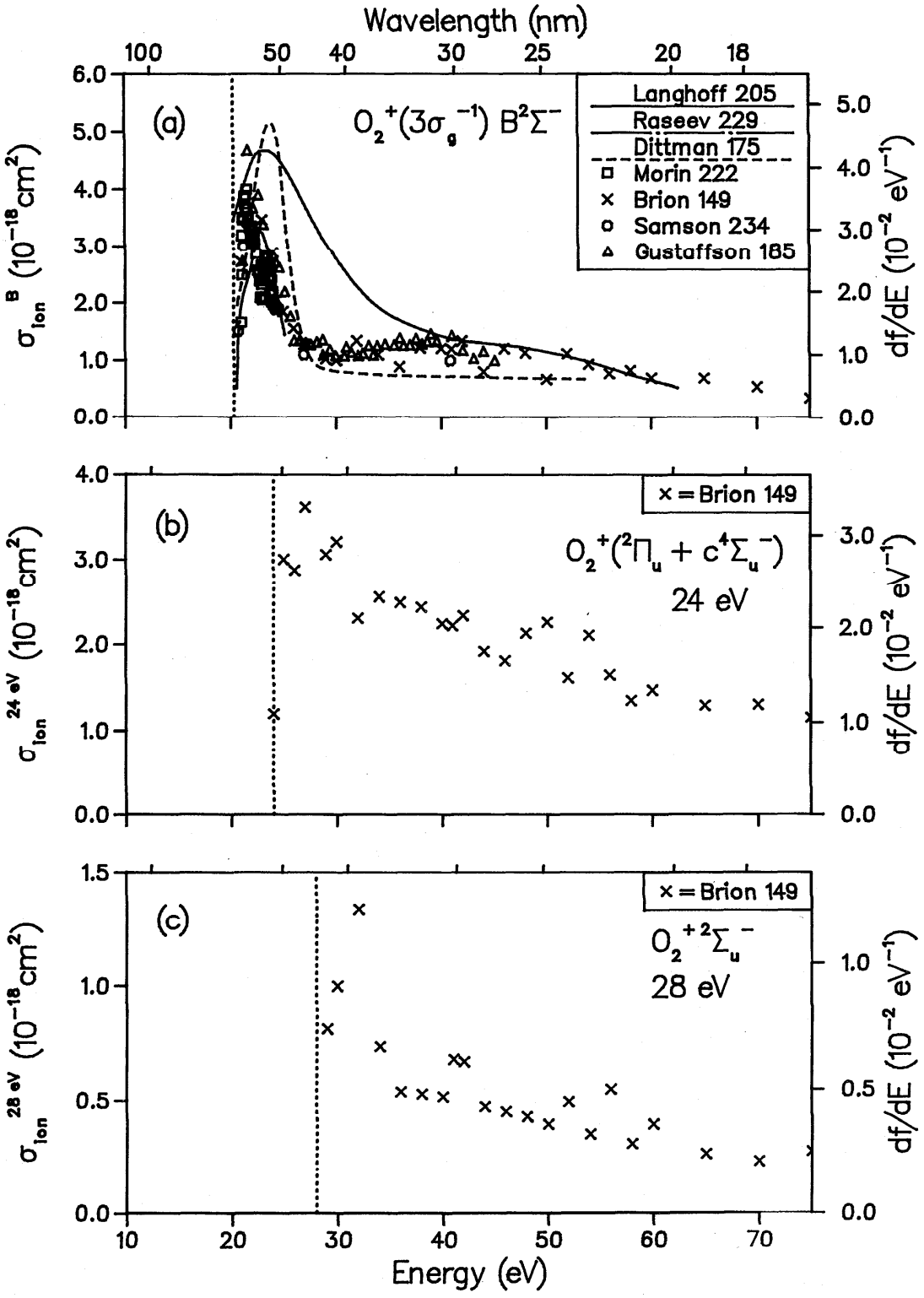

FIG. 21. Partial photoionization cross sections for O_2; (a) final ionic state = $B^2\Sigma^-$, (b) final ionic state = $^2\Pi_u + c^4\Sigma_u^-$, (c) final ionic state = $^2\Sigma_u^-$.

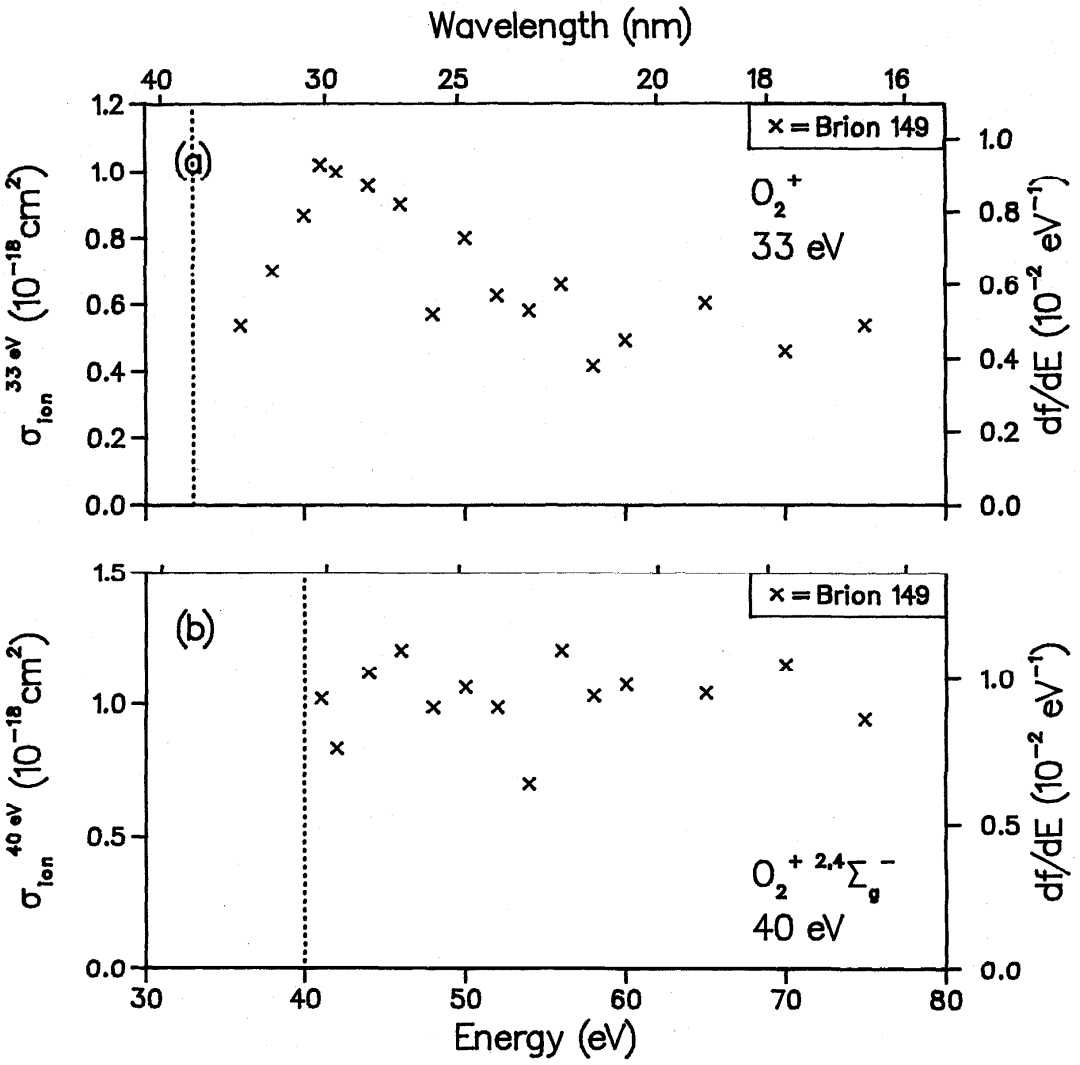

FIG. 22. Partial photoionization cross sections for O_2; (a) PES peak at 33 eV, (b) final ionic state = $^{2,4}\Sigma_g^-$.

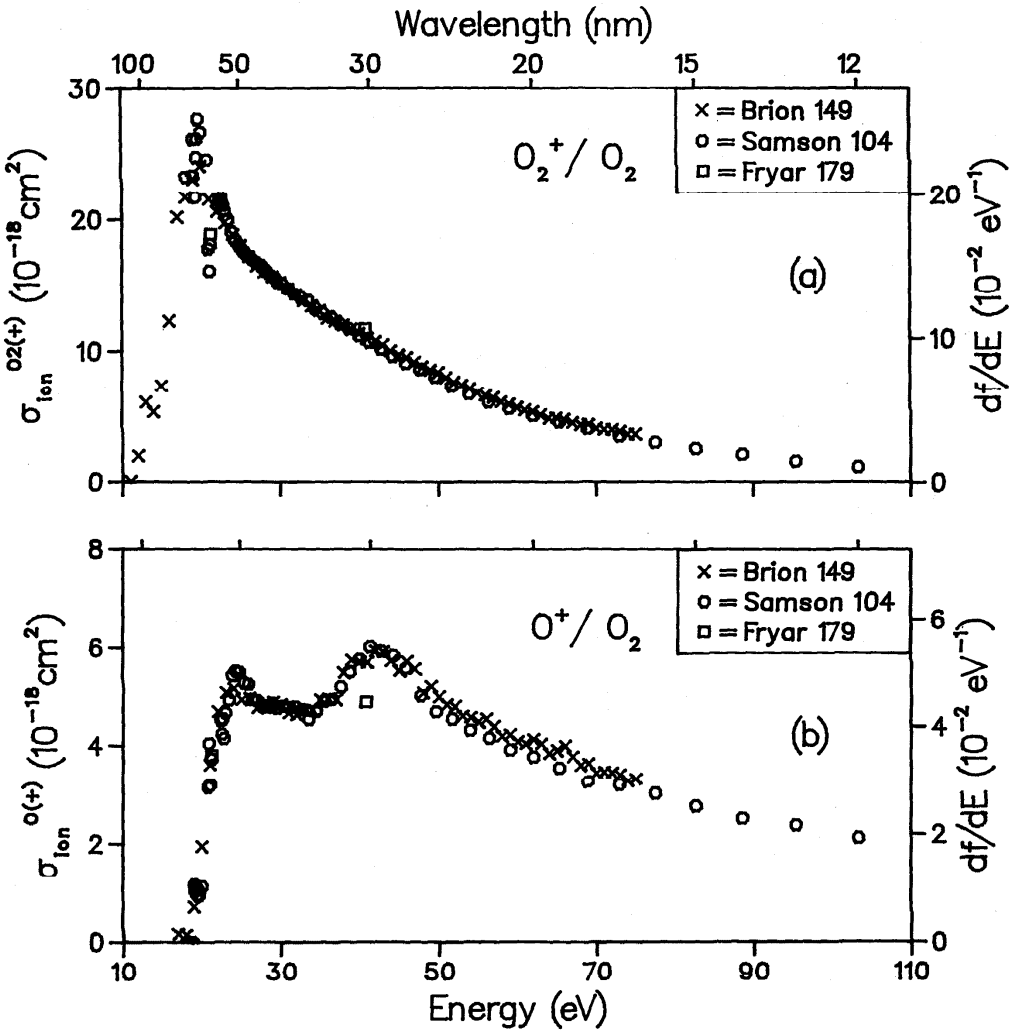

FIG. 23. Partial ionic photofragmentation cross sections of O_2; (a) product ion = O_2^+; (b) product ion = O^+.

Table 5. Data for CO.

Reference	Author	Year	E/T	Method	Experimental normalization	Cross Sections			Betas	Photon energy range (eV)
						Abs	State specific partials	Molecular ions and dissociative fragments	State	
208	Lee	1973	E	P	AB	✓				20- 70
253	Watson	1975	E	P	AB	✓				20- 35
168	Davenport	1976	T	Xα	---		X,B			16- 45
190	Hamnett	1976	E	DIP	TRK		X,A,E,C,$(3\sigma^{-1})$ W, 30-44 eV			18- 50
233	Samson	1976	E	P	AB		X,A,B			16- 40
256	Wight	1976	E	DIP	TRK	✓				18- 70
256	Wight	1976	E	DIP	TRK			CO^+,C^+,O^+,CO^{2+}		18- 60
170	de Reilhac	1977	E	P	AB	✓				25-118
88	Plummer	1977	E	P	AB		X,A,E,W,$(3\sigma^{-1})$			18- 50
164	Cole	1978	E	P	AB	✓				36- 83
224	Padial	1978	T	StEx	---		X,A,B			17- 50
214	Marr	1979	E	P	---				X,A,B	20- 45
252	Wallace	1979	T	Xα	---				A,B	15-150
198	Holmes	1980	E	P	---				X,A	18- 22
206	Langhoff	1981	T	CI	---		C,$(3\sigma^{-1})$			31- 58
215	Masuoka	1981	E	P	AB			CO^+,O^+,C^{2+}		22-140
238	Samson	1981	E	P	AB			C^+		22-140
246	Stephens	1981	T	Xα	---				X	14- 40
123	Thiel	1981	T	Xα	---		A			17- 50
204	Krummacher	1983	E	P	NM		C, 30-44 eV			33-102
211	Lucchese	1983	T	StEx	---		X		X	14- 40
192	Hermann	1984	T	StEx	---		X			14- 50
236	Samson	1984	E	P	AB	✓				14-125

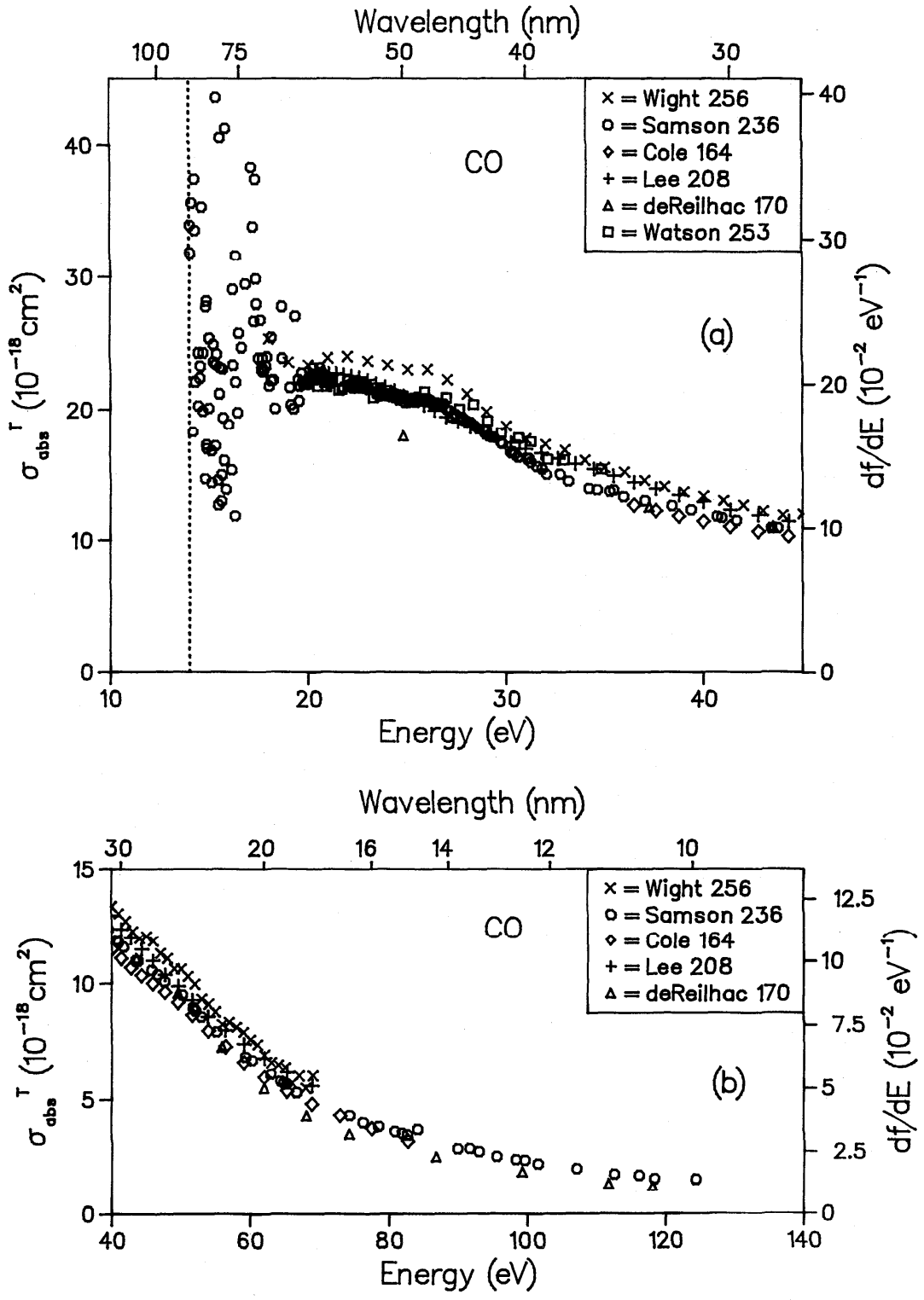

FIG. 24. Total photoabsorption cross section for CO: (a) low-energy range, (b) high-energy range.

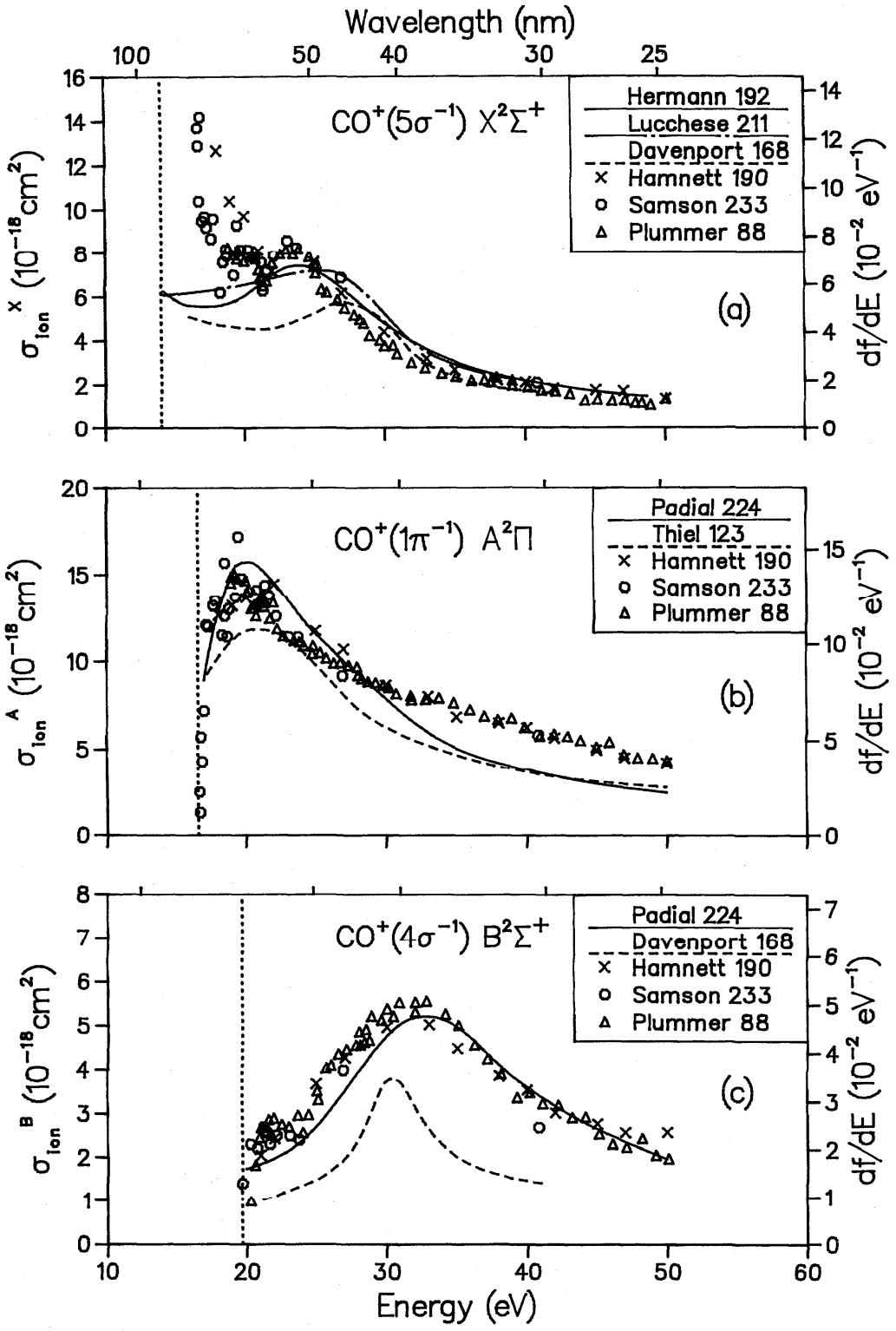

FIG. 25. Partial photoionization cross sections for CO; (a) final ionic state $= X^2\Sigma^+$, (b) final ionic state $= A^2\Pi$, (c) final ionic state $= B^2\Sigma^+$.

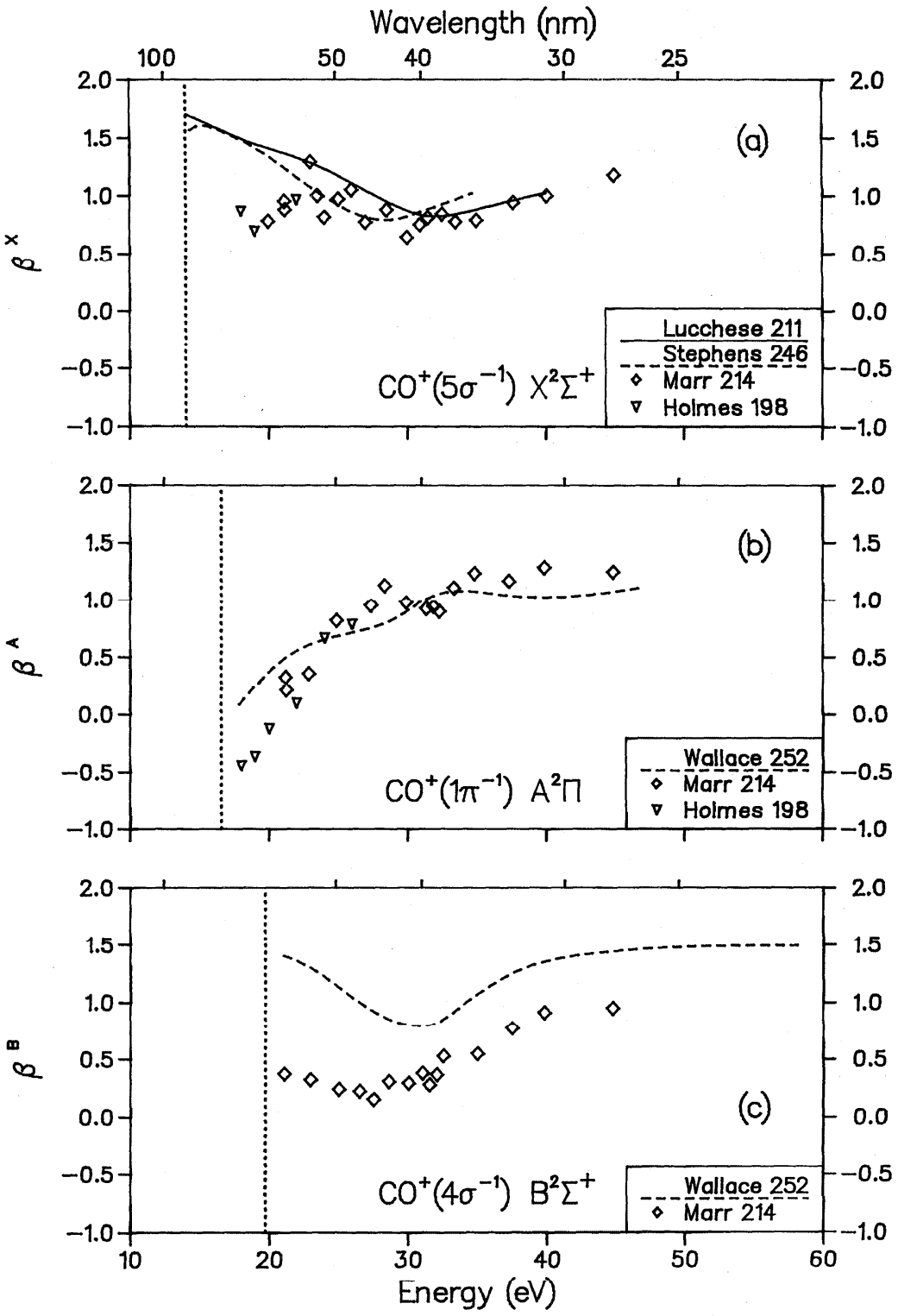

FIG. 26. Photoelectron asymmetry parameters for CO; (a) final ionic state = $X^2\Sigma^+$, (b) final ionic state = $A^2\Pi$, (c) final ionic state = $B^2\Sigma^+$.

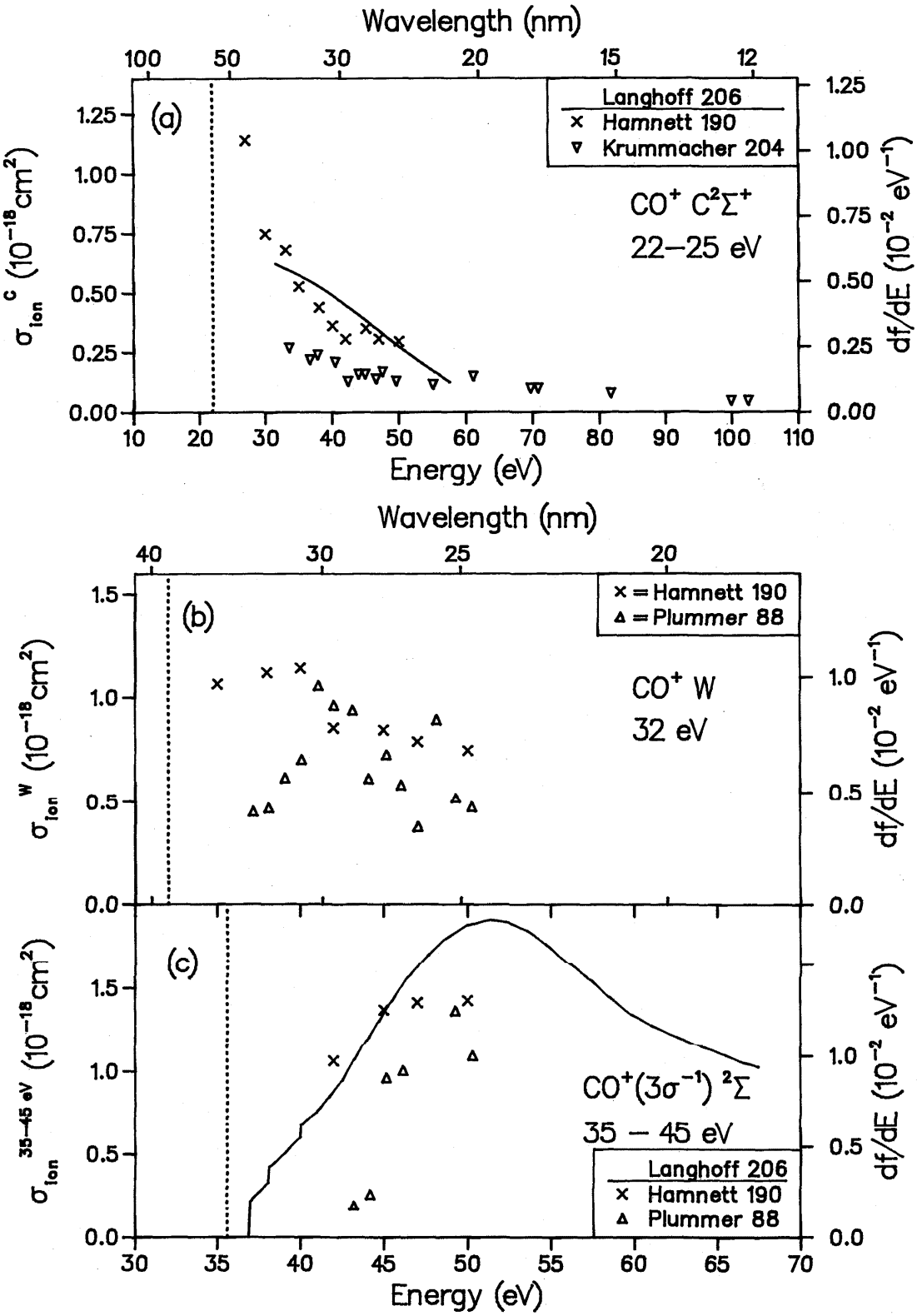

FIG. 27. Partial photoionization cross sections for CO; (a) final ionic state = $C^2\Sigma^+$, (b) final ionic state = W (PES peak at 32 eV), (c) final ionic state = $^2\Sigma$ (PES peak at 35 – 45 eV).

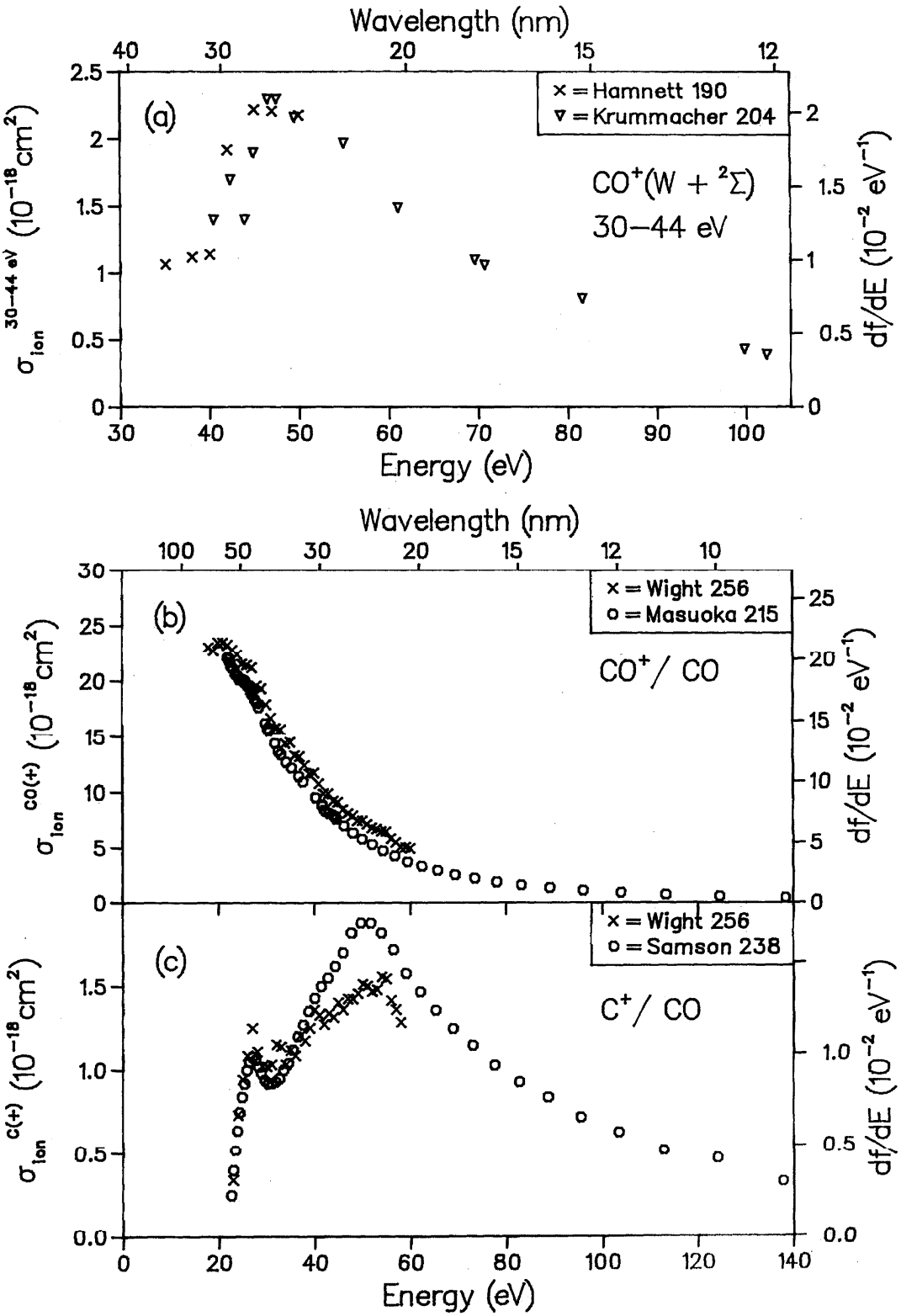

FIG. 28. (a) Partial photoionization cross section for CO, final ionic state = $W + {}^2\Sigma$ (PES peak at 30–44 eV); (b) Partial ionic photofragmentation cross section for CO, product ion = CO^+. (c) Partial ionic photofragmentation cross section for CO, product ion = C^+.

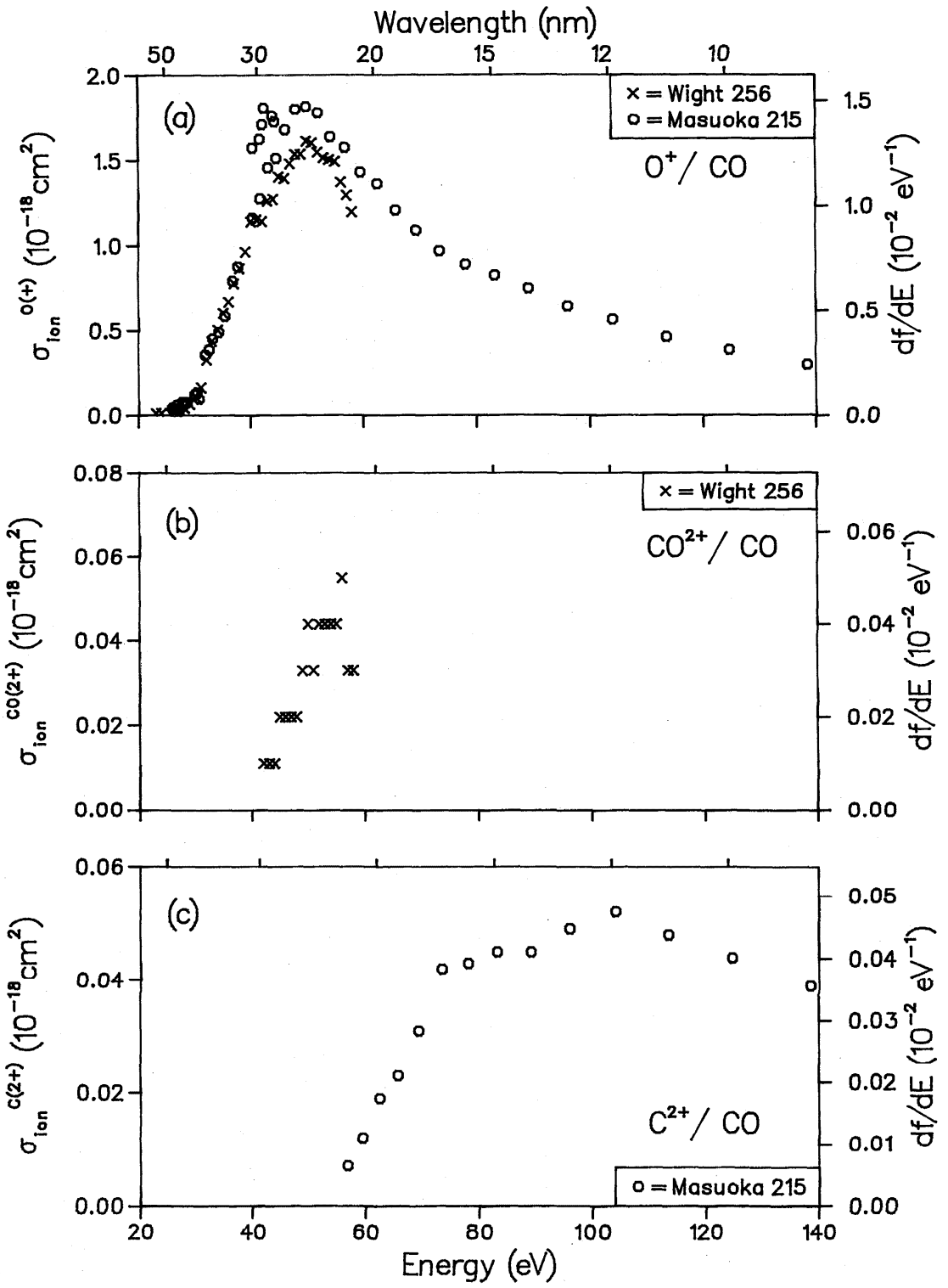

FIG. 29. Partial ionic photofragmentation cross sections for CO; (a) product ion = O^+, (b) product ion = CO^{2+}, (c) product ion = C^{2+}.

Table 6. Data for NO.

Reference	Author	Year	E/T	Method	Experimental normalization	Cross Sections			Betas	Photon energy range (eV)
						Abs	State specific partials	Molecular ions and dissociative fragments	State	
180	Gardner	1973	E	P	AB	✓				20- 33
208	Lee	1973	E	P	AB	✓				20- 70
170	de Reilhac	1977	E	P	AB	✓				24-124
164	Cole	1978	E	P	AB	✓				36-250
187	Gustaffson	1981	E	P	NM		c,B			22- 40
245	Southworth	1982	E	P	NM		X,b,c		X,b,c	16- 31
251	Wallace	1982	T	Xα	---		X,b,B,c,$(3\sigma^{-1})$		X,b,c	10- 50
241	Smith	1983	T	---	---		X		X	9- 40
165	Collins	1984	T	---	---		X		X	9- 40
193	Hermann	1984	T	StEx	---		b,A			
220	Morin	1984	E	P	NM		b,A			22- 30
239	Samson	1985	E	P	NM			NO^+, N^+, O^+, NO^{2+}		20- 80
242	Smith	1985	T	StEx	---		A,b,B,c		b,c	21- 32
191	Hermann	1986	T	StEx	---		X,14-20 eV,B,c			9- 55
200	Iida	1986	E	DIP	TRK	✓				6-190
200	Iida	1986	E	DIP	TRK		X,14-20 eV,c+B+B' 26-36 eV,$(3\sigma^{-1})$			18- 60
200	Iida	1986	E	DIP	TRK			NO^+, N^+, O^+, NO^{2+}		9- 80

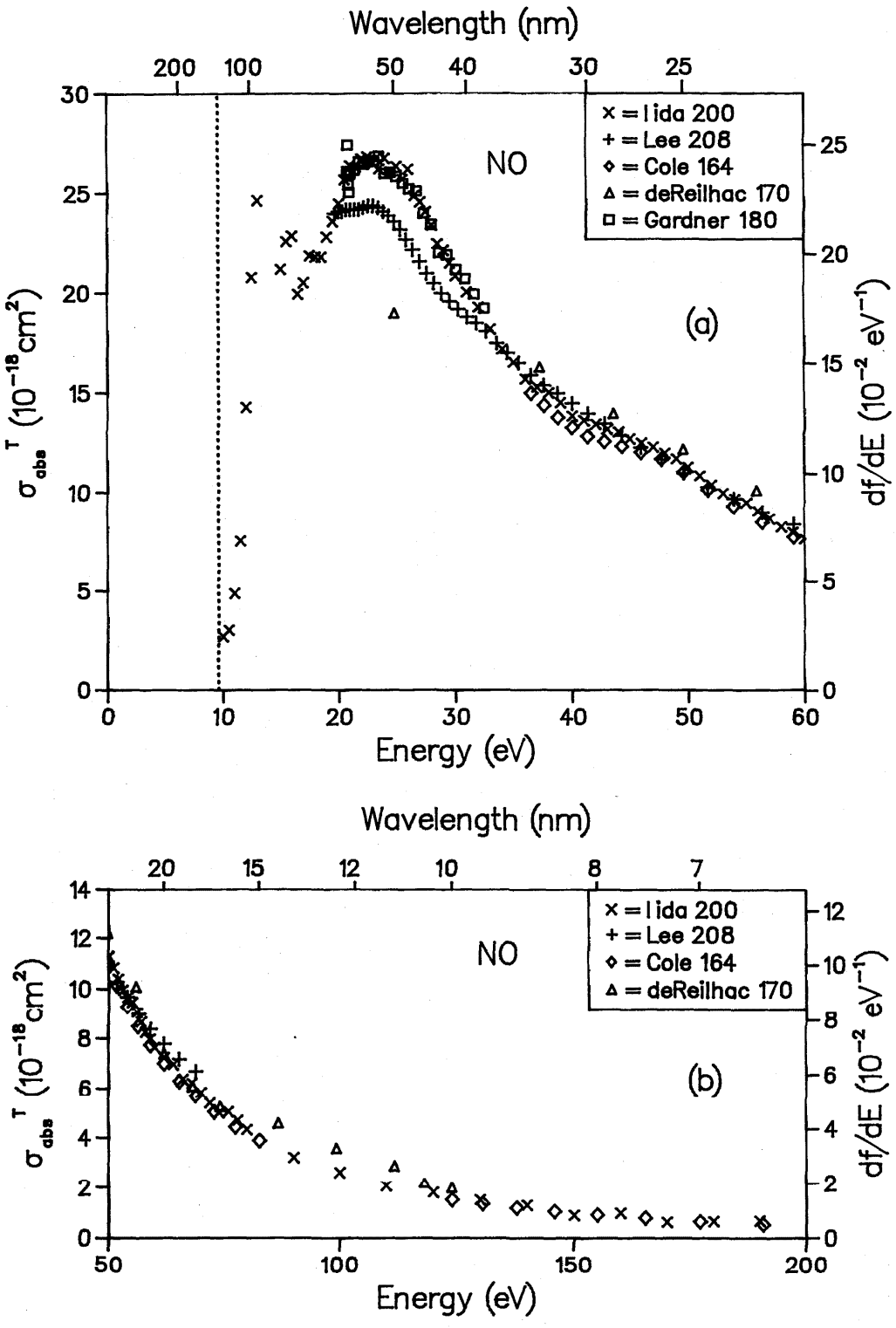

FIG. 30. Total photoabsorption cross section for NO: (a) low-energy range, (b) high-energy range.

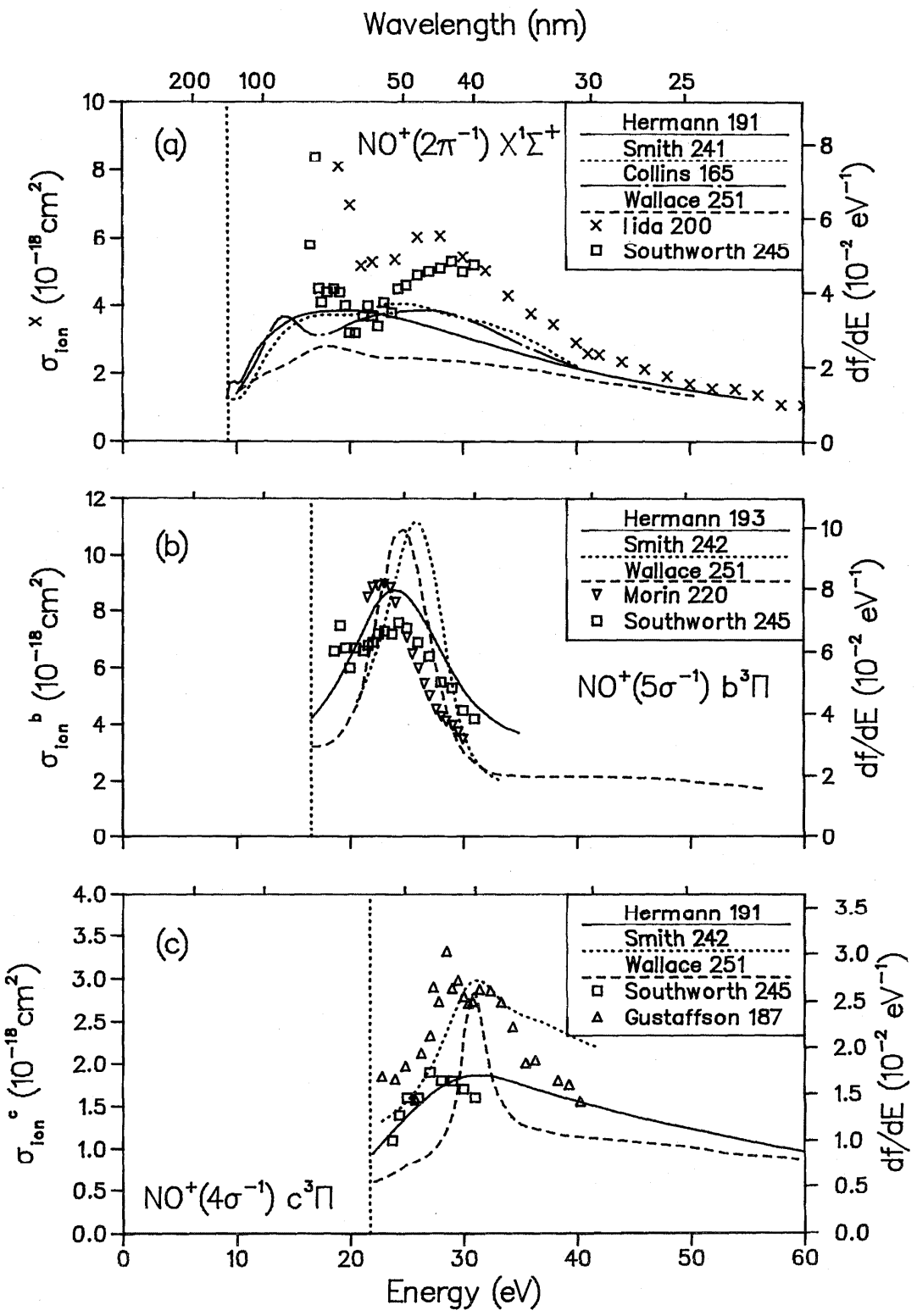

FIG. 31. Partial photoionization cross sections for NO; (a) final ionic state $= X\,^1\Sigma^+$, (b) final ionic state $= b\,^3\Pi$, (c) final ionic state $= c^3\Pi$.

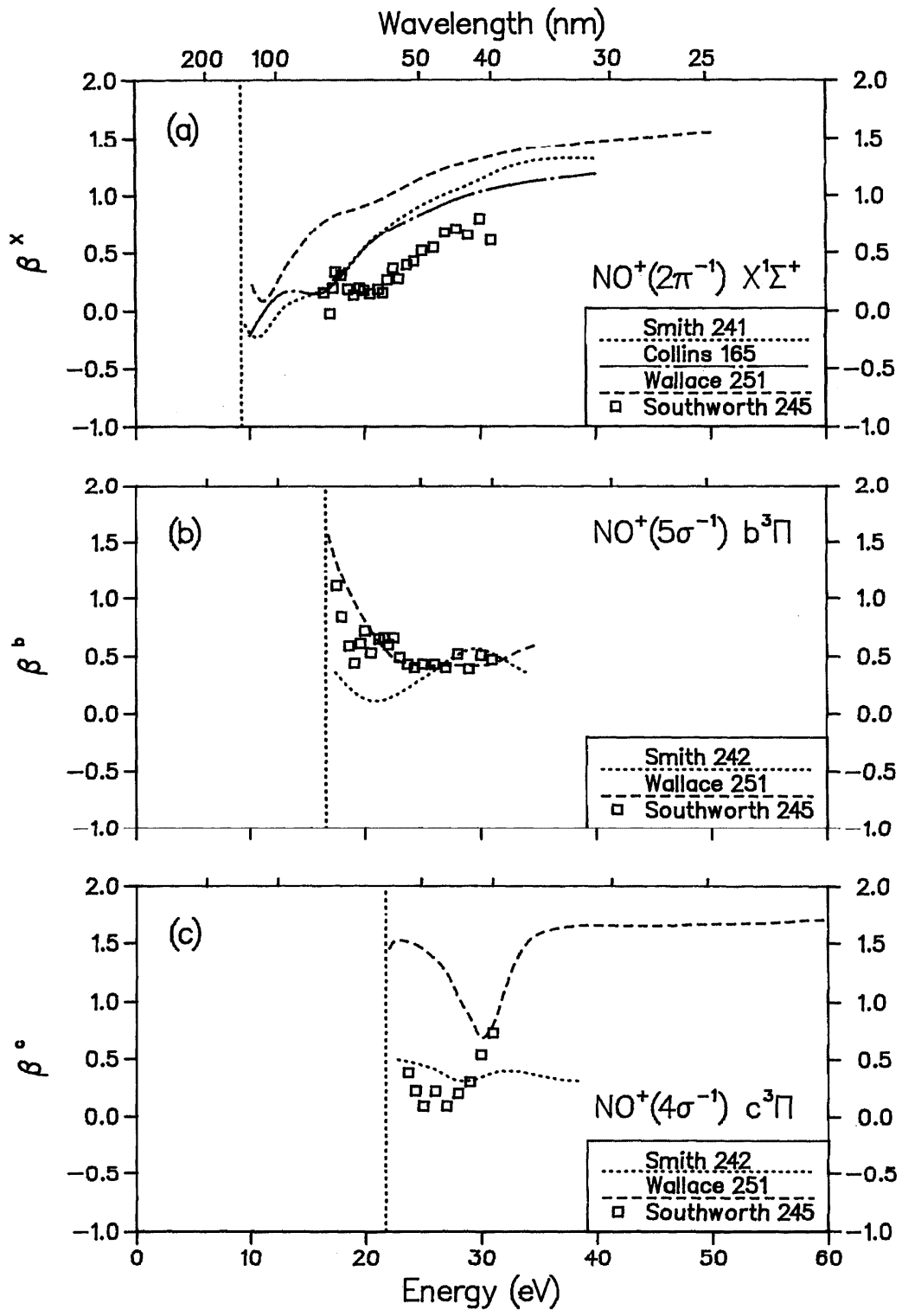

FIG. 32. Photoelectron asymmetry parameters for NO; (a) final ionic state = $X\,^1\Sigma^+$, (b) final ionic state = $b\,^3\Pi$, (c) final ionic state = $c^3\Pi$.

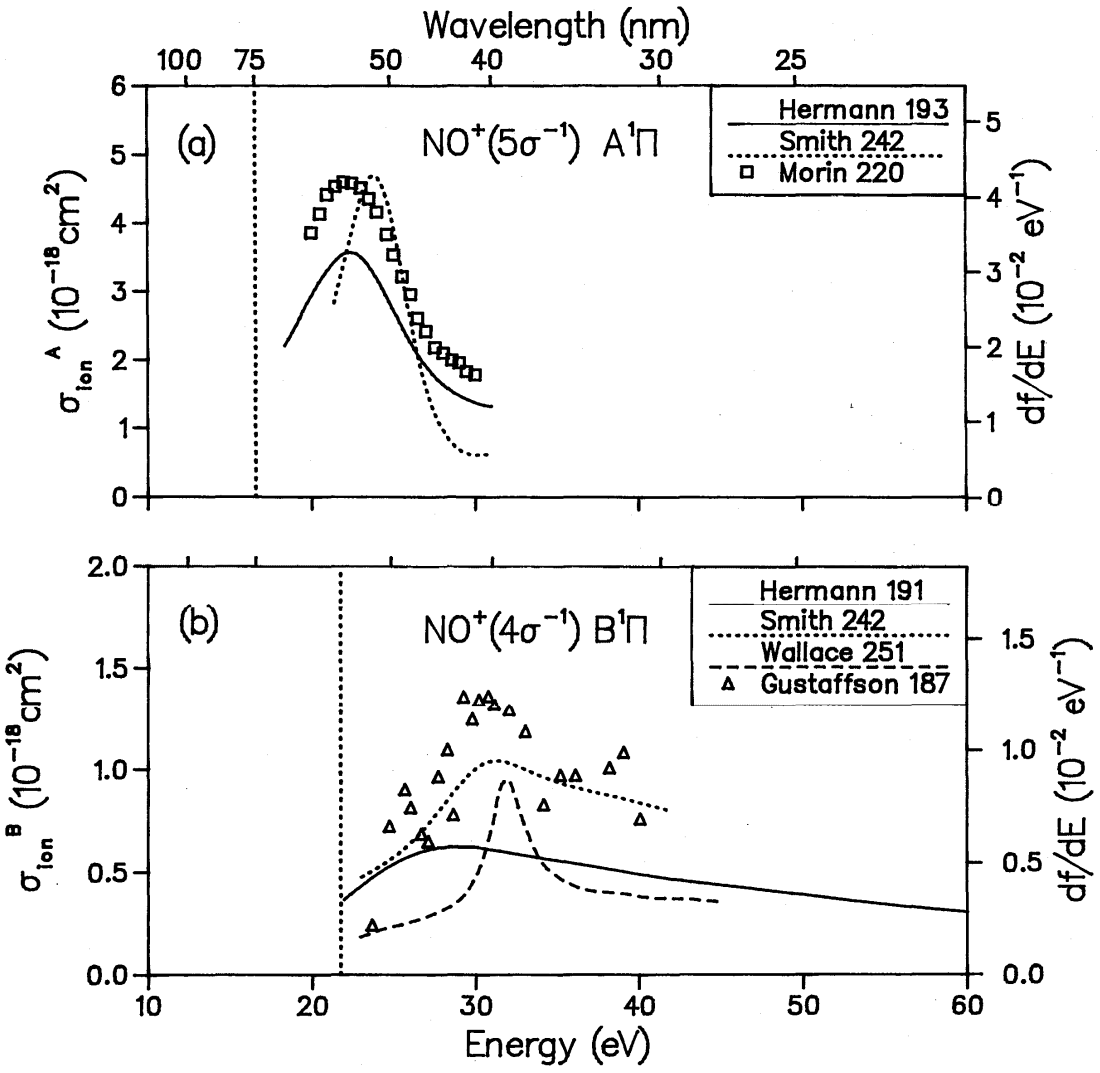

FIG. 33. Partial photoionization cross sections for NO; (a) final ionic state = $A\ ^1\Pi$, (b) final ionic state = $B\ ^1\Pi$.

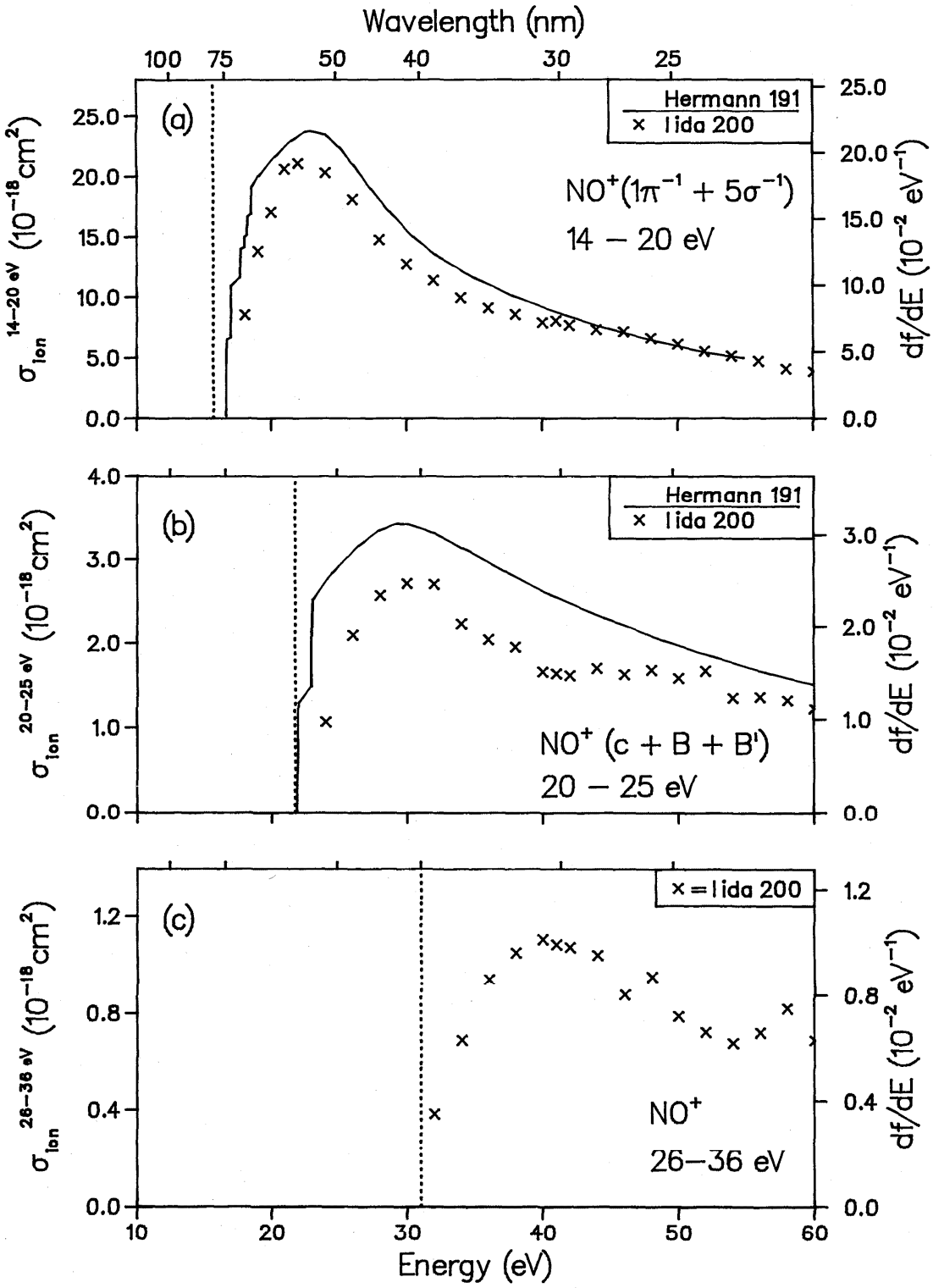

FIG. 34. Partial photoionization cross sections for NO; (a) final ionic state = PES peak at 14–20 eV, (b) final ionic state = $c + B + B'$, (c) final ionic state = PES peak at 26–36 eV.

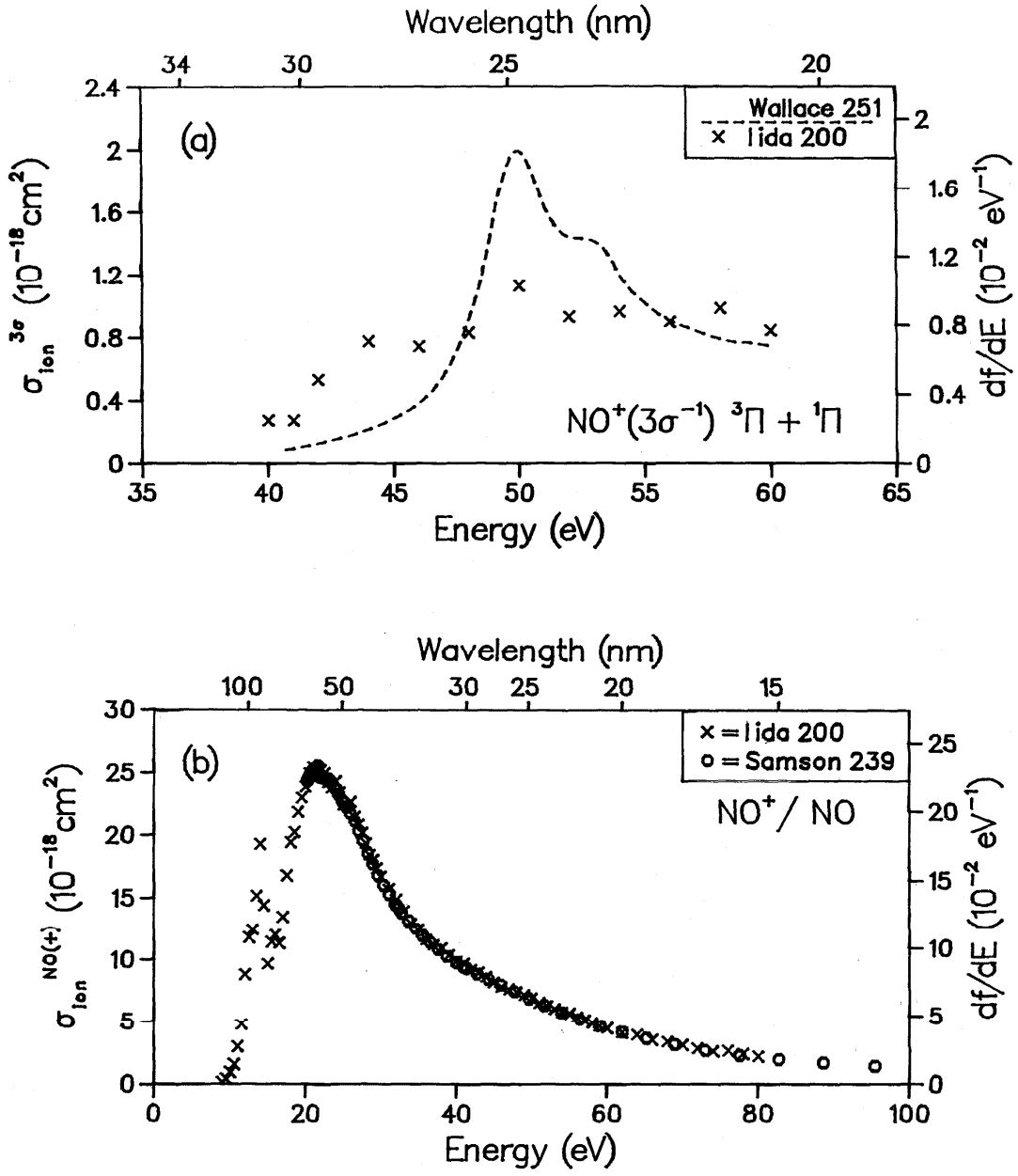

FIG. 35. (a) Partial photoionization cross section for NO, final ionic state = $^3\Pi + {}^1\Pi$; (b) Partial ionic photofragmentation cross section for NO, product ion = NO^+.

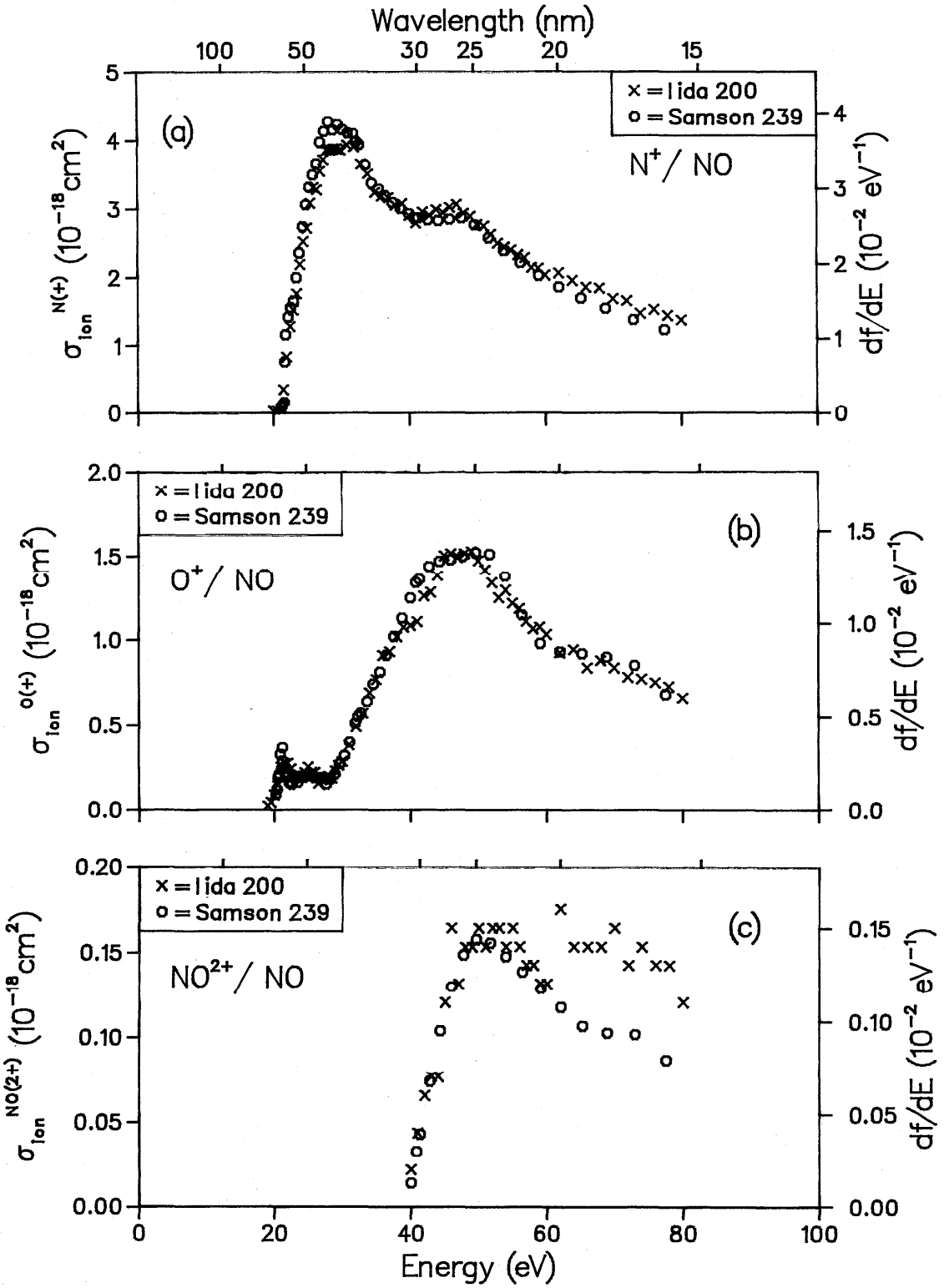

FIG. 36. Partial ionic photofragmentation cross sections for NO; (a) product ion = N^+, (b) product ion = O^+, (c) product ion = NO^{2+}.

Table 7. Data for CO_2.

Reference	Author	Year	E/T	Method	Experimental normalization	Cross Sections			Betas	Photon energy range (eV)
						Abs	State specific partials	Molecular ions and dissociative fragments	State	
179	Fryar	1973	E	P	NM			CO_2^+, CO^+, O^+		21- 40
208	Lee	1973	E	P	AB	✓				17- 70
253	Watson	1975	E	P	AB	✓				19- 33
170	de Reilhac	1977	E	P	AB	✓				24-125
147	Brion	1978	E	DIP	NM		X,A+B,C,MET[a]			21- 60
188	Gustaffson	1978	E	P	NM		X,A+B,C			20- 40
195	Hitchock	1980	E	DIP	TRK	✓		$CO_2^+, CO^+, O^+, C^+, CO_2^{2+}$		8- 80
217	Masuoka	1980	E	P	AB			$CO_2^+, CO^+, O^+, C^+, CO_2^{2+}, C^{2+}$		19-138
247	Swanson	1980	T	$X\alpha$	---		X,C			15- 45
183	Grimm	1981	E	P	NM				X,A,B,C	14- 50
183	Grimm	1981	T	$X\alpha$	---				X,A,B,C	15- 50
225	Padial	1981	T	StEx	---		X,A,A+B,B,C			13- 50
238	Samson	1981	E	P	AB			C^+		22-138
210	Lucchese	1982	T	StEx	---		X,A,A+B,B,C		X,A,B,C	14- 50
165	Collins	1984	T	StEx	---		C		C	25- 45
231	Roy	1984	E	P	NM		C		C	20- 50
236	Samson	1984	E	P	AB	✓				14-107
236	Samson	1984	E	P	AB		X,A+B,C			14- 40

[a]MET = many-body states arising from inner valence ionization.

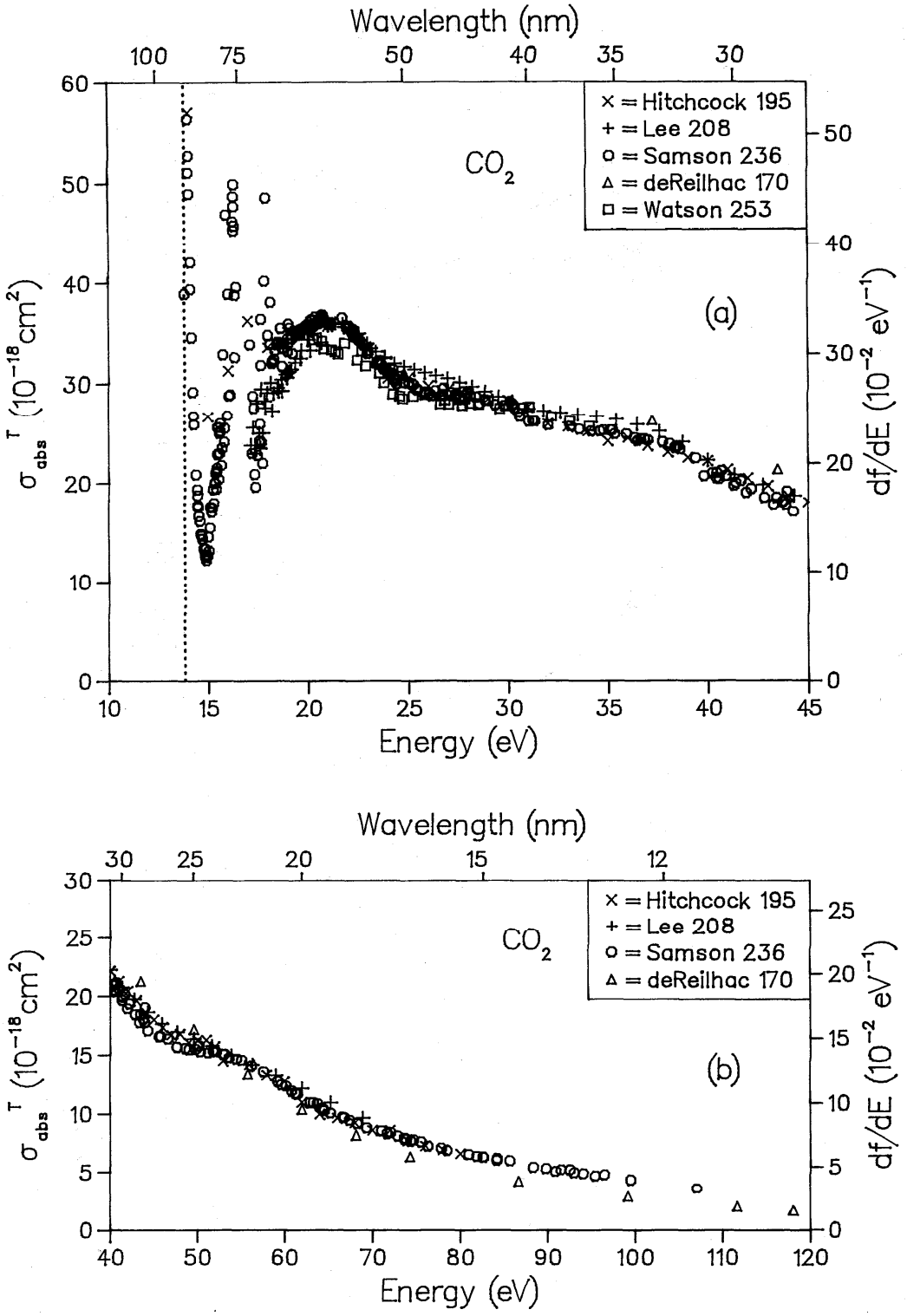

FIG. 37. Total photoabsorption cross section for CO_2: (a) low-energy range, (b) high-energy range.

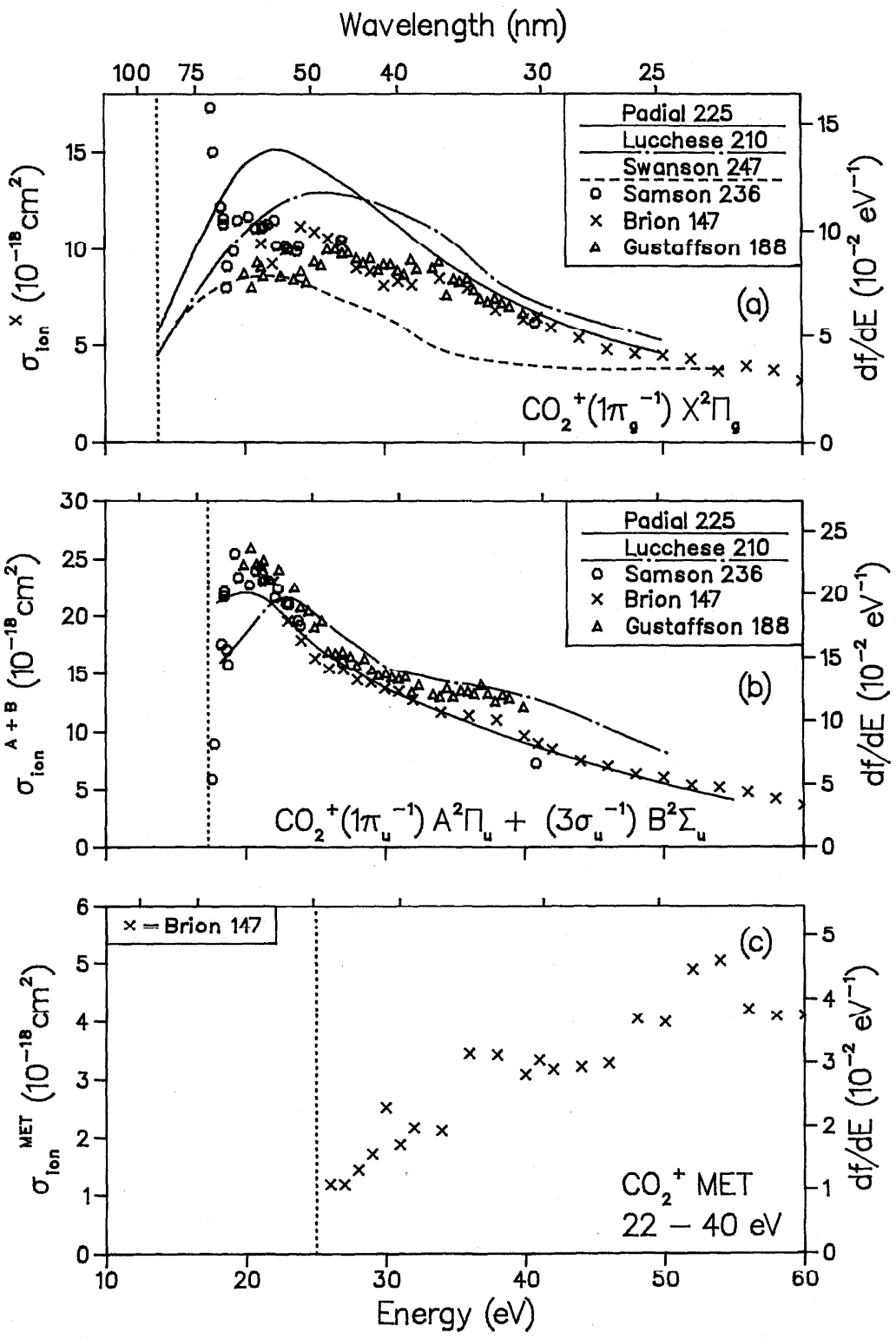

FIG. 38. Partial photoionization cross sections for CO_2; (a) final ionic state = $X^2\Pi_g$, (b) final ionic state = $A^2\Pi_u + B^2\Sigma_u$, (c) final ionic state = PES peak at 22–40 eV.

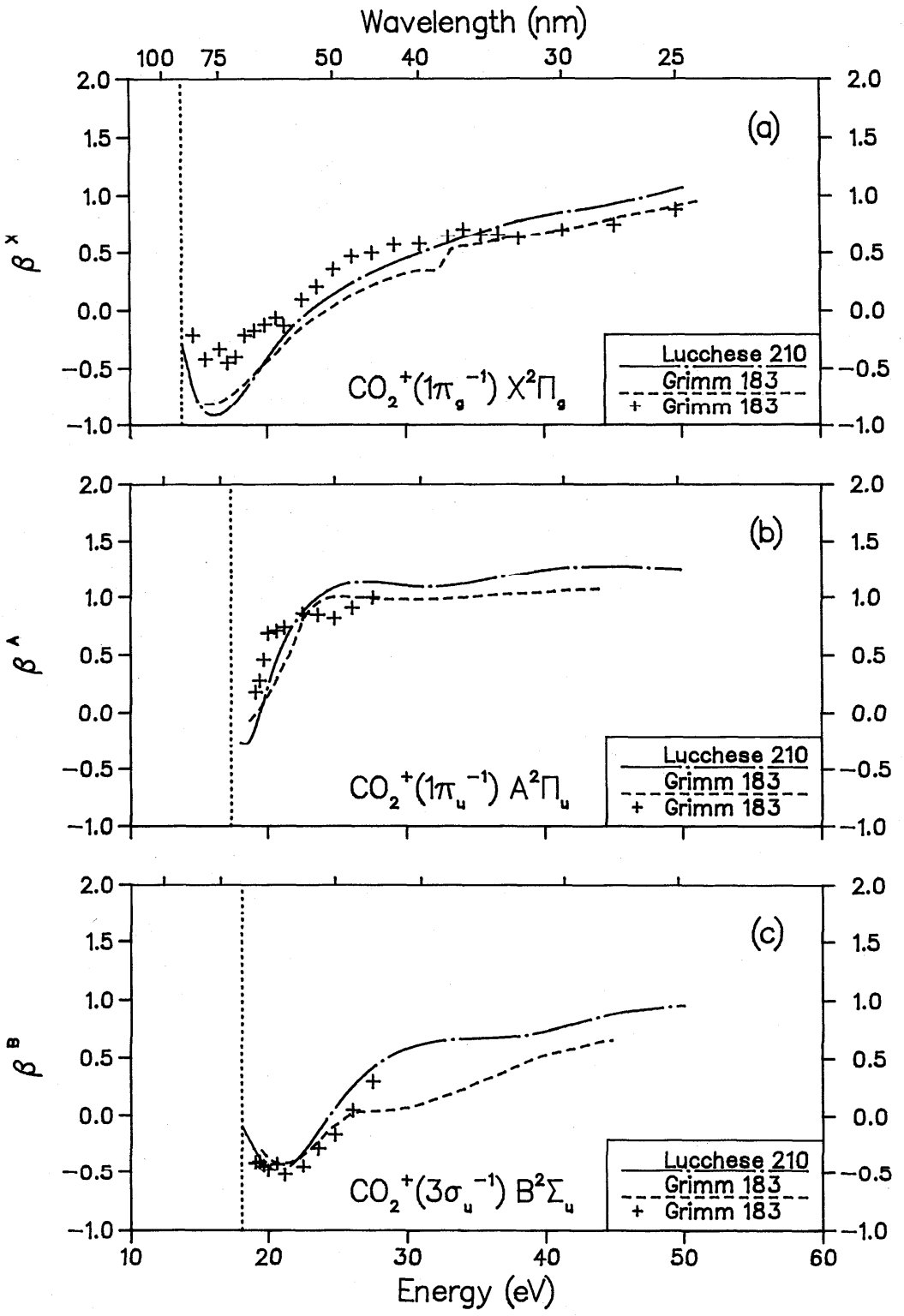

FIG. 39. Photoelectron asymmetry parameters for CO_2; (a) final ionic state $= X\,^2\Pi_g$, (b) final ionic state $= A\,^2\Pi_u$, (c) final ionic state $= B\,^2\Sigma_u$.

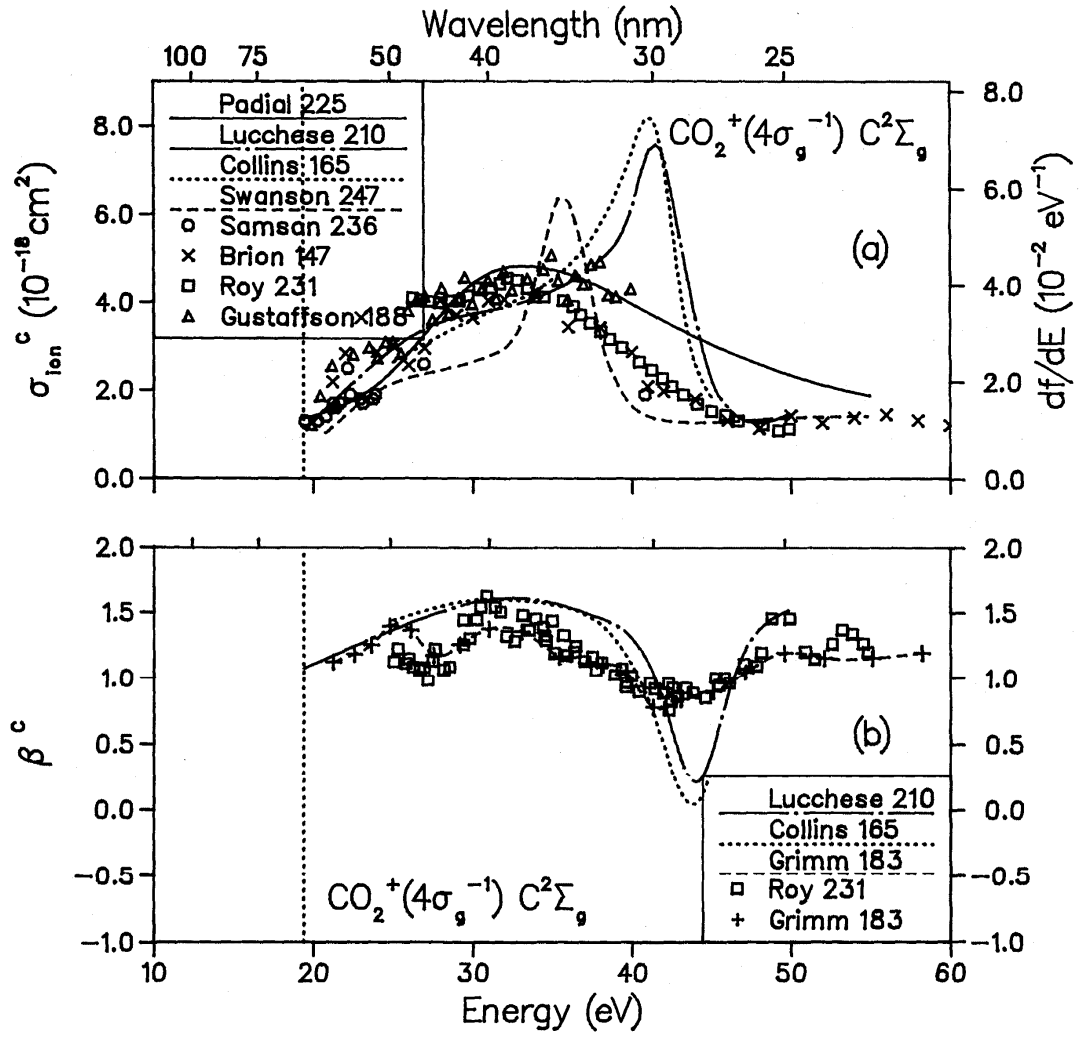

FIG. 40. (a) Partial photoionization cross sections for CO_2, final ionic state = $C^2\Sigma_g$, (b) photoelectron asymmetry parameter for CO_2, final ionic state = $C^2\Sigma_g$.

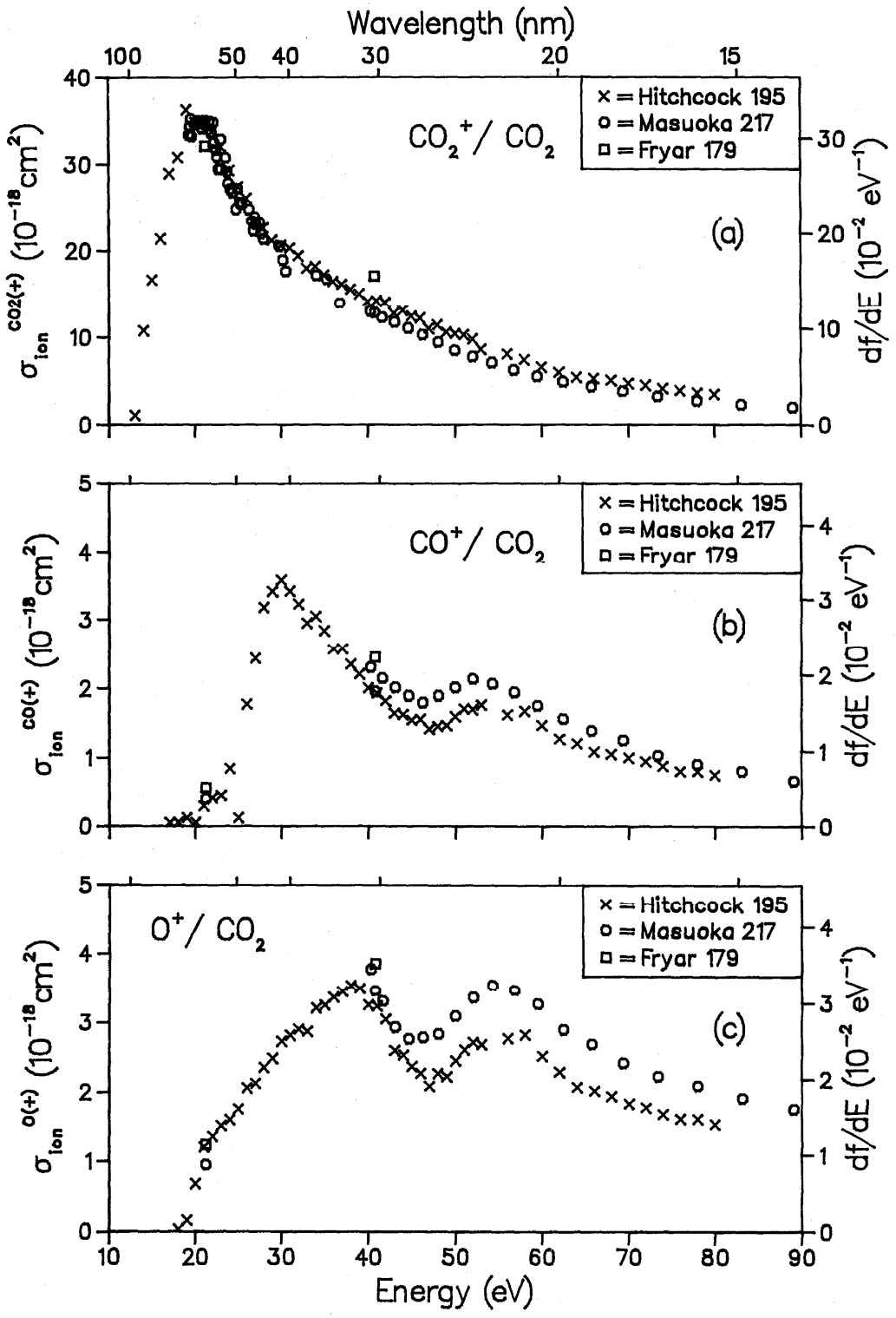

FIG. 41. Partial ionic photofragmentation cross sections for CO_2; (a) product ion = CO_2^+, (b) product ion = CO^+, (c) product ion = O^+.

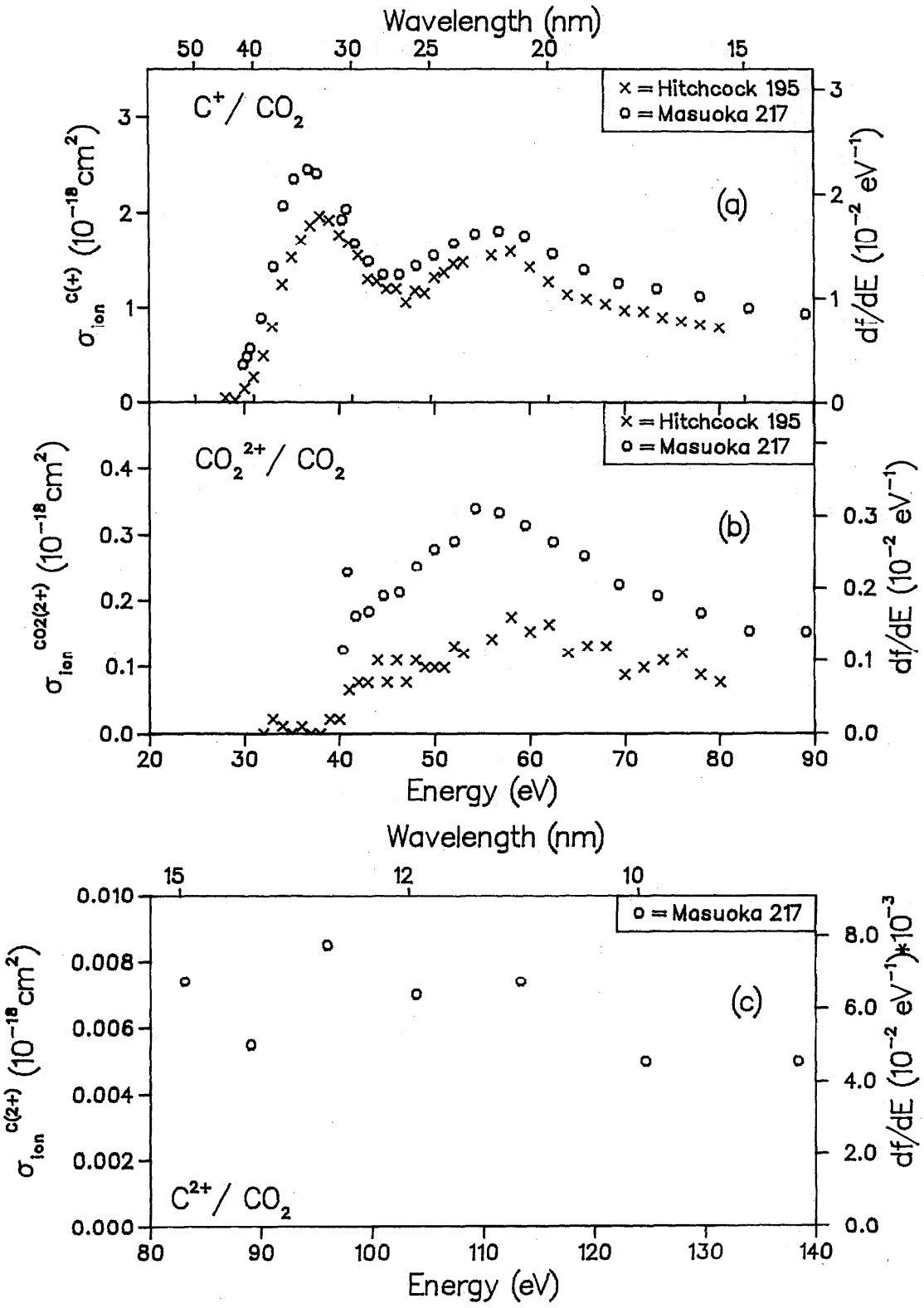

FIG. 42. Partial ionic photofragmentation cross sections for CO_2; (a) product ion = C^+, (b) product ion = CO_2^{2+}, (c) product ion = C^{2+}.

Table 8. Data for N_2O.

Reference	Author	Year	E/T	Method	Experimental normalization	Cross Sections			Betas	Photon energy range (eV)
						Abs	State specific partials	Molecular ions and dissociative fragments	State	
208	Lee	1973	E	P	AB	√				17- 70
170	de Reilhac	1977	E	P	AB	√				25-120
164	Cole	1978	E	P	AB	√				36-250
147	Brion	1978	E	DIP	NM	√				17- 60
147	Brion	1978	E	DIP	NM		X,A,B,C,24 eV,MET[a]			17- 60
195	Hitchcock	1980	E	DIP	TRK	√				8- 74
195	Hitchcock	1980	E	DIP	TRK			$N_2O^+, NO^+, N_2^+, O^+, N^+$		11- 74
156	Carlson	1983	E	P	NM		X,A,B,C		X,A,B,C	19- 70
156	Carlson	1983	T	$X\alpha$	---		X,A,B,C		X,A,B,C	19- 70
248	Truesdale	1983	E	P	NM		X,A,B,C		X,A,B,C	19- 31
237	Samson	1984	E	P	AB			$N_2O^+, NO^+, N_2^+, O^+, N^+$		19- 31
194	Hermann	1987	T	StEx	---		X,A,B,C			13- 52

[a]MET = many-body states arising from inner valence ionization.

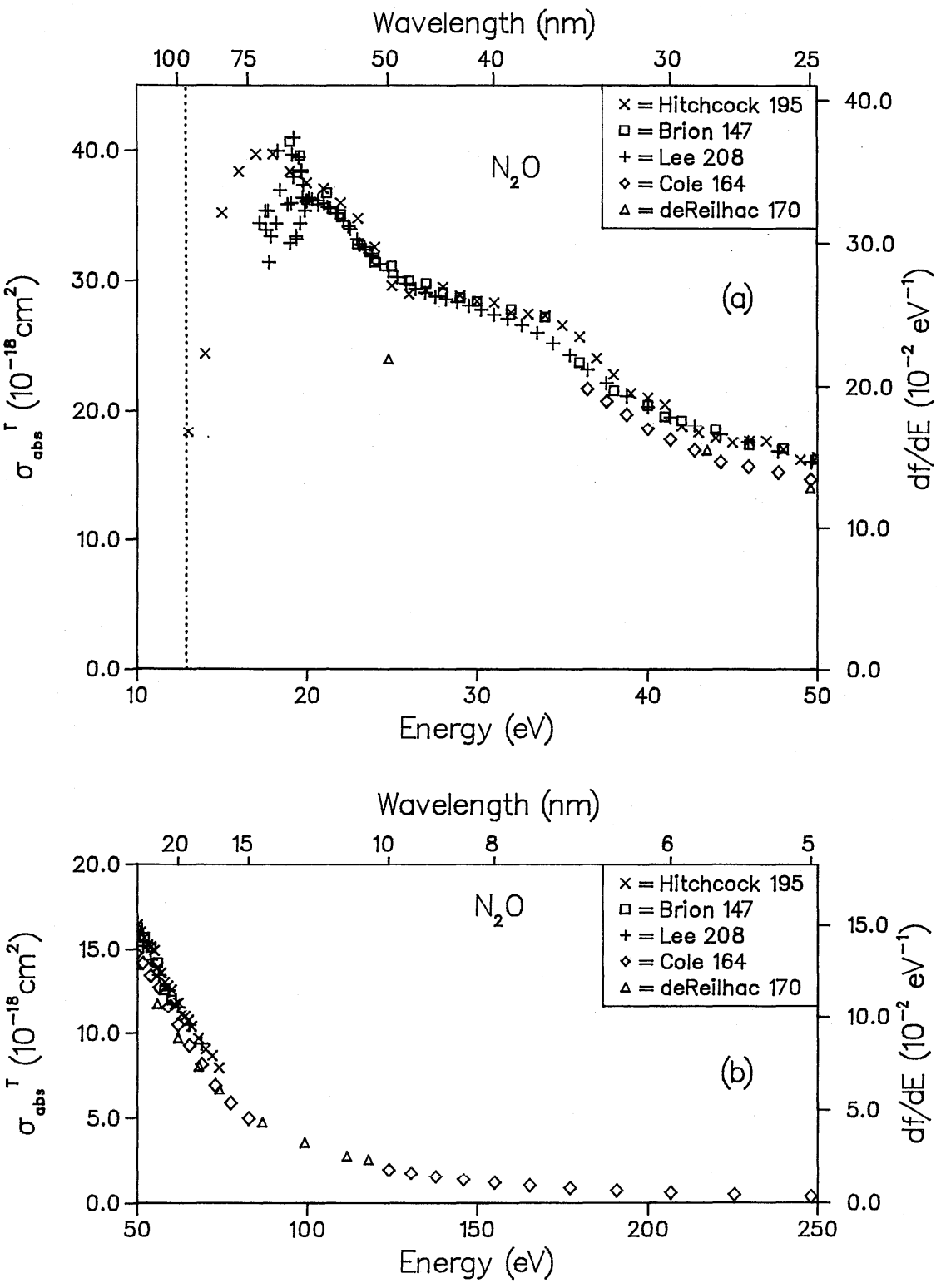

FIG. 43. Total photoabsorption cross section for N_2O: (a) low-energy range, (b) high-energy range.

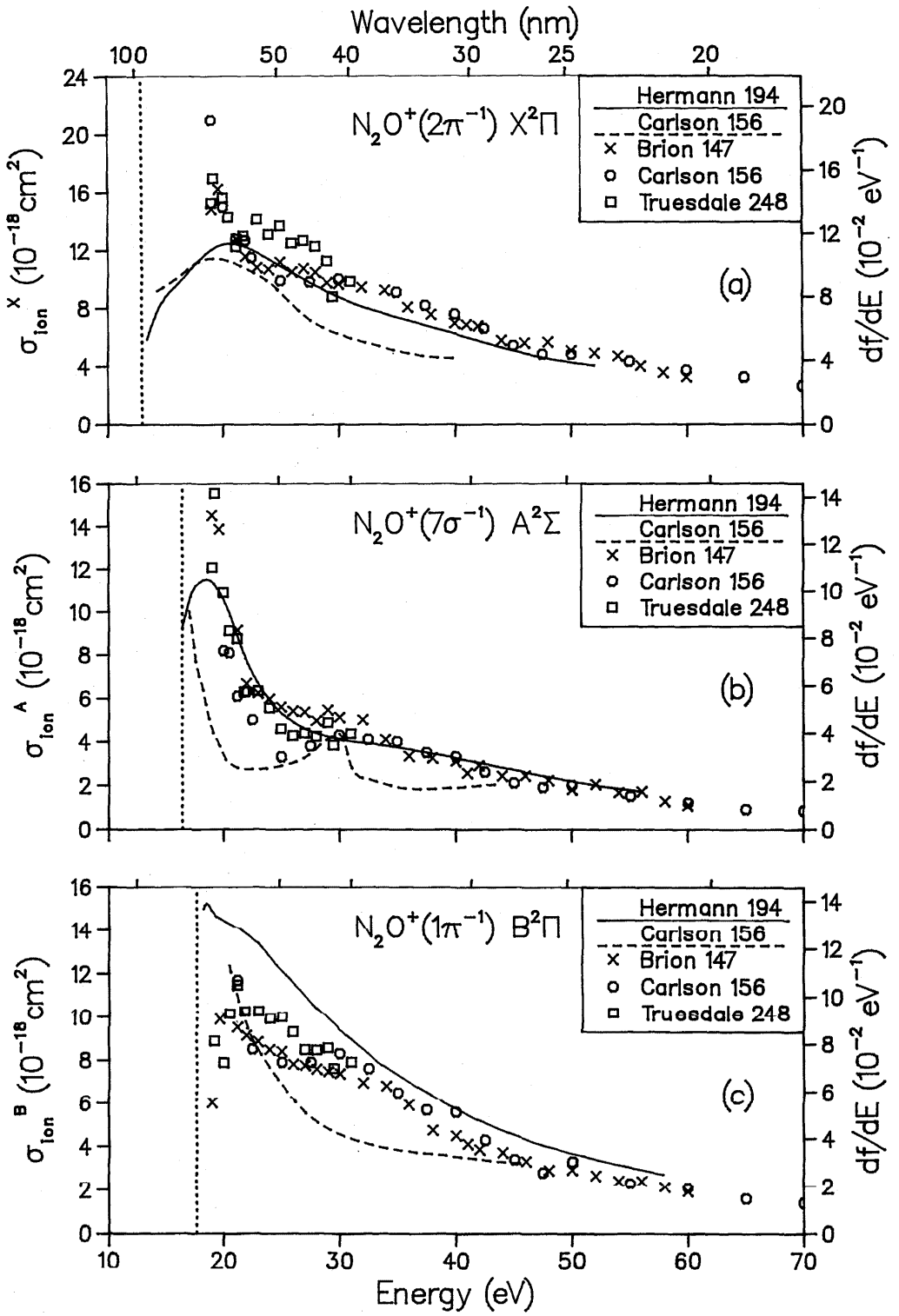

FIG. 44. Partial photoionization cross sections for N_2O; (a) final ionic state $= X^2\Pi$, (b) final ionic state $= A^2\Sigma$, (c) final ionic state $= B^2\Pi$.

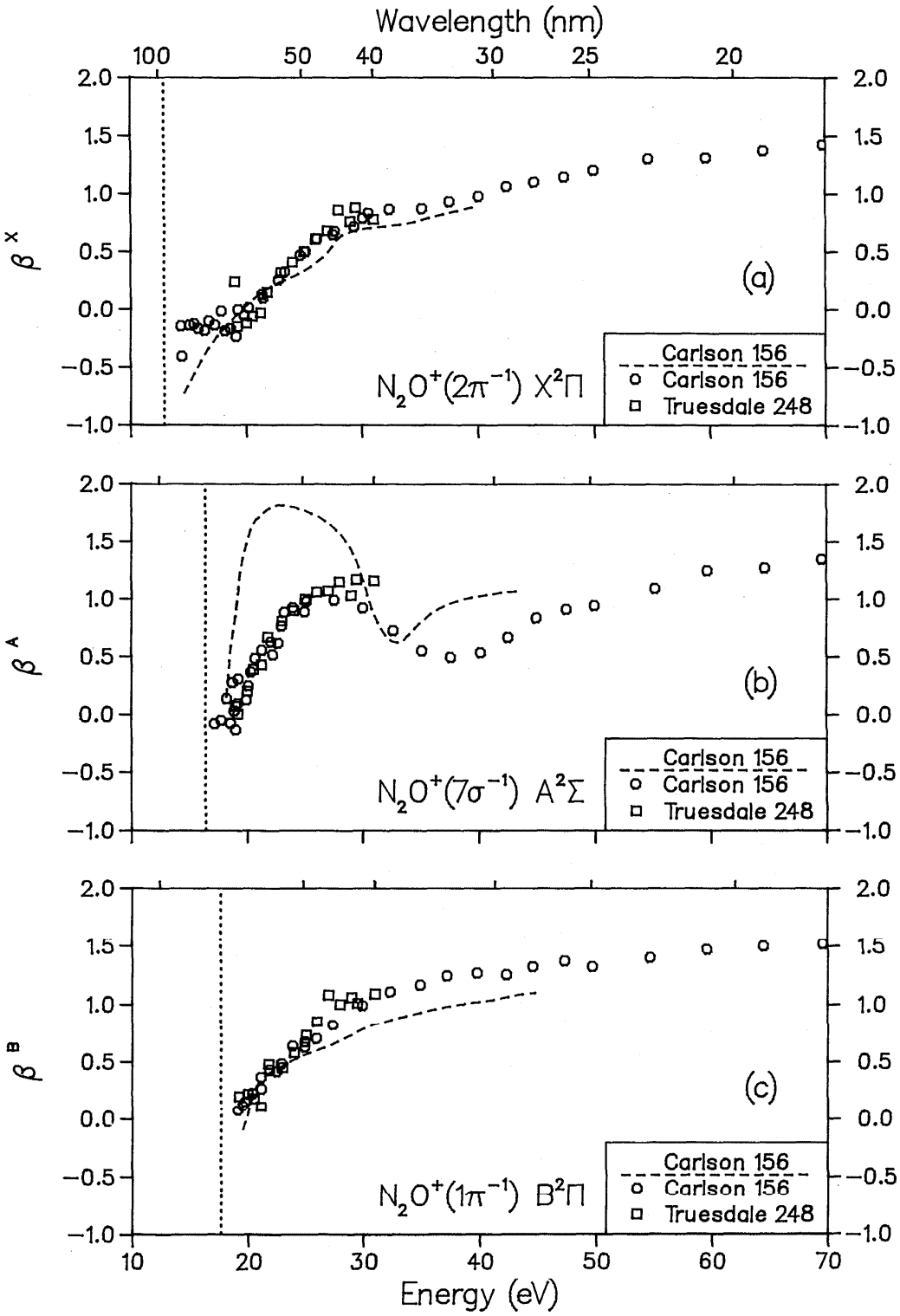

FIG. 45. Photoelectron asymmetry parameters for N_2O; (a) final ionic state = $X^2\Pi$, (b) final ionic state = $A^2\Sigma$, (c) final ionic state = $B^2\Pi$.

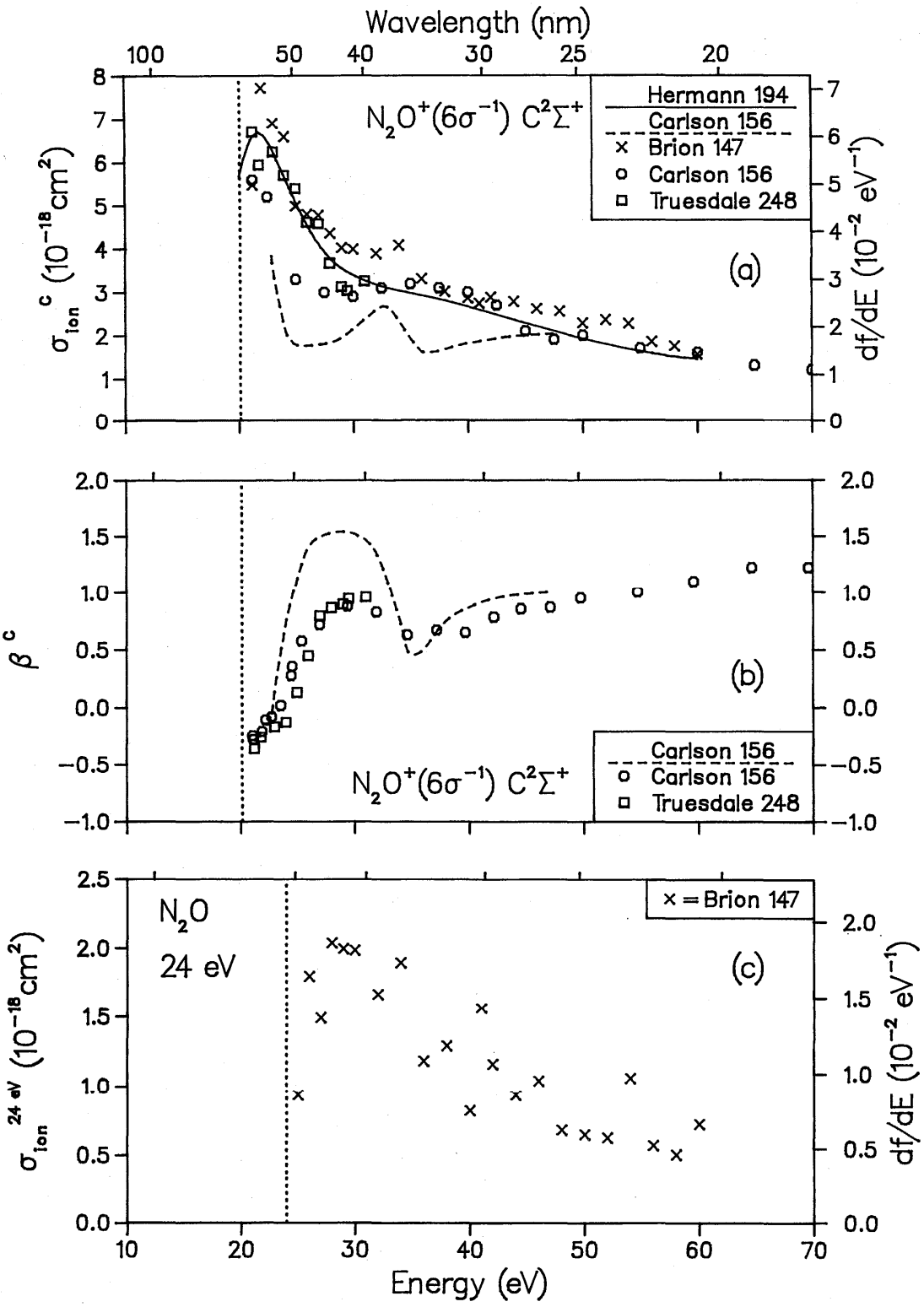

FIG. 46. Partial photoionization cross section for N_2O, final ionic state = $C^2\Sigma^+$, (b) photoelectron asymmetry parameter for N_2O, final ionic state = $C^2\Sigma^+$, (c) partial photoionization cross section for N_2O, final ionic state = PES peak at 24 eV.

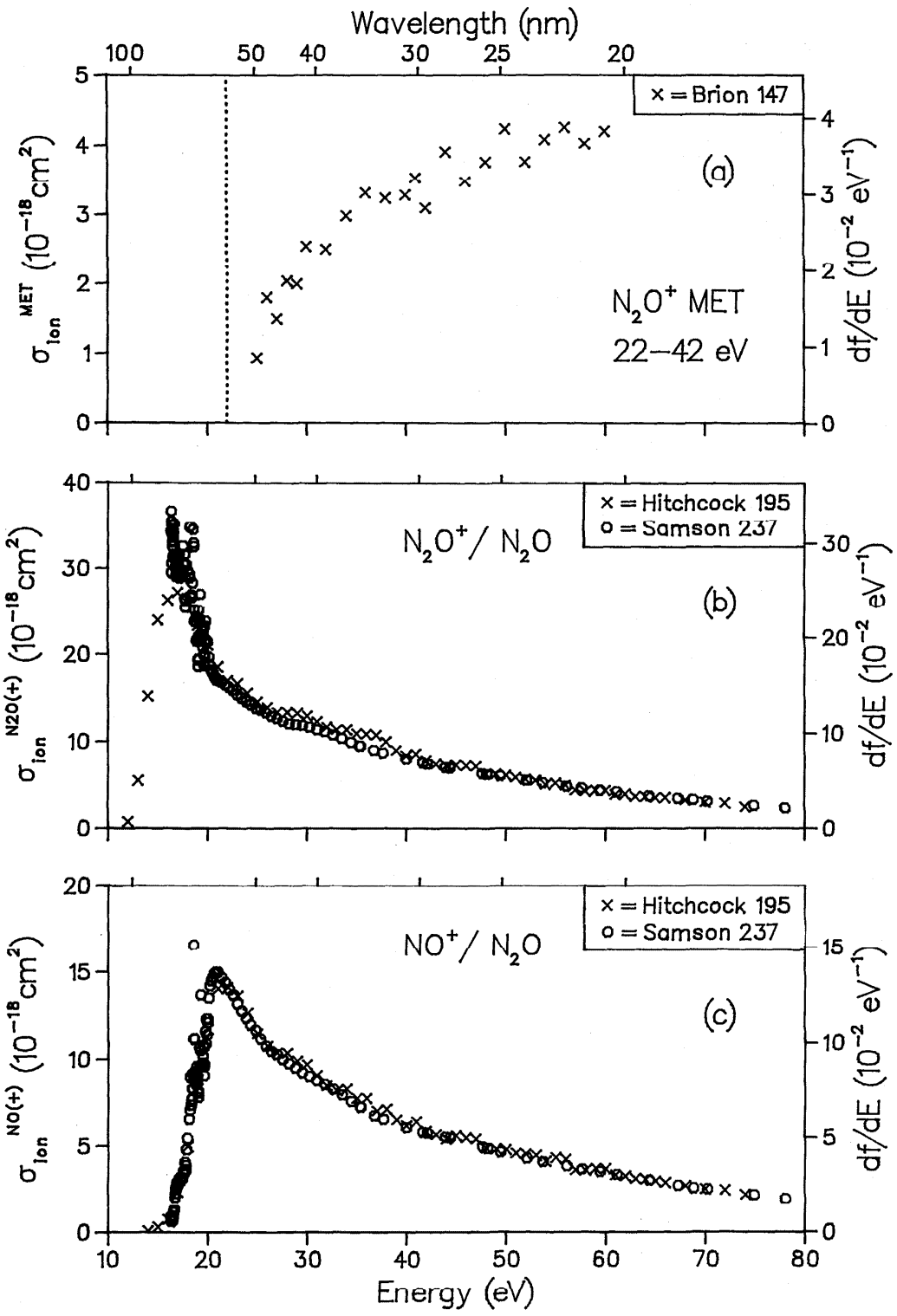

FIG. 47. (a) Partial photoionization cross section for N_2O, final ionic state = PES peak at 22–42 eV. (b) Partial ionic photofragmentation cross sections for N_2O, product ion = N_2O^+. (c) Partial ionic photofragmentation cross sections for N_2O, product ion = NO^+.

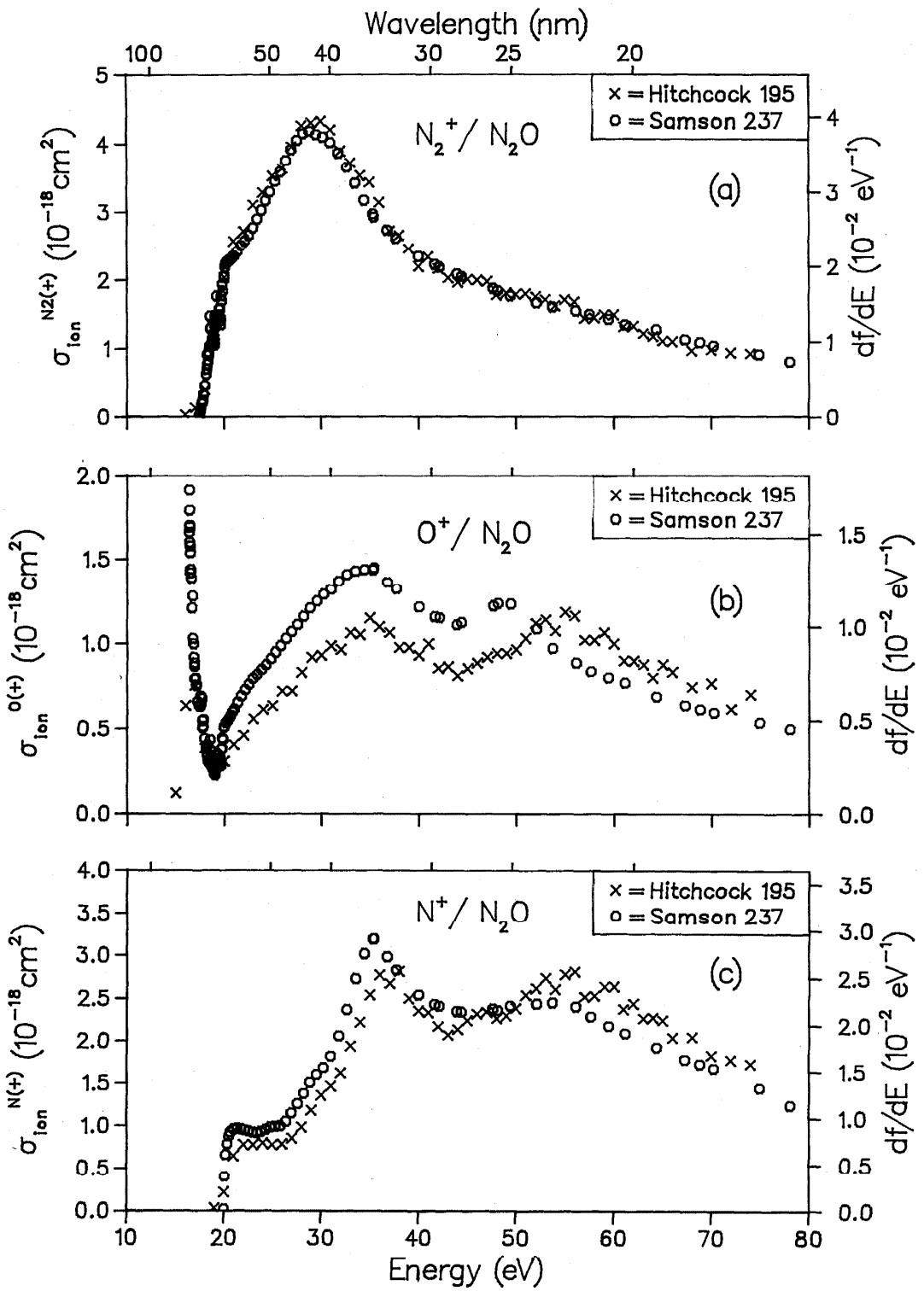

FIG. 48. Partial ionic photofragmentation cross sections for N_2O; (a) product ion = N_2^+, (b) product ion = O^+, (c) product ion = N^+.

Table 9. Data for H_2O.

Reference	Author	Year	E/T	Method	Experimental normalization	Cross Sections			Betas	Photon energy range (eV)
						Abs	State specific partials	Molecular ions and dissociative fragments	State	
153	Cairns	1971	E	P	AB			H_2O^+, OH^+		17- 33
202	Katayama	1973	E	P	AB	√				12- 18
170	de Reilhac	1977	E	P	AB	√				24-118
226	Phillips	1977	E	P	AB	√				15- 70
73	Tan	1978	E	DIP	TRK	√				6-300
73	Tan	1978	E	DIP	TRK		X,A,B,C			16- 61
73	Tan	1978	E	DIP	TRK			H_2O^+,OH^+,H^+,O^+		24- 60
230	Roche	1980	T	Xα	---		X,A,B,C		X,A,B,C	10- 80
74	Diercksen	1982	T	StEx	---		X,A,B,C			16- 70
249	Truesdale	1982	E	P	NM		X,A,B		X,A,B	18- 31
143	Brion	1985	E	DIP	TRK		X			10- 34
152	Cacelli	1984	T	StEx	---		X,A,B,C,$(1a_1^{-1})$			32- 60
140	Banna	1986	E	P	NM		X,A,B,C		X,A,B,C	30-140
146	Brion	1986	E	P	TRK		C			50-200
150	Cacelli	1986	T	StEx	---				X,A,B	15- 50
189	Haddad	1986	E	P	AB	√				12-124

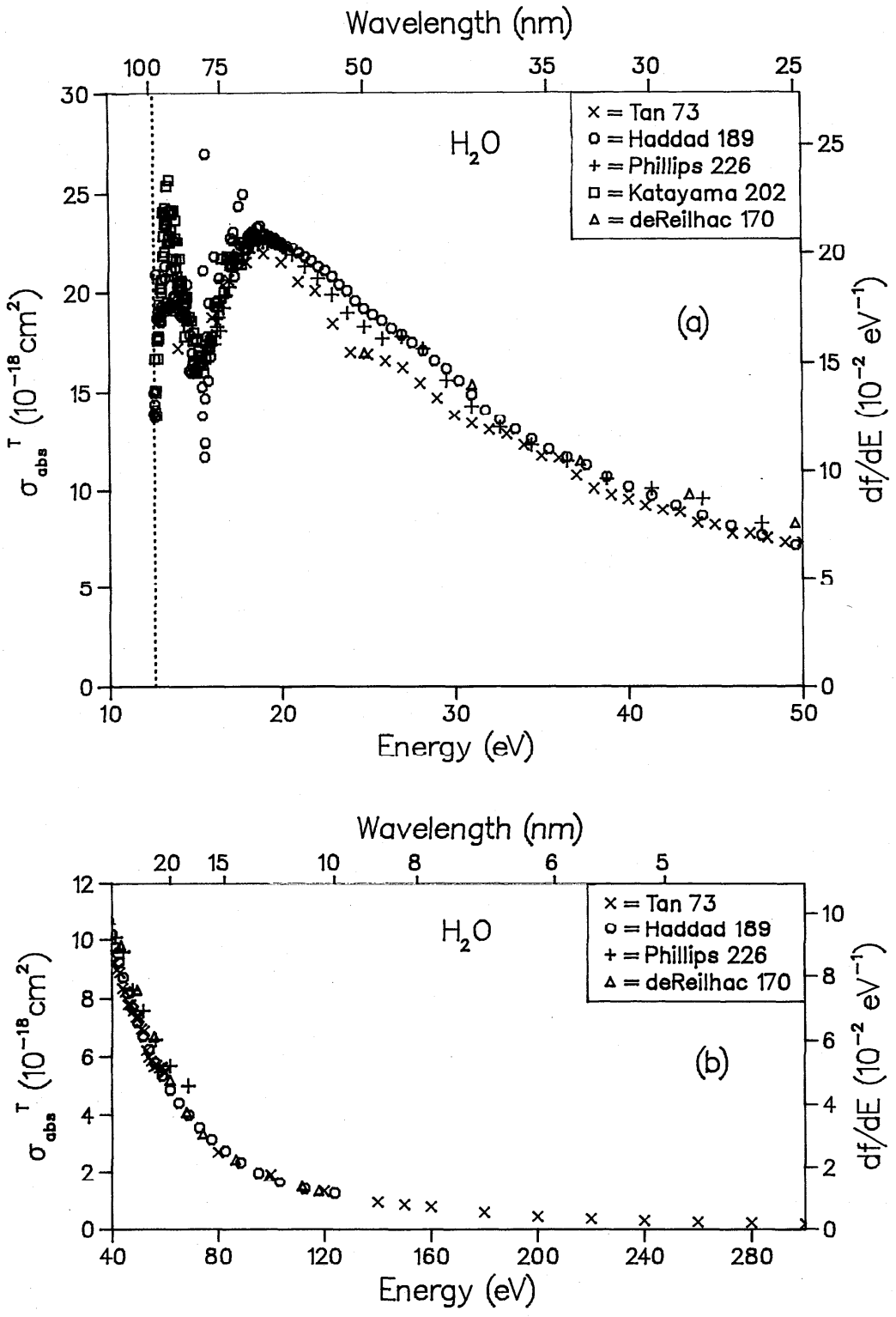

FIG. 49. Total photoabsorption cross section for H_2O: (a) low-energy range, (b) high-energy range.

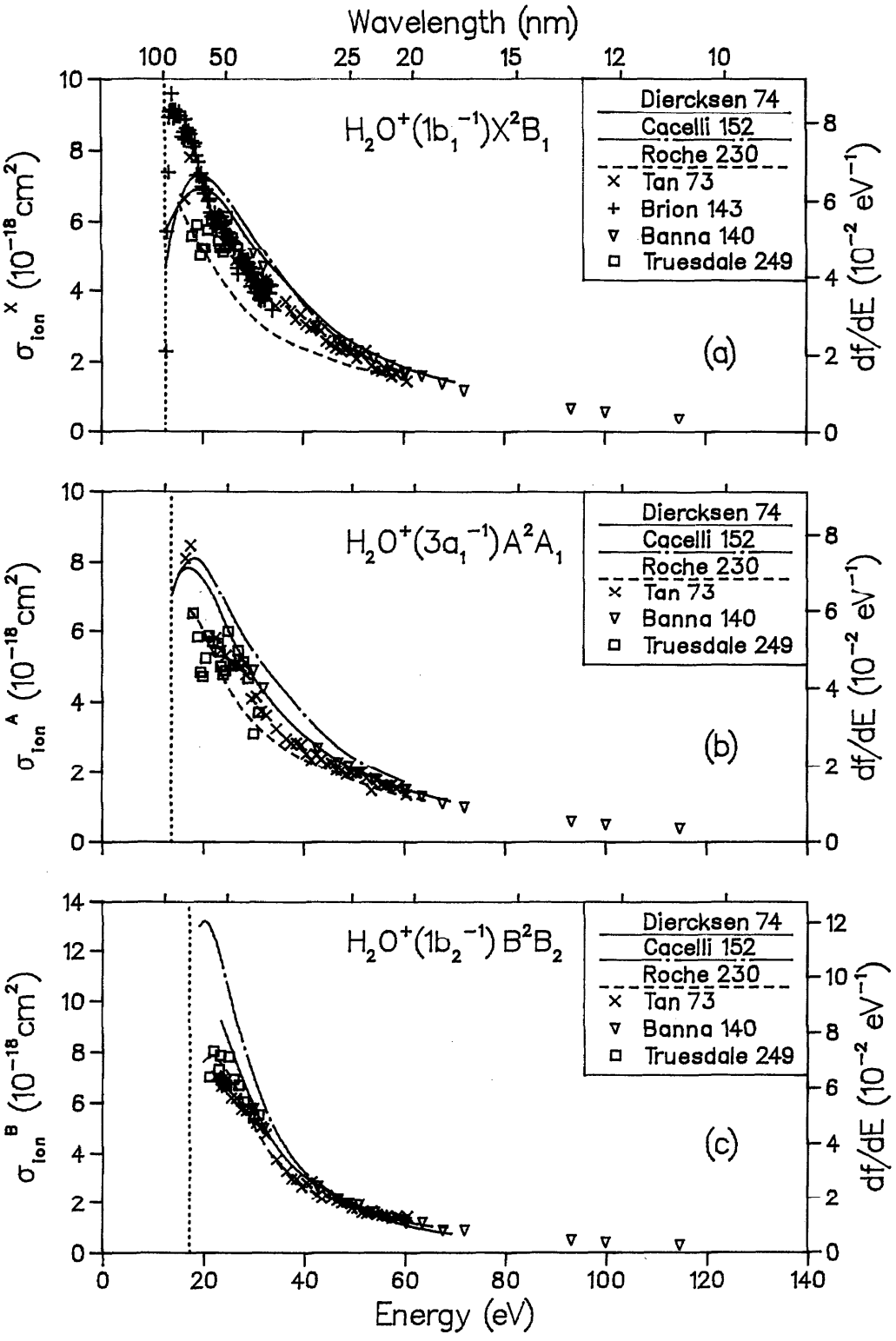

FIG. 50. Partial photoionization cross sections for H_2O; (a) final ionic state = X^2B_1,(b) final ionic state = A^2A_1, (c) final ionic state = B^2B_2.

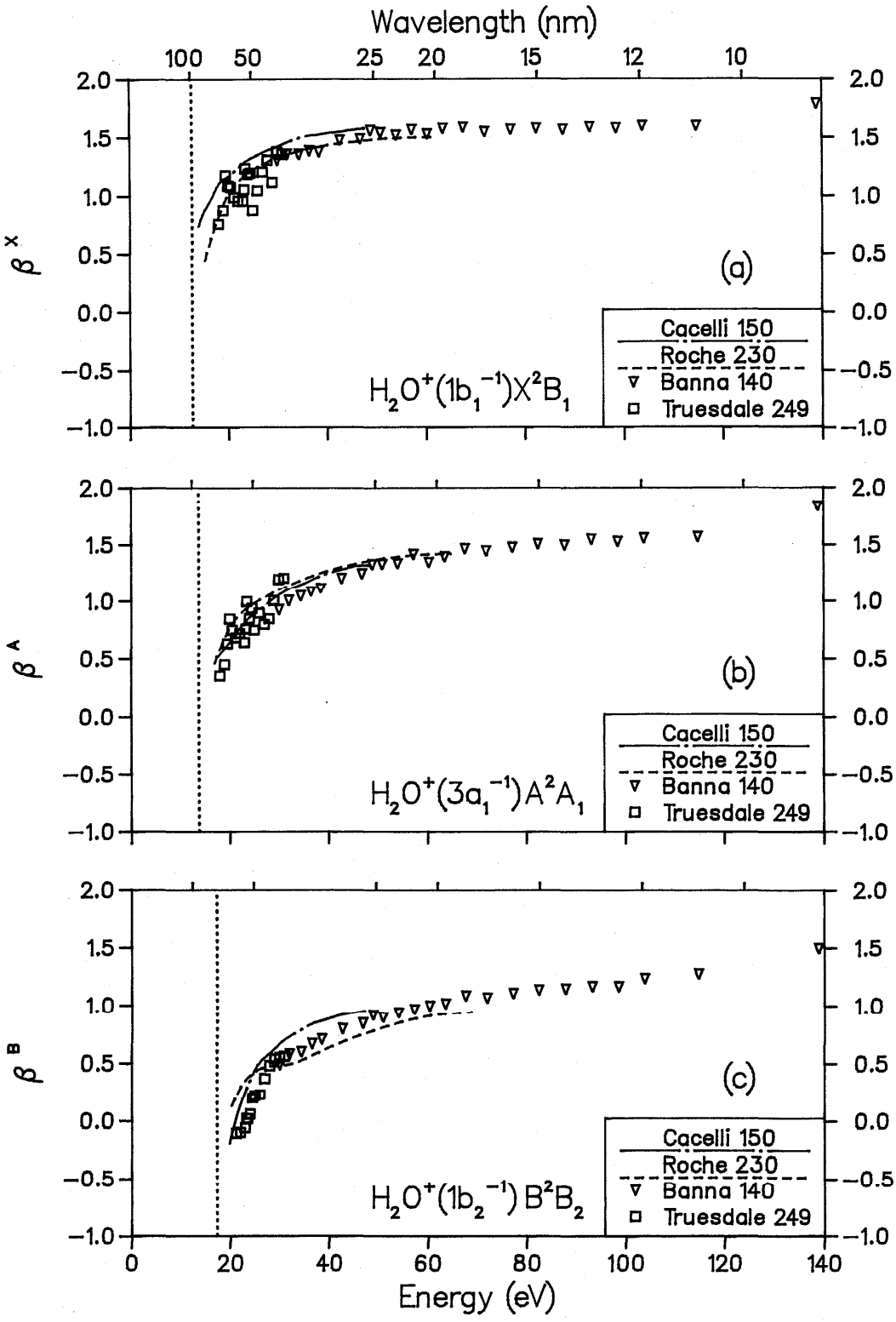

FIG. 51. Photoelectron asymmetry parameters for H_2O; (a) final ionic state = X^2B_1, (b) final ionic state = A^2A_1, (c) final ionic state = B^2B_2.

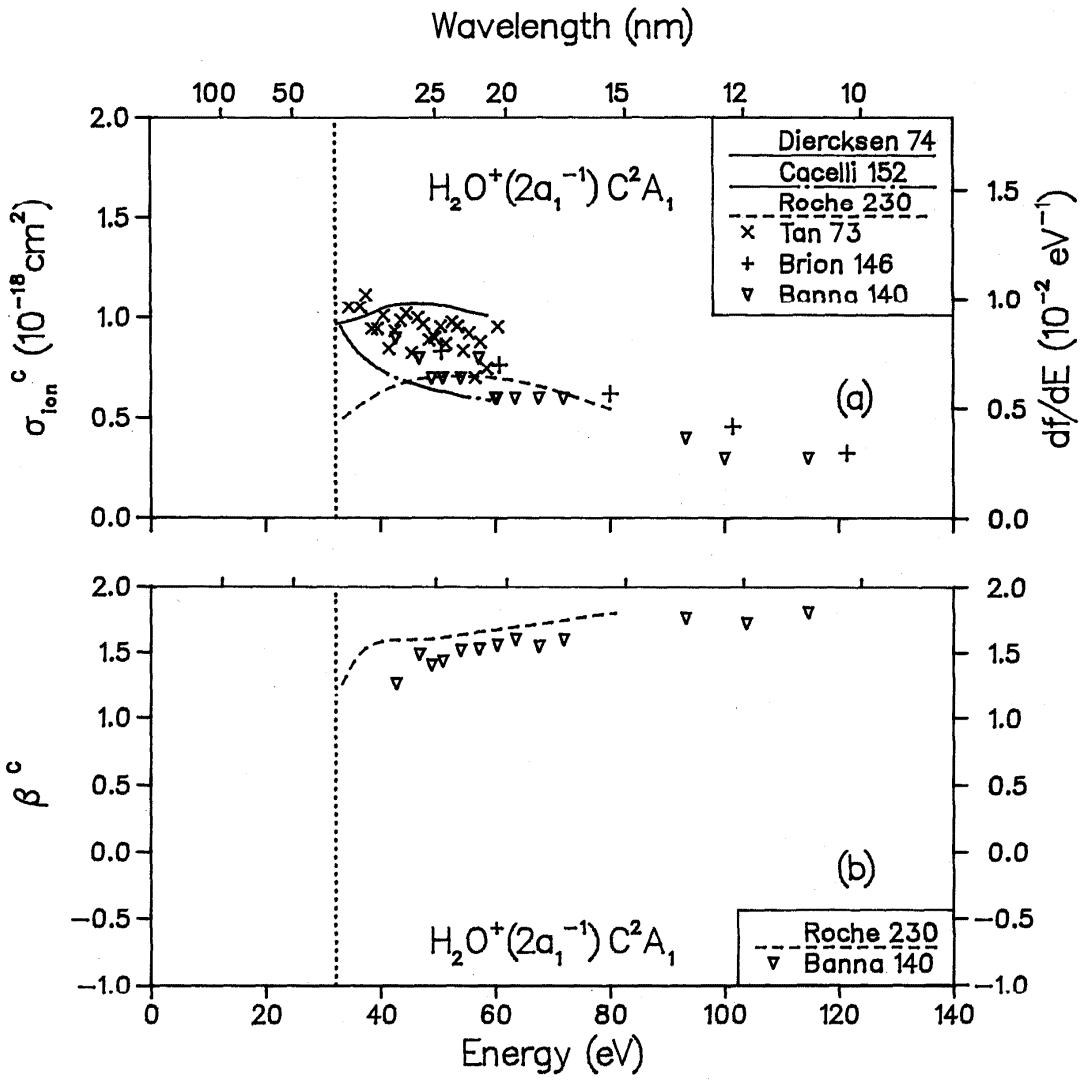

FIG. 52. (a) Partial photoionization cross section for H_2O, final ionic state = C^2A_1, (b) photoelectron asymmetry parameter for H_2O, final ionic state = C^2A_1.

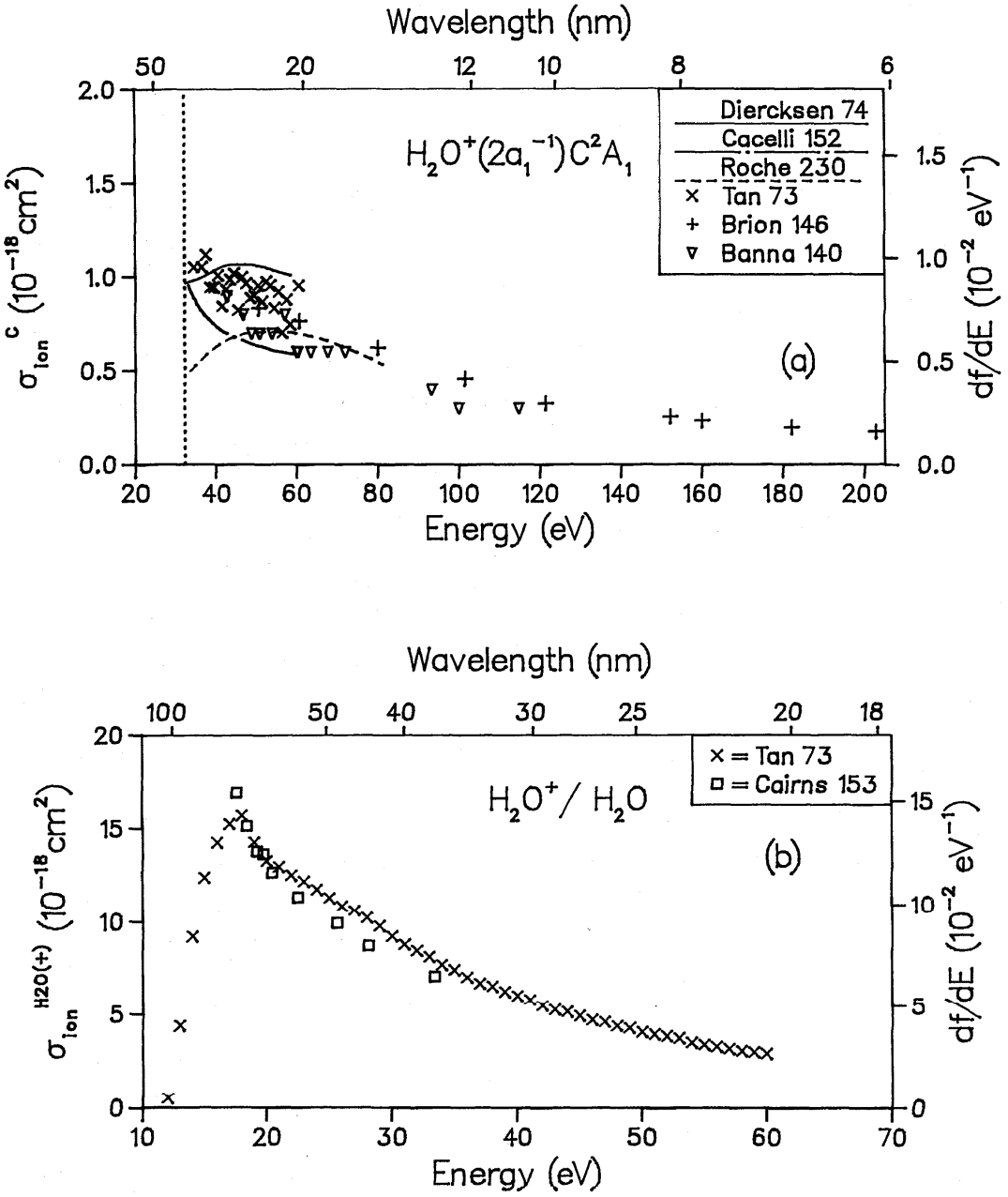

FIG. 53. (a) Partial photoionization cross section for H_2O, final ionic state = C^2A_1, extended energy range. (b) Partial ionic photofragmentation cross section for H_2O, product ion — H_2O^+.

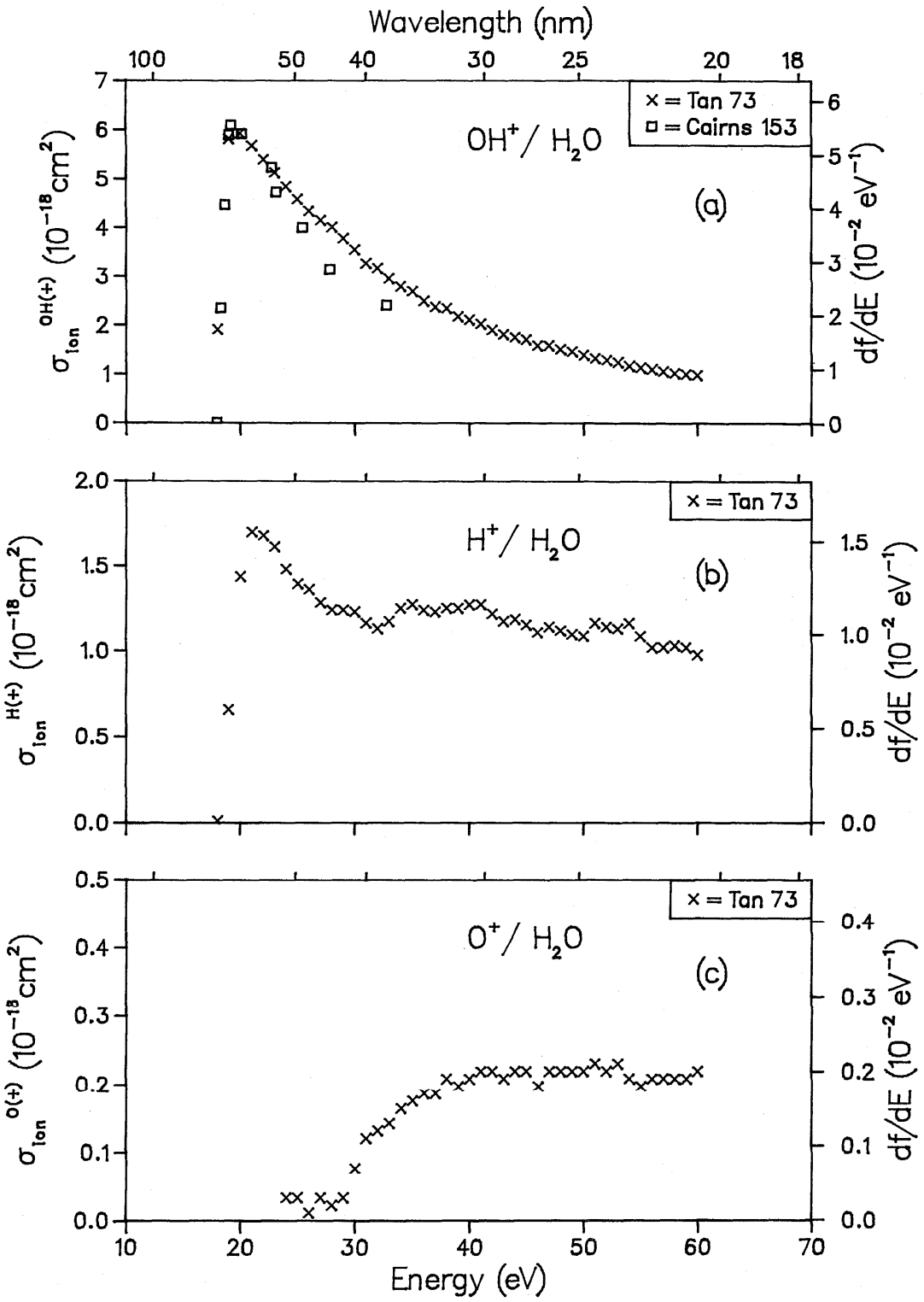

FIG. 54. Partial ionic photofragmentation cross sections for H_2O; (a) product ion = OH^+, (b) product ion = H^+, (c) product ion = O^+.

Table 10. Data for NH_3.

Reference	Author	Year	E/T	Method	Experimental normalization	Cross Sections: Abs	Cross Sections: State specific partials	Cross Sections: Molecular ions and dissociative fragments	Betas: State	Photon energy range (eV)
97	Brion	1977	E	DIP	TRK		X,A,B			15- 50
170	de Reilhac	1977	E	P	AB	√				24-118
257	Wight	1977	E	DIP	TRK	√				10- 60
257	Wight	1977	E	DIP	TRK		A,B			18- 48
257	Wight	1977	E	DIP	TRK			$NH_3^+, NH_2^+, NH^+, N^+, H^+$		10- 60
152	Cacelli	1984	T	StEx	---		X,A,B			15- 60
236	Samson	1984	E	P	AB	√				10-124
139	Banna	1987	E	P	NM		X,A,B		X,A,B	30-130

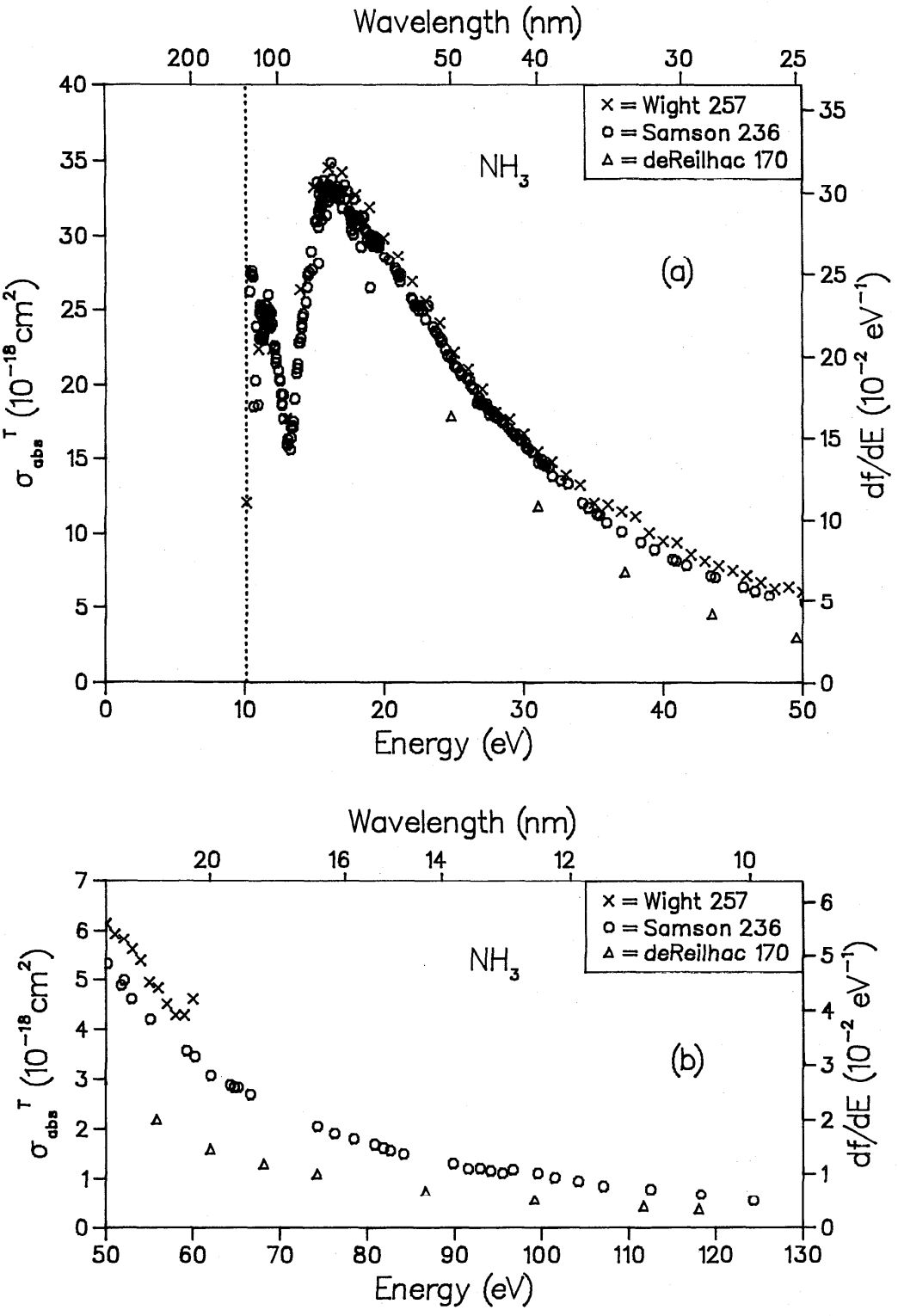

FIG. 55. Total photoabsorption cross section for NH_3: (a) low-energy range, (b) high-energy range.

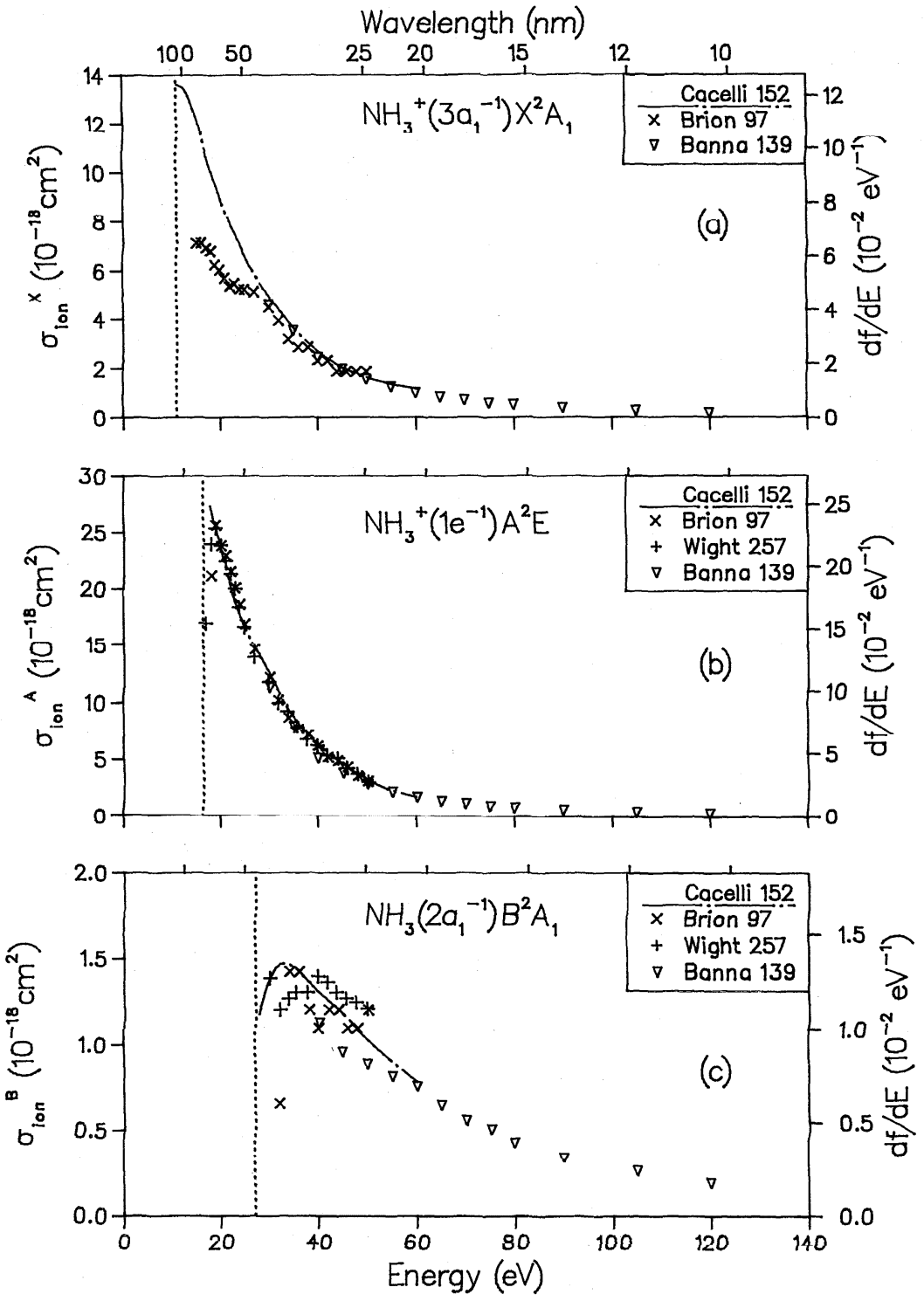

FIG. 56. Partial photoionization cross sections for NH_3; (a) final ionic state $= X^2A_1$, (b) final ionic state $= A^2E$, (c) final ionic state $= B^2A_1$.

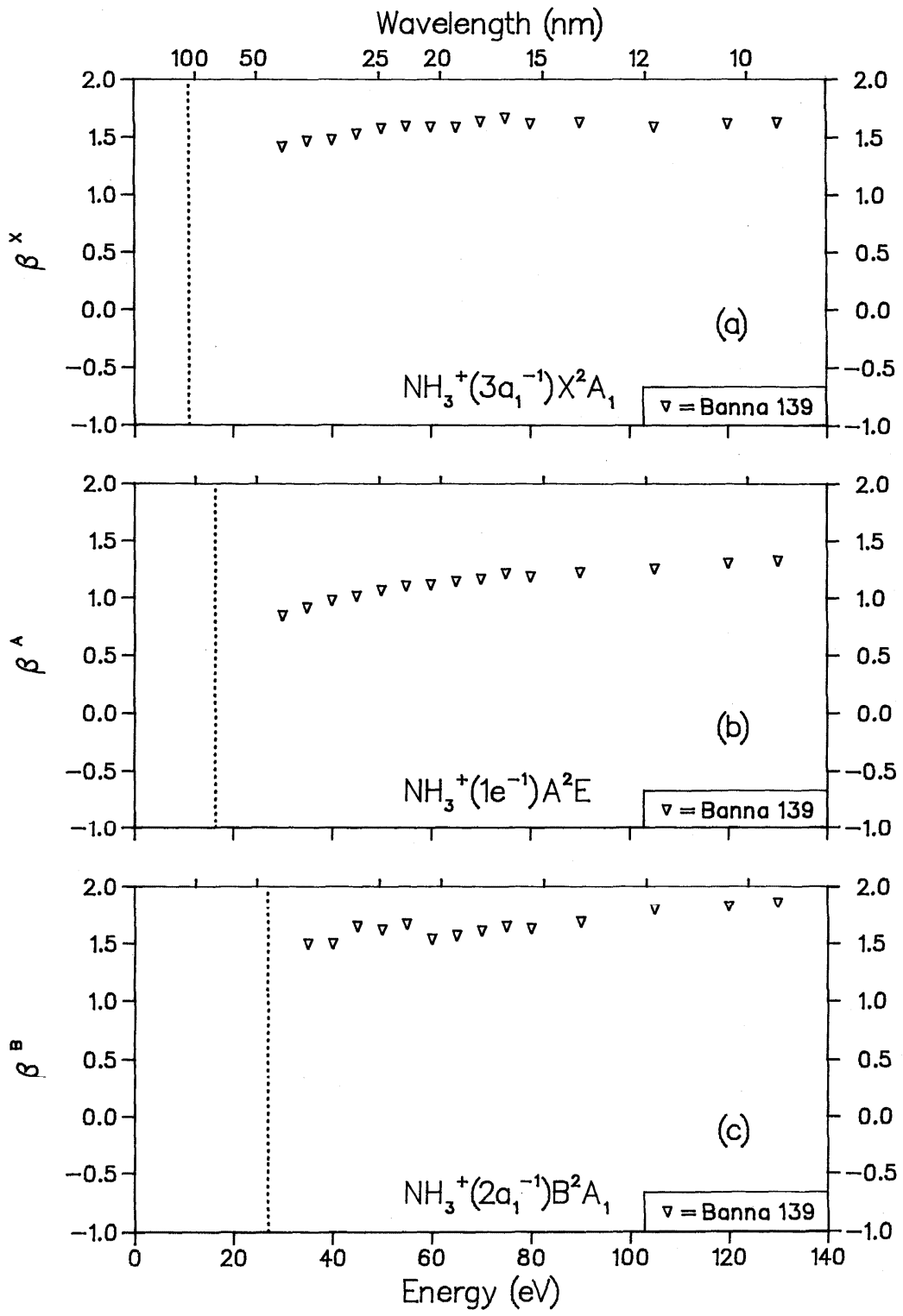

FIG. 57. Photoelectron asymmetry parameters for NH_3; (a) final ionic state = X^2A_1, (b) final ionic state = A^2E, (c) final ionic state = B^2A_1.

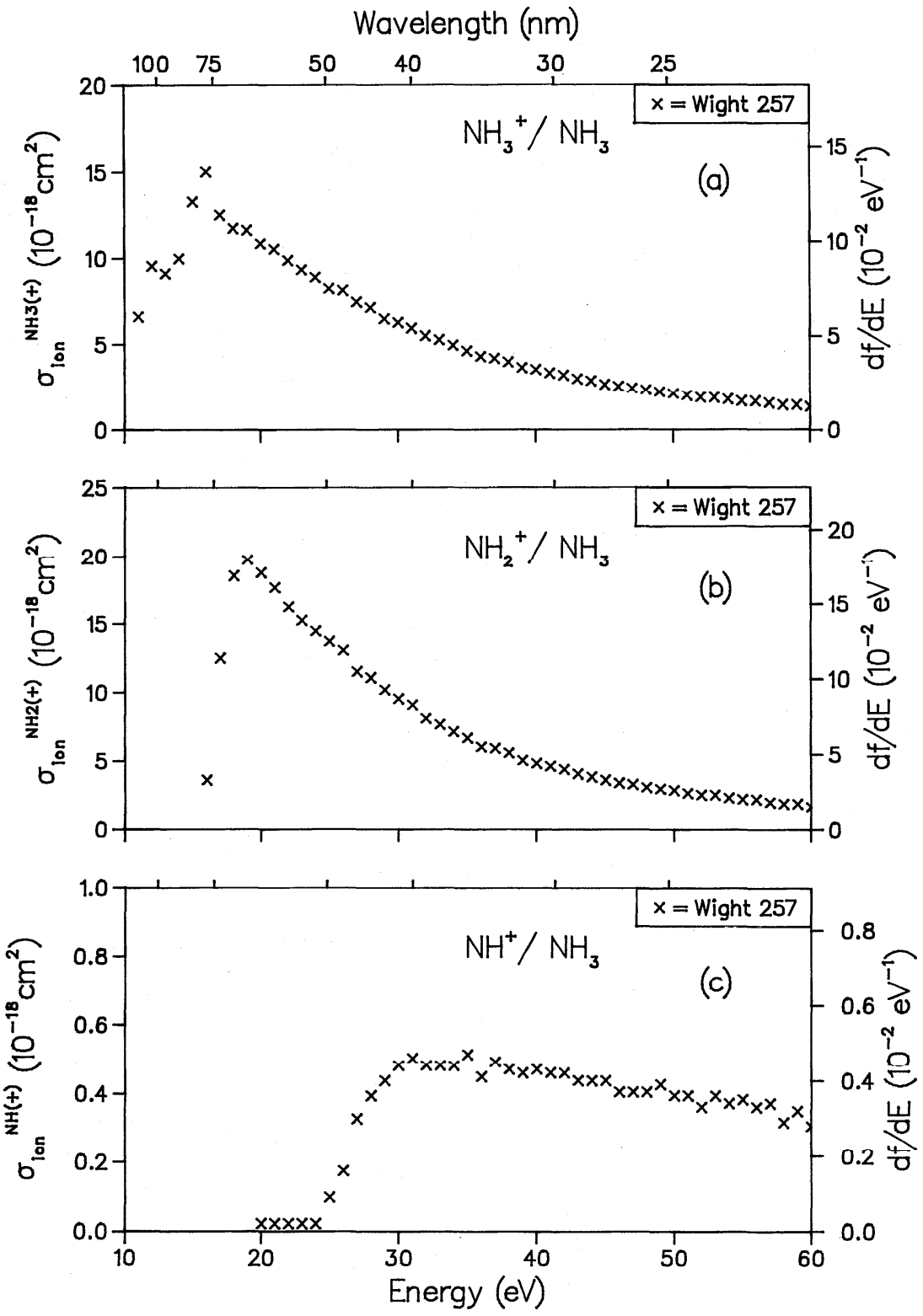

FIG. 58. Partial ionic photofragmentation cross sections for NH_3; (a) product ion = NH_3^+, (b) product ion = NH_2^+, (c) product ion = NH^+.

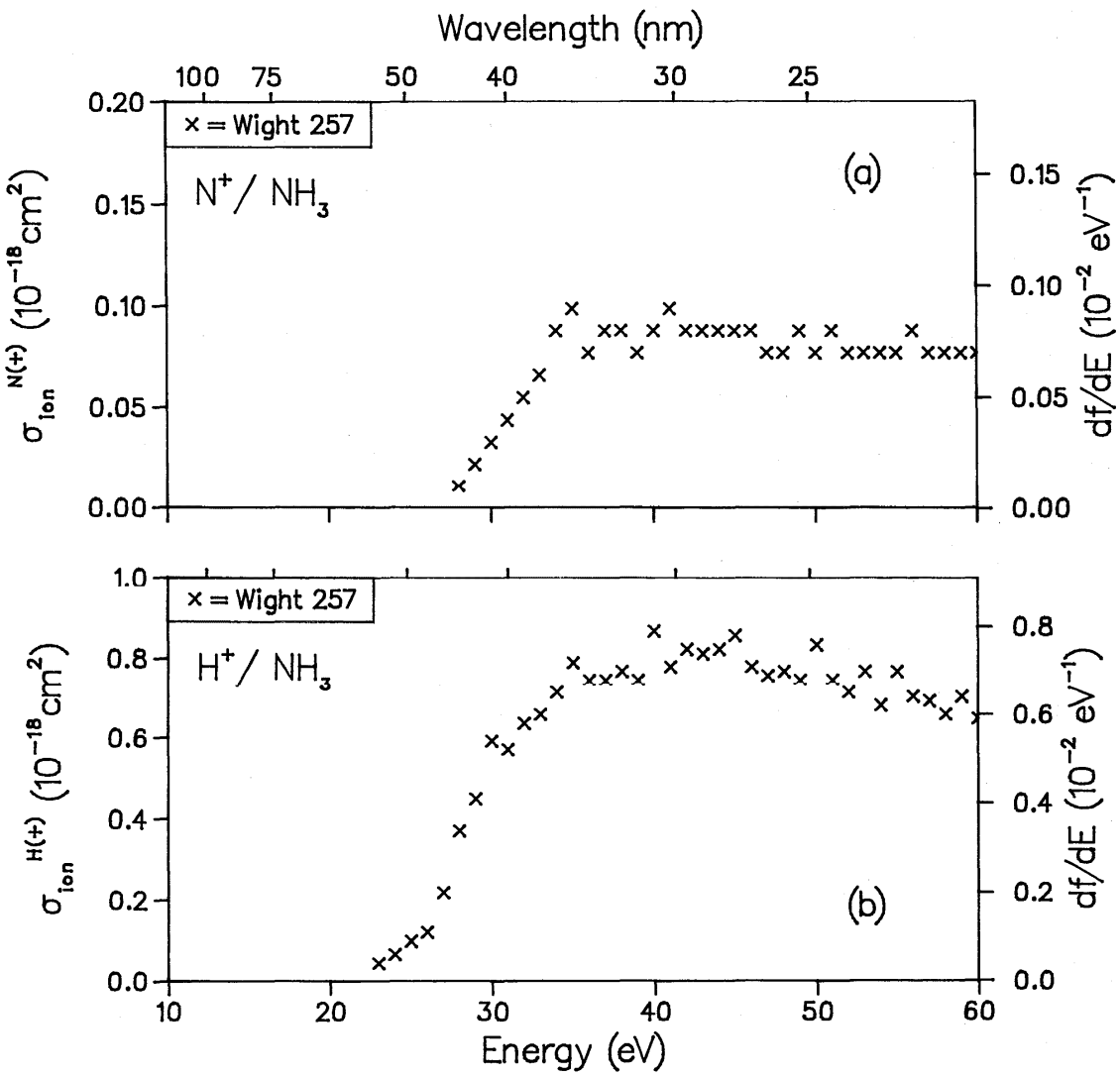

FIG. 59. Partial ionic photofragmentation cross sections for NH_3; (a) product ion = N^+, (b) product ion = H^+.

Table 11. Data for CH_4.

Reference	Author	Year	E/T	Method	Experimental normalization	Cross Sections: Abs	Cross Sections: State specific partials	Cross Sections: Molecular ions and dissociative fragments	Betas: State	Photon energy range (eV)
208	Lee	1973	E	P	AB	✓				19- 68
99	Backx	1975	E	DIF	TRK	✓				14- 80
100	Backx	1975	E	DIF	TRK		X,A,MET[a]			14- 80
100	Backx	1975	E	DIF	TRK			CH_4^+, CH_3^+, CH_2^+ CH^+, H^+, C^+		14- 80
250	Van der Wiel	1976	E	DIF	TRK		X,A			37- 72
170	de Reilhac	1977	E	P	AB	✓				28-100
209	Lee	1977	E	P	AB	✓				17- 24
236	Samson	1984	E	P	AB	✓				13-124
237	Samson	1984	E	P	AB			$CH_4^+, CH_3^+, CH_2^+, CH^+,$ H^+, C^+, H_2^+		14- 40
151	Cacelli	1985	T	StEx	---		X,A			20- 80

[a]MET = many-body states arising from inner-valence ionization.

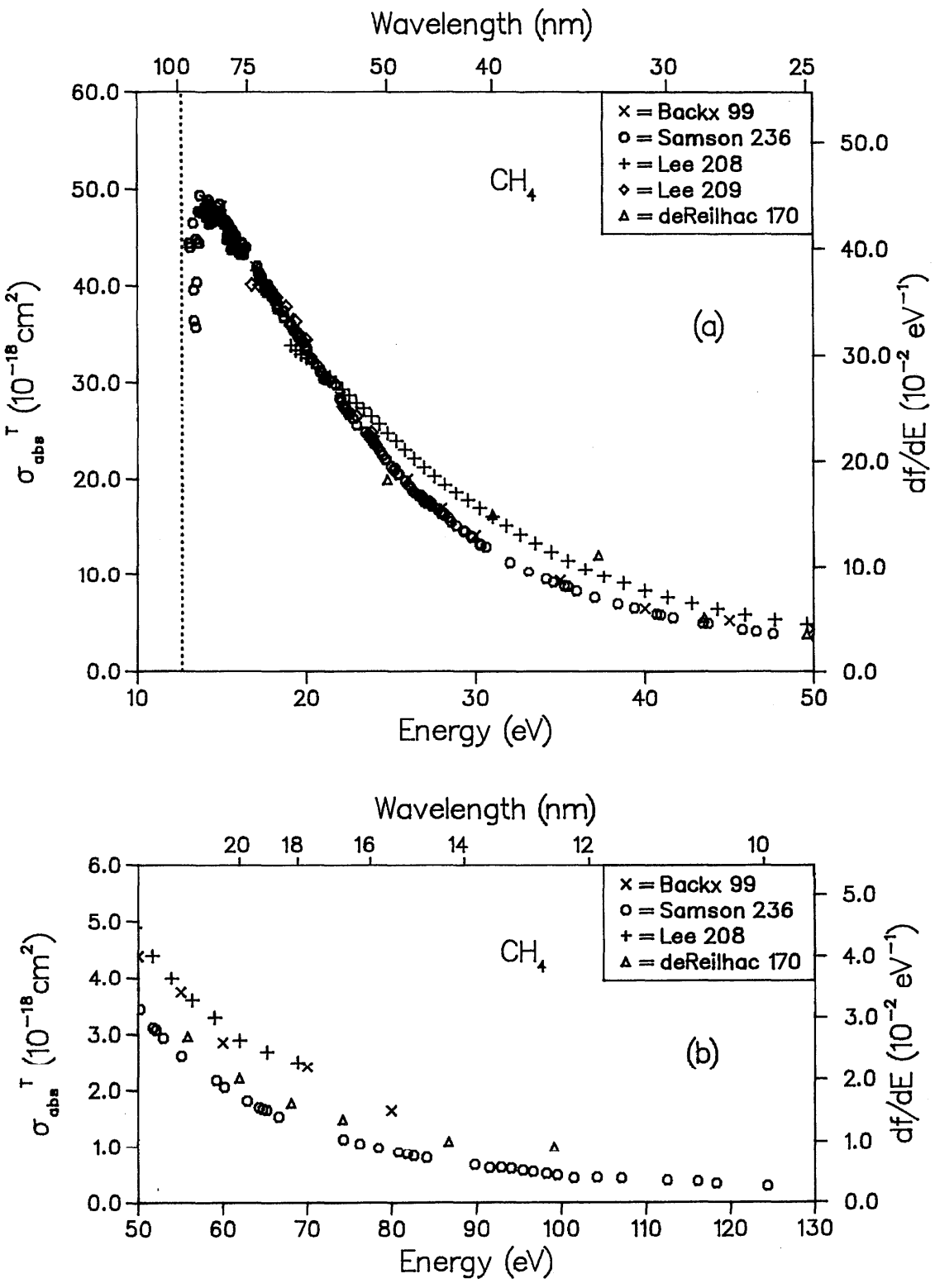

FIG. 60. Total photoabsorption cross section for CH_4: (a) low-energy range, (b) high-energy range.

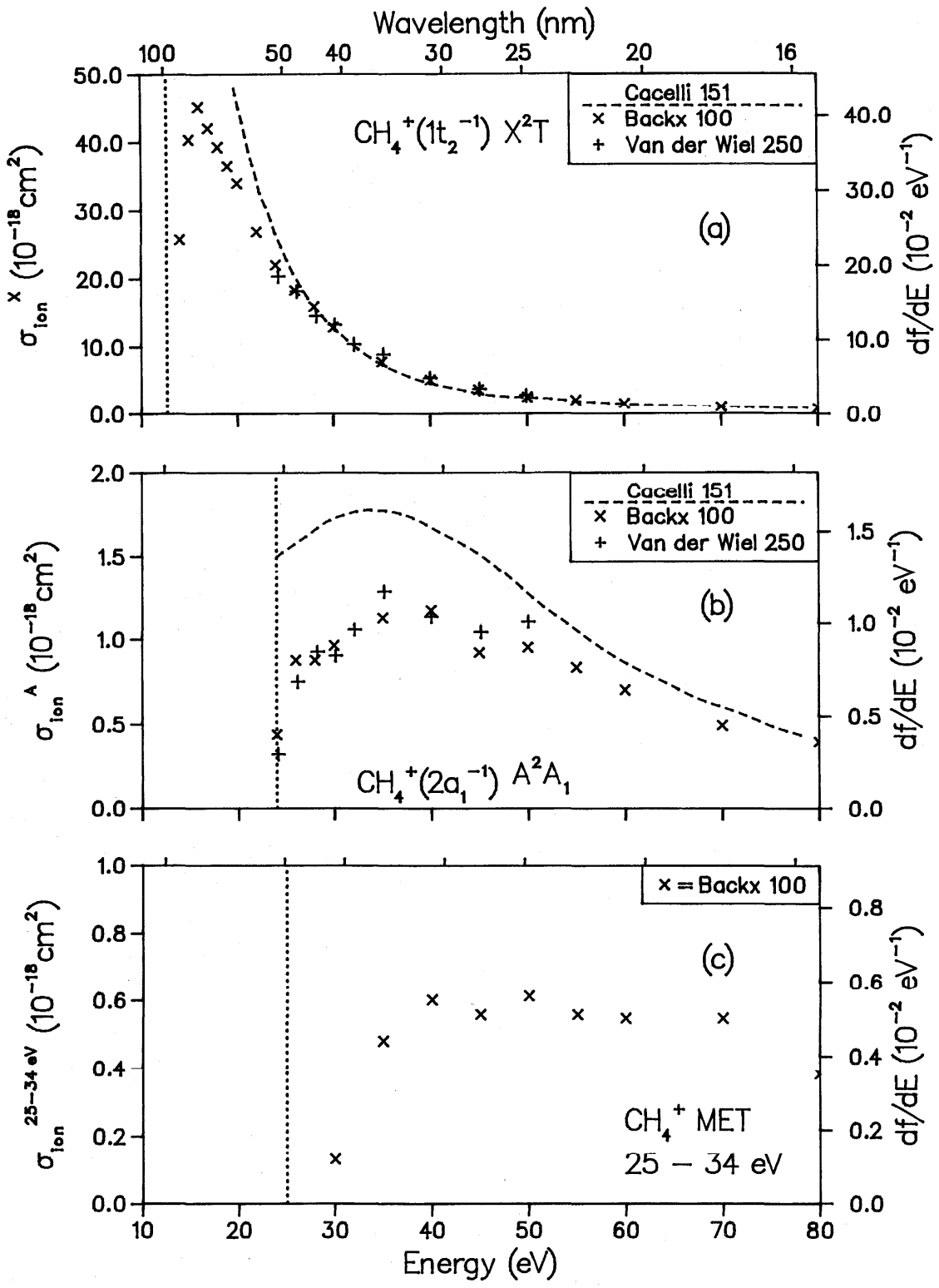

FIG. 61. Partial photoionization cross sections for CH_4; (a) final ionic state = X^2T, (b) final ionic state = A^2A_1, (c) final ionic states = many-body states arising from inner valence ionization.

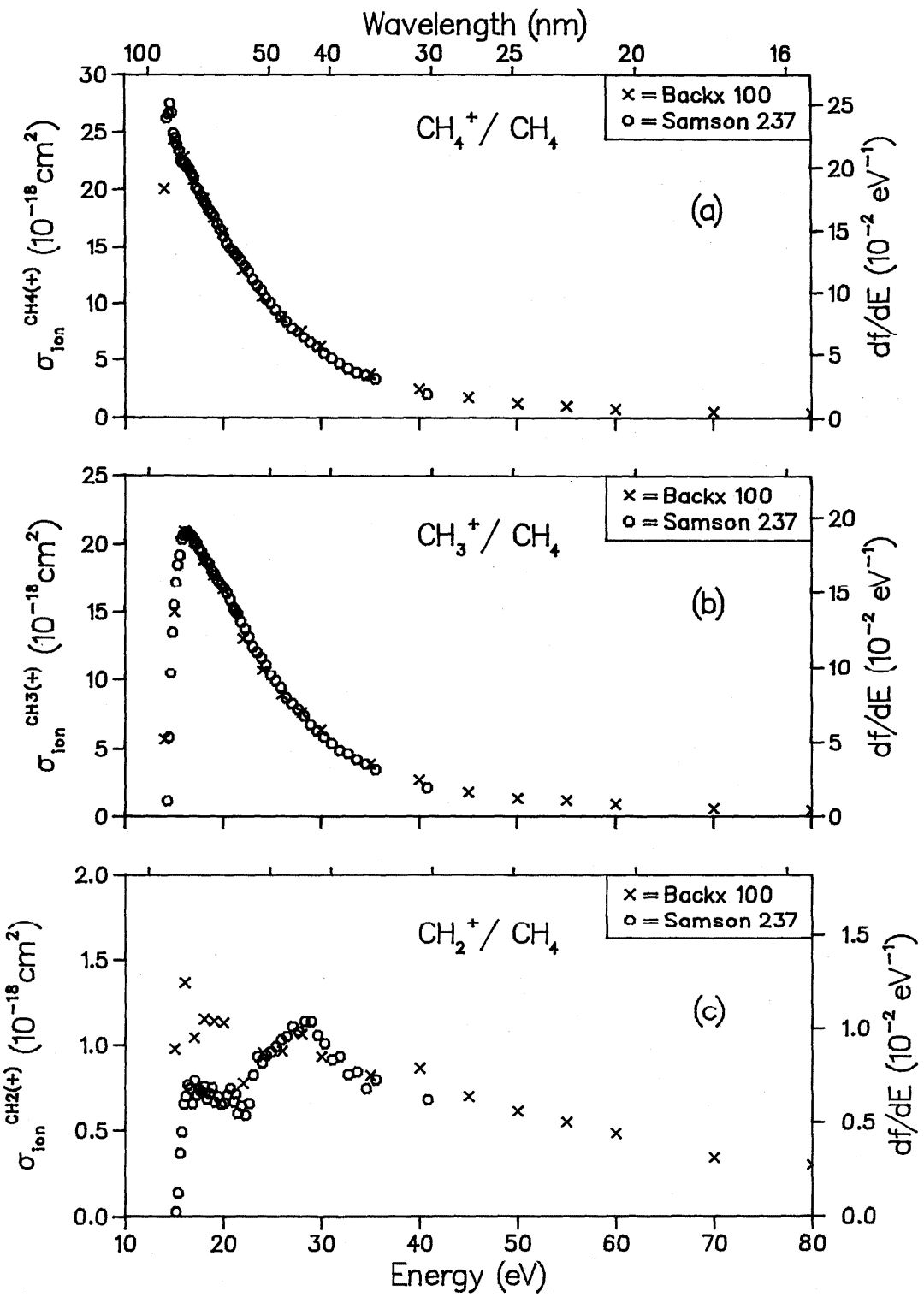

FIG. 62. Partial ionic photofragmentation cross sections for CH_4; (a) product ion = CH_4^+, (b) product ion = CH_3^+, (c) product ion = CH_2^+.

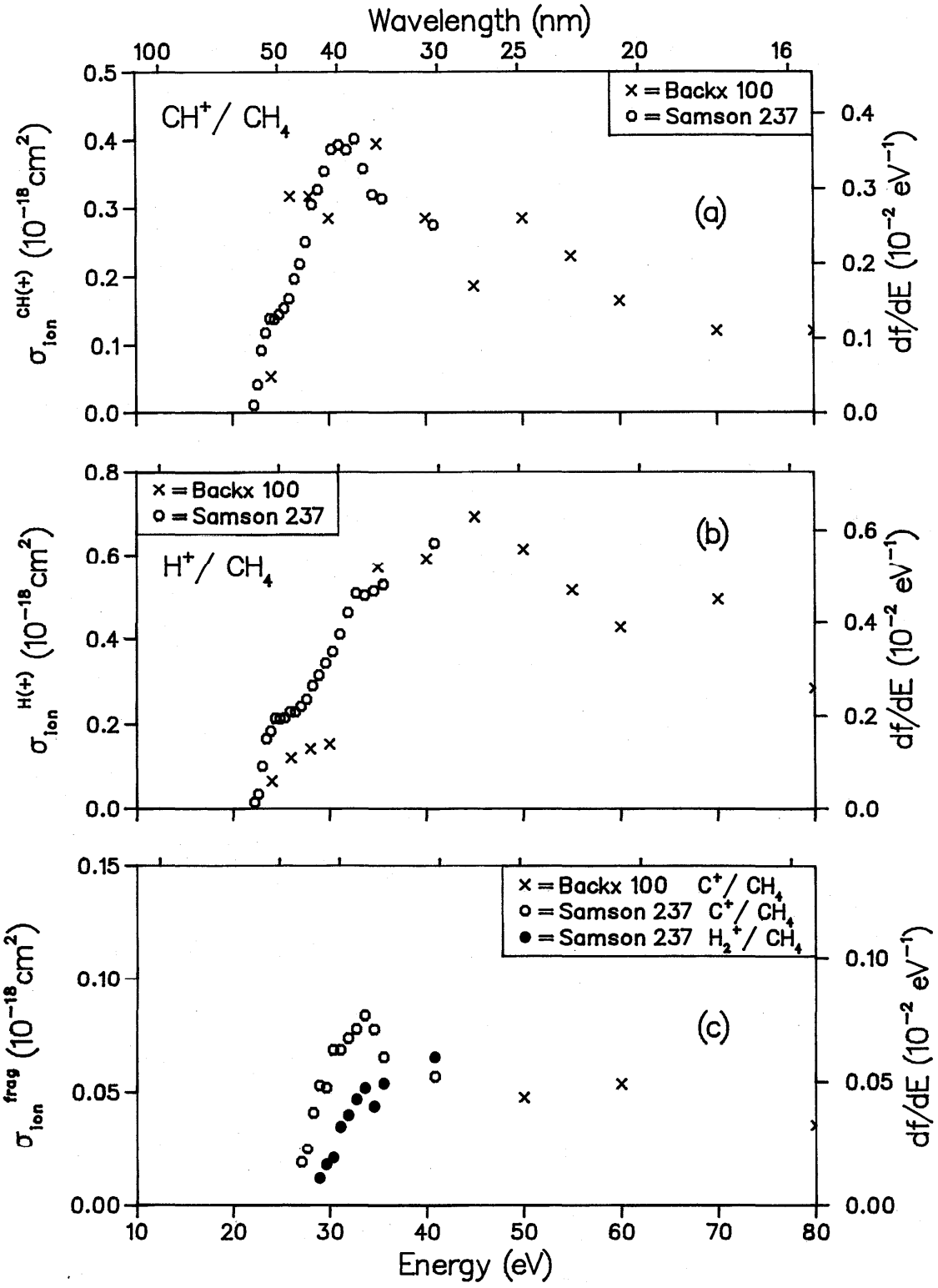

FIG. 63. Partial ionic photofragmentation cross sections for CH_4; (a) product ion = CH^+, (b) product ion = H^+, (c) product ions = C^+ and H_2^+.

Table 12. Data for hydrogen halides.

Reference	Author	Year	E/T	Method	Experimental normalization	Cross Sections: Abs	Cross Sections: State specific partials	Cross Sections: Molecular ions and dissociative fragments	Betas: State	Photon energy range (eV)
HF										
162	Carnovale	1981	E	DIP	TRK	✓				9-150
162	Carnovale	1981	E	DIP	TRK		X,A,B			15- 60
178	Faegri	1981	T	StEx	---		X,A			18- 70
101	Carnovale	1983	E	DIP	TRK			HF^+, F^+, H^+		16- 60
151	Cacelli	1985	T	StEx	---		X,A,B			20- 60
142	Boyle	1987	T	StEx	---		X,A			16- 66
HCℓ										
177	Faegri	1982	T	StEx	---		X,A			13- 32
157	Carlson	1983	E	P	AB		X,A		X,A	20- 80
157	Carlson	1983	T	Xα	---		X,A		X,A	20- 70
169	Daviel	1984	E	DIP	TRK	✓				8- 60
169	Daviel	1984	E	DIP	TRK		X,A,MET[a]			8- 40
169	Daviel	1984	E	DIP	TRK			$HCℓ^+, Cℓ^+, H^+$		8- 40
142	Boyle	1987	T	StEx	---		X,A			13-60
HBr										
155	Carlson	1984	E	P	AB		X,A,B		X,A	14-110
155	Carlson	1984	T	Xα	---		X,A		X,A	20-100
182	Grimm	1984	E	P	AB		X,A			19- 25
144	Brion	1985	E	DIP	TRK	✓				7- 40
144	Brion	1985	E	DIP	TRK	✓				40-100
144	Brion	1985	E	DIP	TRK		X,A,MET[a]			11- 40
144	Brion	1985	E	DIP	TRK			HBr^+, Br^+, H^+		10- 40
142	Boyle	1987	T	StEx	---		X,A			12- 60
HI										
154	Carlson	1984	E	P	AB		X,A		X,A	16- 90
154	Carlson	1984	T	Xα	---		X,A		X,A	16-100
142	Boyle	1987	T	StEx	---		X.A			12- 60

[a]MET = many-body states arising from inner valence ionization.

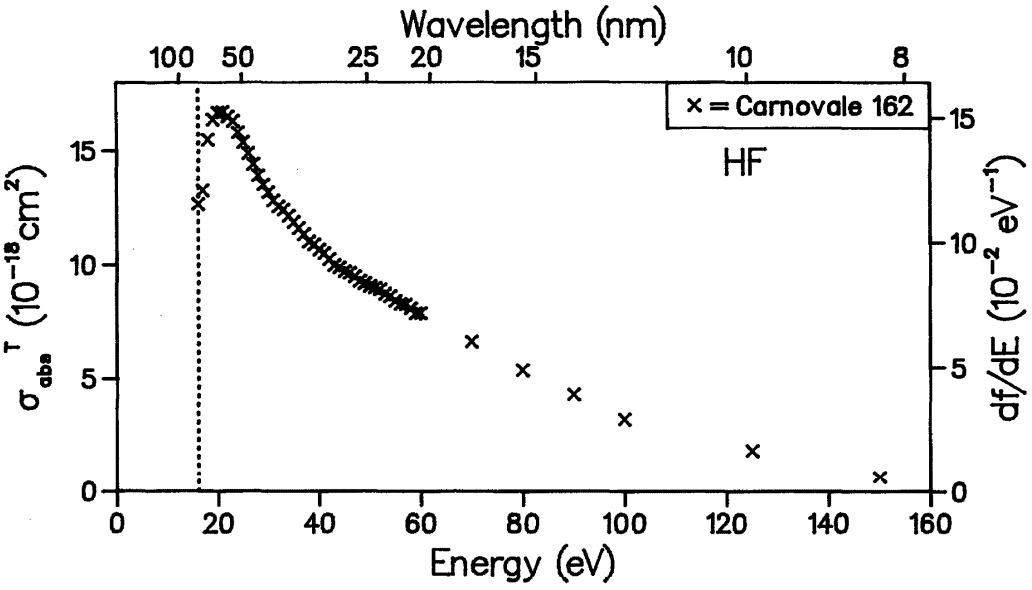

FIG. 64. Total photoabsorption cross section for HF.

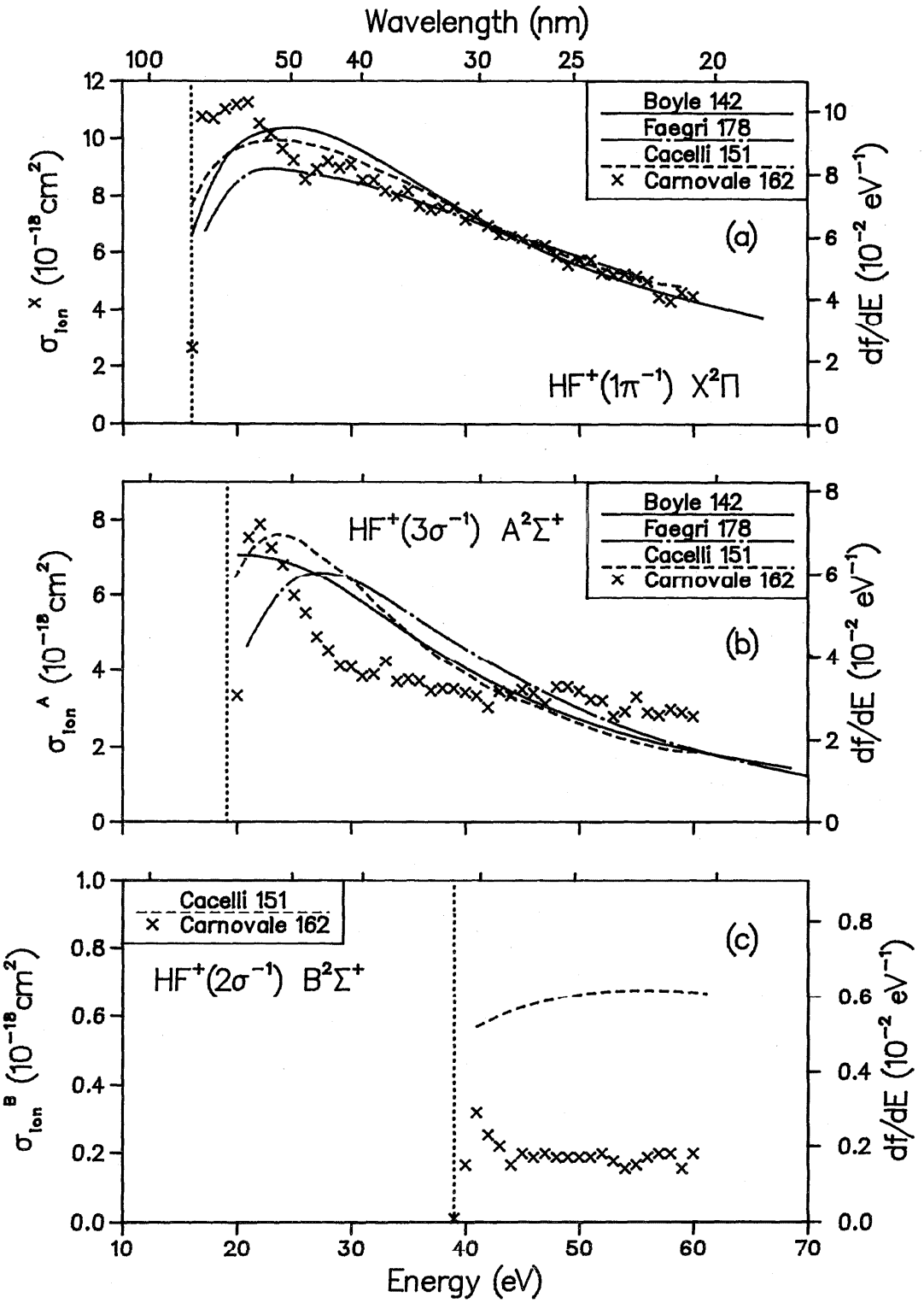

FIG. 65. Partial photoionization cross sections for HF; (a) final ionic state $= X^2\Pi$, (b) final ionic state $= A^2\Sigma^+$, (c) final ionic state $= B^2\Sigma^+$.

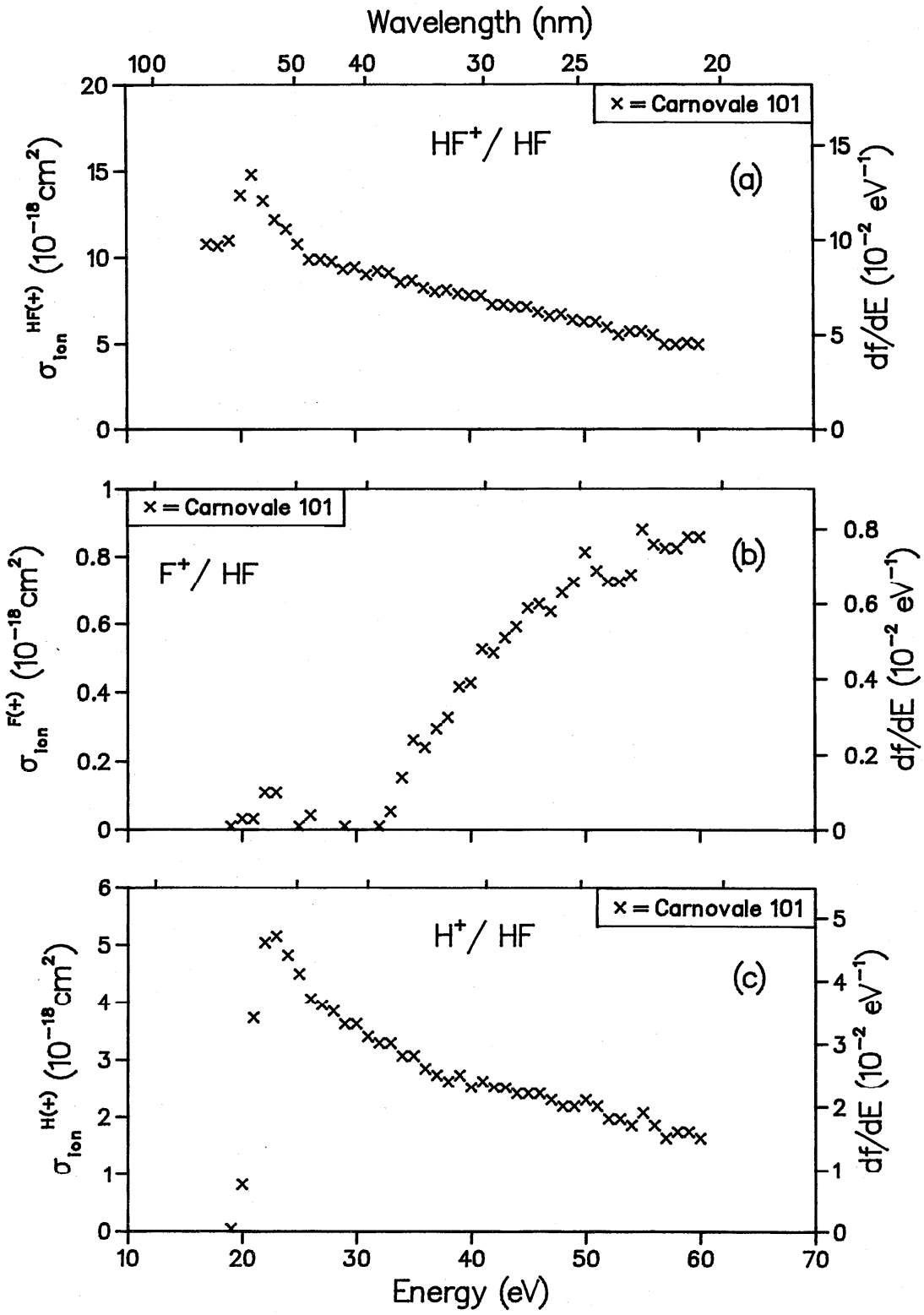

FIG. 66. Partial ionic photofragmentation cross sections for HF; (a) product ion = HF^+, (b) product ion = F^+, (c) product ion = H^+.

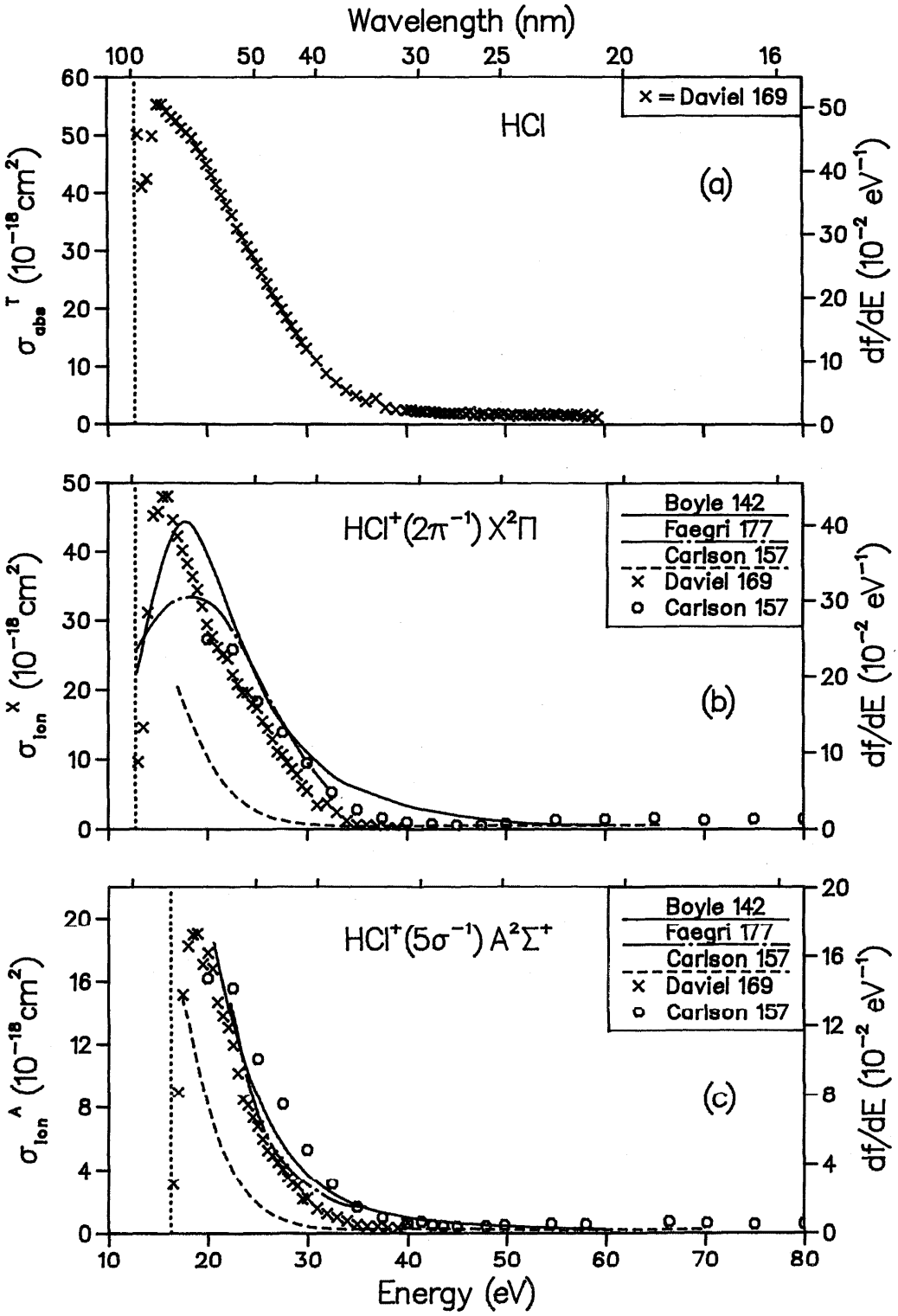

FIG. 67. (a) Total photoabsorption cross section for HCl. (b) Partial photoionization cross section for HCl, final ionic state = $X\,^2\Pi$. (c) Partial photoionization cross section for HCl, final ionic state = $A\,^2\Sigma^+$.

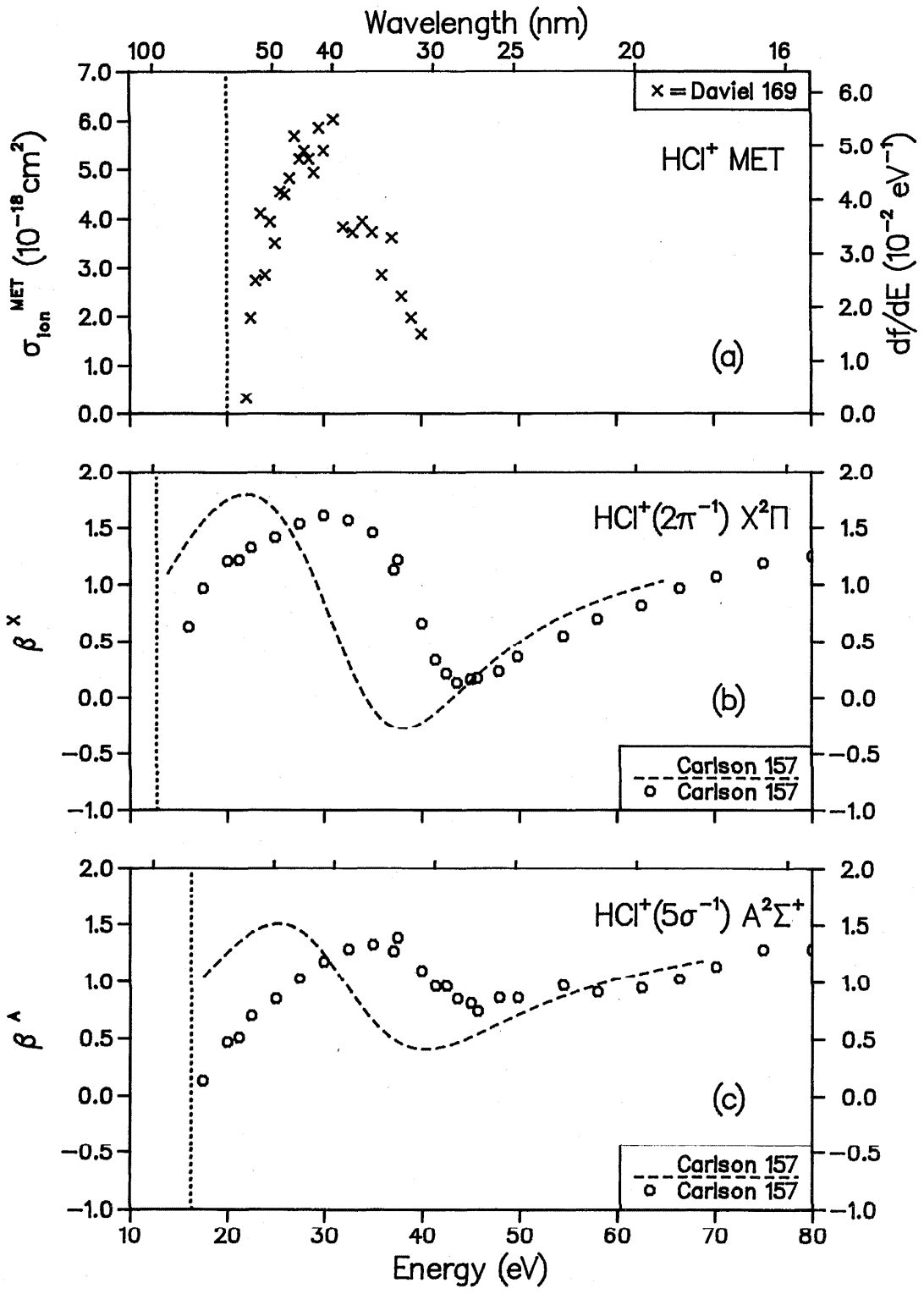

FIG. 68. (a) Partial photoionization cross section for HCl, final ionic states = many-body states arising from inner valence ionization. (b) Photoelectron asymmetry parameter for HCl, final ionic state = $X^2\Pi$. (c) Photoelectron asymmetry parameter for HCl, final ionic state = $A^2\Sigma^+$.

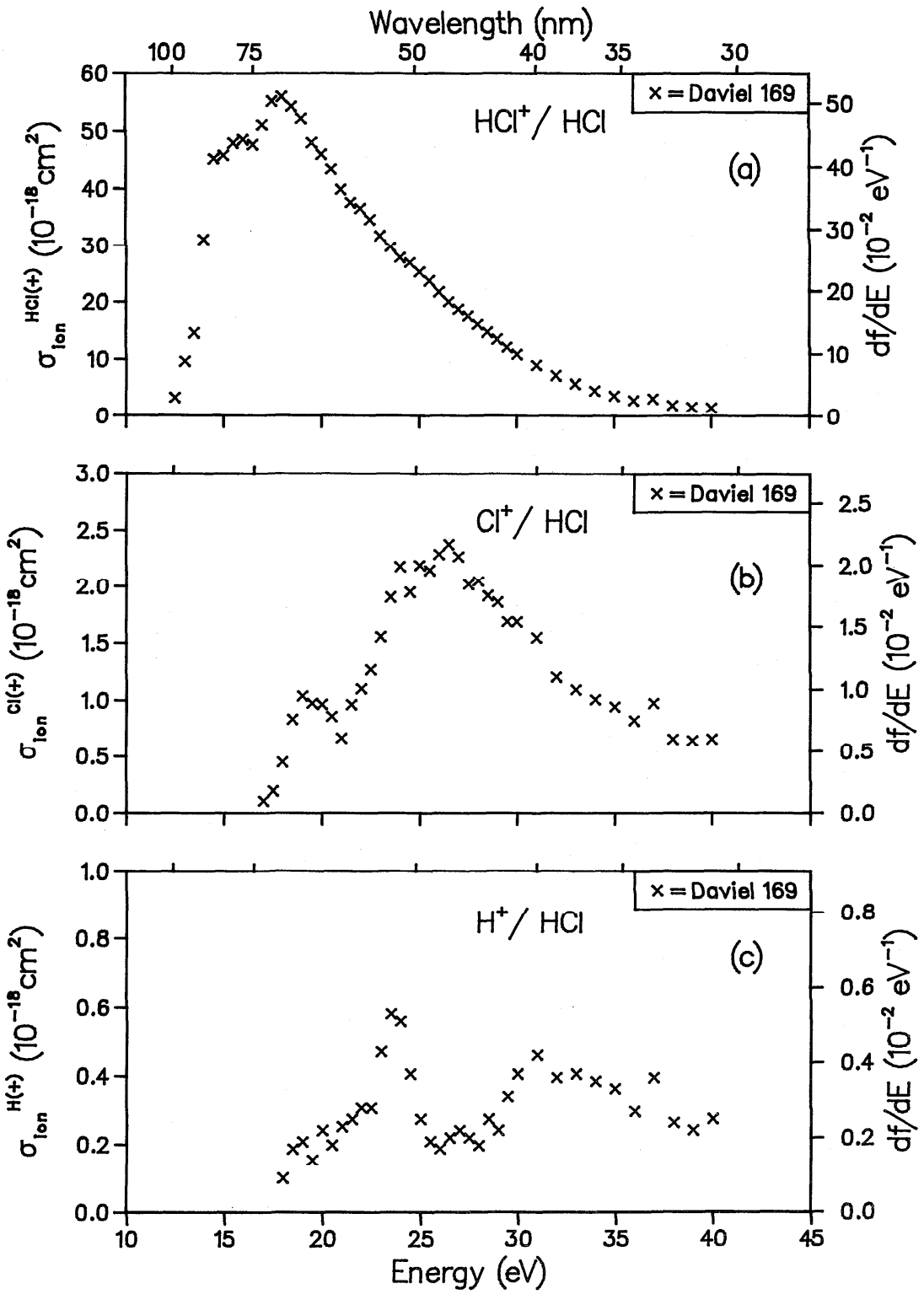

FIG. 69. Partial ionic photofragmentation cross sections for HCl; (a) product ion = HCl^+, (b) product ion = Cl^+, (c) product ion = H^+.

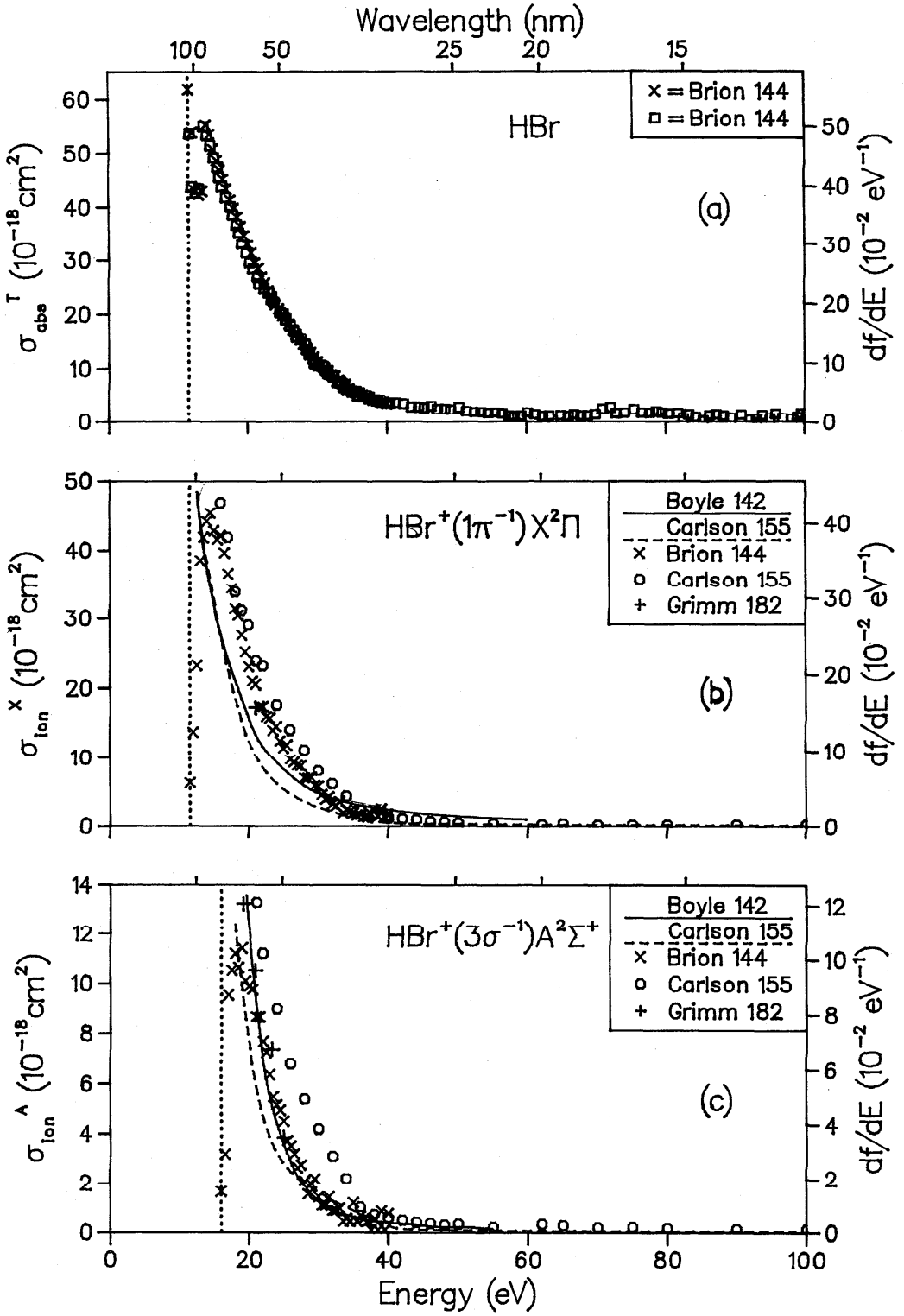

FIG. 70. (a) Total photoabsorption cross section for HBr. (b) Partial photoionization cross section for HBr, final state = $X^2\Pi$. (c) Partial photoionization cross section for HBr, final state = $A^2\Sigma^+$.

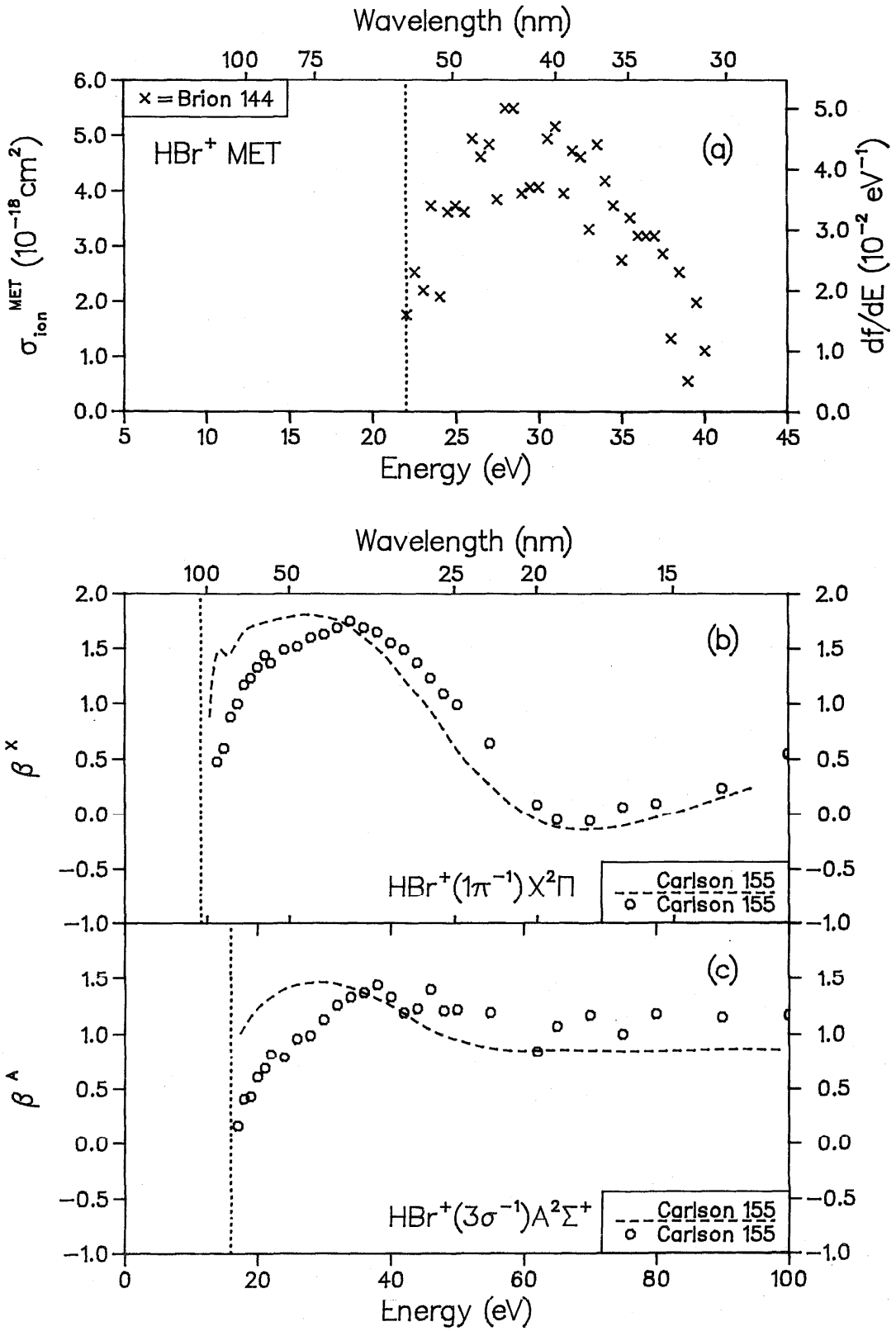

FIG. 71. Partial photoionization cross section for HBr, final ionic states = many-body states arising from inner valence ionization. (b) Photoelectron asymmetry parameter for HBr, final ionic state = $X^2\Pi$. (c) Photoelectron asymmetry parameter for HBr, final ionic state = $A^2\Sigma^+$.

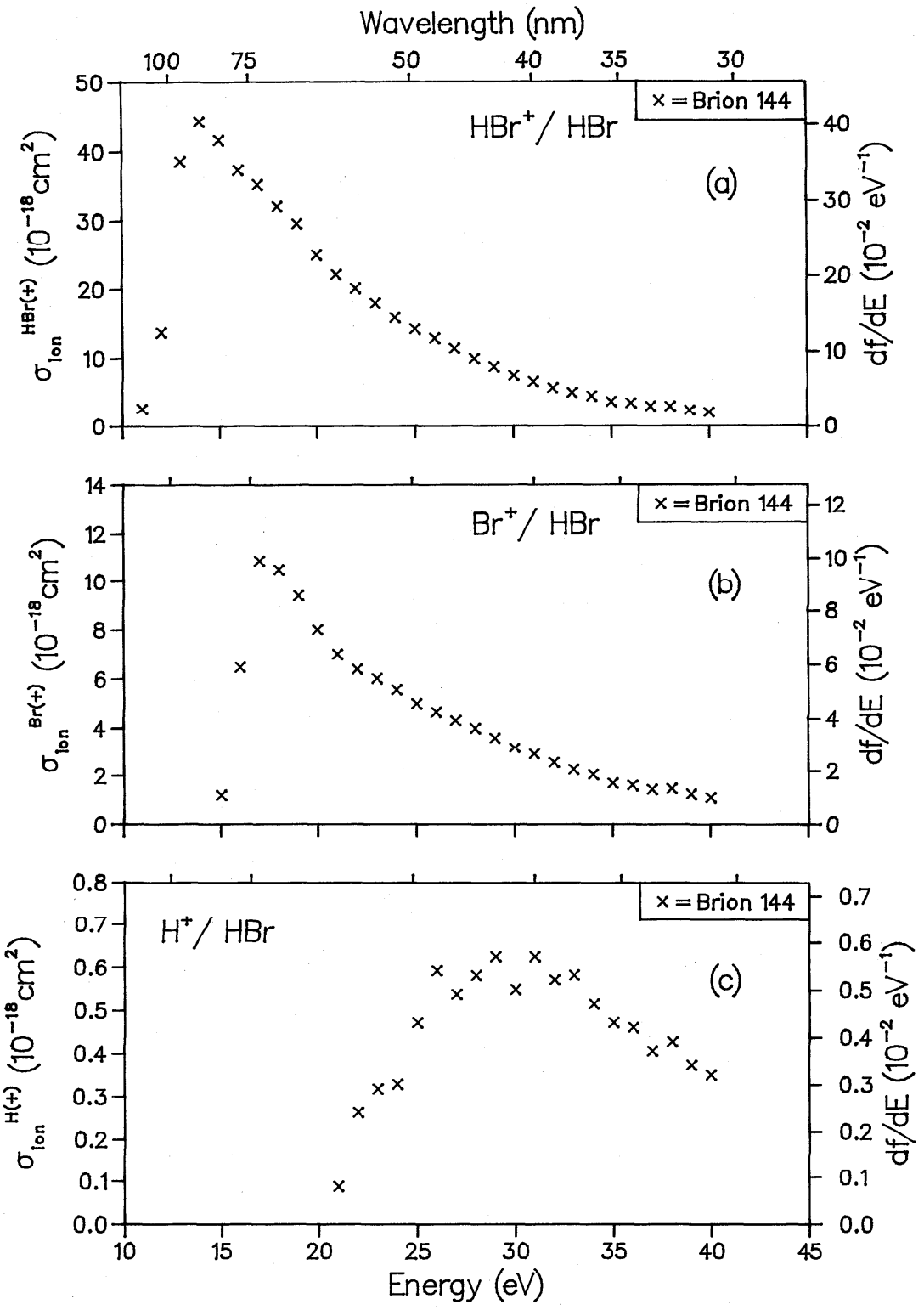

FIG. 72. Partial ionic photofragmentation cross sections for HBr; (a) product ion — HBr^+, (b) product ion = Br^+, (c) product ion = H^+.

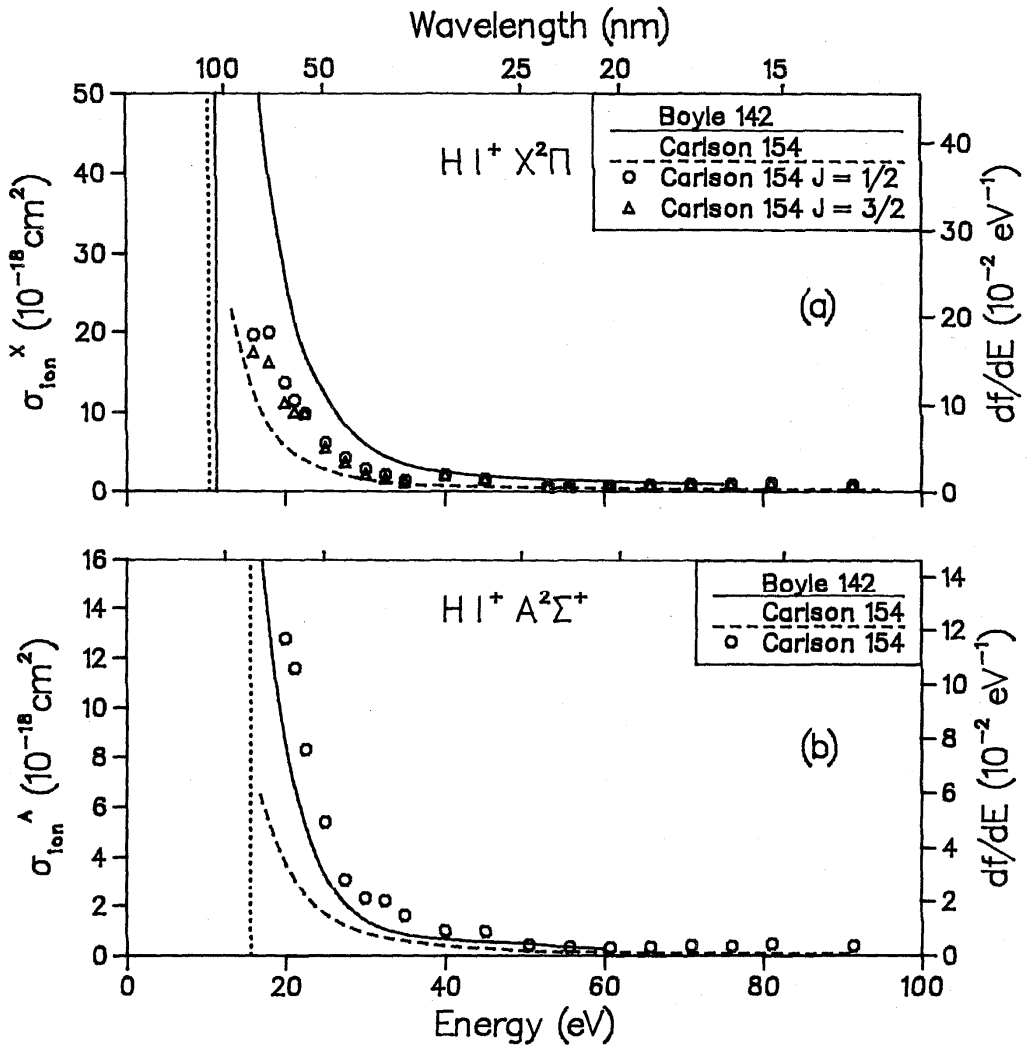

FIG. 73. Partial photoionization cross sections for HI; (a) final ionic state = $X\,^2\Pi$, (b) final ionic state = $A\,^2\Sigma^+$.

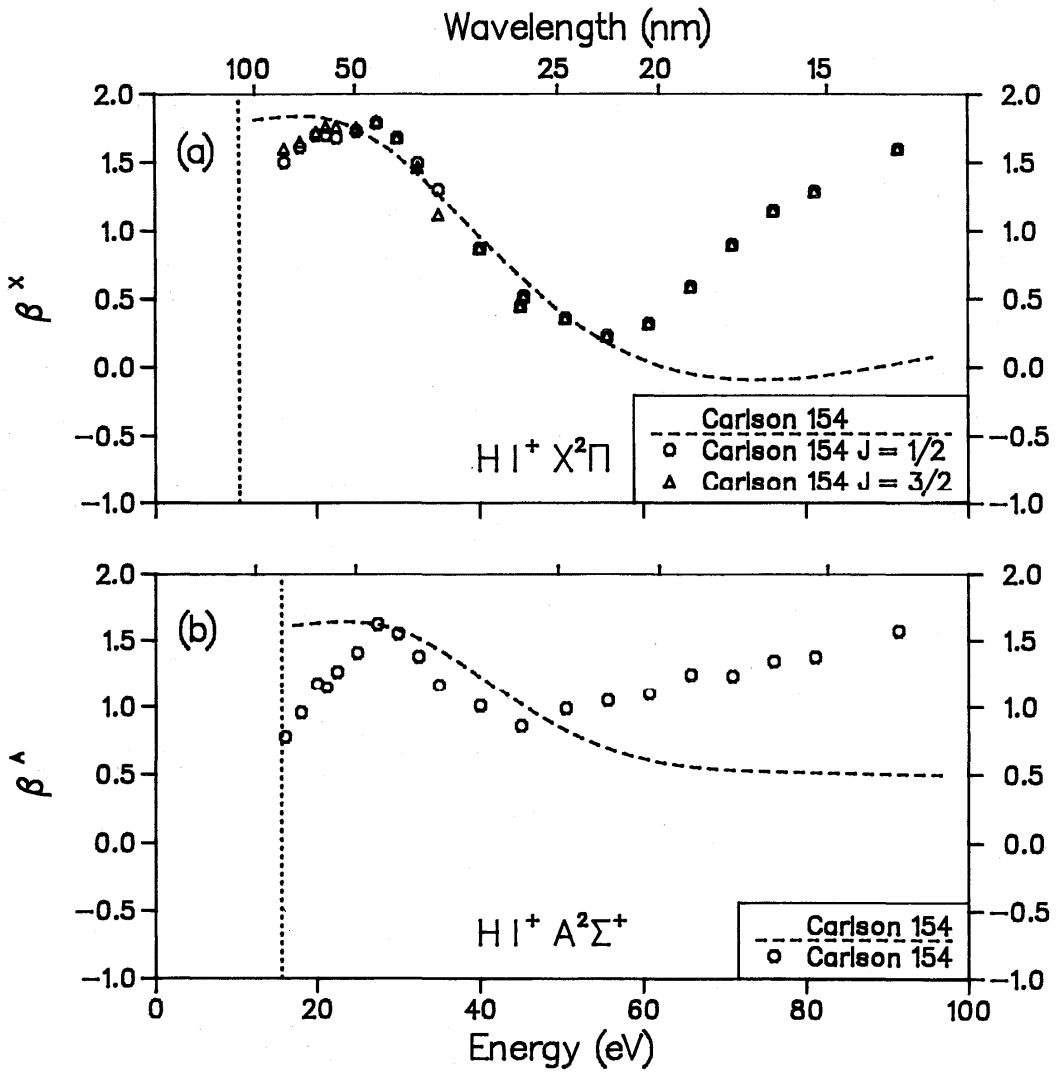

FIG. 74. Photoelectron asymmetry parameters for HI: (a) final ionic state = $X^2\Pi$. (b) final ionic state = $A^2\Sigma^+$.

Table 13. Data for H_2S.

Reference	Author	Year	E/T	Method	Experimental normalization	Cross Sections: Abs	Cross Sections: State specific partials	Cross Sections: Molecular ions and dissociative fragments	Betas: State	Photon energy range (eV)
230	Roche	1980	T	$X\alpha$	---		X,A,B,$(4a_1^{-1})$		X,A,B,$(4a_1)^{-1}$	12- 65
137	Adam	1986	E	P	---				X,A,B,$(4a_1)^{-1}$	25- 70
145	Brion	1986	E	DIP	TRK	✓				10- 90
145	Brion	1986	E	DIP	TRK		X,A,B,$(4a_1^{-1})$			10- 40
145	Brion	1986	E	DIP	TRK			H_2S^+,HS^+,S^+,H^+		10- 40
199	Ibuki	1986	E	P	AB	✓				12- 26
174	Diercksen	1987	T	StEx	---		X.A.B,$(4a_1^{-1})$			22- 55

[a]Branching ratios for X,A,B,$(4a,^{-1})$ states of H_2S^+ were reported by Adam et al. (137).

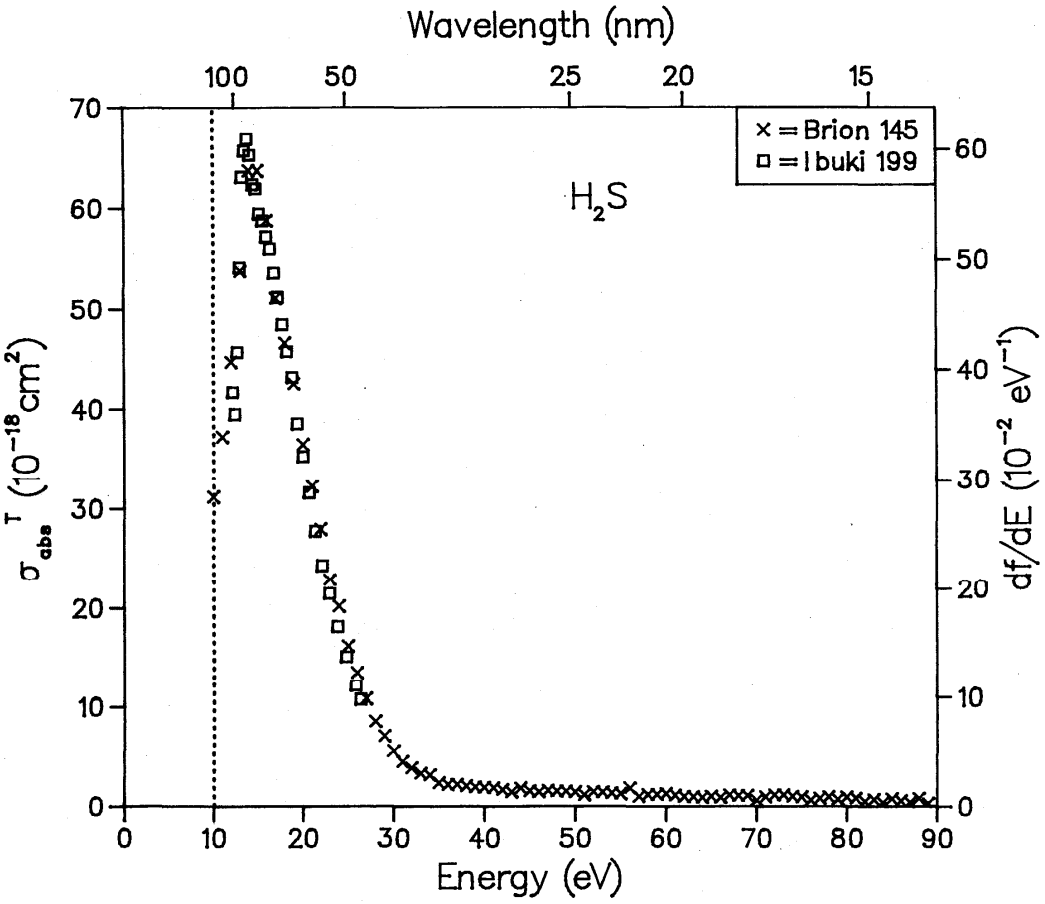

FIG. 75. Total photoabsorption cross section for H_2S.

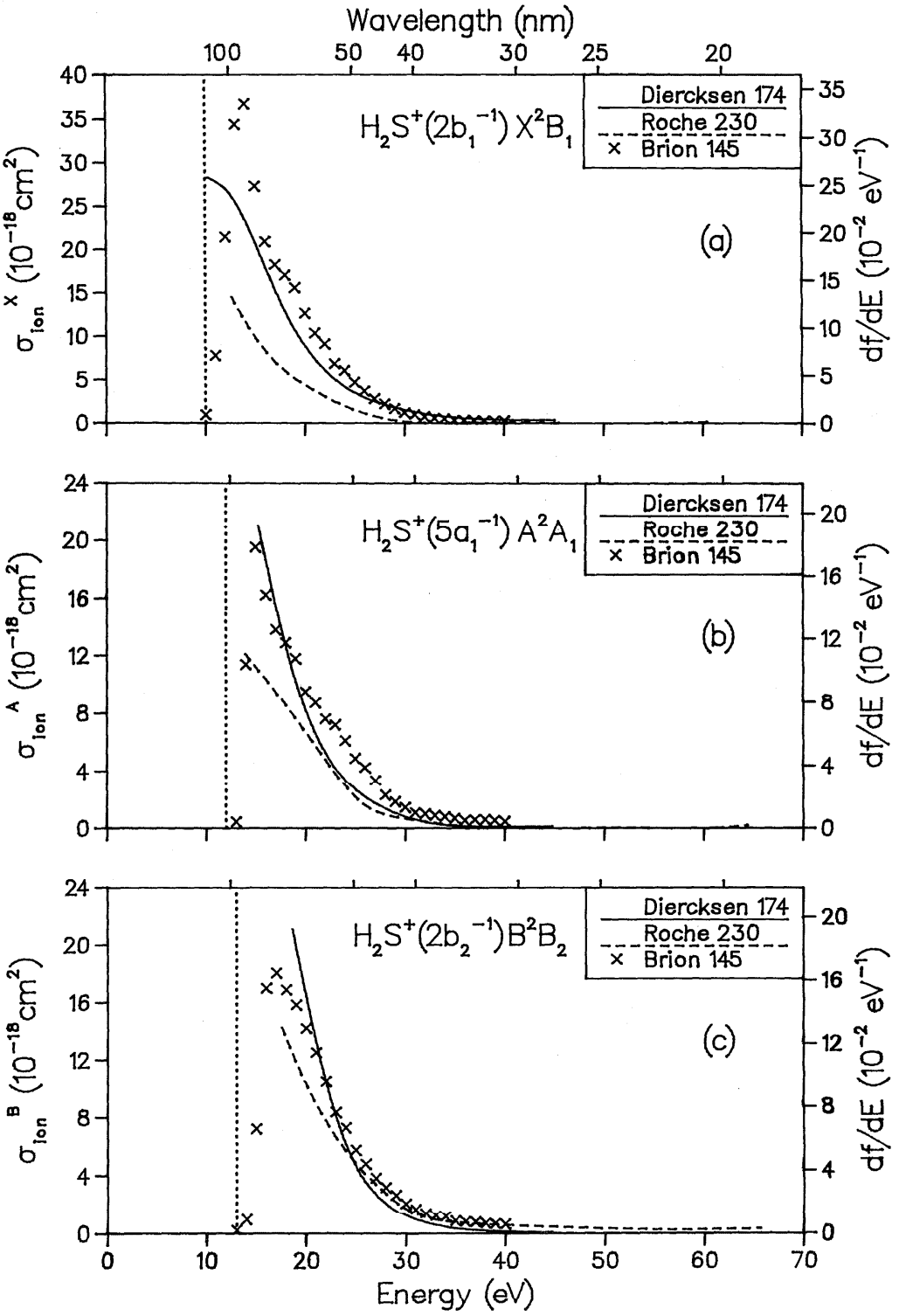

FIG. 76. Partial photoionization cross sections for H_2S; (a) final ionic state = $X\,^2B_1$, (b) final ionic state = $A\,^2A_1$, (c) final ionic state = $B\,^2B_2$.

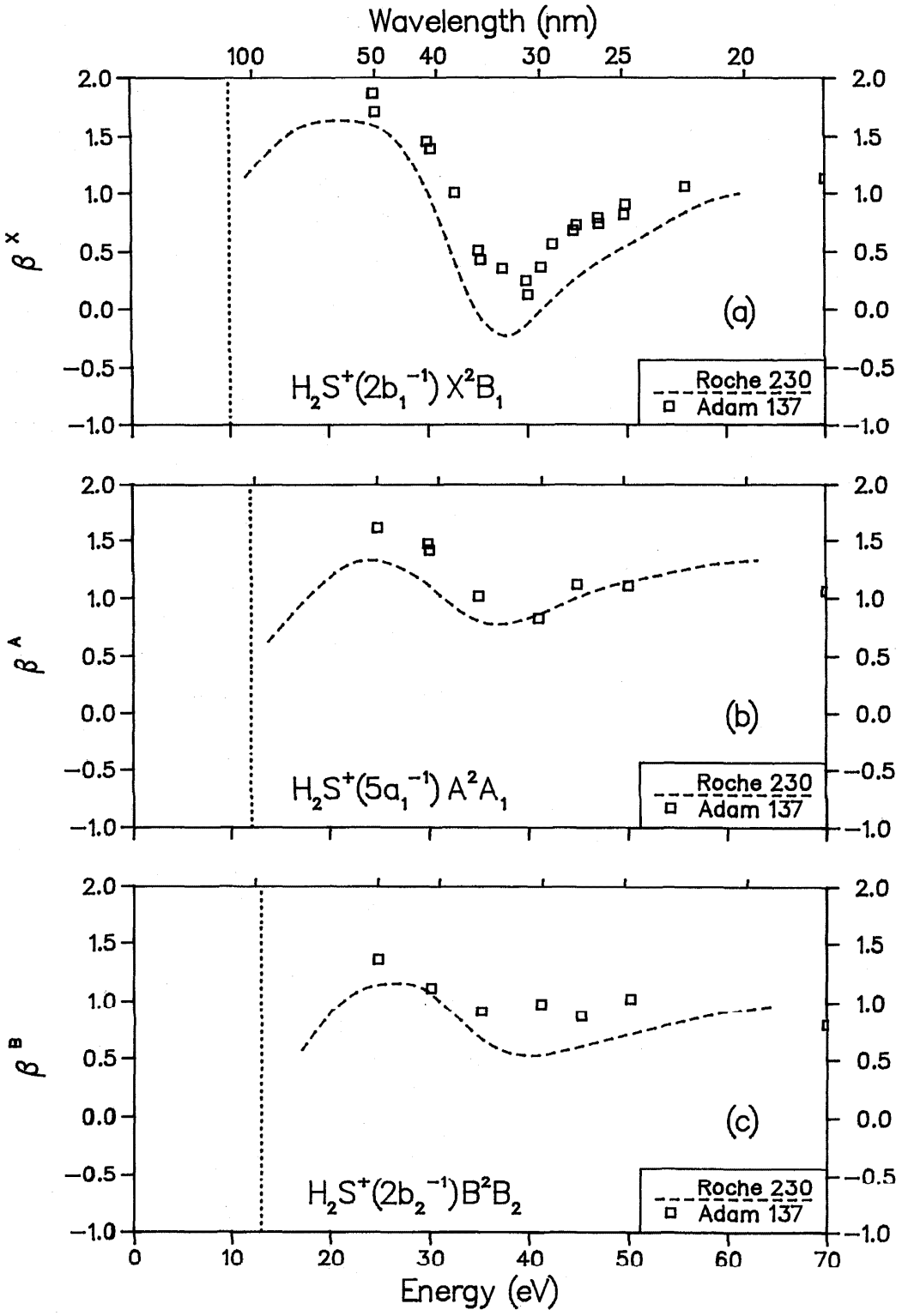

FIG. 77. Photoelectron asymmetry parameters for H_2S; (a) final ionic state $= X^2B_1$, (b) final ionic state $= A^2A_1$, (c) final ionic state $= B^2B_2$.

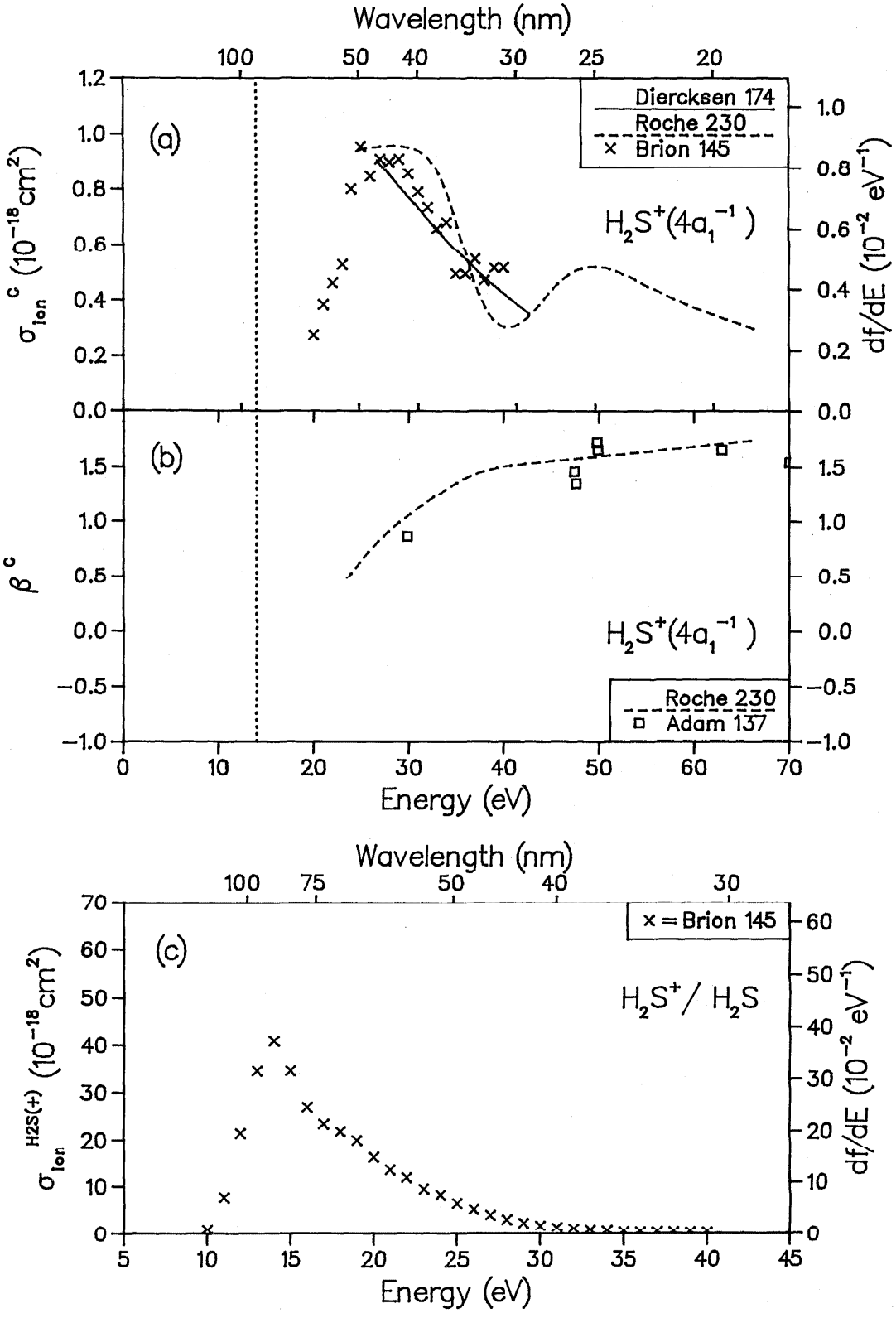

FIG. 78. (a) Partial photoionization cross section for H_2S, final ionic state = *C*, (b) photoelectron asymmetry parameter for H_2S, final ionic state = *C*. (c) Partial ionic photofragmentation cross section for H_2S, product ion = H_2S^+.

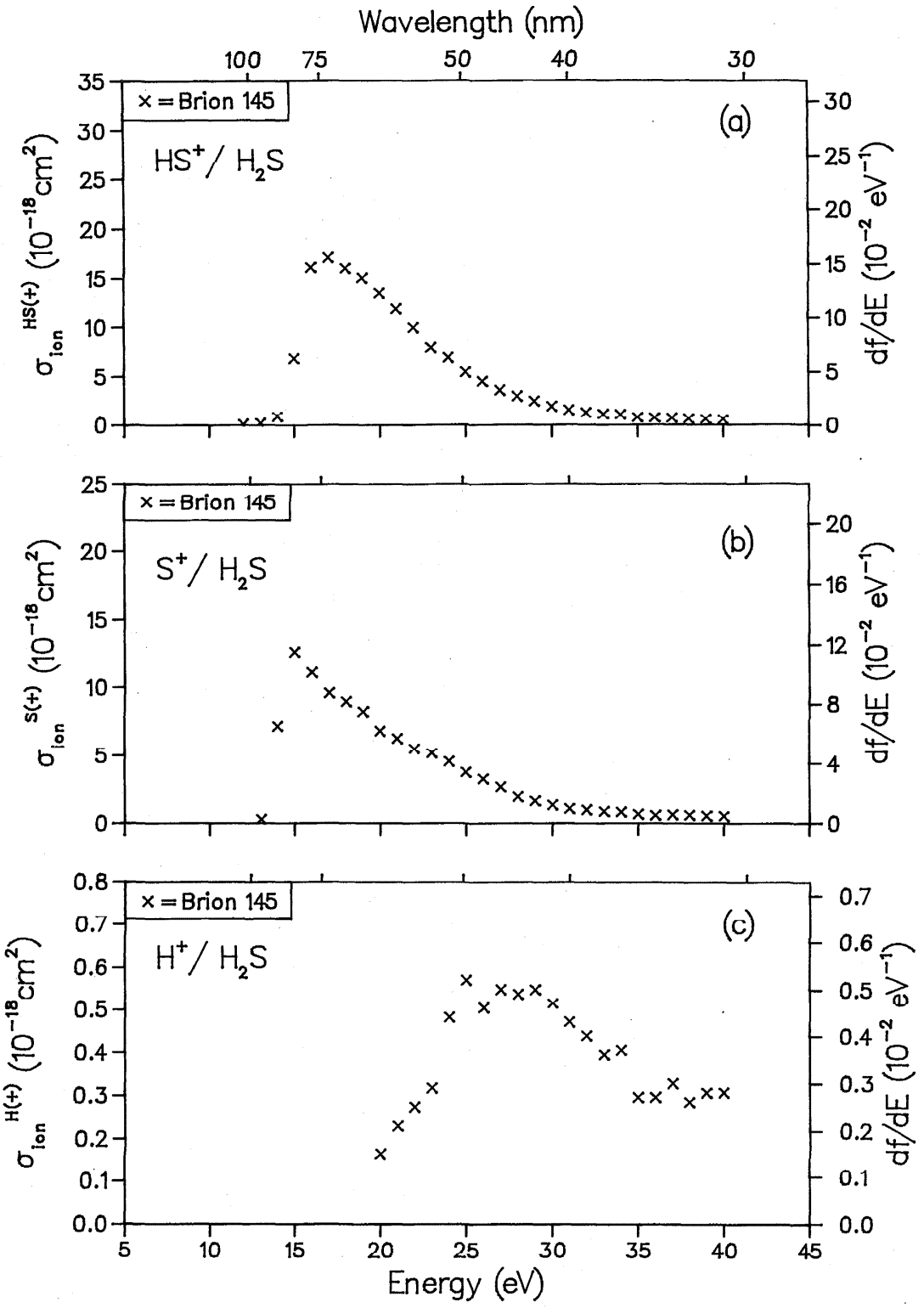

FIG. 79. Partial ionic photofragmentation cross sections for H_2S; (a) product ion = HS^+, (b) product ion = S^+, (c) product ion = H^+.

Table 14. Data for CS_2.

Reference	Author	Year	E/T	Method	Experimental normalization	Cross Sections			Betas	Photon energy range (eV)
						Abs	State specific partials	Molecular ions and dissociative fragments	State	
159	Carlson	1981	E	P	NM				X,A,B,C,D	12-29
163	Carnovale	1981	E	DIP	TRK	✓				5-40
163	Carnovale	1981	E	DIP	TRK		X,A,B,C+D,MET[a]			10-40
158	Carlson	1982	E	P	NM		X,A,B,C,D		X,A,B,C,D	21-70
158	Carlson	1982	T	$X\alpha$	---		X,A,B,C		X,A,B,C	21- 70
105	Carnovale	1982	E	DIP	TRK			CS_2^+,S_2^+,CS^+,CS_2^{2+},C^+,S^+		13-40
261	Wu	1983	E	P	AB	✓				16-67
173	Dierckson	1986	T	StEx	---		X,A,B,C			10-50

[a]MET = many-body states arising from inner valence ionization.

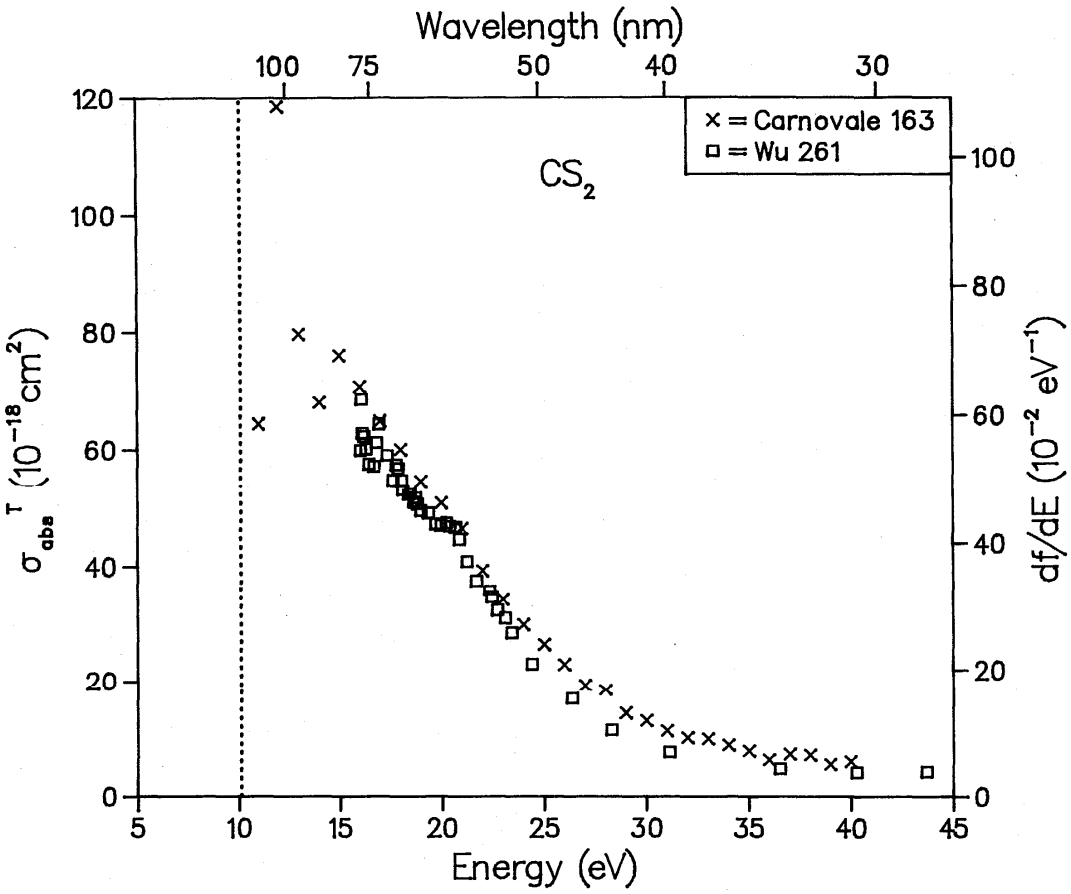

FIG. 80. Total photoabsorption cross section for CS_2.

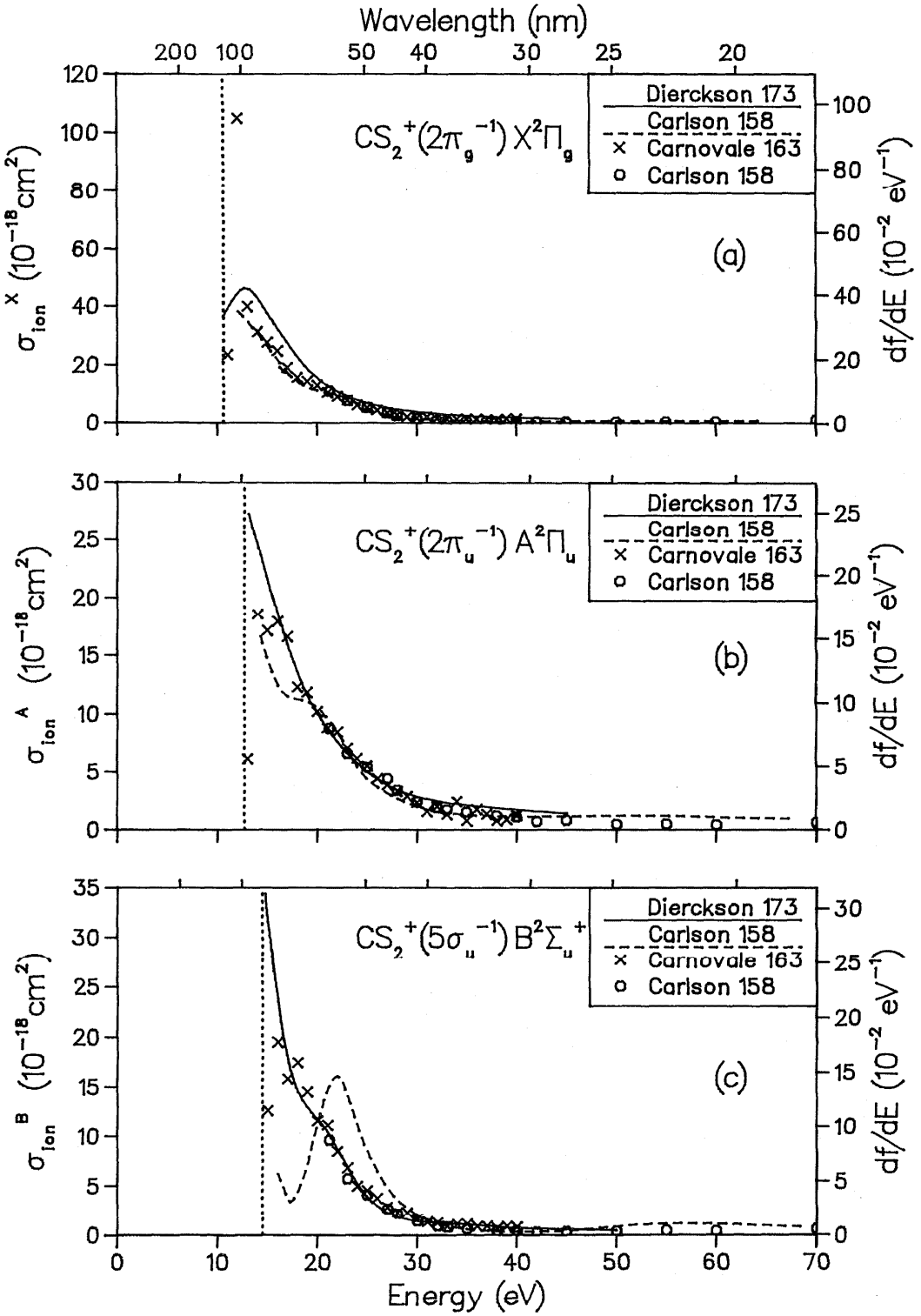

FIG. 81. Partial photoionization cross sections for CS_2; (a) final ionic state = $X^2\Pi_g$, (b) final ionic state = $A^2\Pi_u$,(c) final ionic state = $B^2\Sigma_u$.

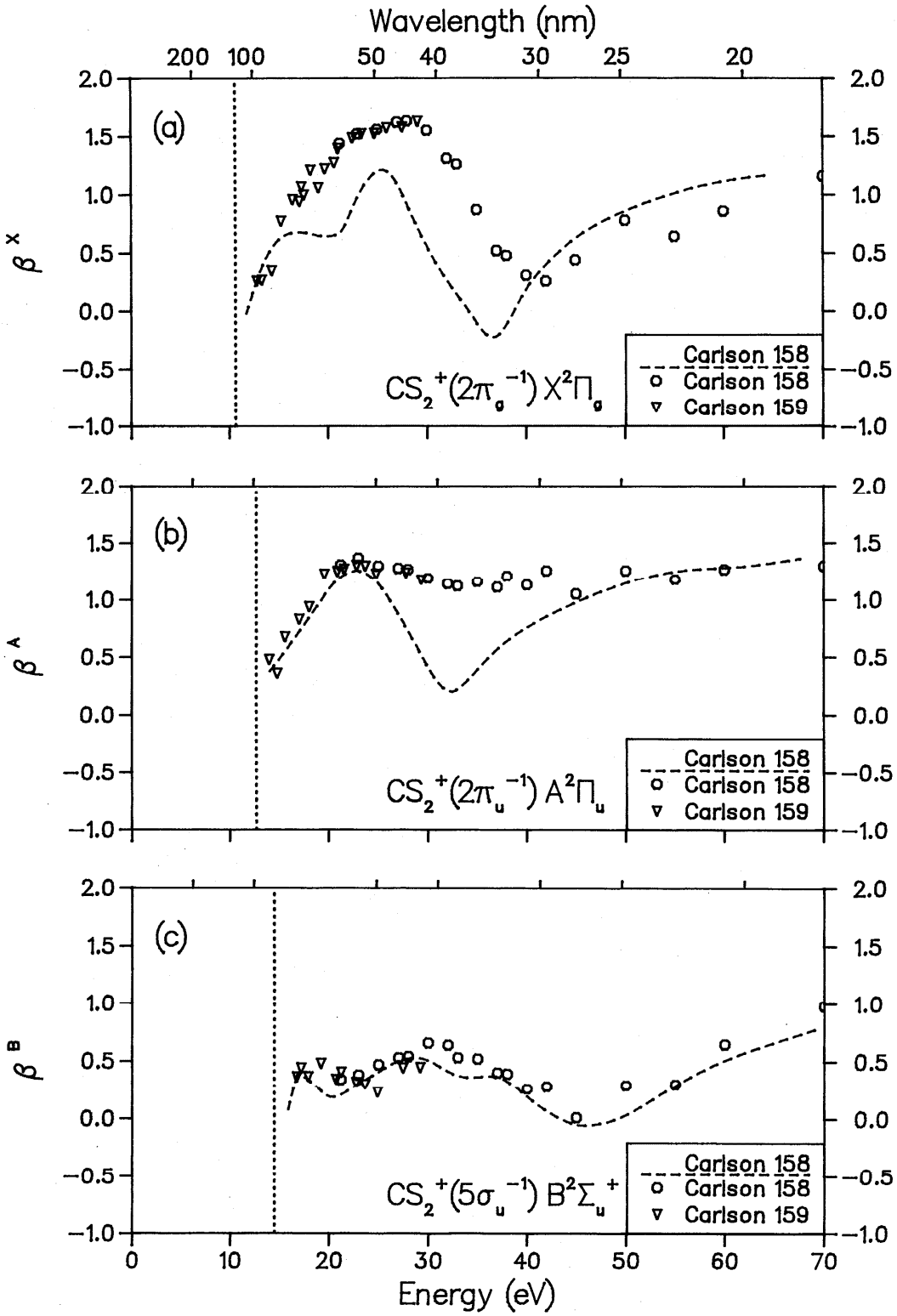

FIG. 82. Photoelectron asymmetry parameters for CS_2; (a) final ionic state = $X^2\Pi_u$, (b) final ionic state = $A^2\Pi_u$, (c) final ionic state = $B^2\Sigma_u$.

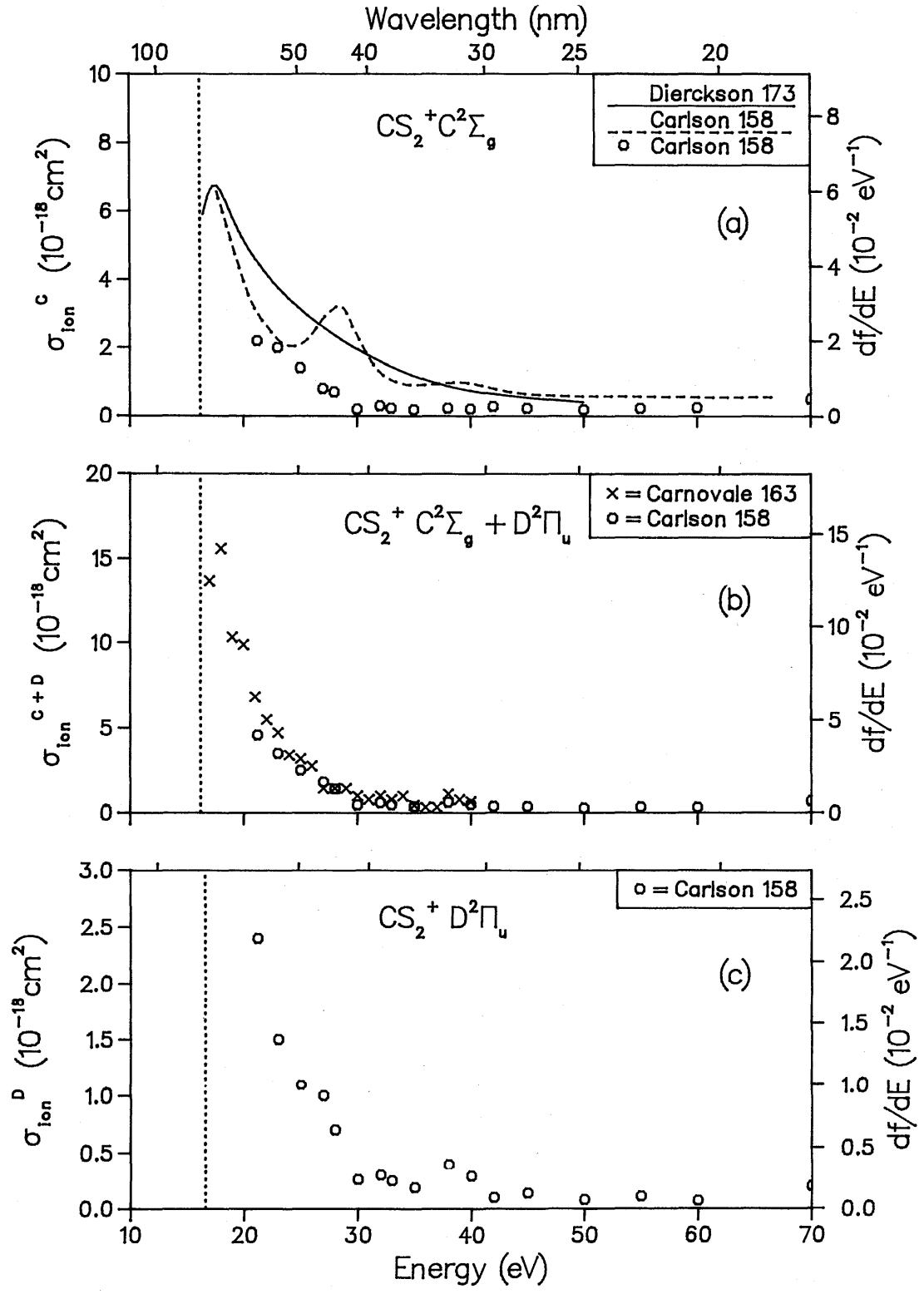

FIG. 83. (a) Partial photoionization cross sections for CS_2; (a) final ionic state = $C^2\Sigma_g$, (b) final ionic state = $C^2\Sigma_g + D^2\Pi_u$, (c) final ionic state = $D^2\Pi_u$.

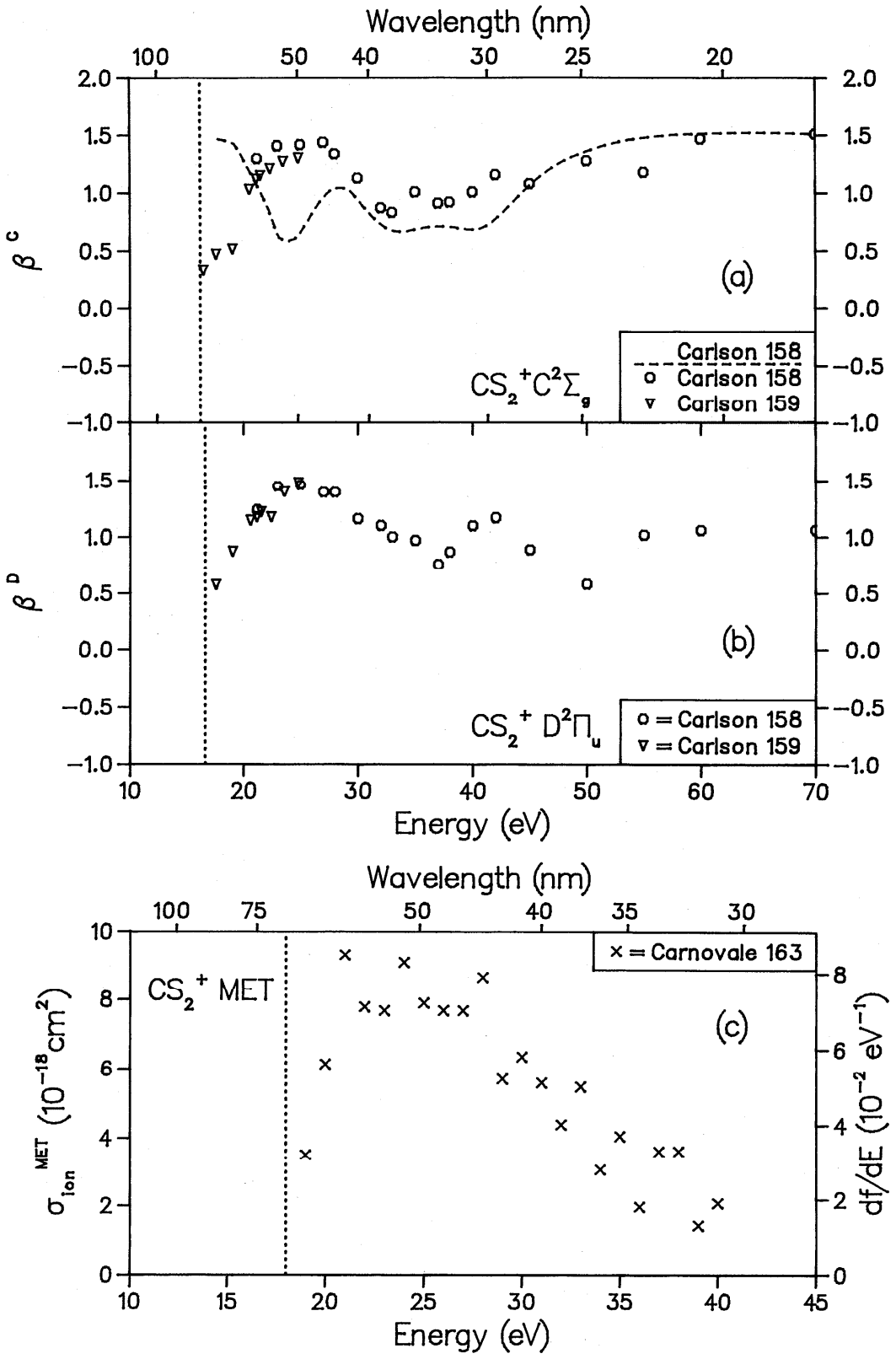

FIG. 84. Photoelectron asymmetry parameters for CS_2; (a) final ionic state = $C^2\Sigma_g$, (b) final ionic state = $D^2\Pi_u$, (c) Partial photoionization cross section for CS_2, final ionic states = many-body states arising from inner valence ionization.

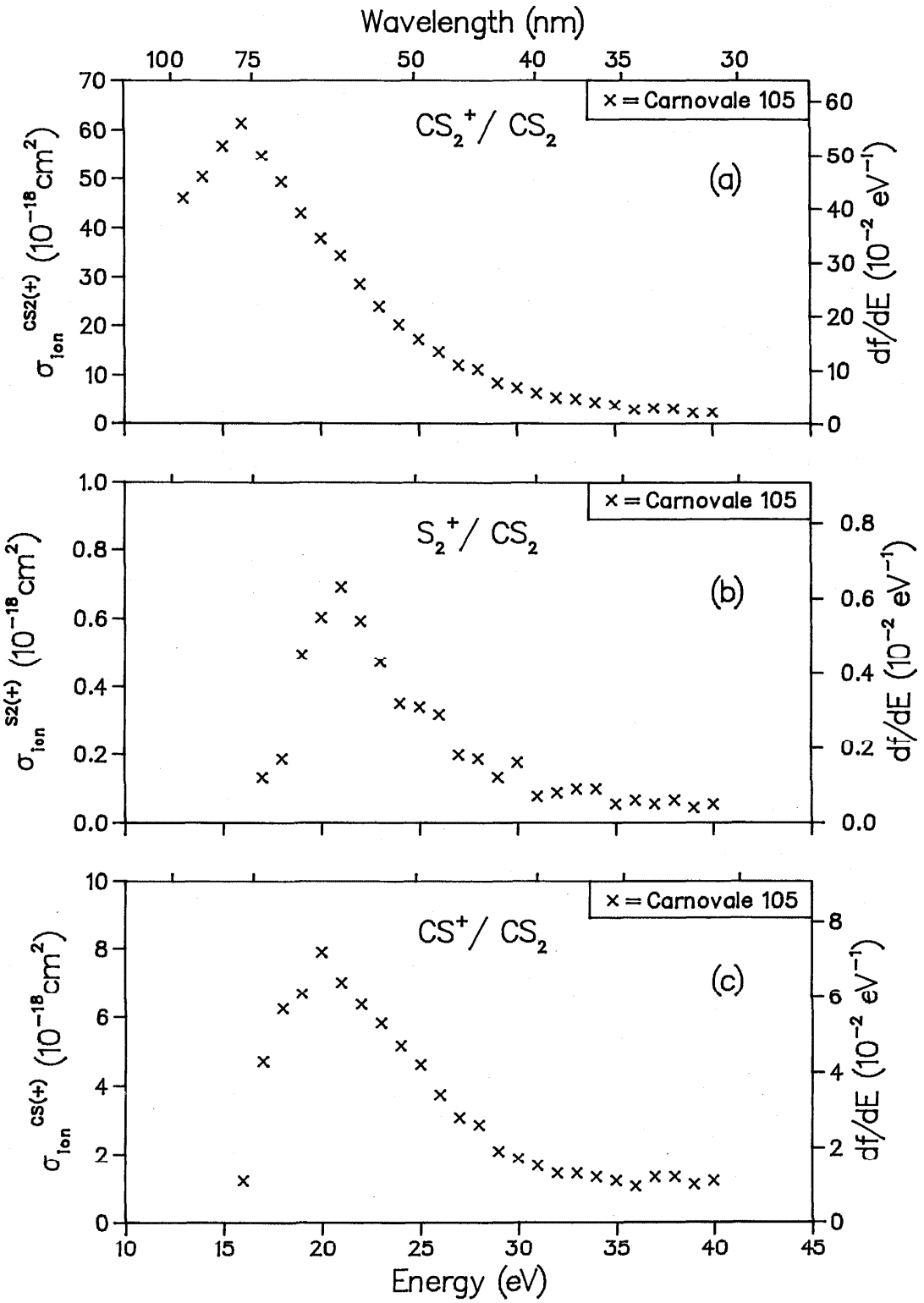

FIG. 85. Partial ionic photofragmentation cross sections for CS_2; (a) product ion = CS_2^+, (b) product ion = S_2^+, (c) product ion = CS^+.

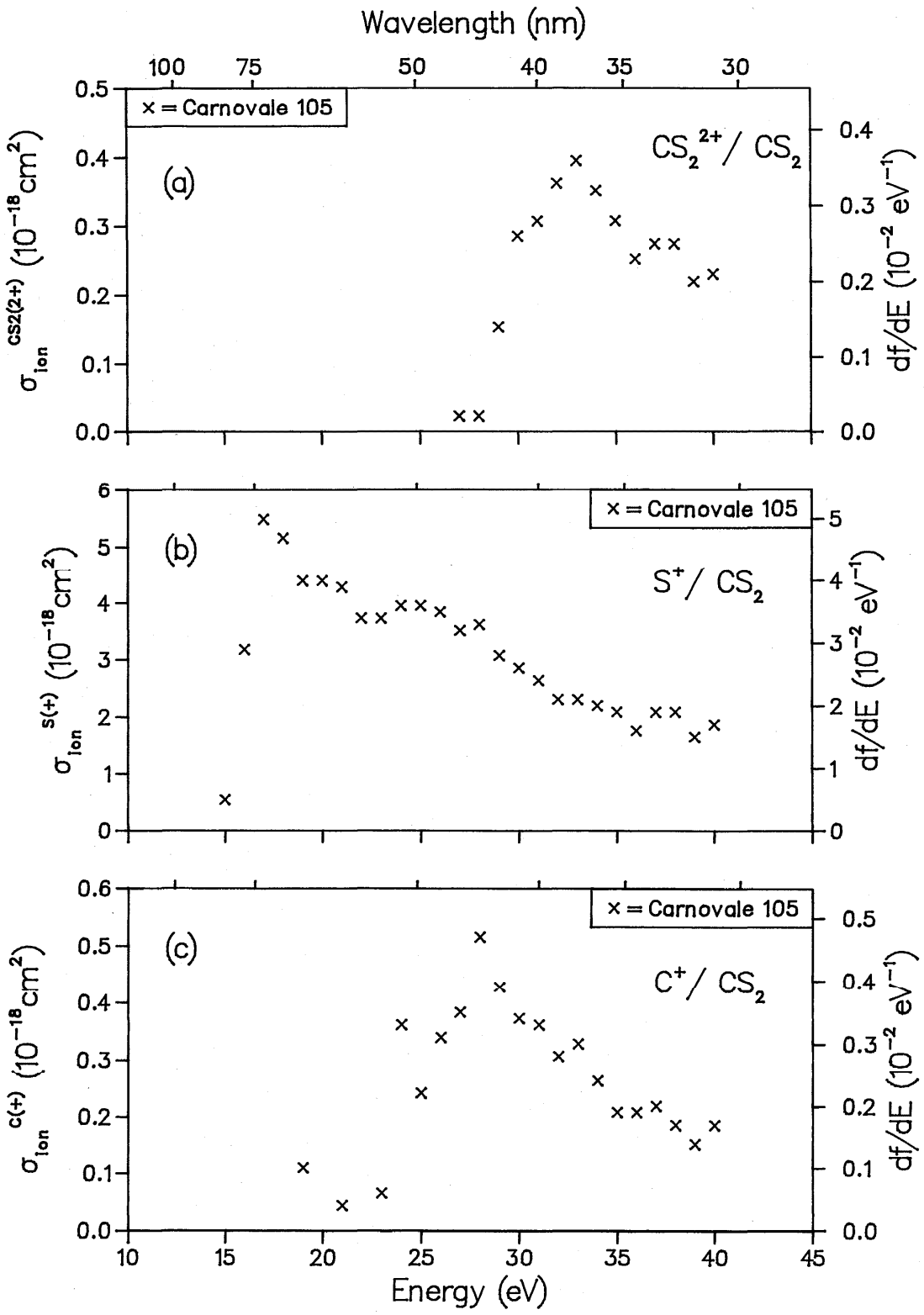

FIG. 86. Partial ionic photofragmentation cross sections for CS_2; (a) product ion = CS_2^{2+}, (b) product ion = S^+, (c) product ion = C^+.

Table 15. Data for OCS.

Reference	Author	Year	E/T	Method	Experimental normalization	Cross Sections			Betas	Photon energy range (eV)
						Abs	State specific partials	Molecular ions and dissociative fragments	State	
159	Carlson	1981	E	P	NM				X,A,B	13- 29
89	White	1981	E	DIP	TRK	✓				6-100
89	White	1981	E	DIP	TRK		X,A+B,C,MET[a]			10-100
158	Carlson	1982	E	P	NM		X,A+B,C		X,A,B,C	21- 40
158	Carlson	1982	T	$X\alpha$	---		X,A+B,C		X,A,B,C	12- 45
105	Carnovale	1982	E	DIP	TRK			$OCS^+,CS^+,S^+,CO^+,O^+,C^+$		13- 50
260	Wu	1982	E	P	AB	✓				16- 68
240	Sheehy	1986	T	StEx	---		X,A+B,C			12- 60

[a]MET = many-body states arising from inner valence ionization.

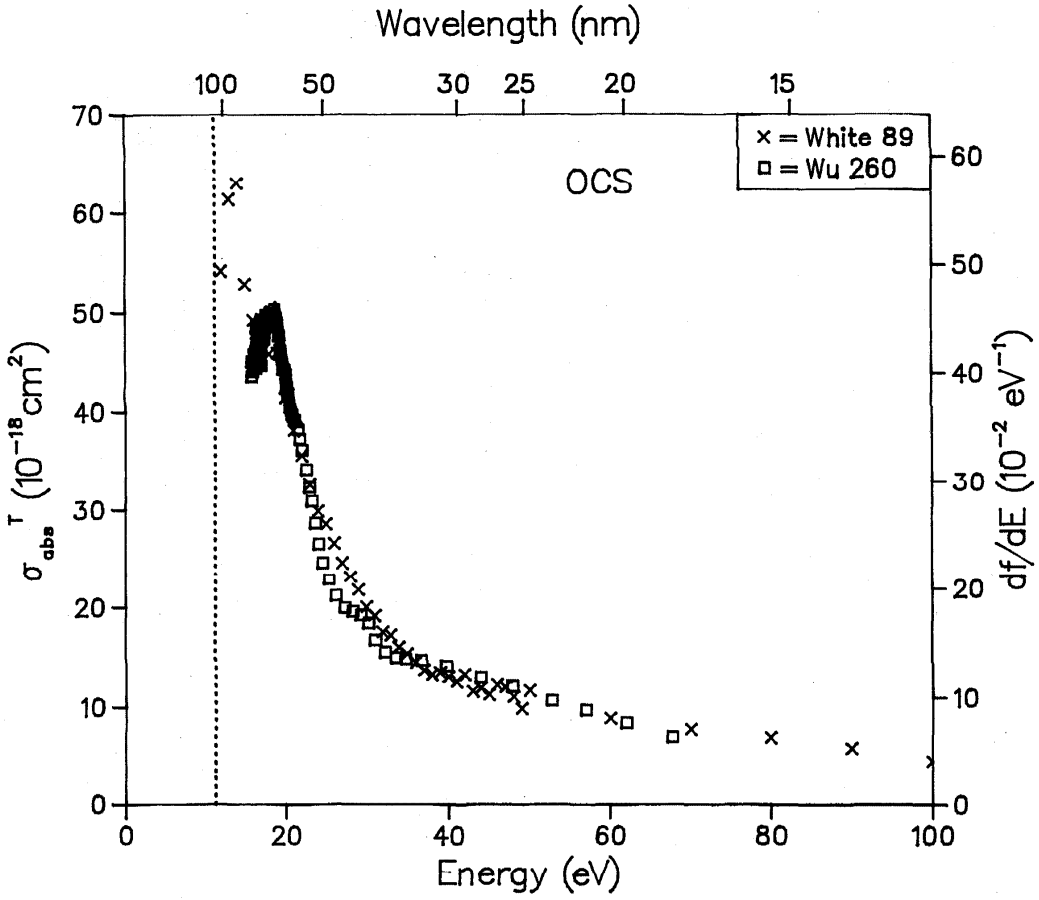

FIG. 87. Total photoabsorption cross section for OCS.

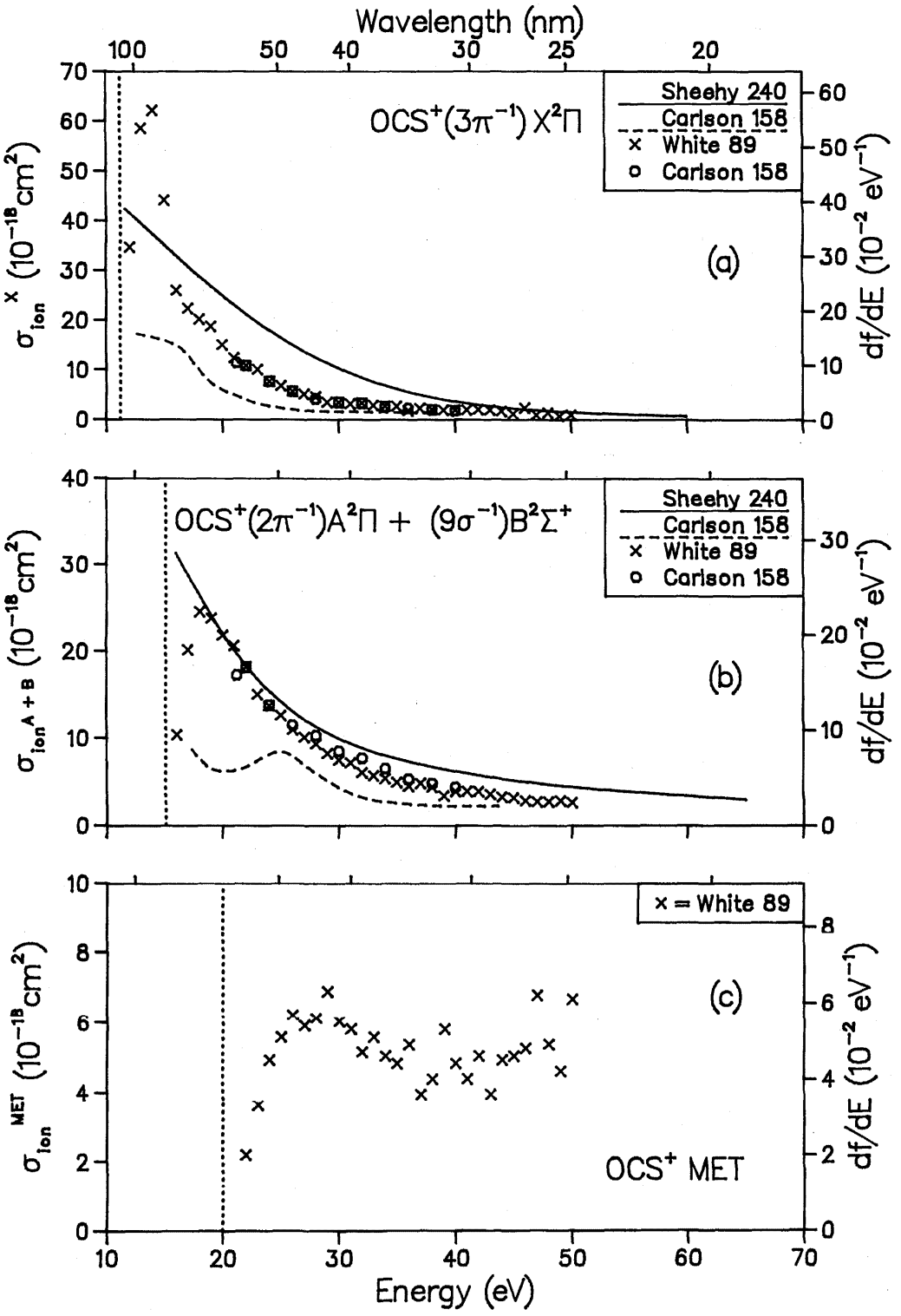

FIG. 88. Partial photoionization cross sections for OCS; (a) final ionic state = $X^2\Pi$, (b) final ionic state = $A^2\Pi + B^2\Sigma^+$, (c) final ionic states = many-body states arising from inner valence ionization.

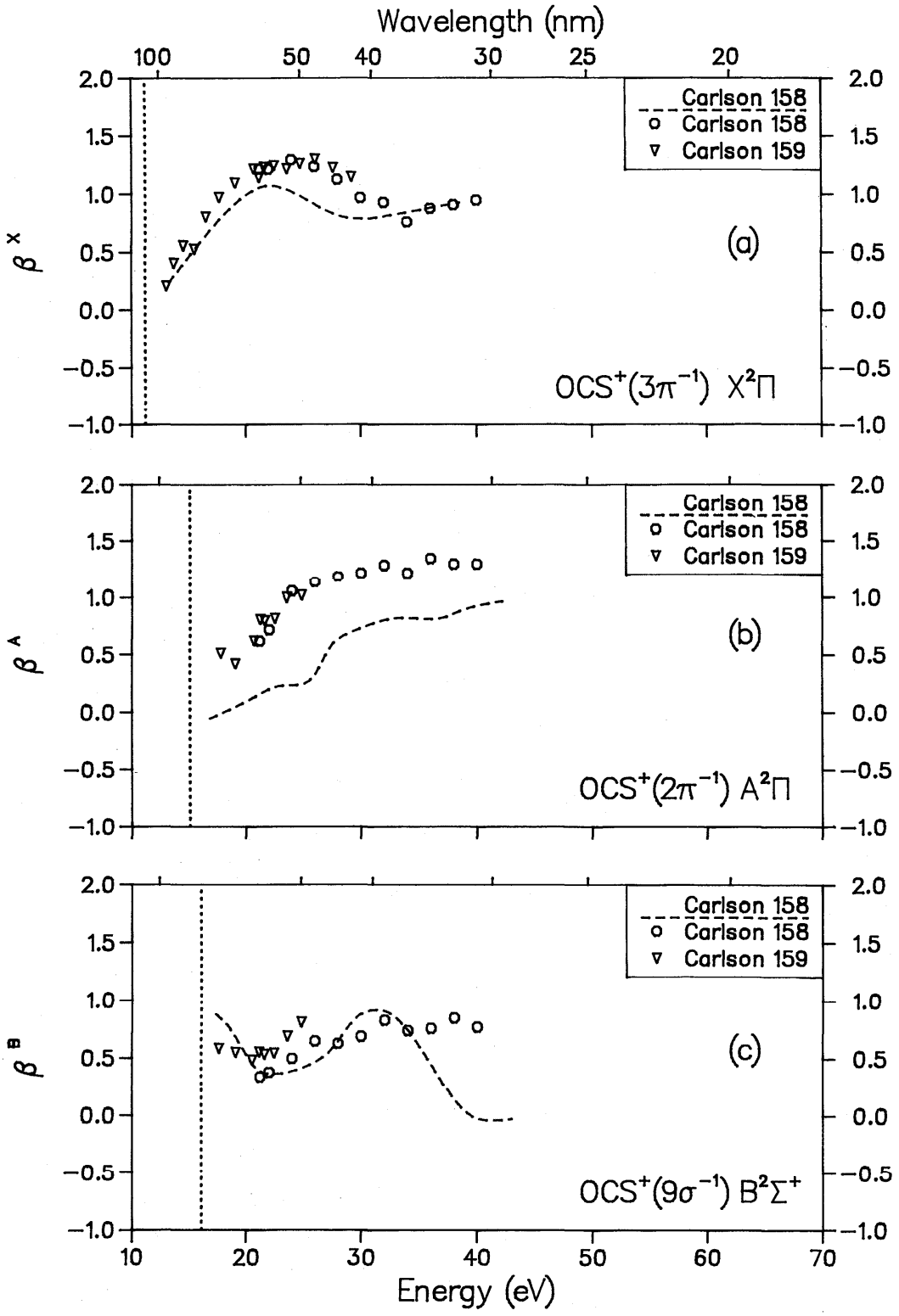

FIG. 89. Photoelectron asymmetry parameters for OCS; (a) final ionic state = $X^2\Pi$, (b) final ionic state = $A^2\Pi$, (c) final ionic state = $B^2\Sigma^+$.

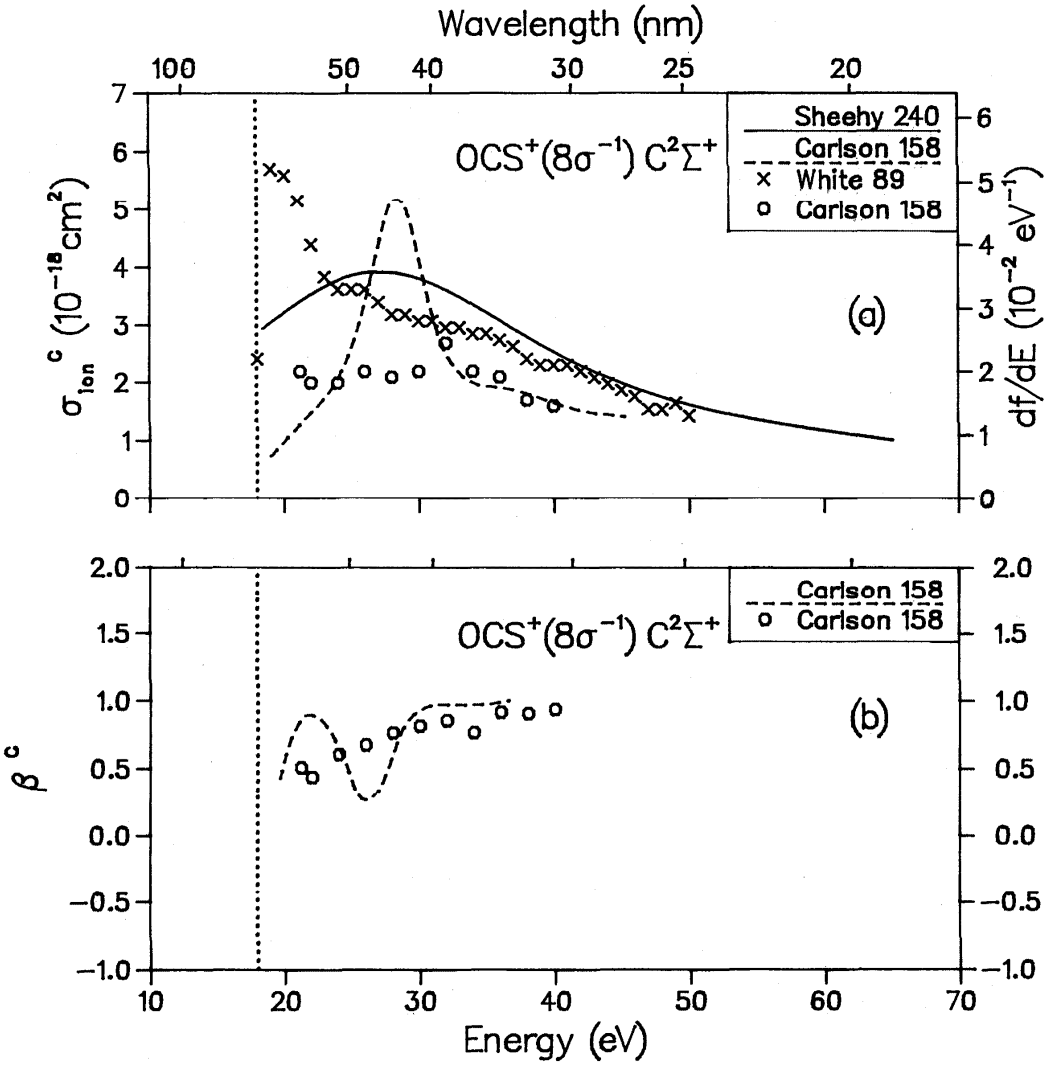

FIG. 90. (a) Partial photoionization cross section for OCS, final ionic state $= C^2\Sigma^+$. (b) Photoelectron asymmetry parameter for OCS, final ionic state $= C^2\Sigma^+$.

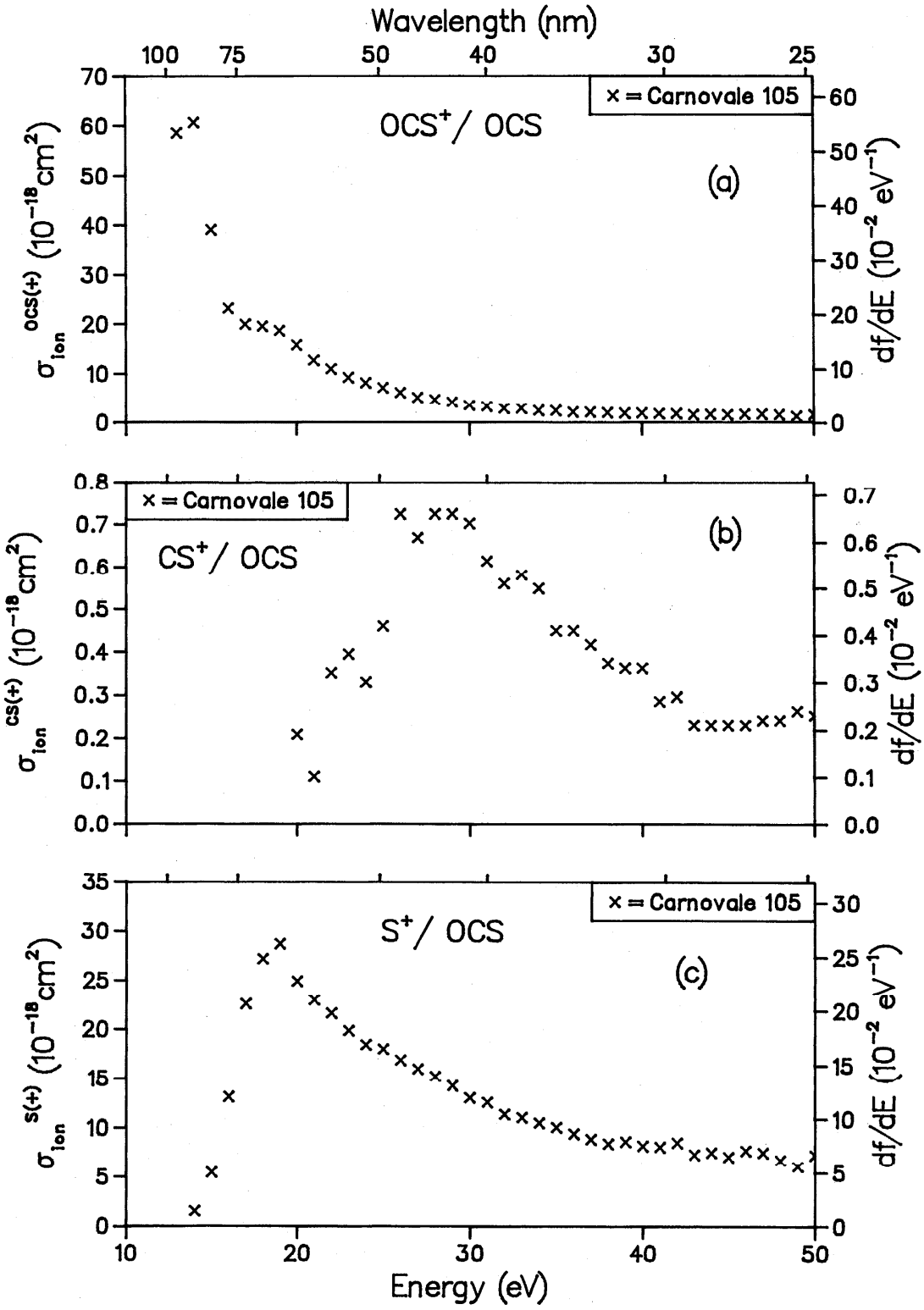

FIG. 91. Partial ionic photofragmentation cross sections for OCS; (a) product ion = OCS^+, (b) product ion = CS^+, (c) product ion = S^+.

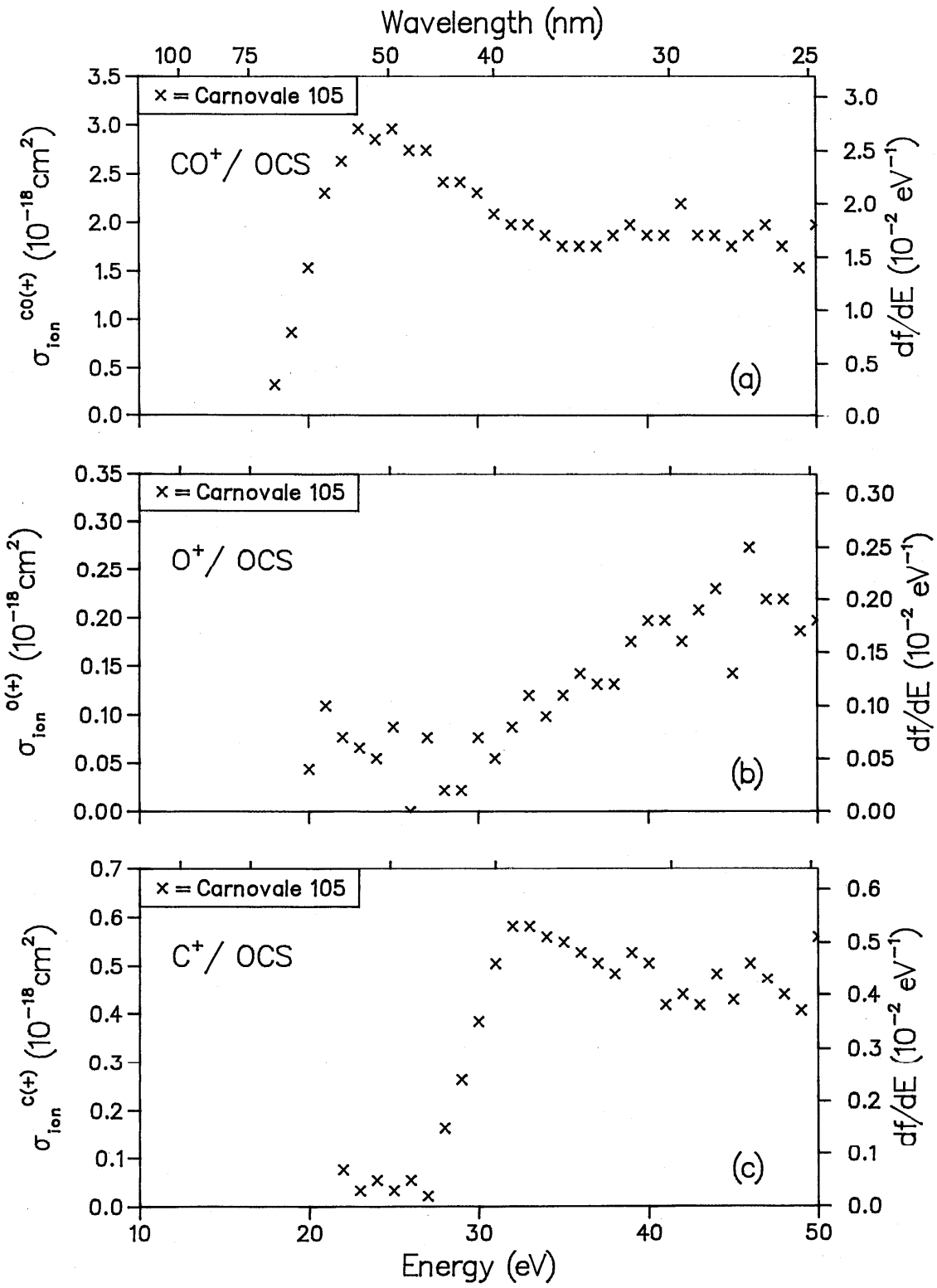

FIG. 92. Partial ionic photofragmentation cross sections for OCS; (a) product ion = CO^+, (b) product ion = O^+, (c) product ion = C^+.

Table 16. Data compiled for SO_2.

Reference	Author	Year	E/T	Method	Experimental normalization	Cross Sections			Betas	Photon energy range (eV)
						Abs	State specific partials	Molecular ions and dissociative fragments	State	
259	Wu	1981	E	P	AB	✓				14-70
237	Samson	1984	E	P	NM			$SO_2^+, SO^+, O^+, S^+, O_2^+$		20-35

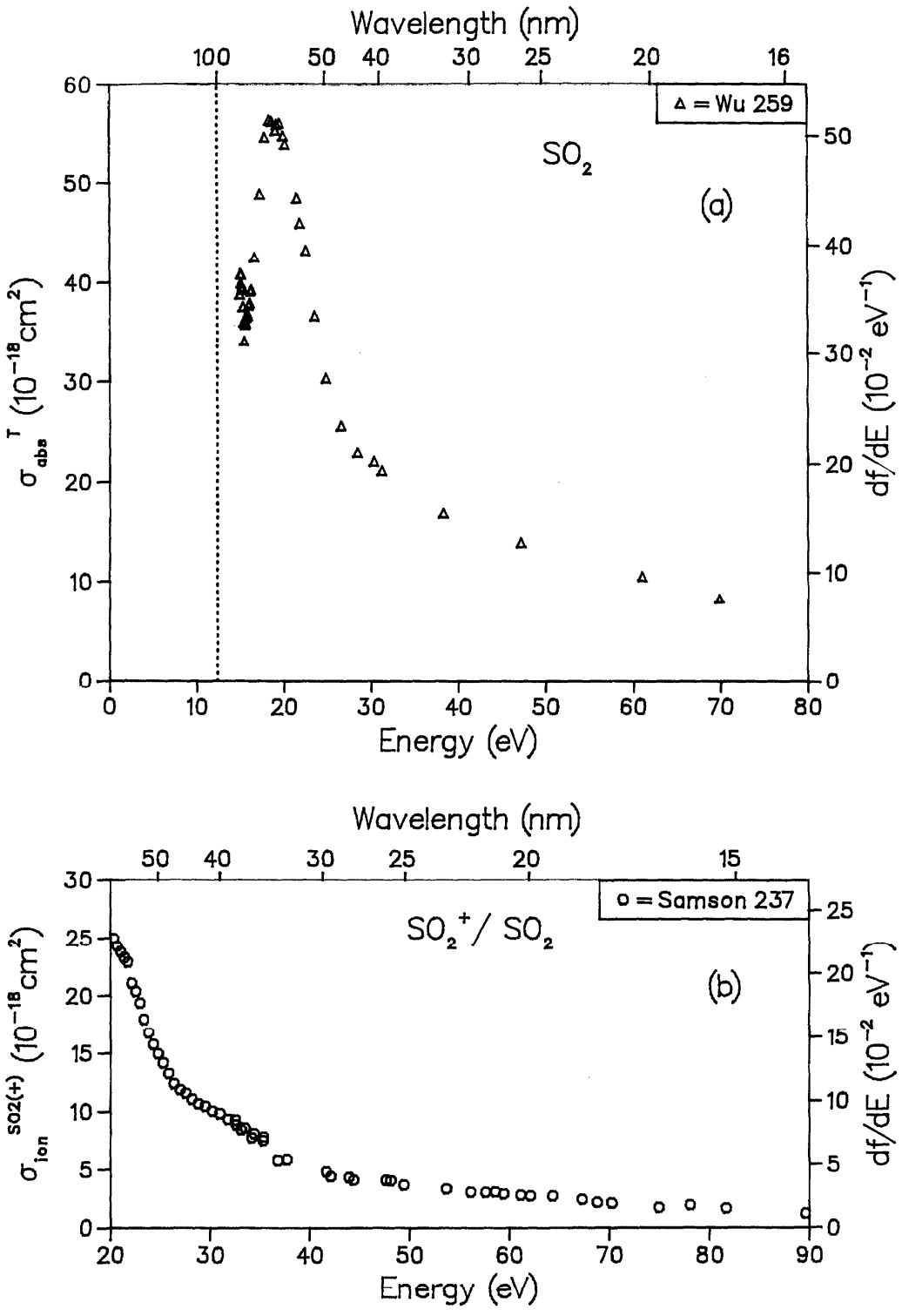

FIG. 93. (a) Total photoabsorption cross section for SO_2. (b) Partial ionic photofragmentation cross sections for SO_2, product ion = SO_2^+.

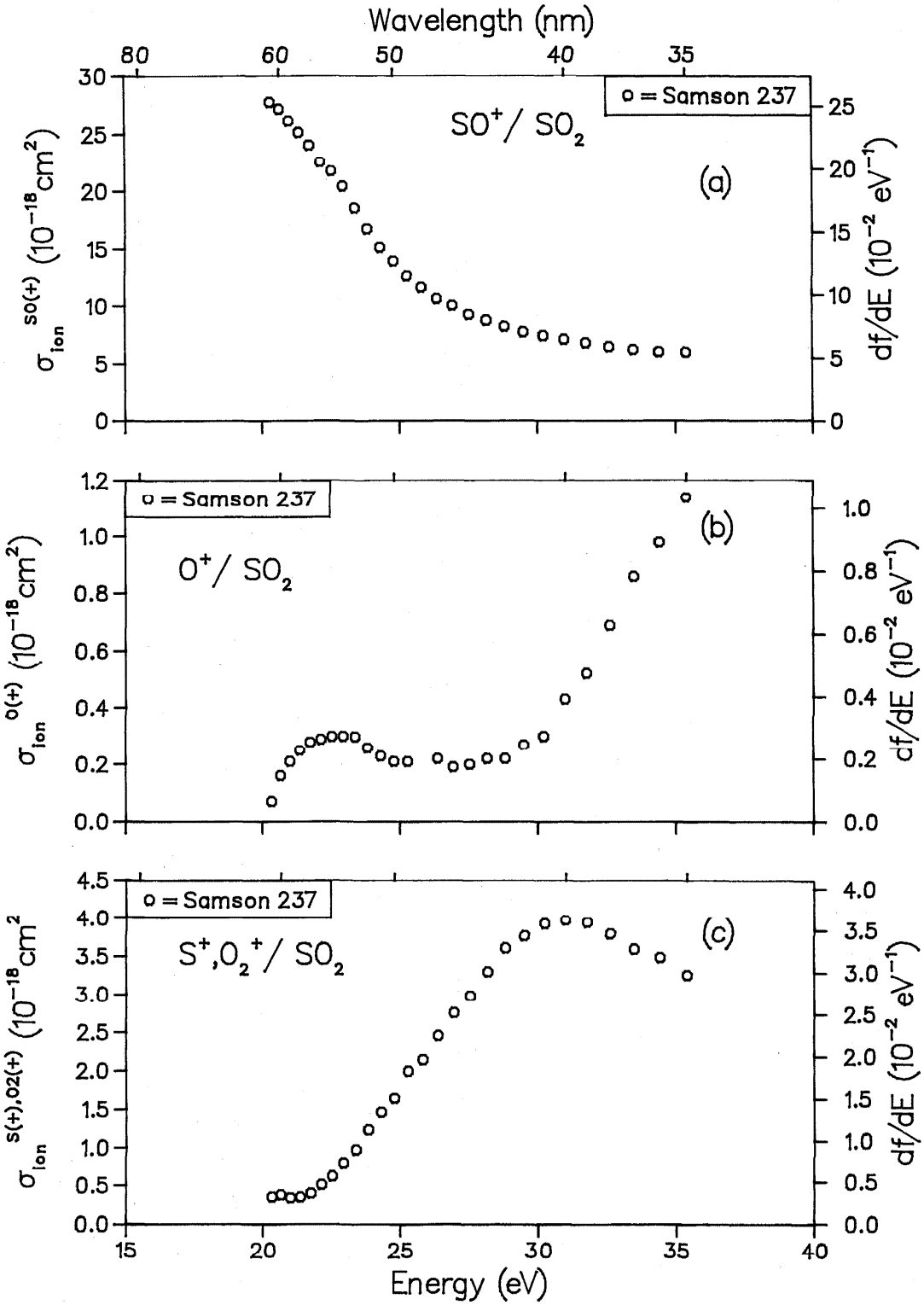

FIG. 94. Partial ionic photofragmentation cross sections for SO_2; (a) product ion = SO^+, (b) product ion = O^+, (c) product ions = S^+, O_2^+.

Table 17. Data for SF_6.

Reference	Author	Year	E/T	Method	Experimental normalization	Cross Sections: Abs	Cross Sections: State specific partials	Cross Sections: Molecular ions and dissociative fragments	Betas: State	Photon energy range (eV)
a	Sasanuma	1971	E	P	Ab	✓				15- 42
141	Blechschmidt	1972	E	P	Ab	✓				15- 50
209	Lee	1977	E	P	Ab	✓				16- 65
186	Gustaffson	1978	E	P	NM		$(1t_{1g}^{-1}),(5t_{1u}^{-1}+3eg^{-1}),$ $(1t_{2u}^{-1}),(1t_{2g}^{-1}),(4t_{1u}^{-1})$			19- 54
196	Hitchcock	1978	E	DIP	TRK	✓				5-230
197	Hitchcock	1979	E	DIP	TRK	✓				5- 63
197	Hitchcock	1979	E	DIP	TRK			$SF_5^+,SF_4^+,SF_3^+,SF_2^+,SF^+,S^+$ $F^+,SF_2^{2+},SF_4^{2+},$		15- 63
216	Masuoka	1981	E	P	NM			$SF_5^+,SF_4^+,SF_3^+,SF_2^+,SF^+,S^+,$ $F^+,SF_2^{2+},SF_3^{2+},SF_4^{2+},$ SF^{2+},S^{2+}		78-124
171	Dehmer	1982	E	P	NM		$(1t_{1g}^{-1}),(5t_{1u}^{-1}+1t_{2u}^{-1}),(3eg^{-1})$ $(1t_{2g}^{-1}),(4t_{1u}^{-1})$		$(1t_{1g}^{-1}),(5d_{1u}^{-1}+1t_{2u}^{-1}),(3e_g^{-1})$ $(1t_{2g}^{-1}),(4t_{1u}^{-1})$	17- 30
171	Dehmer	1982	T	X_α	---		$(1t_{1g}^{-1}),(5t_{1u}^{-1}+1t_{2u}^{-1}),$ $(1t_{2g}^{-1}),(4t_{1u}^{-1})$		$(1t_{1g}^{-1}),(5t_{1u}^{-1}+1t_{2u}^{-1}),$ $(1t_{2g}^{-1}),(4t_{1u}^{-1})$	17- 30

[a] M. Sasanuma, E. Ishiguro, Y. Morioka, M. Nakamura, III International Conference on Vacuum Ultraviolet Radiation Physics, Tokyo, 1971. Data taken from Lee et al., Ref. 209.

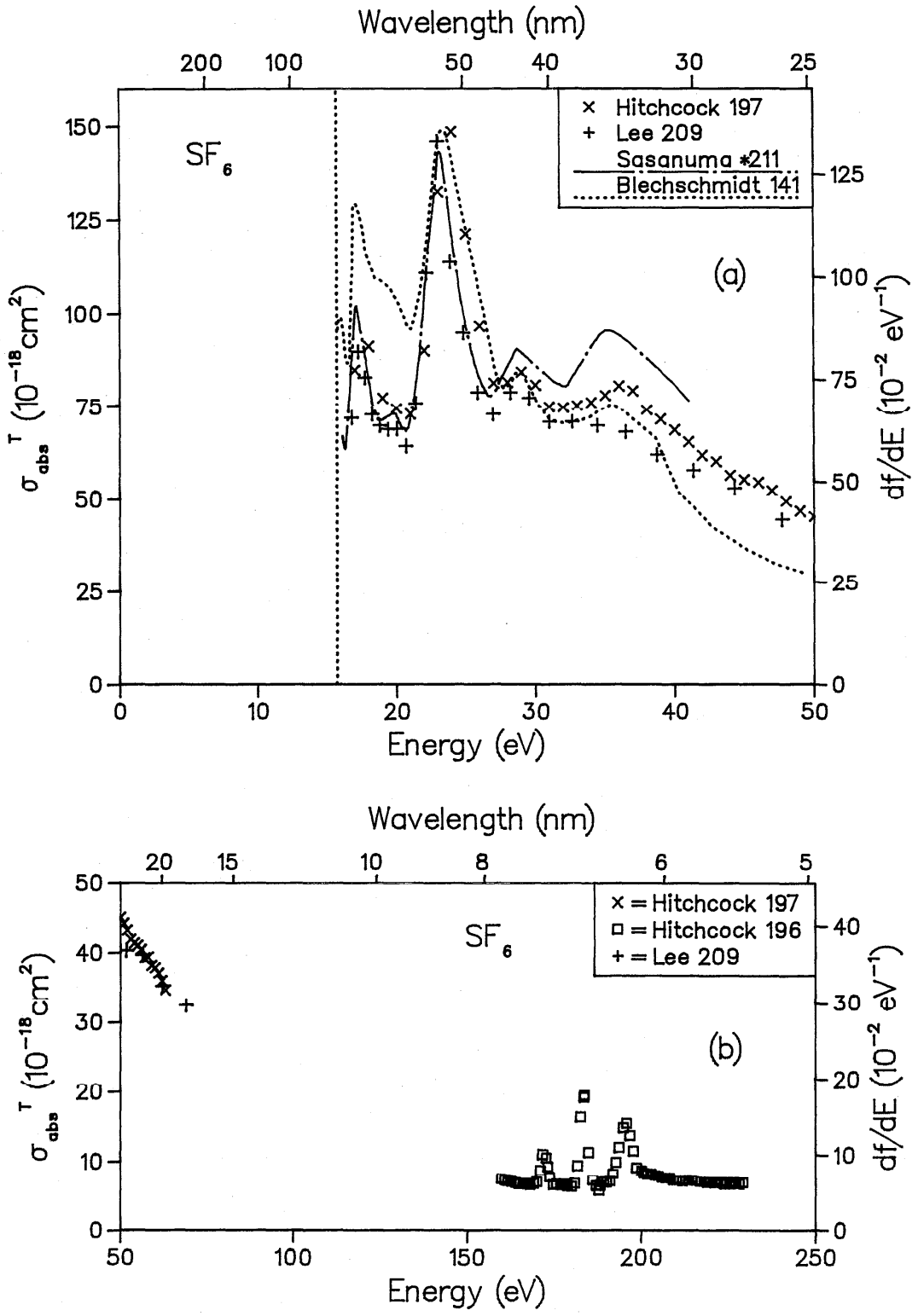

FIG. 95. Total photoabsorption cross section for SF_6: (a) low-energy range, (b) high-energy range.

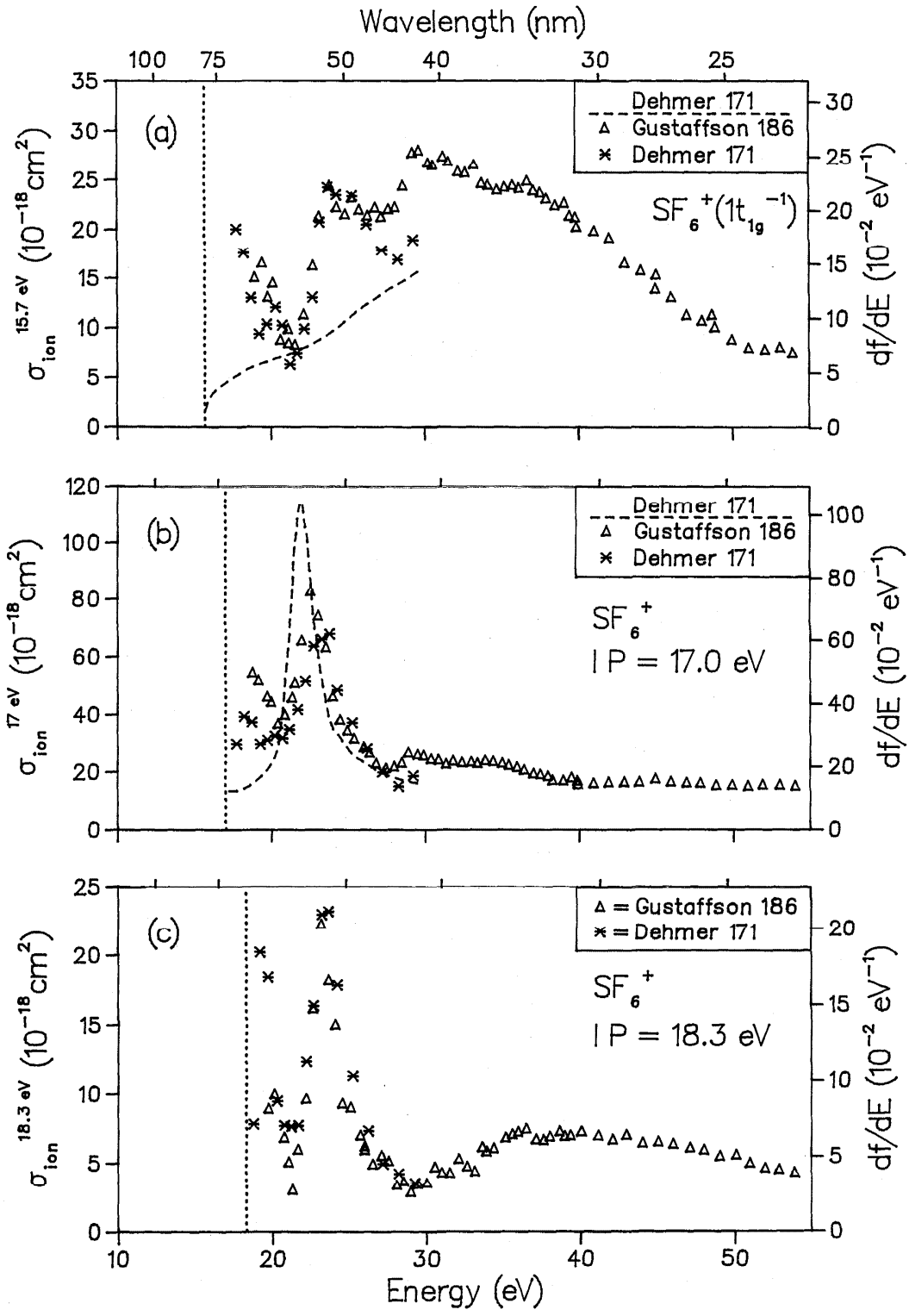

FIG. 96. Partial photoionization cross sections for SF_6; PES peak at (a) 15.7, (b) 17.0, and (c) 18.3 eV.

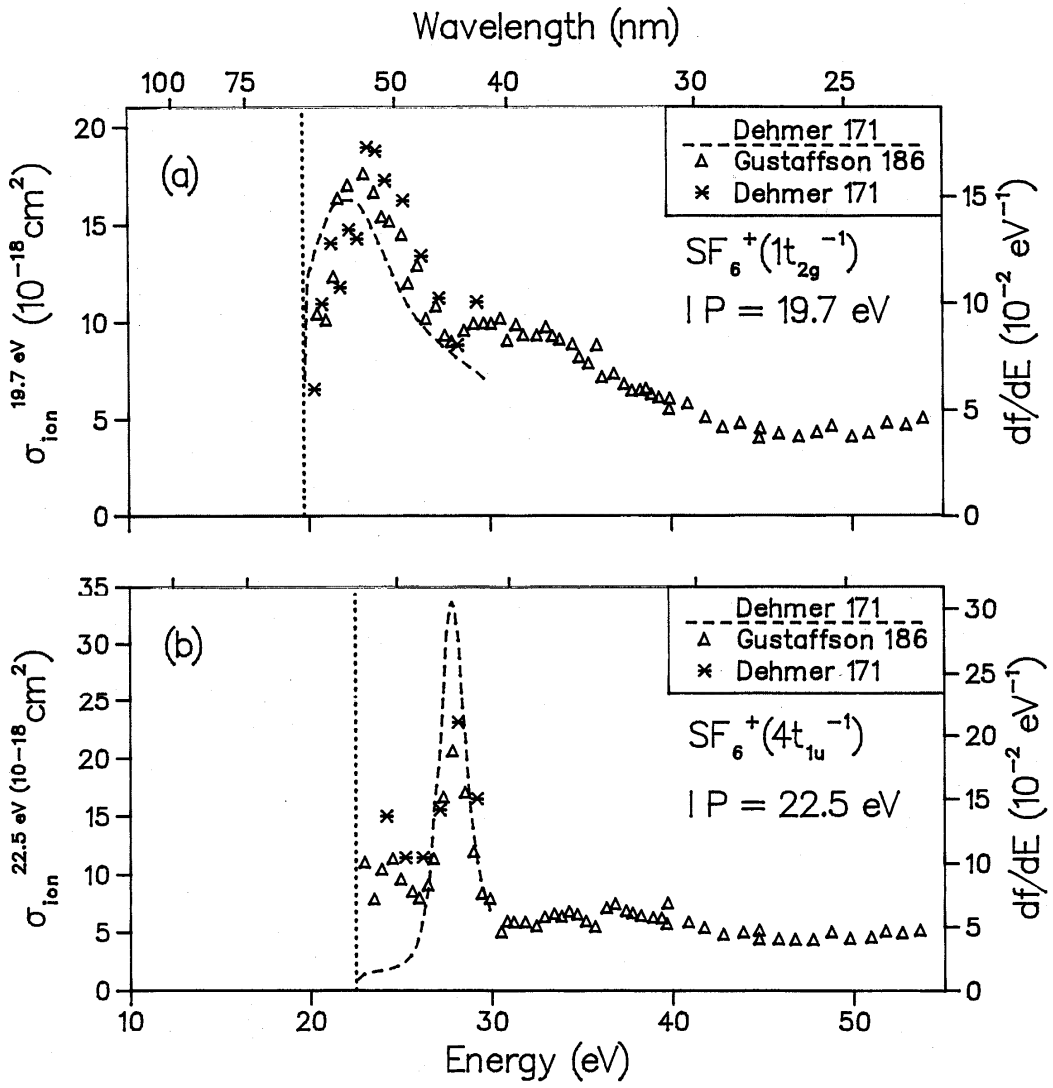

FIG. 97. Partial photoionization cross sections for SF_6; PES peak at (a) 19.7 and (b) 22.5 eV.

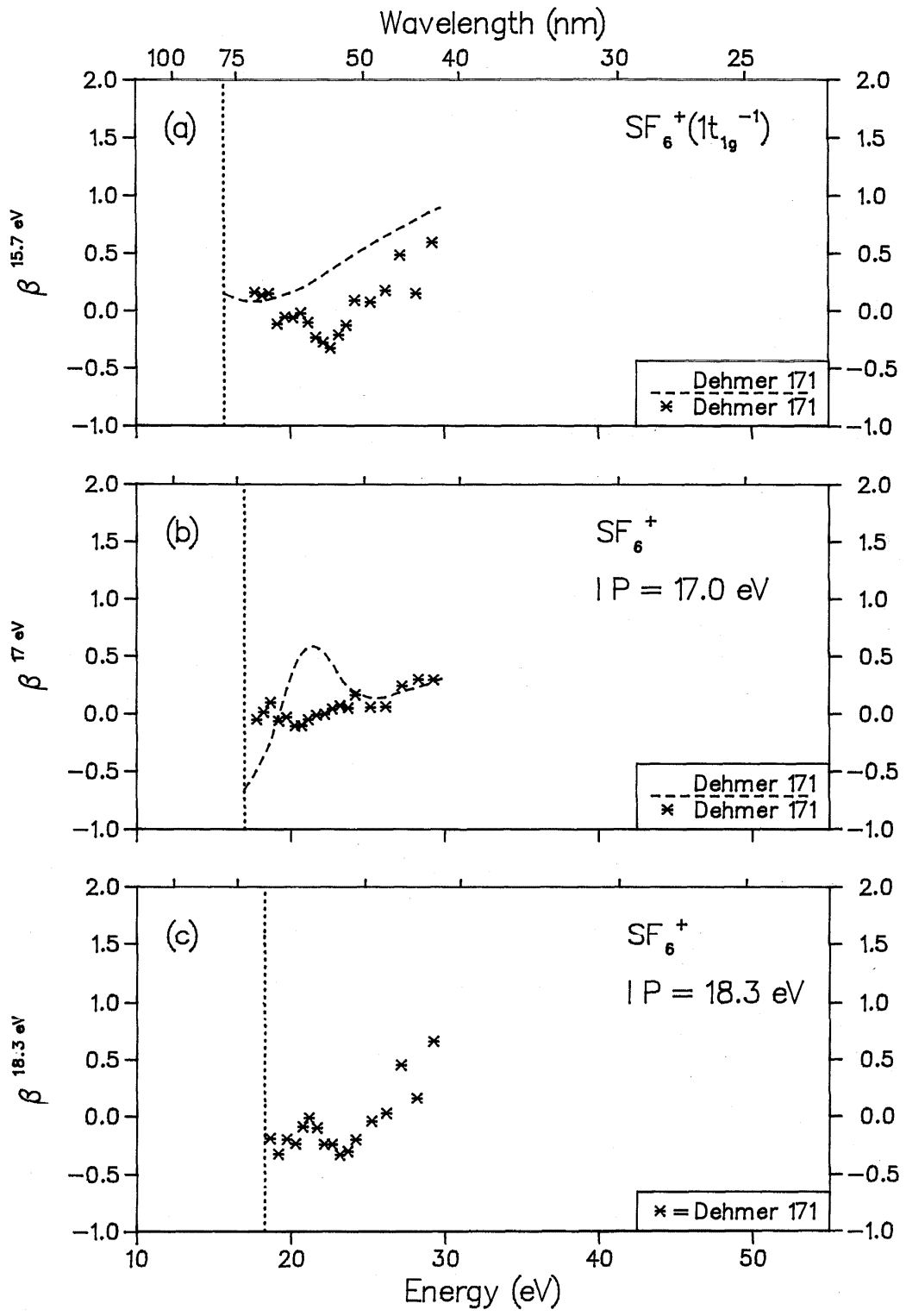

FIG. 98. Photoelectron asymmetry parameters for SF_6; PES peak at (a) 15.7 (b) 17.0, and (c) 18.3 eV.

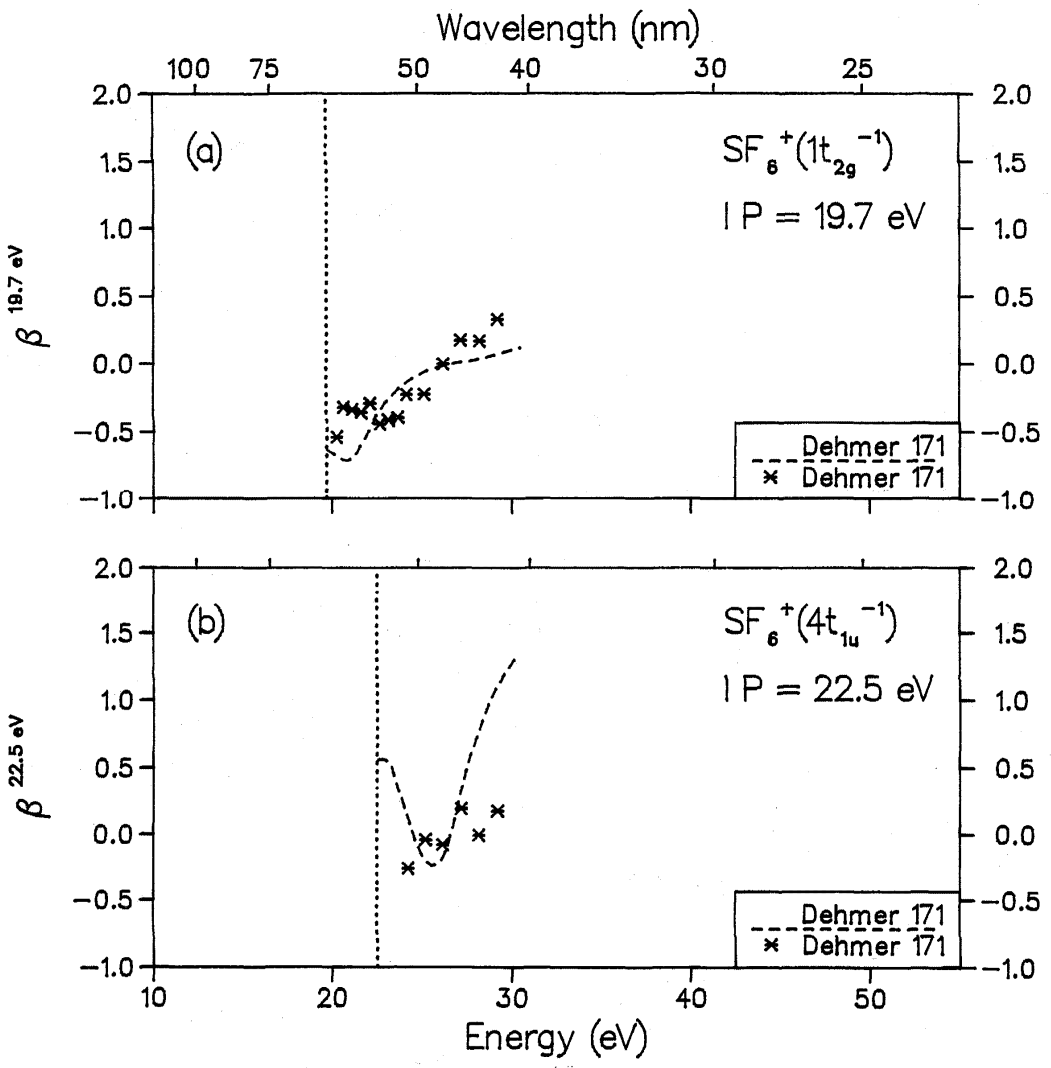

FIG. 99. Photoelectron asymmetry parameters for SF_6; PES peak at (a) 19.7 and (b) 22.5 eV.

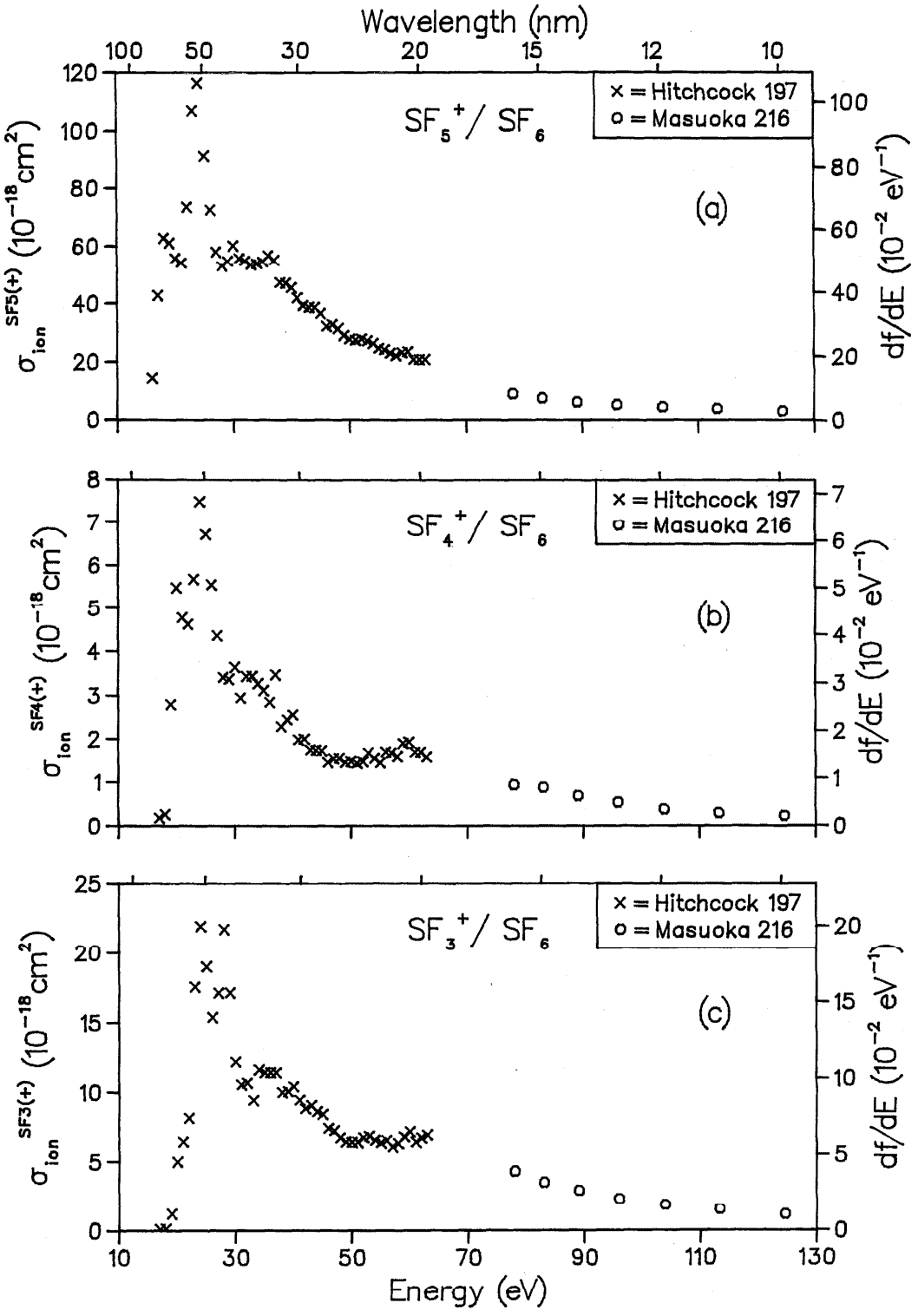

FIG. 100. Partial ionic photofragmentation cross sections for SF_6: (a) product ion = SF_5^+, (b) product ion = SF_4^+, (c) product ion = SF_3^+.

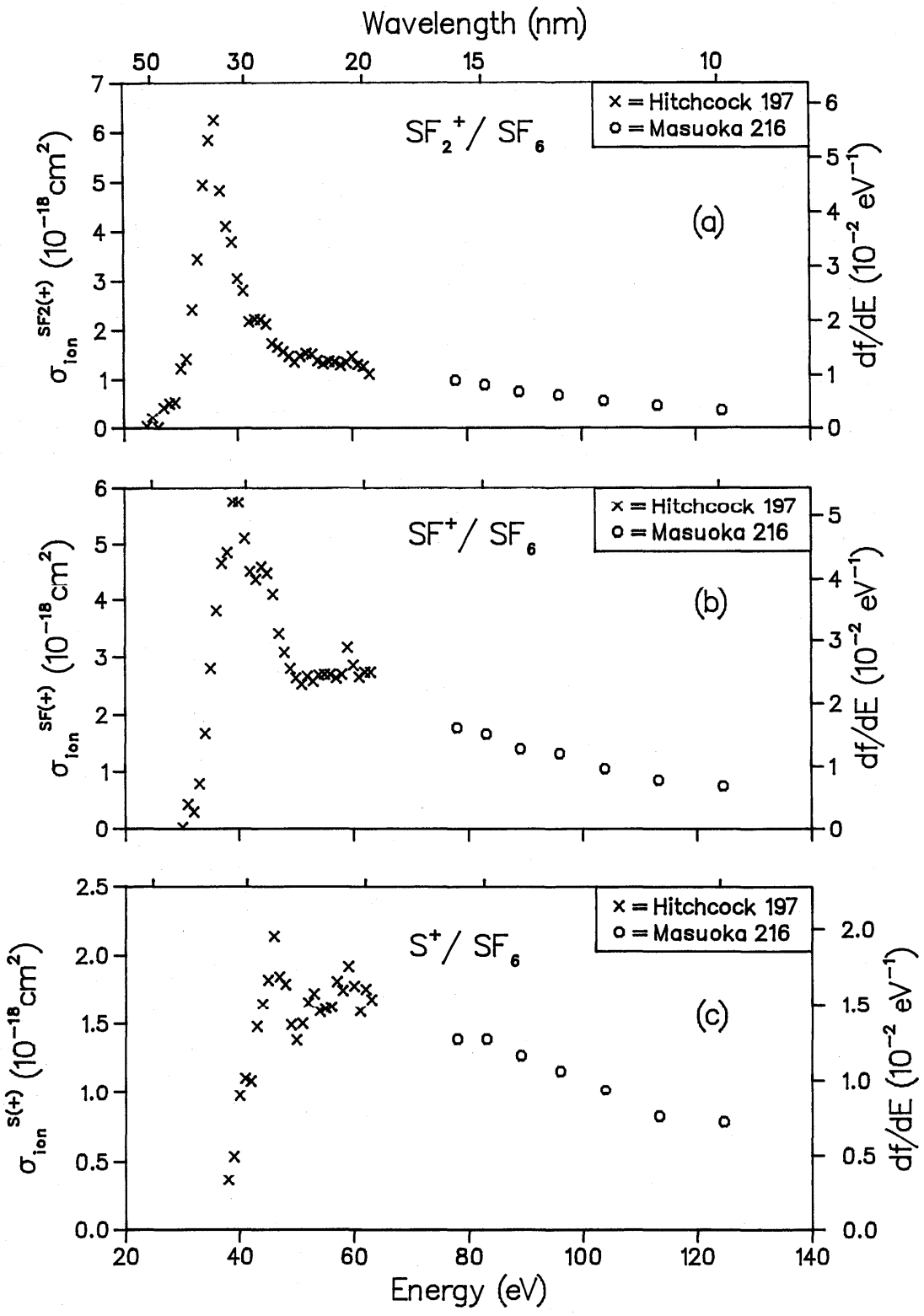

FIG. 101. Partial ionic photofragmentation cross sections for SF_6; (a) product ion = SF_2^+, (b) product ion = SF^+, (c) product ion = S^+.

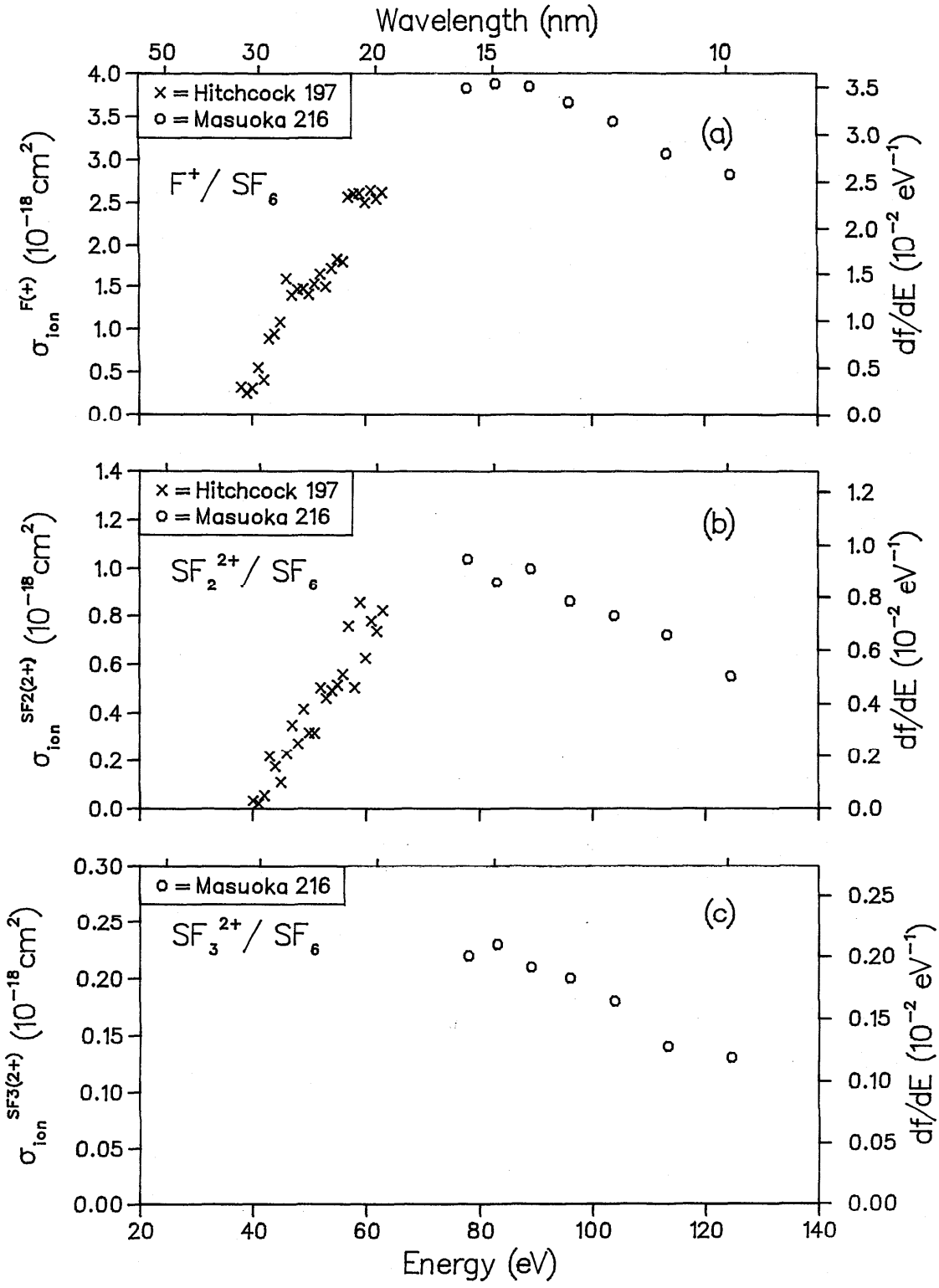

FIG. 102. Partial ionic photofragmentation cross sections for SF_6; (a) product ion = F^+, (b) product ion = SF_2^{2+}, (c) product ion = SF_3^{2+}.

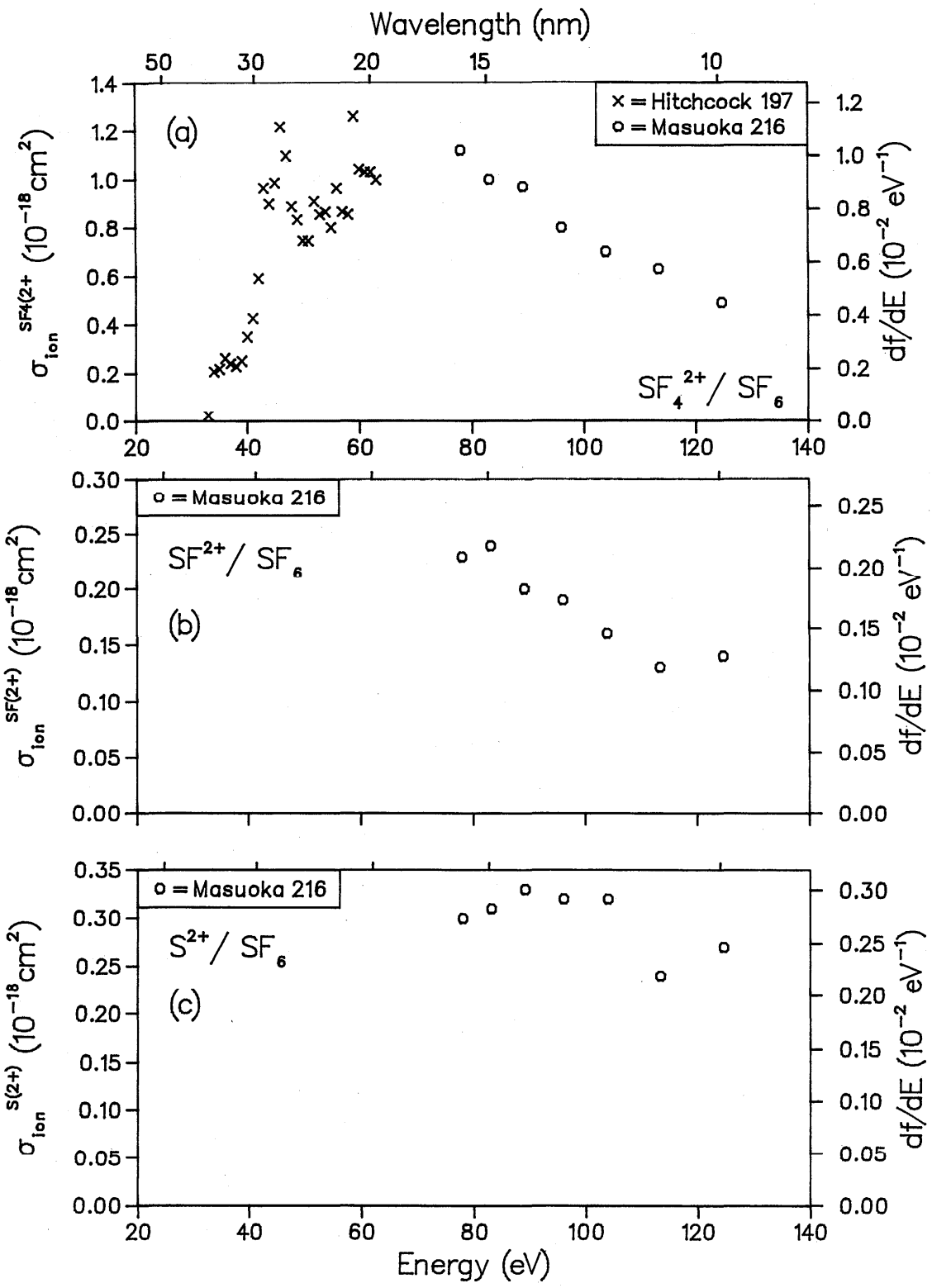

FIG. 103. Partial ionic photofragmentation cross sections for SF_6; (a) product ion = SF_4^{2+}, (b) product ion = SF^{2+}, (c) product ion = S^{2+}.

Table 18. Data for Cl_2.

Reference	Author	Year	E/T	Method	Experimental normalization	Cross Sections			Betas	Photon energy range (eV)
						Abs	State specific partials	Molecular ions and dissociative fragments	State	
161	Carlson[a]	1983	E	P	NM		X,A,E		X,A,B	18-70
161	Carlson[a]	1983	T	$X\alpha$	---		X,A,B		X,A,B	12-65
232	Samson	1986	E	P	AB	✓				12-80
232	Samson	1986	E	P	AB			Cl_2^+, Cl^+, Cl_2^{2+}		12-80

[a]Data were renormalized to Samson and Angel, Ref. 20151.

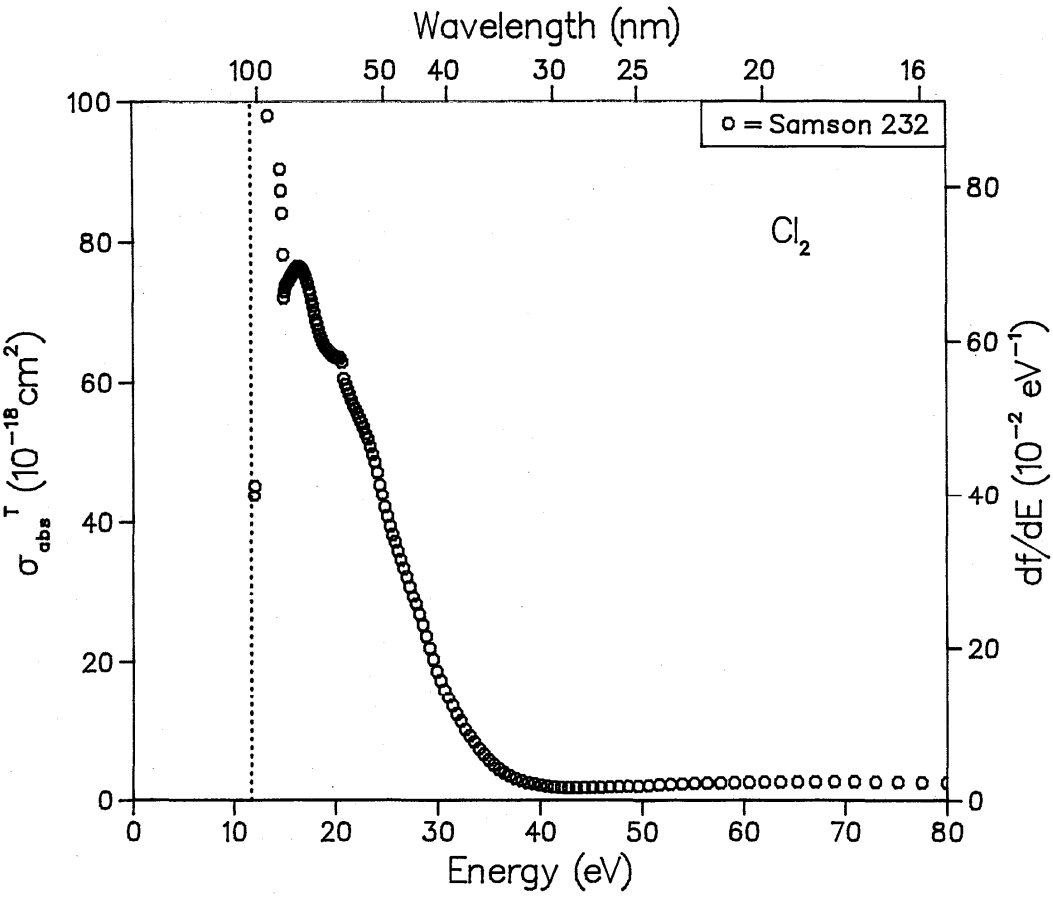

FIG. 104. Total photoabsorption cross section for Cl_2.

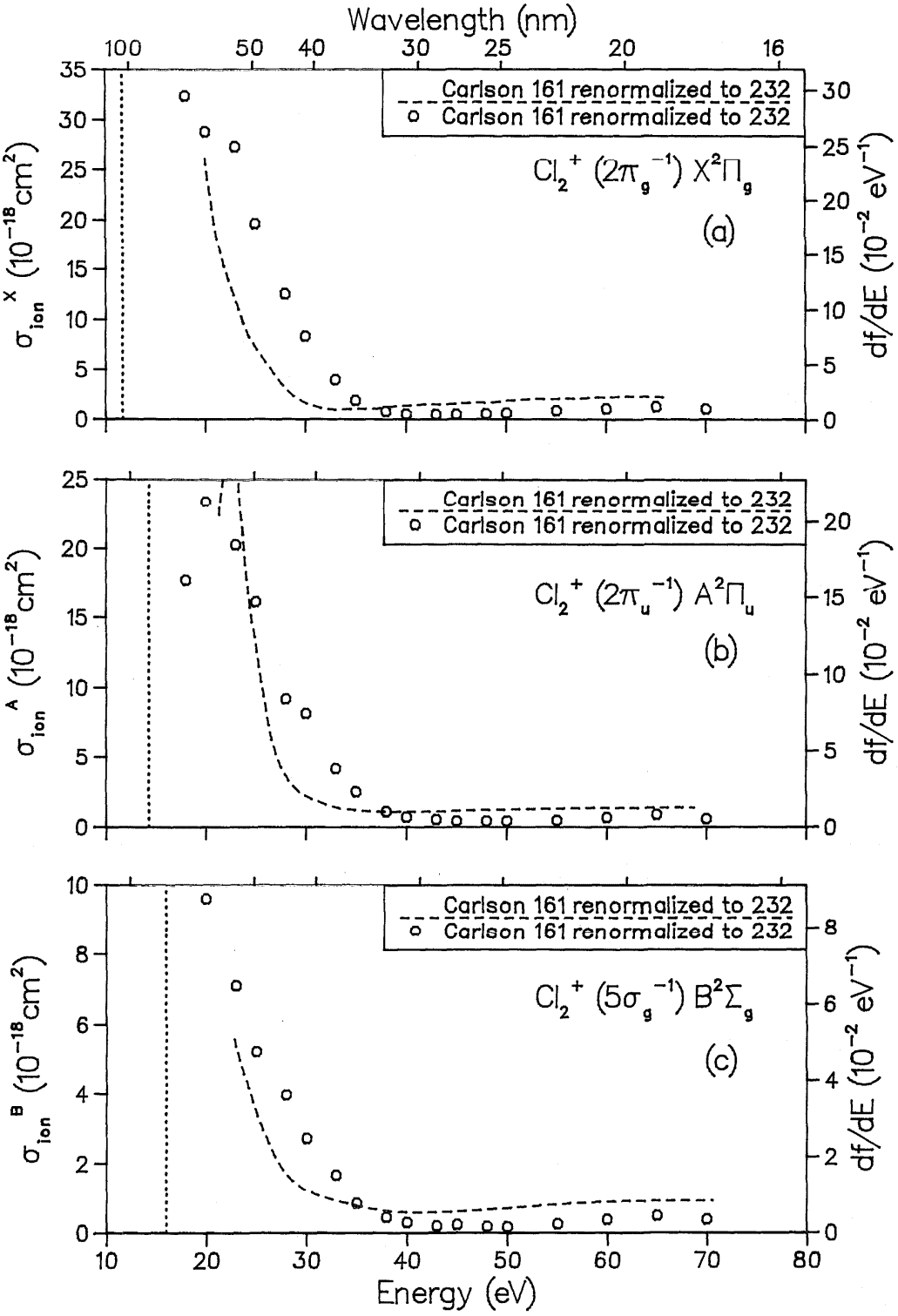

FIG. 105. Partial photoionization cross sections for Cl_2; (a) final ionic state = $X^2\Pi_g$, (b) final ionic state = $A^2\Pi_u$, (c) final ionic state = $B^2\Sigma_g$.

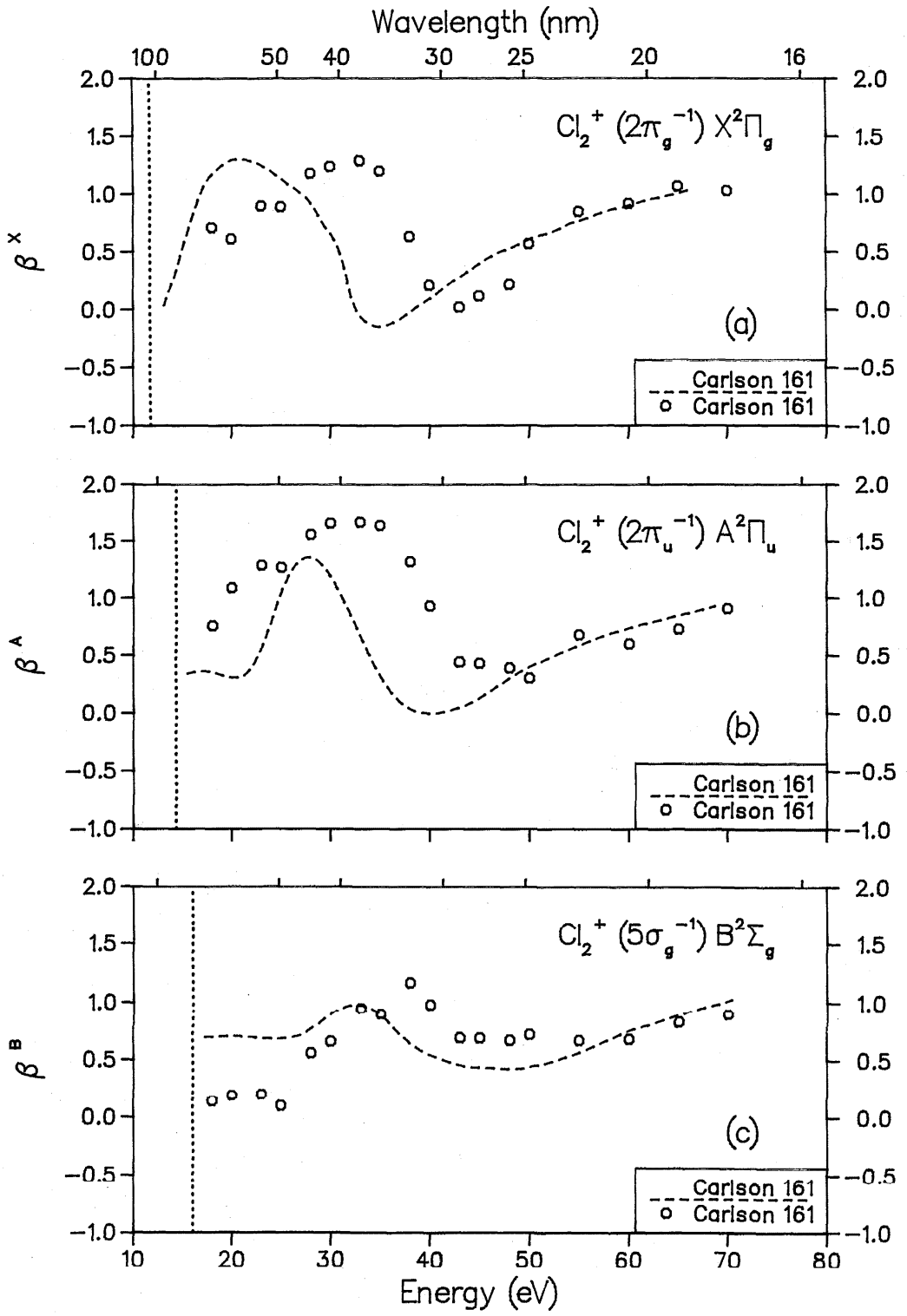

FIG. 106. Photoelectron asymmetry parameters for Cl_2; (a) final ionic state = $X^2\Pi_g$, (b) final ionic state = $A^2\Pi_u$,(c) final ionic state = $B^2\Sigma_g$.

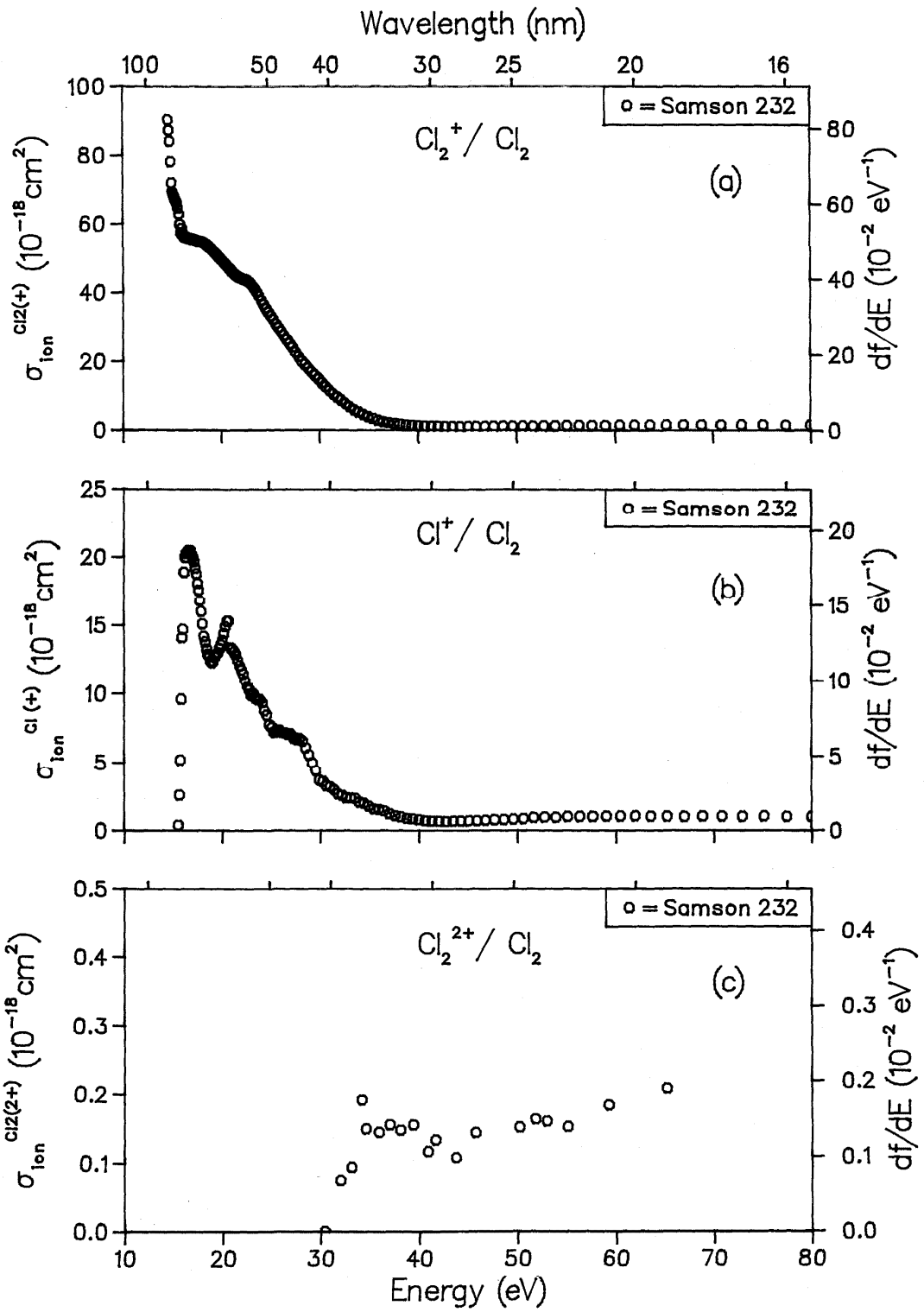

FIG. 107. Partial ionic photofragmentation cross sections for Cl_2; (a) product ion = Cl_2^+, (b) product ion = Cl^+, (c) product ion = Cl_2^{2+}.

Table 19. Data for CCl_4.

Reference	Author	Year	E/T	Method	Experimental normalization	Cross Sections			Betas	Photon energy range (eV)
						Abs	State specific partials	Molecular ions and dissociative fragments	State	
160	Carlson[a]	1982	E	P	NM		X,A,B,C,D		X,A,B,C,D	20-60
160	Carlson	1982	T	$X\alpha$	---		X,A,B,C,D		X,A,B,C	22-56

[a]Author estimates accuracy to within a factor of 2.

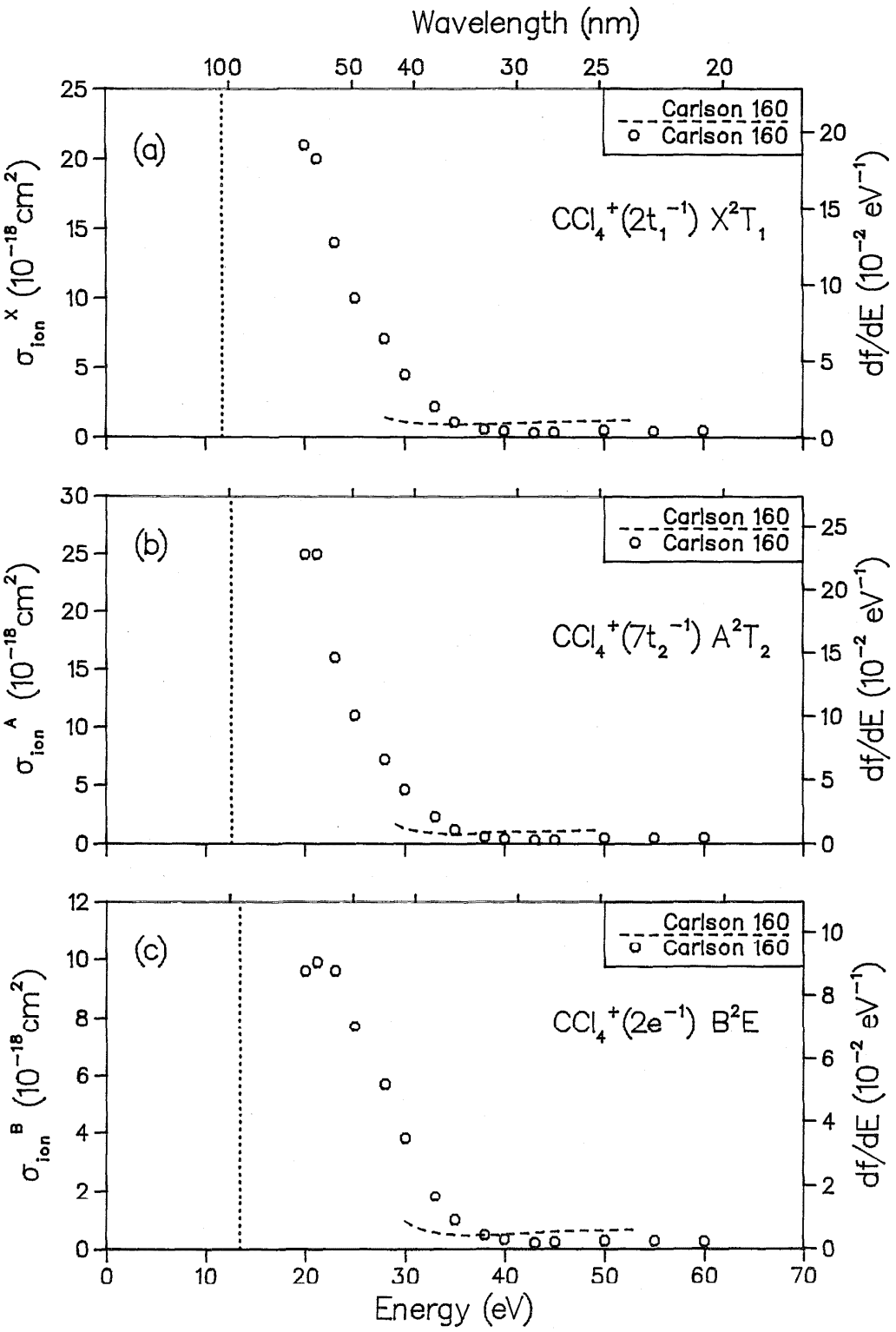

FIG. 108. Partial photoionization cross sections for CCl_4; (a) final ionic state $= X^2T_1$, (b) final ionic state $= A^2T_2$, (c) final ionic state $= B^2E$.

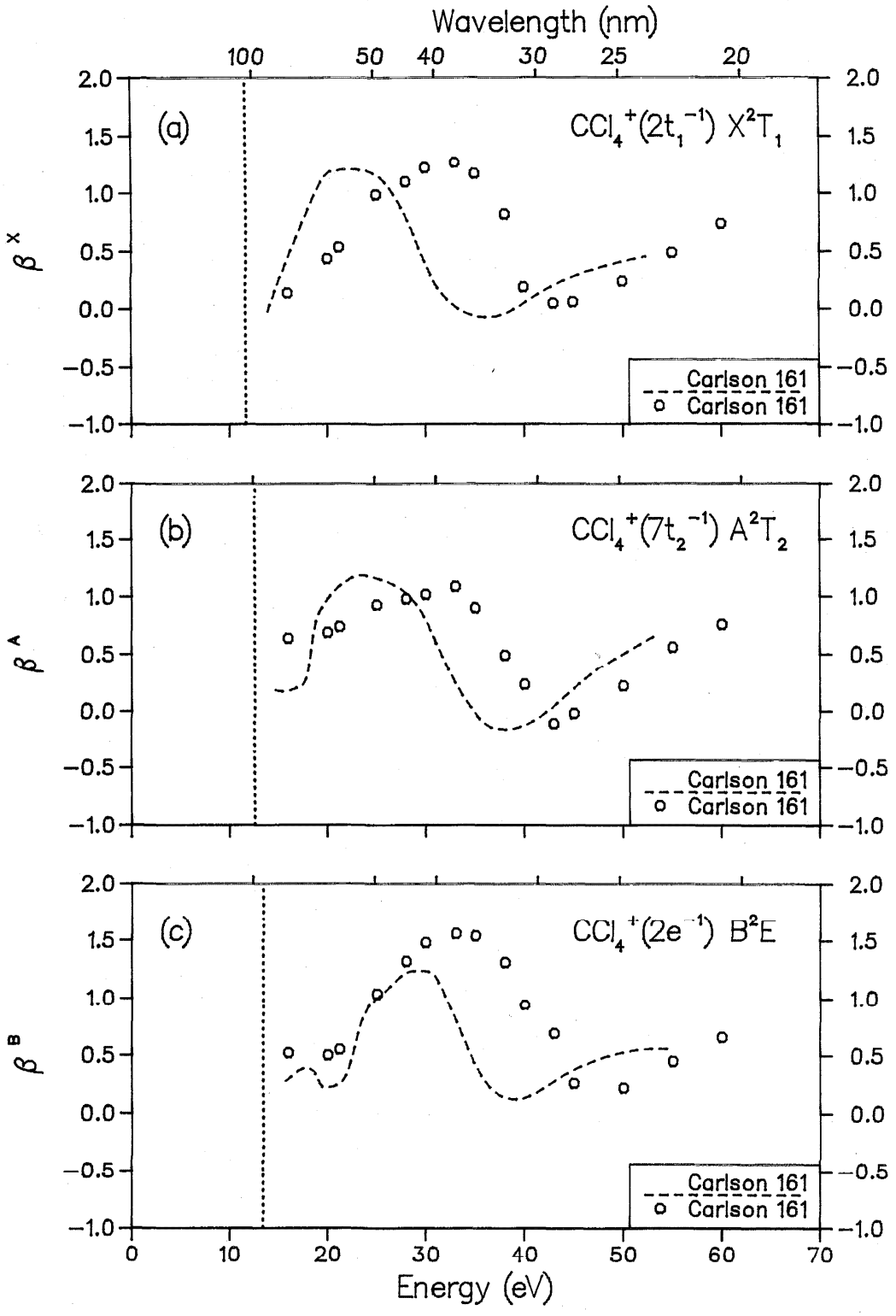

FIG. 109. Photoelectron asymmetry parameters for CCl_4; (a) final ionic state = X^2T_1, (b) final ionic state = A^2T_2, (c) final ionic state = B^2E.

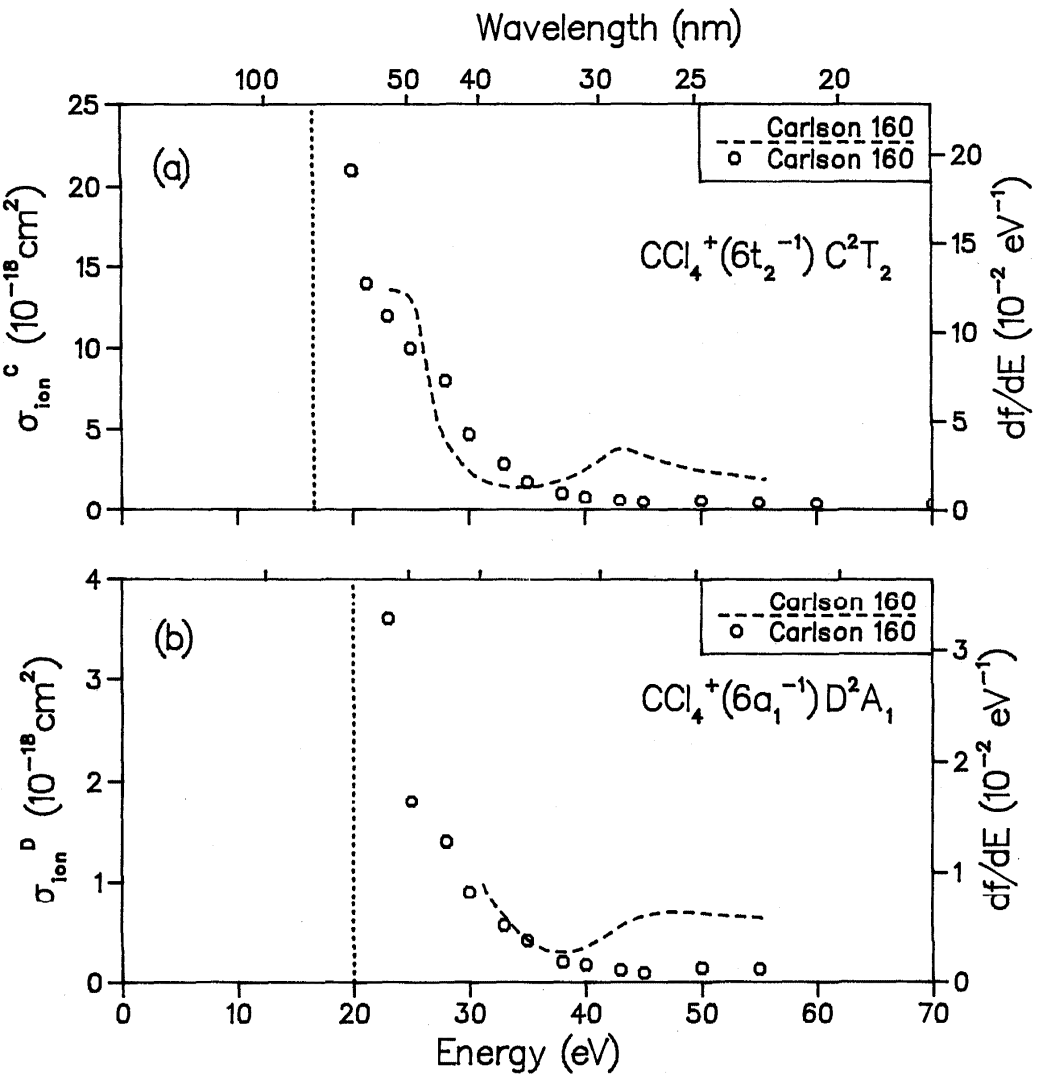

FIG. 110. Partial photoionization cross sections for CCl_4; (a) final ionic state = C^2T_2, (b) final ionic state = D^2A_1.

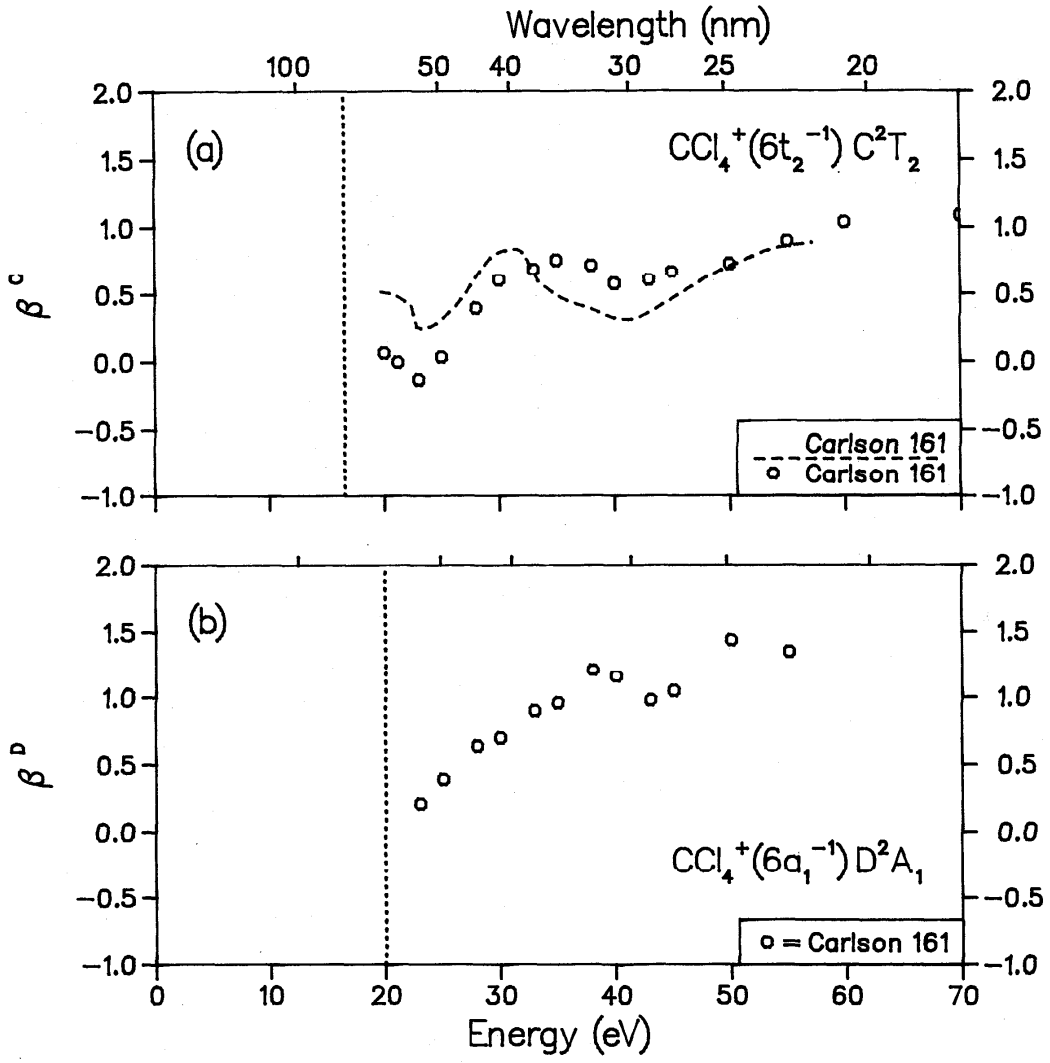

FIG. 111. Photoelectron asymmetry parameters for CCL_4; (a) final ionic state = C^2T_2, (b) final ionic state = D^2A_1.

7. Acknowledgments

Financial support for this work was provided by the Office of Standard Reference Data of the National Bureau of Standards, the National Science Foundation, the Natural Sciences and Engineering Research Council of Canada, and the Petroleum Research Fund administered by the American Chemical Society. We acknowledge the receipt of a Canada Council Killam Research Fellowship by CEB for 1984 to 1986. We acknowledge support for JARS by NSF Grant ATM-8412820 and NASA Grant No. NGR28-002-01. We thank Dr. M. Inokuti for a careful reading of the manuscript and for his very helpful suggestions.

8. References

[1]R. W. Ditchburn and U. Opik, "Photoionization Processes," in *Atomic and Molecular Processes*, edited by D. R. Bates (Academic, New York, 1962), p. 79.

[2]G. V. Marr, *Photoionization Processes in Gases* (Academic, New York, 1967).

[3]J. A. R. Samson, *Techniques of Vacuum Ultraviolet Spectroscopy* (Wiley, New York, 1967).

[4]K. Siegbahn, C. Nordling, A. Fahlman, R. Nordberg, K. Hamerin, J. Hedman, G. Johansson, T. Bergmark, S.-E. Karlsson, I. Lindgrin, and B. Lindberg, *Electron Spectroscopy for Chemical Analysis—Atomic, Molecular, and Solid State Structure Studies by Means of Electron Spectroscopy* (Almquist and Wiksells, Boktryekeri AB, Stockholm, Sweden, 1967).

[5]J. A. R. Samson and G. L. Weissler, "Absorption, Photoionization, and Scattering Cross Sections," in *Methods of Experimental Physics, Atomic and Electron Physics,* edited by B. Bederson and W. L. Fite (Academic, New York, 1968), Vol. 7, Part A.

[6]K. Siegbahn, C. Nordling, G. Johansson, J. Hedman, P. F. Heden, K. Hamrin, U. Gelius, T. Bergmark, L. O. Werme, R. Manne, and Y. Baer, *ESCA Applied to Free Molecules* (North-Holland, Amsterdam, 1969).

[7]D. W. Turner, "Photoelectron Spectroscopy," Ann. Rev. Phys. Chem. **21**, 107 (1970).

[8]D. W. Turner, C. Baker, A. D. Baker, and C. R. Brundle, *Molecular Photoelectron Spectroscopy* (Wiley, London, 1970).

[9]J. H. D. Eland, *Photoelectron Spectroscopy* (Wiley, New York, 1974).

[10]*Electron Spectroscopy*, edited by D. A. Shirley (North-Holland, Amsterdam, 1972).

[11]*Electron Spectroscopy: Progress in Research and Applications* edited by R. Caudano and J. Verbist (Elsevier, Amsterdam, 1974).

[12]W. C. Price, "Photoelectron Spectroscopy," Adv. At. Mol. Phys. **10**, 131 (1974).
[13]*Chemical Spectroscopy and Photochemistry in the Vacuum Ultraviolet* edited by C. Sandorfsky, P. J. Ausloos, and M. B. Robin (Reidel, Boston, MA, 1974).
[14]T. A. Carlson, *Photoelectron and Auger Spectroscopy* (Plenum, New York, 1975).
[15]T. A. Carlson, "Photoelectron Spectroscopy," Ann. Rev. Phys. Chem. **26**, 211 (1975).
[16]J. W. Rabalais, *Principles of Ultraviolet Photoelectron Spectroscopy* (Wiley, New York, 1976).
[17]W. C. Price, "Photoelectron Spectroscopy in the Study of Molecular Orbitals," in *Very High Resolution Spectroscopy*, edited by A. Smith (Academic, New York, 1976), p. 187.
[18]J. A. R. Samson, "Photoionization of Atoms and Molecules," Phys. Rep. **28**, 303 (1976).
[19]*Photoionization and Other Probes of Many-Electron Interactions*, edited by F. J. Wuilleumier, NATO–ASI Series B (Plenum, New York, 1976), Part I, pp. 187–198; Part II, 198.
[20]*Electron Spectroscopy: Theory, Techniques, and Applications*, edited by C. R. Brundle and A. D. Baker (Academic, New York, 1977–1981) Vols. 1–4.
[21]H. Okabe, *Photochemistry of Small Molecules* (Wiley, New York, 1978).
[22]J. A. R. Samson, "Vacuum Ultraviolet Photoelectron Spectroscopy of Atoms and Molecules," J. Electron Spectrosc. Relat. Phenom. **15**, 257 (1979).
[23]J. Berkowitz, *Photoabsorption, Photoionization, and Photoelectron Spectroscopy* (Academic, New York, 1979).
[24]J. Heicklein, *Atmospheric Chemistry* (Academic, New York, 1976).
[25]L. Spitzer, Jr., *Physical Processes in the Interstellar Medium* (Wiley, New York, 1978).
[26]J. W. Chamberlain, *Theory of Planetary Atmospheres* (Academic, New York, 1978).
[27]*Proceedings of the Workshop on Electronic and Ionic Collision Cross Sections Needed in the Modeling of Radiation Interactions with Matter*, 6–8 December 1983, edited by M. Inokuti (Argonne National Lab. Report No. ANL 84-28, Argonne, IL, 1984).
[28]*Atmospheric Physics and Chemistry*, edited by H. S. W. Massey and D. R. Bates (Academic, New York, 1982).
[29]*Molecular Astrophysics*, edited by G. H. F. Dierckson, W. Huebner, and P. W. Langhoff (Reidel, Dordrecht, Holland, 1985).
[30]E. J. McCartney, *Absorption and Emission by Atmospheric Gases* (Wiley, New York, 1983).
[31]K. Watanabe, M. Zelikof, and E. C. Y. Inn, "Absorption Coefficients of Several Atmospheric Gases," AFCRC Technical Report No. 52-53 (1953).
[32]G. L. Weissler, Handbuch der Physik **21**, 304 (1956).
[33]K. Watanabe, Adv. Geophys. **2**, 153 (1958).
[34]J. R. McNesby and H. Okabe, Adv. Photochem. **3**, 157 (1964).
[35]J. O. Sullivan and A. C. Holland, "A Congeries of Absorption Cross Sections for Wavelengths Less Than 3000 Å," NASA Report No. CR 371 (1966).
[36]R. I. Schoen, Can. J. Chem. **47**, 1879 (1969).
[37]R. D. Hudson and L. J. Kieffer, "Compilation of Atomic Ultraviolet Photoabsorption Cross Sections for Wavelengths Between 3000 and 10 Å," At. Data **2**, 205 (1971).
[38]R. D. Hudson and L. J. Kieffer, "Compilation of Atomic Ultraviolet Photoabsorption Cross Sections for Atoms Between 5 and 3500 Å," NASA Spec. Publ. 3064 (1971), JILA Information Center, University of Colorado, Boulder, CO 80302.
[39]R. D. Hudson, "Critical Review of Ultraviolet Photoabsorption Cross Sections for Molecules of Astrophysical and Aeronomic Interest," Rev. Geophys. Space Phys. **9**, 306 (1971).
[40]K. Way, Jpn. J. Appl. Phys. **17**, Suppl. 17-2, 497 (1978).
[41]L. J. Kieffer, "Bibliography of Low Energy Electron and Photon Cross Section Data," Natl. Bur. Stand. (U.S.), Spec. Publ. 426, 219 pgs. (1976).
[42]J. W. Gallagher, J. R. Rumble Jr., and E. C. Beaty, "Bibliography of Low Energy Electron and Photon Cross Section Data," Natl. Bur. Stand (U. S.), Spec. Publ. 426, Suppl. 1, 115 pgs. (1979).
[43]J. W. Gallagher and E. C. Beaty, "Bibliography of Low Energy Electron and Photon Cross Section Data," JILA Inf. Cent. Report No. 18, 145 pgs. (1980).
[44]J. W. Gallagher and E. C. Beaty, "Bibliography of Low Energy Electron and Photon Cross Section Data," JILA Inf. Cent. Report. No. 21, 122 pgs. (1981).
[45]E. E. Koch and B. F. Sonntag, Top. Curr. Phys. **10**, 269 (1979).
[46]M. O. Krause, "Electron Spectrometry of Atoms and Molecules," in *Synchrotron Radiation Research*, edited by H. Winick and S. Doniach (Plenum, New York, 1980), Chap. 5, p. 101.
[47]J. A. R. Samson, "Photoelectron Angular Distributions and Photoionization Cross Sections in the Vacuum Ultraviolet," in *Electron Spectroscopy: Theory Techniques and Applications*, edited by C. R. Brundle and A. D. Baker (Academic, New York, 1981), Vol. 4, Chap. 6, p. 369.
[48]C. E. Brion and A. Hamnett, Adv. Chem. Phys. **45**, 2 (1981).
[49]C. E. Brion, "Electron Scattering at High and Intermediate Energies: Quantitative Measurements in Molecular Spectroscopy," in *Physics of Electronic and Atomic Collisions*, edited by S. Datz, (North–Holland, Amsterdam, 1982), p. 579.
[50]J. A. R. Samson, "Atomic Photoionization," in *Handbuch der Physik*, edited by S. Flugge (Springer, Berlin, 1982), Vol. 31, p. 187.
[51]I. Nenner, "Photophysical Processes in Simple Molecules Excited by Synchrotron Radiation," Laser Chem. **3**, 339 (1983).
[52]C. E. Brion, "Dipole Oscillator Strengths Observed in Electron Impact" (Argonne National Lab. Report. No. ANL 84-28, Argonne, IL, 1983), p. 85.
[53]C. E. Brion and J. P. Thomson, "Compilation of Valence-Shell Molecular Photoelectron Branching Ratios as a Function of Energy," J. Electron Spectrosc. **33**, 287 (1984).
[54]C. E. Brion and J. P. Thomson, "Compilation of Dipole Oscillator Strengths (Cross Sections) for the Photoabsorption, Photoionization and Ionic Fragmentation of Molecules," J. Electron Spectrosc. **33**, 301 (1984).
[55]B. V. McKoy, T. A. Carlson, and R. R. Lucchese, J. Phys. Chem. **88**, 3188 (1984).
[56]C. E. Brion, Comm. At. Mol. Phys. **16**, 249 (1985).
[57]I. Nenner and J. A. Beswick, "Molecular Photodissociation and Photoionization," in *Handbook of Synchroton Radiation*, edited by G. W. Marr (North–Holland, Amsterdam, 1986), Vol. II, p. 355.
[58]T. A. Carlson, M. O. Krause, W. A. Svensson, P. Gerard, F. A. Grimm, T. A. Whitely, and B. P. Pullen, Z. Physik **D2**, 309 (1986).
[59]P. W. Langhoff, "Stieltjes-Tchebycheff Moment-Theory Approach to Molecular Photoionization Studies," in *Electron-Molecule and Photon-Molecule Scattering*, edited by T. Rescigno, V. McKoy, and B. Schneider (Plenum, New York, 1979), p. 183.
[60]J. L. Dehmer and D. Dill, "The Continuum Multiple Scattering Approach to Electron-Molecule Scattering and Molecular Photoionization," in Ref. 59, p. 225.
[61]P. W. Langhoff, "Stieltjes-Tchebycheff Moment-Theory Approach to Photoeffect Studies in Hilbert Space," in *Moment Methods in Many-Fermion Systems*, edited by B. J. Dalton, S. M. Grimes, J. P. Vary, and S. A. Williams (Plenum, New York, 1980), p. 191.
[62]P.W. Langhoff, "Aspects of Electronic Configuration Interaction in Molecular Photoionization," in *Electron-Atom and Electron-Molecule Collisions*, edited by J. Hinze (Plenum, New York, 1983), p. 297.
[63]J. L. Dehmer, D. Dill, and A. C. Parr, "Photoionization Dynamics of Small Molecules," in *Photophysics and Photochemistry in the Vacuum Ultraviolet*, edited by S. McGlynn, G. Findley, and R. Huebner (Reidel, Dordrecht, Holland, 1985), p. 341.
[64]R. R. Lucchese and B. V. McKoy, "Studies of Molecular Photoionization," in *Electron-Molecule Collisons and Photoionization Processes*, edited by V. McKoy, H. Suzuki, K. Takayanagi, and S. Trajmar (Verlag Chemie. International, Deerfield Beach, FL, 1983), p. 13.
[65]P. W. Langhoff, "Schrodinger Spectra," in *Methods in Computational Molecular Physics*, edited by G. H. F. Diercksen and S. Wilson (Reidel, Dordrecht, Holland, 1983), p. 299.
[66]B. I. Schneider and L. A. Collins, "Linear Algebraic Approach to Molecular Photoionization," in *Resonances in Electron-Molecule Scattering, van der Waals Complexes, and Reactive Chemical Dynamics*, edited by D. G. Truhlar (American Chemical Society, Washington, DC, 1984), p. 65.
[67]D. L. Lynch, V. McKoy, and R. R. Lucchese, in Ref. 66, p. 89.
[68]P. W. Langhoff, "Molecular Photoionization Resonances, a Theoretical Chemist's Perspective," Ref. 66, p. 113.
[69]J. L.Dehmer, in Ref. 66, p. 139.
[70]J. L. Dehmer, A. C. Parr, and S. H. Southworth, "Resonances in Molecular Photoionization," in *Handbook on Synchrotron Radiation* edited by G. V. Marr (North–Holland, Amsterdam, 1986), Vol. II, p. 241.
[71]R. R. Lucchese, K. Takatsuka, and V. McKoy, "Applications of the

Schwinger Variational Principle to Electron-Molecule Collisions and Molecular Photoionization," Phys. Rep. **131**, 147 (1986).
[72]M. Ya. Amusia, Adv. At. Mol. Phys. **17**, 1 (1981).
[73]K. H. Tan, C. E. Brion, Ph. E. Van der Leeuw, and M. J. Van der Wiel, Chem. Phys. **29**, 299 (1978).
[74]G. H. F. Diercksen, W. P. Kraemer, T. N. Rescigno, C. F. Bender, B. V. McKoy, S. R. Langhoff, and P. W. Langhoff, J. Chem. Phys. **76**, 1043 (1983).
[75]F. C. Brown, "Inner-Shell Threshold Spectra," in *Synchrotron Radiation Research*, edited by H. Winck and S. Doniach (Plenum, New York, 1980), Chap. 4, p. 61.
[76]C. E. Brion, S. Daviel, R. Sodhi, and A. P. Hitchcock, "Recent Advances in Inner-Shell Excitation of Free Molecules by Electron Energy Loss Spectroscopy," edited by B. Crasemann, AIP Conference Proceedings No. 94, American Institute of Physics, 1982, pp. 429–446.
[77]J. E. Pollard, D. J. Trevor, J. E. Reutt, Y. T. Lee, and D. A. Shirley, Chem. Phys. **77**, 34 (1982).
[78]A. Tabché-Fouhaile, K. Ito, H. Frölich, P. M. Guyon, and I. Nenner, J. Chem. Phys. **77**, 182 (1982).
[79]*Molecular Ions*, edited by J. Berkowitz and K.-O. Groeneveld (Plenum, New York, 1983).
[80]J. A. Guest, M. A. O'Halloran, and R. N. Zare, J. Chem. Phys. **81**, 2689 (1984).
[81]T. Baer, in *Gas Phase Ion Chemistry*, edited by M. T. Bower (Academic, New York, 1979), Chap. 5.
[82]V. A. Antonov and V. S. Letokhov, Appl. Phys. **24**, 89 (1981).
[83]U. Fano and J. W. Cooper, Rev. Mod. Phys. **40**, 441 (1968).
[84]J. A. R. Samson and R. B. Cairns, Phys. Rev. **173**, 80 (1968).
[85]L. C. Lee and J. A. Guest, J. Phys. B **14**, 3415 (1981).
[86]R. J. Tunnicliffe and J. A. Rees, Vacuum **17**, 457 (1967).
[87]K. F. Poulter, M.-J. Rodgers, P. J. Nash, T. J. Thompson, and M. P. Perkin, Vacuum **33**, 311 (1983).
[88]E. W. Plummer, T. Gustafsson, W. Gudat, and D. E. Eastman, Phys. Rev. A **15**, 2339 (1977).
[89]M. G. White, K. T. Leung and C. E. Brion, J. Electron Spectrosc. **23**, 127 (1981).
[90]S. Daviel, C. E. Brion, and A. P. Hitchcock, "A New High Performance Electron Energy Loss Spectrometer for Valence and Inner-Shell Excitation Studies," Rev. Sci. Instrum. **55**, 182 (1984).
[91]H.Bethe, Ann. Phys. (Leipzig) **5**, 325 (1930).
[92]E. N. Lassettre, Radiat. Research (Suppl.) **1**, 530 (1959).
[93]E. N. Lassettre and A. Skerbele, Methods Exp. Phys. **3B**, 868 (1974).
[94]M. J. Van der Wiel, Physica **49**, 411 (1970).
[95]M. Inokuti, Rev. Mod. Phys. **43**, 297 (1971).
[96]M. J. Van der Wiel and C. E. Brion, J. Electron Spectrosc. **1**, 309 (1972/73).
[97]C. E. Brion, A. Hamnett, G. R. Wight, and M. J. Van der Wiel, J. Electron Spectrosc. **12**, 323 (1977).
[98]A. Hamnett, W. Stoll, G. Branton, M. J. Van der Wiel, and C. E. Brion, J. Phys. B **9**, 945 (1976).
[99]C. Backx, G. R. Wight, R. R. Tol, and M. J. Van der Wiel, J. Phys. B **8**, 3007 (1975).
[100]C. Backx and M. J. Van der Wiel, J. Phys. B **8**, 3020 (1975).
[101]F. Carnovale and C. Brion, Chem. Phys. **74**, 253 (1983).
[102]A. P. Hitchcock, G. R. J. Williams, C. E. Brion, and P. W. Langhoff, Chem. Phys. **88**, 65 (1984).
[103]J. A. Wheeler and J. A. Bearden, Phys. Rev. **46**, 755 (1934).
[104]J. A. R. Samson, G. H. Rayborn, and P. N. Pareek, J. Chem. Phys. **76**, 393 (1982).
[105]F. Carnovale, A. P. Hitchcock, J. P. D. Cook and C. E. Brion, Chem. Phys. **66**, 249 (1982).
[106]H. A. Bethe, in *Handbuch der Physik*, edited by S. Fugge (Springer, Berlin, 1933), Vol. 24, pp. 457–487.
[107]G. Briet and H. A. Bethe, Phys. Rev. **93**, 888 (1954).
[108]H. A. Bethe and E. E. Salpeter, *Quantum Mechanics of One- and Two-Electron Atoms and Ions* (Springer, Berlin, 1957).
[109]J. Cooper and R. N. Zare, J. Chem. Phys. **48**, 942 (1968).
[110]J. C. Tully, R. S. Berry, and B. J. Dalton, Phys. Rev. **176**, 95 (1968).
[111]A. D. Buckingham, B. J. Orr, and J. M. Sichel, Philos. Trans. Roy. Soc. London, Series A **268**, 147 (1970).
[112]D. Dill and J. L. Dehmer, J. Chem. Phys. **61**, 692 (1974).
[113]Y. Itikawa, Chem. Phys. **28**, 461 (1978).
[114]Y. Itikawa, Chem. Phys. **30**, 109 (1978).
[115]M. White, Phys. Rev. A **26**, 1907 (1982).
[116]R. A. Bonham and M. L. Lively, Phys. Rev. A **29**, 1224 (1984).
[117]L. D. Landau and E. M. Lifschitz, *Quantum Mechanics, Non-Relativistic Theory* (Pergamon, Oxford, 1962).
[118]C. N. Yang, Phys. Rev. **74**, 764 (1948).
[119]U. Fano and D. Dill, Phys Rev. A **6**, 185 (1972).
[120]E. P. Wigner, Phys. Rev. **73**, 1002 (1948).
[121]S. Iwata and S. Nagukura, Mol. Phys. **27**, 425 (1974).
[122]F. Hirota, J. Electron Spectrosc. Relat. Phenom. **9**, 149 (1976).
[123]W. Thiel, Chem. Phys. **57**, 227 (1981).
[124]P. R. Hilton, S. Nordholm, and N. S. Hush, Chem. Phys. Lett. **64**, 515 (1979).
[125]B. W. Fatyga, C. L. Winstead, and P. W. Langhoff, Chem. Phys. Lett. (to be published).
[126]U. Fano and A. R. P. Rau, *Atomic Collisions and Spectra* (Academic, New York, 1986).
[127]G. R. J. Williams and P. W. Langhoff, Chem. Phys. Lett. **78**, 21 (1981).
[128]Z. H. Levine and P. Soven, Phys. Rev. Lett. **50**, 2074 (1983).
[129]Z. H. Levine and P. Soven, Phys. Rev. A **29**, 625 (1984).
[130]S. H. Southworth, A. C. Parr, J. E. Hardis, and J. L. Dehmer, Phys. Rev. A **33**, 1020 (1986).
[131]H. M. Rosenstock, K. Draxl, B. W. Steiner, and J. T. Herron, J. Chem. Phys. Ref. Data **6**, Suppl. 1 (1977).
[132]H. Hartmann, in *Landholt-Börnstein Tables* (Springer, Berlin, 1951), Band I, Te. 13, pp. 359–368.
[133]K. Kimura, S. Katsumata, Y. Achiba, T. Yamazaki, and S. Iwata, *Handbook of He I Photoelectron Spectra of Fundamental Organic Molecules* (Japan Scientific Society, Tokyo and Halsted Press, New York, 1981).
[134]R. D. Levin and S. G. Lias, *Ionization Potential and Appearance Potential Measurements*, 1971–1982 (U. S. Department of Commerce, National Bureau of Standards, 1982), NSRDS-NBS71.
[135]W. von Niessen, L. S. Cederbaum, J. Schirmer, G. H. F. Diercksen, and W. P. Kraemer, J. Electron. Spectrosc. Relat. Phenom. **28**, 45 (1982).
[136]J. Franklin, J. G. Dillard, H. M. Rosenstock, J. T. Herron, and K. Draxl, "Ionization Potentials, Appearance Potentials, and Heats of Formation of Gaseous Positive Ions," NSRDS-NBS 26 (1969).
[137]M. Y. Adam, P. Morin, C. Cauletti, and M. N. Piancastelli, J. Electron Spectrosc. Relat. Phenom. **36**, 377 (1985).
[138]C. Backx, G. R. Wight, and M. J. Van Der Wiel, J. Phys. B **9**, 315 (1976).
[139]M. S. Banna, H. Kossmann, and V. Schmidt, Chem. Phys. **114**, 157 (1987).
[140]M. S. Banna, B. H. McQuaide, R. Malutzki, and V. Schmidt, J. Chem. Phys. **84**, 4739 (1986).
[141]D. Blechschmidt, R. Haensel, E. E. Koch, U. Nielsen, and T. Sagawa, Chem. Phys. Lett. **14**, 33 (1972).
[142]C. Boyle and P. W. Langhoff, Chem. Phys. Lett. (submitted).
[143]C. E. Brion and F. Carnovale, Chem. Phys. **100**, 291 (1985).
[144]C. E. Brion, Y. Iida, F. Carnovale, and J. P. Thomson, Chem. Phys. **98**, 327 (1985).
[145]C. E. Brion, Y. Iida, and J. P. Thomson, Chem. Phys. **101**, 449 (1986).
[146]C. E. Brion, D. W. Lindle, P. A. Heimann, T. A. Ferrett, M. N. Piancastelli, and D. A. Shirley, Chem. Phys. Lett. **128**, 118 (1986).
[147]C. E. Brion and K. H. Tan, Chem. Phys. **34**, 141 (1978).
[148]C. E. Brion and K. H. Tan, J. Electron Spectrosc. Relat. Phenom. **23**, 1 (1981).
[149]C. E. Brion, K. H. Tan, M. J. Van Der Wiel, and P. E. Van Der Leeuw, J. Electron Spectrosc. Relat. Phenom. **17**, 101 (1979).
[150]I. Cacelli, V. Caravetta, and R. Moccia, J. Chem. Phys. **85**, 7038 (1986).
[151]I. Cacelli, V. Caravetta, and R. Moccia. J. Phys. B **18**, 1375 (1985).
[152]I. Cacelli, R. Moccia, and V. Carravetta, Chem. Phys. **90**, 313 (1984).
[153]R. B. Cairns, H. Harrison, and R. I. Schoen, J. Chem. Phys. **55**, 4886 (1971).
[154]T. A. Carlson, A. Fahlman, M. O. Krause, P. R. Keller, J. W. Taylor, T. A. Whitley, and F. A. Grimm, J. Chem. Phys. **80**, 3521 (1984).
[155]T. A. Carlson, A. Fahlman, M. O. Krause, T. A. Whitley, and F. A. Grimm, J. Chem. Phys. **81**, 5389 (1984).
[156]T. A. Carlson, P. R. Keller, J. W. Taylor, T. Whitley, and F. A. Grimm, J. Chem. Phys. **79**, 97 (1983).
[157]T. A. Carlson, M. O. Krause, A. Fahlman, P. R. Keller, J. W. Taylor, T. A. Whitley, and F. A. Grimm, J. Chem. Phys. **79**, 2157 (1983).
[158]T. A. Carlson, M. O. Krause, and F. A. Grimm, J. Chem. Phys. **77**, 1701 (1982).
[159]T. A. Carlson, M. O. Krause, F. A. Grimm, J. D. Allen Jr., D. Mehaffy, P. R. Keller, and J. W. Taylor, J. Chem. Phys. **75**, 3288 (1981).
[160]T. A. Carlson, M. O. Krause, F. A. Grimm, P. R. Keller, and J. W. Taylor, J. Chem. Phys. **77**, 5340 (1982).
[161]T. A. Carlson, M. O. Krause, F. A. Grimm, and T. A. Whitley, J. Chem.

Phys. **78**, 638 (1983).
[162]F. Carnovale, R. Tseng, and C. E. Brion, J. Phys. B **14**, 4771 (1981).
[163]F. Carnovale, M. G. White, and C. E. Brion, J. Electron Spectrosc. Relat. Phenom. **24**, 63 (1981).
[164]B. E. Cole and R. N. Dexter, J. Phys. B **11**, 1011 (1978).
[165]L. A. Collins and B. I. Schneider, Phys. Rev. A **29**, 1695 (1984).
[166]G. R. Cook and P. H. Metzger, J. Opt. Soc. Am. **54**, 968 (1964).
[167]J. W. Davenport, Int. J. Quantum Chem. Symp. **11**, 89 (1977).
[168]J. W. Davenport, Phys. Rev. Lett. **36**, 945 (1976).
[169]S. Daviel, Y. Iida, F. Carnovale, and C. E. Brion, Chem. Phys. **83**, 391 (1984).
[170]L. De Reilhac and N. Damany, J. Quant. Spectrosc. Radiat. Transfer **18**, 121 (1977).
[171]J. L. Dehmer, A. C. Parr, S. Wallace, and D. Dill, Phys. Rev. A **26**, 3283 (1982).
[172]D. R. Denne, J. Phys. D **3**, 1392 (1970).
[173]G. H. F. Diercksen, M. R. Hermann, B. W. Fatyga, and P. W. Langhoff, Chem. Phys. Lett. **123**, 345 (1986).
[174]G. H. F. Diercksen and P. W. Langhoff, Chem. Phys. **112**, 227 (1987).
[175]P. M. Dittmen, D. Dill, and J. L. Dehmer, J. Chem. Phys. **76**, 5703 (1982).
[176]C. M. Dutta, F. M. Chapman, Jr., and E. F. Hayes, J. Chem. Phys. **67**, 1904 (1977).
[177]K. Faegri Jr. and H. P. Kelly, Chem. Phys. Lett. **85**, 472 (1982).
[178]K. Faegri Jr. and H. P. Kelly, Phys. Rev. A **23**, 52 (1981).
[179]J. Fryar and R. Browning, Planet. Space Sci. **21**, 709 (1973).
[180]A. B. Gardner, M. J. Lynch, D. T. Stewart, and W. S. Watson, J. Phys. B **6**, L262 (1973).
[181]A. Gerwer, C. Asaro, B. V. McKoy, and P. W. Langhoff, J. Chem. Phys. **72**, 713 (1980).
[182]F. A. Grimm (private communication).
[183]F. A. Grimm, J. D. Allen Jr., T. A. Carlson, M. O. Krause, D. Mehaffy, P. R. Keller, and J. W. Taylor, J. Chem. Phys. **75**, 92 (1981).
[184]F. A. Grimm and T. A. Carlson, Chem. Phys. **80**, 389 (1983).
[185]T. Gustafsson, Chem. Phys. Lett. **75**, 505 (1980).
[186]T. Gustafsson, Phys. Rev. A **18**, 1481 (1978).
[187]T. Gustafsson and H. J. Levinson, Chem. Phys. Lett. **78**, 28 (1981).
[188]T. Gustafsson, E. W. Plummer, D. W. Eastman, and W. Gudat, Phys. Rev. A **17**, 175 (1978).
[189]G. N. Haddad and J. A. R. Samson, J. Chem. Phys. **84**, 6623 (1986).
[190]A. Hamnett, W. Stoll, and C. E. Brion, J. Electron Spectrosc. Relat. Phenom. **8**, 367 (1976).
[191]M. R. Hermann, C. W. Bauschlicher Jr., W. M. Huo, S. R. Langhoff, and P. W. Langhoff, Chem. Phys. **109**, 1 (1986).
[192]M. R. Hermann, G. H. F. Diercksen, B. W. Fatyga, and P. W. Langhoff, Int. J. Quantum Chem. Symp. **18**, 719 (1984).
[193]M. R. Hermann, S. R. Langhoff, and P. W. Langhoff, Chem. Phys. Lett. **109**, 150 (1984).
[194]M. R. Hermann, S. R. Langhoff, and P. W. Langhoff, Chem. Phys. Lett. (submitted).
[195]A. P. Hitchcock, C. E. Brion, and M. J. Van Der Wiel, Chem. Phys. **45**, 461 (1980).
[196]A. P. Hitchcock, C. E. Brion, and M. J. Van Der Wiel, J. Phys. B **11**, 3245 (1978).
[197]A. P. Hitchcock and M. J. Van Der Wiel, J. Phys. B **12**, 2153 (1979).
[198]R. M. Holmes and G. V. Marr, J. Phys. B **13**, 945 (1980).
[199]T. Ibuki, H. Koizumi, T. Yoshimi, M. Morita, S.Arai, K. Hironaka, K. Shinsaka, Y. Hatano, and Y. Yagishita, Chem. Phys. Lett. **119**, 327 (1985).
[200]Y. Iida, F. Carnovale, S. Daviel, and C. E. Brion, Chem. Phys. **105**, 211 (1986).
[201]Y. Itikawa, H. Takagi, H. Nakamura, and H. Sato, Phys. Rev. A **27**, 1319 (1983).
[202]D. H. Katayama, R. E. Huffman, and C. L. O'Bryan, J. Chem. Phys. **59**, 4309 (1973).
[203]S. Krummacher, V. Schmidt, and F. Wuilleumier, J. Phys. B **13**, 3993 (1980).
[204]S. Krummacher, V. Schmidt, F. Wuilleumier, J. M. Bizau, and D. Ederer, J. Phys. B **16**, 1733 (1983).
[205]P. W. Langhoff, A. Gerwer, C. Asaro, and B. V. McKoy, Int. J. Quantum Chem. Symp. **13**, 645 (1979).
[206]P. W. Langhoff, S. R. Langhoff, T. N. Rescigno, J. Schirmer, L. S. Cederbaum, W. Domcke, and W. Von Niessen, Chem. Phys. **58**, 71 (1981).
[207]L. C. Lee, R. W. Carlson, and D. L. Judge, J. Quant. Spectrosc. Radiat. Transfer **16**, 873 (1976).
[208]L. C. Lee, R. W. Carlson, D. L. Judge, and M. Ogawa, J. Quant. Spectrosc. Radiat. Transfer **13**, 1023 (1973).
[209]L. C. Lee, E. Phillips, and D. L. Judge, J. Chem. Phys. **67**, 1237 (1977).
[210]R. R. Lucchese and V. McKoy, Phys. Rev. A **26**, 1406 (1982).
[211]R. R. Lucchese and V. McKoy, Phys. Rev. A **28**, 1382 (1983).
[212]R. R. Lucchese, G. Raseev, and V. McKoy, Phys. Rev. A **25**, 2572 (1982).
[213]G. V. Marr, R. M. Holmes, and K. Codling, J. Phys. B **13**, 283 (1980).
[214]G. V. Marr, J. M. Morton, R. M. Holmes, and D. G. McCoy, J. Phys. B **12**, 43 (1979).
[215]T. Masuoka and J. A. R. Samson, J. Chem. Phys. **74**, 1093 (1981).
[216]T. Masuoka and J. A. R. Samson, J. Chem. Phys. **75**, 4946 (1981).
[217]T. Masuoka and J. A. R. Samson, J. Chim. Phys. Phys. Chim. Biol. **77**, 623 (1980).
[218]D. G. McCoy, J. M. Morton, and G. V. Marr, J. Phys. B **11**, L547 (1978).
[219]G. Mehlman, D. L. Ederer, and E. B. Saloman, J. Chem. Phys. **68**, 1862 (1978).
[220]P. Morin, M. Y. Adam, P. Lablanquie, I. Nenner, M. J. Hubin-Franskin, and J. Delwiche, Ann. Isr. Phys. Soc. **6**, 613 (1984).
[221]P. Morin, M. Y. Adam, I. Nenner, J. Delwiche, M. J. Hubin-Franskin, and P. Lablanquie, Nucl. Instrum. Methods **208**, 761 (1983).
[222]P. Morin, I. Nenner, M. Y. Adam, M. J. Hubin-Franskin, J. Delwiche, H. Lefebvre-Brion, and A. Giusti-Suzor, Chem. Phys. Lett. **92**, 609 (1982).
[223]S. V. Oneil and W. P. Reinhardt, J. Chem. Phys. **69**, 2126 (1978).
[224]N. T. Padial, G. Csanak, B. V. McKoy, and P. W. Langhoff, J. Chem. Phys. **69**, 2992 (1978).
[225]N. Padial, G. Csanak, B. V. McKoy, and P. W. Langhoff, Phys. Rev. A **23**, 218 (1981).
[226]E. Phillips, L. C. Lee, and D. L. Judge, J. Quant. Spectrosc. Radiat. Transfer **18**, 309 (1977).
[227]H. F. Prest, W.-B. Tzeng, J. M. Brom Jr., and C. Y. Ng, Int. J. Mass Spectrom. Ion Phys. **50**, 315 (1983).
[228]G. Raseev and H. Le Rouzo, Phys. Rev. A **27**, 268 (1983).
[229]G. Raseev, H. Lefebvre-Brion, H. Le Rouzo, and A. L. Roche, J. Chem. Phys. **74**, 6686 (1981).
[230]M. Roche, D. R. Salahub, and R. P. Messmer, J. Electron Spectrosc. Relat. Phenom. **19**, 273 (1980).
[231]P. Roy, I. Nenner, M. Y. Adam, J. Delwiche, M. J. Hubin-Franskin, P. Lablanquie, and D. Roy, Chem. Phys. Lett. **109**, 607 (1984).
[232]J. A. R. Samson and G. C. Angel, J. Chem. Phys. **86**, 1814 (1987).
[233]J. A. R. Samson and J. L. Gardner, J. Electron Spectrosc. Relat. Phenom. **8**, 35 (1976).
[234]J. A. R. Samson, J. L. Gardner, and G. N. Haddad, J. Electron Spectrosc. Relat. Phenom. **12**, 281 (1977).
[235]J. A. R. Samson, G. N. Haddad, and J. L. Gardner, J. Phys. B **10**, 1749 (1977).
[236]J. A. R. Samson and G. Haddad (private communication).
[237]J. A. R. Samson and T. Masuoka (private communication).
[238]J. A. R. Samson, T. Masuoka, and W. T. Huntress, Geophys. Res. Lett. **8**, 405 (1981).
[239]J. A. R. Samson, T. Masuoka, and P. N. Pareek, J. Chem. Phys. **83**, 5531 (1985).
[240]J. A. Sheehy and P. W. Langhoff, Chem. Phys. Lett. (submitted).
[241]M. E. Smith, R. R. Lucchese, and V. McKoy, J. Chem. Phys. **79**, 1360 (1983).
[242]M. E. Smith, V. McKoy, and R. R. Lucchese, J. Chem. Phys. **82**, 4147 (1985).
[243]S. H. Southworth, A. C. Parr, and J. E. Hardis, Phys. Rev. A **33**, 1020 (1986).
[244]S. Southworth, W. D. Brewer, C. M. Truesdale, P. H. Kobrin, D. W. Lindle, and D. A. Shirley, J. Electron Spectrosc. Relat. Phenom. **26**, 43 (1982).
[245]S. Southworth, C. M. Truesdale, P. H. Kobrin, D. W. Lindle, W. D. Brewer, and D. A. Shirley, J. Chem. Phys. **76**, 143 (1982).
[246]J. A. Stephens, D. Dill, and J. L. Dehmer, J. Phys. B **14**, 3911 (1981).
[247]J. R. Swanson, D. Dill, and J. L. Dehmer, J. Phys. B **13**, L231 (1980).
[248]C. M. Truesdale, S. Southworth, P. H. Kobrin, D. W. Lindle, and D. A. Shirley, J. Chem. Phys. **78**, 7117 (1983).
[249]C. M. Truesdale, S. Southworth, P. H. Kobrin, D. W. Lindle, G. Thornton, and D. A. Shirley, J. Chem. Phys. **76**, 860 (1982).
[250]M. J. Van Der Wiel, W. Stoll, A. Hamnett, an C. E. Brion, Chem. Phys. Lett. **37**, 240 (1976).
[251]S. Wallace, D. Dill, and J. L. Dehmer, J. Chem. Phys. **76**, 1217 (1982).

[252]S. Wallace, D. Dill, and J. L. Dehmer, J. Phys. B **12**, L417 (1979).
[253]W. C. Watson, D. T. Stewart, A. B. Gardner, and M. J. Lynch, Planet. Space Sci. **23**, 384 (1975).
[254]W. S. Watson, J. Lang, and D. T. Stewart, J. Phys. B **6**, L148 (1973).
[255]W. S. Watson, J. Lang, and D. T. Stewart, Phys. Lett. A **44**, 293 (1973).
[256]G. R. Wight, M. J. Van Der Wiel, and C. E. Brion, J. Phys. B **9**, 675 (1976).
[257]G. R. Wight, M. J. Van Der Wiel, and C. E. Brion, J. Phys. B **10**, 1863 (1977).
[258]P. R. Woodruff and G. V. Marr, Proc. R. Soc. London, Ser. A **358**, 87 (1977).
[259]C. Y. R. Wu and D. L. Judge, J. Chem. Phys. **74**, 3804 (1981).
[260]C. Y. R. Wu and D. L. Judge, J. Chem. Phys. **76**, 2871 (1982).
[261]C. Y. R. Wu and D. L. Judge, J. Chem. Phys. **78**, 2180 (1983).